CONTENTS

Page

INTENTIONALLY LEFT BLANK

TABLES

Page

INTENTIONALLY LEFT BLANK

FIGURES

Page

INTENTIONALLY LEFT BLANK

2.3.10 Biosphere Transport and Exposure

[NUREG-1804, Section 2.2.1.3.13.3: AC 1, AC 2, AC 3, AC 4, AC 5; Section 2.2.1.3.14.3: AC 1, AC 2, AC 3, AC 4, AC 5]

The information presented in this section addresses the requirements for conducting a performance assessment included in 10 CFR 63.102(i); proposed 10 CFR 63.114(a)(1) through (a)(5), (a)(7), and (b); 63.305(a), (b), and (d); proposed 63.305(c); proposed 63.311; and 63.312(a) through (e), with respect to the area of biosphere transport and exposure. Proposed 10 CFR 63.114(a)(6) is not referenced below because the degradation, deterioration, and alteration processes that are the subject of that section are addressed in Sections 2.2, 2.3.4 to 2.3.7, and 2.3.11. This section also provides information that addresses specific acceptance criteria in Sections 2.2.1.3.13.3 and 2.2.1.3.14.3 of NUREG-1804.

With regard to biosphere transport and receptor exposure, this section presents the following:

- A description of the biosphere conceptual and mathematical model
- Descriptions of input data used in the model that were representative of the site and surrounding region and of the receptor, the reasonably maximally exposed individual (RMEI), along with discussion of uncertainties and variabilities in the model parameter values, and consideration of alternative conceptual models
- Specific features, events, and processes (FEPs) included in the analyses and the technical bases for inclusion
- Discussion of the biosphere model results, their bases, and their use as input to the total system performance assessment (TSPA) model.

The categories of information provided in this section, as well as the corresponding regulatory requirements and NUREG-1804 acceptance criteria, are presented in the table below. With regard to Acceptance Criteria 1(4) and 3(5) in Section 2.2.1.3.13.3 as well as Section 2.2.1.3.14.3 of NUREG-1804 no formal peer reviews or expert elicitations were used directly to support development of the current biosphere model discussed in this section (2.3.10). In addition, this section does not discuss the approach used for data qualification. However, scientific analyses, model development, and data qualification activities were conducted in accordance with project procedures that comply with Quality Assurance Program requirements. The project procedures governing data qualification are consistent with NUREG-1298 (Altman et al. 1988) in keeping with the Acceptance Criteria 1(4) from Sections 2.2.1.3.13.3 and 2.2.1.3.14.3 of NUREG-1804.

SAR Section	Information Category	Proposed 10 CFR Part 63 Reference	NUREG-1804 Reference
2.3.10	Biosphere Transport and Exposure	63.102(i)[a] 63.114(a)(1) 63.114(a)(2) 63.114(a)(3) 63.114(a)(4) 63.114(a)(5) 63.114(a)(7) 63.114(b) 63.305(a)[a] 63.305(b)[a] 63.305(c) 63.305(d)[a] 63.311 63.312(a)[a] 63.312(b)[a] 63.312(c)[a] 63.312(d)[a] 63.312(e)[a] 63.342(c)	Section 2.2.1.3.13.3: Acceptance Criterion 1 Acceptance Criterion 2 Acceptance Criterion 3 Acceptance Criterion 4 Acceptance Criterion 5 Section 2.2.1.3.14.3: Acceptance Criterion 1 Acceptance Criterion 2 Acceptance Criterion 3 Acceptance Criterion 4 Acceptance Criterion 5
2.3.10.1	Summary and Overview	Not applicable	Not applicable
2.3.10.2	Conceptual Model of Biosphere Transport, Receptor, and Receptor Exposure	63.102(i)[a] 63.114(a)(1) 63.114(a)(2) 63.114(a)(3) 63.114(a)(4) 63.114(a)(5) 63.114(a)(7) 63.114(b) 63.305(a)[a] 63.305(b)[a] 63.305(c) 63.305(d)[a] 63.312(a)[a] 63.312(b)[a] 63.312(c)[a] 63.312(d)[a] 63.312(e) 63.342(c)	Section 2.2.1.3.13.3: Acceptance Criterion 1(1) Acceptance Criterion 1(2) Acceptance Criterion 1(3) Section 2.2.1.3.14.3: Acceptance Criterion 1(1) Acceptance Criterion 1(2) Acceptance Criterion 1(3)
2.3.10.3	Data and Data Uncertainty	63.114(a)(1) 63.114(a)(2)	Section 2.2.1.3.13.3: Acceptance Criterion 2 Acceptance Criterion 3(1) Acceptance Criterion 3(2) Acceptance Criterion 3(3) Acceptance Criterion 3(4) Section 2.2.1.3.14.3: Acceptance Criterion 2 Acceptance Criterion 3(1) Acceptance Criterion 3(2) Acceptance Criterion 3(3) Acceptance Criterion 3(4)

SAR Section	Information Category	Proposed 10 CFR Part 63 Reference	NUREG-1804 Reference
2.3.10.4	Model Uncertainty	63.114(a)(5) 63.114(a)(7) 63.114(b) 63.342(c)	Section 2.2.1.3.13.3: Acceptance Criterion 4 Section 2.2.1.3.14.3: Acceptance Criterion 4
2.3.10.5	Abstraction	63.114(b) 63.311 63.342(c)	Section 2.2.1.3.13.3: Acceptance Criterion 5 Section 2.2.1.3.14.3: Acceptance Criterion 3(6) Acceptance Criterion 5
2.3.10.6	Conclusions	Not applicable	Not applicable

NOTE: [a]Not changed by the proposed rule.

2.3.10.1 Summary and Overview

The performance assessment is defined as a systematic analysis that identifies the FEPs that might affect performance of the geologic repository; examines their effects on performance; and estimates the radiological exposures to the RMEI (10 CFR 63.102). The evaluation of how well the Yucca Mountain natural and engineered barrier systems are projected to perform in their capacity to retain or retard the migration of radionuclides from the repository to the accessible environment is the focus of geosphere modeling (described in Sections 2.3.1 to 2.3.9). The evaluation of doses to the defined receptor, the RMEI, when the radionuclide release to the accessible environment occurs, is the focus of biosphere modeling.

The biosphere model simulates the processes and pathways contributing to dose to the RMEI at Yucca Mountain. According to 10 CFR 63.312, the RMEI is the receptor defined for the purpose of performance assessment of the Yucca Mountain repository. Two potential sources of radionuclides are considered. Radionuclides present in groundwater may reach the biosphere when groundwater is drawn from wells and used for agricultural and domestic purposes. Alternatively, in the unlikely event of an igneous eruption through the repository, radionuclides attached to tephra could be transported directly to the biosphere and to the RMEI (Section 2.3.11). Because the biosphere model addresses features and processes in the accessible environment outside of the repository system boundary, the model provides no information regarding the capability of the natural and engineered barriers.

The biosphere model, known as the Environmental Radiation Model for Yucca Mountain Nevada (ERMYN), tracks the environmental transport of radionuclides that originate from the repository through the biosphere and calculates annual dose to the RMEI per unit of radionuclide concentration in groundwater or in surface soil mixed with volcanic tephra. The primary outputs of the biosphere model are biosphere dose conversion factors (BDCFs), equivalent to the annual dose from all potential exposure pathways that the RMEI would experience as a result of a unit concentration of a radionuclide in groundwater (Section 2.3.10.5.1) or in surface soil mixed with volcanic tephra (Section 2.3.10.5.2). The TSPA model combines the BDCFs with estimates of radionuclide concentrations in groundwater and in surface soil mixed with volcanic tephra from the saturated

zone transport abstraction models and the volcanic tephra redistribution model, respectively, at the location of the RMEI, to calculate the predicted annual total dose required to evaluate compliance with the individual protection standards in proposed 10 CFR 63.311 and proposed 10 CFR 63.321 (Sections 2.3.10.5.1.2 and 2.3.10.5.2.2). This quantity represents the incremental annual dose that the RMEI would receive as a result of radionuclide releases from the geologic repository at Yucca Mountain, in addition to, and exclusive of, the dose contributions from other sources, whether natural or man-made.

Site-specific conditions in the Yucca Mountain region (Section 2.3.10.2.1) are incorporated in the reference biosphere (i.e., the biosphere model's representation of the environment). The lifestyle of the people living in Amargosa Valley (Section 2.3.10.2.2) provides the bases for the representation of the RMEI. Separate conceptual and mathematical models, and resulting sets of BDCFs, were developed for the groundwater (Section 2.3.10.2.5) and volcanic ash exposure scenarios (Section 2.3.10.2.6) because the transport mechanisms differ depending on the source. The groundwater exposure scenario considers radionuclides entering the biosphere from wells used for drinking, irrigating commercial and garden crops, watering livestock, raising fish, and running evaporative coolers. These water usage practices may lead to radioactive contamination of the environmental media, such as soil, air, fauna, and flora, and the consequent radiation exposure of the RMEI. The BDCFs for the groundwater exposure scenario include contributions from ingesting water, crops, fish, animal products, and soil; external exposure to soil; and inhaling resuspended soil, aerosols from evaporative coolers, and radioactive gases and their decay products (Section 2.3.10.2.5).

The sources of contamination for the volcanic ash exposure scenario are radionuclides deposited by a volcanic eruption in the area occupied by the hypothetical community that includes the RMEI, or by the later redistribution of contaminated volcanic tephra to that location. The biosphere model considered transport of radionuclides from the soil mixed with contaminated volcanic tephra to air, crops, and animal products. The term “tephra” is used as a general term for pyroclastic material regardless of size. The term “ash” means erupted material less than 2 mm in diameter. The RMEI could receive a dose from inhaling resuspended soil and radon (^{222}Rn) decay products; from ingesting crops, animal products, and soil; and from external exposure to soil (Section 2.3.10.2.6).

The mathematical representations of transport processes and exposure pathways are based on the methods generally applied in radiological assessments and included in other biosphere models. Where necessary, representations of site-specific processes and pathways were developed. Input parameter distributions were developed from site-specific data and surveys, data from analogue sites, and other sources (Section 2.3.10.3). The distributions of parameters describing the reference biosphere were stochastically sampled to incorporate variation and uncertainty in the conditions in the Yucca Mountain region. Parameter distributions incorporating variation and uncertainty about the diets and living styles of the population of Amargosa Valley are used to describe the RMEI.

Alternative conceptual models were considered and evaluated during development of the biosphere model. The evaluation included several criteria, such as consistency with the available data and scientific understanding of the modelled processes, applicability of a model to the conditions in the Yucca Mountain region, representation of the uncertainty, and whether an alternative model could result in underestimating the risk to the RMEI. In addition, mathematical model uncertainty was evaluated by comparison of biosphere model results to results from alternative models at the process

or submodel levels. No alternative system-level model was identified because of the inclusion of site-specific environmental transport and exposure pathways in the biosphere model (Section 2.3.10.4.1). The alternative conceptual model evaluation resulted in the conclusion that the models selected for incorporation into the biosphere model presented a better choice with respect to the aforementioned criteria. Also, the differences noted between the models were small relative to the total variability in BDCFs. The propagation of uncertainty and variability through the model resulted in BDCFs that varied by about 1 to 2 orders of magnitude for most radionuclides.

In the biosphere model, the effect of climate change on the BDCFs for the groundwater exposure scenario must be weighed against two requirements. One requirement is not to project changes in society, the biosphere (other than climate), human biology, or increases or decreases of human knowledge or technology (10 CFR 63.305(b)). The other requirement is to vary factors related to climate based on cautious, but reasonable assumptions consistent with present knowledge (proposed 10 CFR 63.305(c)). Because BDCFs are a function of climate factors that depend on human activities and those that do not, the effect of climate change on BDCFs needed to be evaluated from the perspective of these two requirements. It was concluded that human activities, which should not be projected to change, have the largest effect on the BDCFs, and that the BDCFs are relatively insensitive to climate change effects on those parameters that are independent of human activities (SNL 2007a, Section 6.11.3). Furthermore, the BDCFs for the future climate, which is predicted to be cooler and wetter than the present-day climate (BSC 2004a), are lower than the corresponding present-day climate BDCFs and would result in lower doses to the RMEI (SNL 2007a, Section 6.11.3). BDCFs for the volcanic ash exposure scenario were almost insensitive to the effects of climate change on the model parameters. Based on these considerations, the present-day climate BDCFs represent a suitable balance between the requirements of 10 CFR 63.305(b) and proposed 10 CFR 63.305(c), meet the requirements of 10 CFR 63.305(a) and (b), and are appropriate for the assessment of doses to the RMEI for the entire 10,000 year period following repository closure, and for the period beyond 10,000 years, within the period of geologic stability, as prescribed by proposed 10 CFR Part 63 (Section 2.3.10.5.1.1).

Role of the Biosphere Model in the TSPA—The TSPA model integrates the essential components of the conceptual and process models to simulate repository behavior. Figure 2.3.10-1 represents the information flow from source data to the conceptual and mathematical biosphere process models used to calculate BDCFs, which are inputs to the TSPA model. Figure 2.3.10-2 is a schematic representation of the principal TSPA model components for the nominal scenario class. This and other scenario classes and modeling cases involving radionuclide release to groundwater use BDCFs for the groundwater exposure scenario. Biosphere exposure scenarios should not be confused with TSPA scenario classes. The biosphere exposure scenario is a well-defined, connected sequence of FEPs that describes characteristics of the biosphere, where radionuclide transport and human exposure occurs, and is constructed to evaluate radiological consequences of radionuclide releases to the reference biosphere in a given medium, such as the groundwater, irrespective of the cause of contamination in the groundwater. The TSPA scenario classes pertain to the characteristics and evolution of the whole repository system. Figure 2.3.10-2 demonstrates the role and relationship of the biosphere model to other models. The biosphere component of the TSPA model receives input from the saturated zone transport abstraction models in the form of mass concentration of radionuclides in a unit volume of water. This quantity is calculated by dividing the mass flux of radionuclides at the boundary of accessible environment by an annual water demand of 3,000 acre-feet (10 CFR 63.312(c)). Within the biosphere model

component of the TSPA model, this quantity is converted to activity concentration per unit volume of groundwater and combined with the BDCFs from the biosphere model to calculate annual dose to the RMEI for comparison to regulatory standards. Figure 2.3.10-3 shows the relationship of the biosphere model to other TSPA model components for the volcanic eruption modeling case of the igneous scenario class. In this case, the biosphere component of the TSPA model receives information on radionuclide concentration on the ground as input from the tephra redistribution model. The TSPA model combines the input from the tephra redistribution model with BDCFs from the biosphere model to generate annual dose histories.

Summary of FEPs Evaluated in the Biosphere Transport and Exposure Models and Analyses—The complete set of FEPs, both included and excluded, is provided in Section 2.2 (Table 2.2-5). The included FEPs that describe the biosphere system and associated chemical, physical, and biological processes in the region surrounding Yucca Mountain were used to define the reference biosphere and to develop the biosphere conceptual model (Section 2.2 and SNL 2007a, Sections 6.2 and 6.7). These FEPs are presented in Table 2.3.10-1, along with summaries of the technical basis and approach for disposition within the biosphere model.

2.3.10.2 Conceptual Model of Biosphere Transport, Receptor, and Receptor Exposure

[NUREG-1804, Section 2.2.1.3.13.3: AC 1(1) to (3); Section 2.2.1.3.14.3: AC 1(1) to (3)]

The following actions were taken to identify and incorporate important site features, physical phenomenon, couplings, and appropriate assumptions into the conceptual model of biosphere transport and receptor exposure. First, the biosphere and population to be modeled were characterized (Sections 2.3.10.2.1 and 2.3.10.2.2). The characteristics of the local biosphere and the population were used to construct the reference biosphere and the receptor for the biosphere model (the RMEI). This information was considered in the identification of the FEPs applicable to the biosphere model. The processes that would transport radionuclides to environmental media, and the pathways by which the RMEI would be exposed to radionuclides in those media, were then identified (Section 2.3.10.2.3). The identified processes were used to develop an interaction matrix of radionuclide transfer and exposure pathways that must be included in the model (i.e., in the reference biosphere). Methods for modeling radioactive decay and ingrowth, and submodels that account for interactions, were then developed for the environmental media and exposure pathways, and assumptions were developed that allow for implementation of the submodels (Sections 2.3.10.2.4 to 2.3.10.2.6) (SNL 2007a, Sections 6.1 to 6.3). Section 2.3.10.2 describes the conceptual biosphere model and identifies those aspects of biosphere characteristics modeling (FEP 2.3.13.01.0A) that are important for repository performance, including the technical bases for those descriptions.

2.3.10.2.1 Information Used to Characterize the Reference Biosphere

To ensure that the required characteristics of the reference biosphere specified in proposed 10 CFR 63.305 were incorporated into the biosphere model, present knowledge of the conditions in the region surrounding Yucca Mountain was used to characterize local climate, geography, soils, flora and fauna, communities, and infrastructure. This characterization focused on Amargosa Valley, which is the inhabited region south of Yucca Mountain at or near the accessible environment (SNL 2007a, Section 6.1.1), because this region currently supports a community whose dietary and

lifestyle characteristics were used to construct a stylized exposure scenario for a hypothetical receptor, the RMEI (Section 2.3.10.2.2), as required by 10 CFR 63.312(b).

Climate—Today, the Yucca Mountain region has low precipitation, hot summers, cool winters, low relative humidity, and a high rate of evaporation (BSC 2004b, Section 6.3.3.2). Data collected at Meteorological Monitoring Site 9 in northern Amargosa Valley (Section 2.3.1, Figure 2.3.1-3) were used in biosphere modeling to characterize the present-day climate of the area. These data were selected because Site 9 is approximately at the boundary of the accessible environment specified in 10 CFR 63.302 (BSC 2004c, Section 4.1.5.1). Average annual precipitation is about 100 mm, and average monthly temperatures range from 6.9°C in December to 31.2°C in July (BSC 2004c, Table 4.1-2). The present-day climate in the Yucca Mountain region is further described in Section 2.3.1. Measurements of annual precipitation used in the biosphere model for the present-day climate are lower than those considered in Section 2.3.1 for the calculation of infiltration rates because the location of the RMEI specified in 10 CFR 63.312(a) is at a lower elevation than the area of water infiltration above the repository (BSC 2004c, Section 4.1.5.1).

Topography and Soils—Amargosa Valley is a broad northwest-trending basin approximately 80 km long and up to 30 km wide. The basin floor slopes gently to the southeast from elevations of about 975 m at the northern end (near Beatty, Nevada) to about 600 m toward the south end. There are no perennial streams at Yucca Mountain or northern Amargosa Valley. The ephemeral Amargosa River, which infrequently carries runoff from the Yucca Mountain area via Fortymile Wash, flows southeast along the western edge of the basin (SNL 2007a, Section 6.1.1.1; BSC 2004b, Sections 3.4.2 and 3.4.3).

The soils on alluvial fans and in stream channels in northern Amargosa Valley generally are deep and well- to excessively drained. The surface soil layer generally is less than 20 cm thick; subsurface soils are up to 150 cm deep. Soil textures vary from gravelly fine sands to sandy loams. The soils are calcareous and moderately alkaline. The site-specific information on soils in Amargosa Valley was obtained from the Natural Resource Conservation Service (USDA 2004) and other sources (CRWMS M&O 1999a). Information on topography and soils was used to develop soil erosion rates, leaching rates, crop growth characteristics, crop irrigation requirements, airborne particulate concentrations, and other parameter distributions that are consistent with the current knowledge of the conditions in the Yucca Mountain region (SNL 2007b, Section 6; BSC 2004c, Section 6).

Native Flora and Fauna—The native vegetation of northern Amargosa Valley is dominated by shrubs typical of the northern Mojave Desert, such as creosote bush (*Larrea tridentata*) and white bursage (*Ambrosia dumosa*). There are no forested areas in Amargosa Valley or elsewhere in the immediate region south of Yucca Mountain (DOE 2002, Section 3.1.5.1.1). Wildlife in the Yucca Mountain region is dominated by species associated with the Mojave Desert, with some species from the Great Basin Desert at higher elevations. Game species found in the region include Gambel's quail (*Callipepla gambelii*), chukar (*Alectoris chukar*), mourning dove (*Zenaida macroura*), and mule deer (*Odocoileus hemionus*). Those species are most common in the mountains surrounding Amargosa Valley and Yucca Mountain and in areas where water is available from springs, seeps, and man-made water developments (CRWMS M&O 1999b, Section 3.3.2.3; DOE 2002, Section 3.1.5.1.2). Based on the presence of native game species and the results of the food consumption survey, human consumption of native game animals was

included in the calculation of food consumption rates in the biosphere model by including consumption rates of wild game and game hen in the corresponding food types that were considered in the biosphere model. Because there are no locally produced wood products used for production of building materials or furniture, the use of wood products was not included in the model (SNL 2007a, Section 6.3.1.6; BSC 2005, Section 6.4.2).

Communities—The region surrounding Yucca Mountain is rural and sparsely populated. In 2003, an estimated 23,180 people lived within 84 km of Yucca Mountain. About 80% lived more than 64 km from Yucca Mountain in and near Pahrump, Nevada. An estimated 1,412 people lived in the Amargosa Valley region about 20 to 56 km south of Yucca Mountain (BSC 2003, Table 1 and Figure 1). The closest residents to Yucca Mountain in 2003 lived in northern Amargosa Valley, at the intersection of U.S. Highway 95 and Nevada State Route 373, about 20 km south of Yucca Mountain (Figure 2.3.10-4). Other communities and employment centers in south-central Nevada, and the approximate highway distance from the intersection of Highway 95 and State Route 373, are Beatty (45 km); Pahrump (70 km); Indian Springs (70 km); and Las Vegas (120 km). Information about the communities in the region surrounding Yucca Mountain was used to characterize the RMEI and the reference biosphere (BSC 2005, Sections 5.1 and 6.1; Rasmuson 2004, Enclosure 2; SNL 2007a, Sections 6.1.1 and 6.1.2).

Infrastructure—In 2004, government and other community and social services in the Town of Amargosa Valley included a public library, an elementary school, churches, a community center and park, a senior center, a small medical clinic, an ambulance service, and a post office. There also were small convenience or general stores; restaurants, saloons, and gambling establishments; miscellaneous retail stores; and a motel (Rasmuson 2004, Enclosure 2). Most of the major roads in the Amargosa Valley area were paved. The nearest other indoor recreation (e.g., movie theaters, other restaurants), larger stores, and hospitals were in Pahrump and Las Vegas. Because some Amargosa Valley residents leave the area for employment and to obtain some goods and services, the biosphere model accounted for the RMEI spending some time away from areas where radionuclides originating from the repository may be present in the environment (BSC 2005, Sections 5 and 6).

Water used for domestic, municipal, and agricultural purposes in Amargosa Valley comes from groundwater. There are no public water treatment systems in Amargosa Valley. Therefore, the biosphere model considered that water used by the RMEI would be from groundwater and would not be treated prior to use (SNL 2007a, Section 6.3.1.1).

Agriculture—There is a small agricultural industry in Amargosa Valley. Approximately 2,000 acres are commercially farmed, of which more than 90% is planted in alfalfa or other hay. Commercial crops are irrigated with groundwater, primarily using center pivot and other overhead sprinkler systems. Small grains, pistachios, grapes, orchard crops, garlic, and onions are also grown commercially. In addition, evergreen trees are grown on about 1,000 acres for commercial sale as landscape products or Christmas trees. There is a dairy with more than 5,000 cows, and a catfish farm operated in the 1990s. Many residences have gardens with vegetable plots, and some have a few cattle, sheep, chickens, and other farm animals (CRWMS M&O 1997, Section 3.4; Horak and Carns 1997, pp. 4 to 18; YMP 1999, Section 3.4; BSC 2004c, Appendix A).

Information on agriculture in the Amargosa Valley was used to identify some of the important environmental media and site features to include in the biosphere model (e.g., commercial and garden crops, locally grown feed for livestock, and locally raised fish). This agricultural information was also used to select representative crops and animal products for developing input parameters related to crop and livestock production that are consistent with the current conditions in the Yucca Mountain region (e.g., BSC 2004c, Appendix A).

Summary of Biosphere Characteristics—The information above was used to construct the reference biosphere for the TSPA model by incorporating into the biosphere model applicable FEPs that describe the Yucca Mountain region. The characteristics of the environment in the Yucca Mountain region that may affect potential pathways of radionuclide transport and exposure were incorporated in the biosphere model primarily through the model parameters that characterized climate, soil, communities, agriculture, and other conditions in the region surrounding the Yucca Mountain site. The information described above, and thus the parameter values and associated FEPs that describe the reference biosphere, were consistent with present knowledge of conditions in the Yucca Mountain region, as required by 10 CFR 63.305(a).

2.3.10.2.2 Information Used to Characterize the Reasonably Maximally Exposed Individual

The receptor used in the performance assessment of the repository is the RMEI. The RMEI is the hypothetical individual that represents the exposed population for the purpose of performance assessment. The RMEI has average diet and living style characteristics for a hypothetical community with characteristics of the Town of Amargosa Valley that is situated at the specified compliance location. The RMEI is selected to represent those persons in the vicinity of Yucca Mountain who are reasonably expected to receive the greatest exposure to radioactive material released from a geologic repository at Yucca Mountain. In accordance with 10 CFR 63.102(i), characteristics of the RMEI are based on current human behavior and biospheric conditions in the region (FEPs 2.4.04.01.0A, 2.4.07.00.0A, and 2.4.08.00.0A). The following information was used to develop model parameters characterizing the diet, lifestyle, and metabolic and physiological considerations of the RMEI (FEP 2.4.01.00.0A) that are consistent with the requirements of 10 CFR 63.312.

Diet—Based on a survey of Amargosa Valley residents (DOE 1997), it was determined that many people in that region consume some locally produced vegetables, fruit, grain, meat, poultry, fish, eggs, and milk. This information was used to identify the ingestion pathways to be included in the biosphere model (Section 2.3.10.2.5), and to calculate the average consumption rates of locally produced foods (Section 2.3.10.3.1.9) (BSC 2005, Section 6.4).

Use of Evaporative Coolers—About 74% of Amargosa Valley residents surveyed used evaporative coolers, and they used them for an average of 5 months per year (BSC 2005, Section 6.3.4). Therefore, the biosphere model includes exposure to radionuclides resulting from the use of evaporative coolers during part of the year (Section 2.3.10.3.1.8) (SNL 2007a, Section 6.4.2.2).

Gardens—About 46% of Amargosa Valley residents surveyed had gardens (DOE 1997, Table 2.4.2). Crops commonly grown in gardens include onions, garlic, watermelon, squash, and

numerous other plants (Horak and Carns 1997, pp. 5 to 6 and Table 1; Mills et al. n.d.). Because gardens are common in the region, characteristics of these garden crops were considered during development of input parameters that characterized irrigation requirements and farming methods (Sections 2.3.10.3.1.1 and 2.3.10.3.1.3) (BSC 2004c, Section 6 and Appendix A).

Employment—About 39% of Amargosa Valley residents that were 16 years of age or older were not employed at the time of the 2000 Census (Bureau of the Census 2002, Table P47). Of the residents who were employed, the largest proportion (27%) worked in mining and about 6% worked in agriculture (Bureau of the Census 2002, Table P49). Information about employment in Amargosa Valley was used to determine the proportion of the population that works indoors and outdoors in Amargosa Valley and to calculate exposure times (Sections 2.3.10.3.1.7 and 2.3.10.3.2.5) (BSC 2005, Section 6.3).

Commute Time—In 2000, about 64% of employed Amargosa Valley residents that were 16 years of age or older commuted 10 minutes or more to work one way. About 20% of employed residents commuted 35 minutes or more one way (Bureau of the Census 2002, Table P31). Information about commute times in Amargosa Valley was used to model the proportion of the Amargosa Valley population who would work in areas where radionuclides might be present, and the amount of time that local workers would commute within those areas (Sections 2.3.10.3.1.7 and 2.3.10.3.2.5) (BSC 2005, Section 6.3).

Housing Type—About 89% of occupied housing units in Amargosa Valley during 2000 were mobile homes, and about 91% of the total population lived in mobile homes (Bureau of the Census 2002, Tables H30, H31, and H33). Information about housing types in Amargosa Valley was used to select building shielding factors for lightly constructed housing (Section 2.3.10.3.1.7) (BSC 2005, Section 6.6), along with parameters related to evaporative coolers, house ventilation rates, and equilibrium factors for ^{222}Rn decay products indoors (Sections 2.3.10.3.1.2 and 2.3.10.3.1.8) (BSC 2004d, Sections 6.5 and 6.6).

Metabolic and Physiological Considerations—The biosphere model used dose coefficients from *Federal Guidance Report 13* (EPA 2002) to convert radionuclide intake or external exposure to dose (Sections 2.3.10.3.1.7 to 2.3.10.3.1.9). Dose coefficients for external exposure are equal to the effective dose per unit time per unit radionuclide concentration in the soil and were developed using tissue weighting factors consistent with ICRP Publication 60 (ICRP 1991). The dose coefficients for inhalation and ingestion are equal to the committed effective dose per unit radionuclide intake by inhalation or ingestion and were also developed using tissue weighting factors and the dosimetric methods based on ICRP Publication 60 (ICRP 1991). This approach was in compliance with 40 CFR Part 197, Appendix A, as required by proposed 10 CFR 63.2. The dose coefficients for intake of radionuclides used in the biosphere model are those for adults (consistent with the requirement of 10 CFR 63.312(e) that the RMEI be an adult) and used the commitment period of 50 years (EPA 2002, FGR 13 Help, Data Application and Limitations). The biokinetic and dosimetric models used in the development of the dose coefficients were based on a hypothetical average adult person with the anatomical and physiological characteristics defined in *Report of the Task Group on Reference Man: A Report Prepared by a Task Group of Committee 2 of the International Commission on Radiologic Protection* (ICRP 1975) with further modifications as described in *Federal Guidance Report 13* (EPA 1999). Breathing rates used in the biosphere model were based on the more recent biometric results for adults used in the

respiratory track model developed by the International Commission on Radiological Protection (ICRP 1994a; BSC 2005, Section 6.3.3).

Summary of RMEI Characteristics—The RMEI is a hypothetical receptor that is assumed to have the dietary and lifestyle characteristics of the Amargosa Valley population. Only those dietary and lifestyle characteristics of the Amargosa Valley population that may affect the dose to the RMEI are relevant to biosphere modeling and, as such, were considered in the biosphere model. These characteristics were incorporated in the biosphere model through those model parameters that characterize the lifestyle, diet, metabolism, and physiology of the RMEI (BSC 2005, Section 6). Consistent with 10 CFR 63.312, numerical values for the parameters that quantify the diet and living style of the RMEI were developed based on information from surveys of the people who reside in Amargosa Valley. Development of information used to characterize the RMEI, associated parameter distributions, and use of those parameters in the biosphere model are further described in Section 2.3.10.3.

2.3.10.2.3 Radionuclide Transport and Exposure Pathways

Based on the applicable FEPs (Table 2.3.10-1) and the required characteristics of the reference biosphere and RMEI, the environmental transport pathways, human exposure pathways, and related environmental media that are important for evaluating repository performance were identified and described (SNL 2007a, Section 6.3). Environmental transport pathways are the routes by which radionuclides move among, and accumulate in, environmental media. Human exposure pathways arise when people are exposed, internally or externally, to radionuclides in those media. The pathways included in the biosphere model were selected based on the arid and semiarid climatic conditions in the Yucca Mountain region, as required by 10 CFR 63.305(d).

Groundwater Exposure Scenario—The groundwater exposure scenario was used to evaluate the RMEI's exposure to radionuclides released from the groundwater into the biosphere. Under this scenario, radionuclides could be released into the biosphere from groundwater drawn from a well. The RMEI may be exposed to radionuclide concentrations in the following six environmental media when water is used for domestic and agricultural purposes (SNL 2007a, Section 6.3.1.2):

1. Groundwater
2. Soil irrigated with groundwater
3. Indoor and outdoor air containing resuspended particles, radioactive gases, or aerosols from evaporative coolers
4. Crops irrigated with groundwater
5. Food products from animals fed with irrigated crops
6. Fish raised in groundwater at a fish farm.

The radionuclide concentration in groundwater for all exposure pathways included in the biosphere model that involved these media was calculated by dividing the annual mass flux of radionuclides by an annual water demand of 3,000 acre-ft. A radionuclide interaction transfer matrix was constructed to identify the important pathways of radionuclide transfer among environmental media and RMEI exposure (Figure 2.3.10-5). Pathways identified in the matrix in Figure 2.3.10-5 were considered in the biosphere conceptual model and evaluated quantitatively in the biosphere mathematical model (SNL 2007a, Section 6.3.1.3).

The environmental transport pathways identified in the interaction matrix in Figure 2.3.10-5, and explicitly included in the biosphere model for the groundwater exposure scenario, are listed in Table 2.3.10-2. The conceptual representation of the transport of radionuclides among environmental media and resulting exposure to the RMEI are displayed in Figure 2.3.10-6. Exposure could occur when the RMEI is exposed to radionuclides in environmental media external to the body or by inhalation or ingestion of those media into the body.

The activities and the related pathways that could lead to radiation exposure are summarized in Table 2.3.10-3. As described in Section 2.3.10.2.5, other environmental media and transport pathways that could lead to exposure were considered during development of the biosphere model (e.g., external exposure to air and water, inhalation of soil particles by farm animals), but were excluded because they have a negligible influence on the biosphere model results (SNL 2007a, Sections 6.3.3, 7.3, and 7.4).

Volcanic Ash Exposure Scenario—The conceptual model for the volcanic ash exposure scenario considered the same characteristics of the biosphere and receptor as the groundwater exposure scenario. The major difference between the exposure scenarios was the source of radionuclides. For the volcanic ash exposure scenario, the source would be radionuclides associated with tephra from an eruptive event through the repository. Volcanic tephra and associated radionuclides could be transported into the biosphere during and after an eruption by aeolian and fluvial processes. On cultivated soils, the tephra would become mixed with surface soil and radionuclides could be transferred to crops and animals, which could result in exposure when contaminated crops and animal products are ingested. On cultivated and noncultivated land, the volcanic ash, a fine-grained component of tephra, less than 2 mm in diameter, could be resuspended, causing exposure from inhalation of radionuclides in contaminated ash and soil particles. The ash also may be inadvertently ingested. The RMEI would also be exposed to radionuclides external to the body (SNL 2007a, Section 6.3.2).

The effects of a volcanic intrusion on concentrations of radionuclides in groundwater, and subsequent dose to the RMEI from use of that groundwater, are evaluated in the TSPA igneous intrusion modeling case (Section 2.4.1), which uses BDCFs from the groundwater exposure scenario. Similarly, the contribution to dose received during a volcanic eruption (i.e., before the deposition of volcanic tephra on the ground is completed) is evaluated in the TSPA using inhalation dose factors for the exposure during volcanic eruption, and using BDCFs for the volcanic ash exposure scenario for the conditions following tephra deposition (SNL 2008, Section 6.5.2.4). Thus, the volcanic ash exposure scenario included only those radionuclide transport pathways (soil, air, plants, and animals) and RMEI exposure pathways (external, inhalation, and ingestion) that could result from an initial deposition in, or a subsequent redistribution to, the RMEI location of radionuclides attached to volcanic tephra particles. These pathways were incorporated into the

interaction matrix for the volcanic ash exposure scenario (Figure 2.3.10-7) (SNL 2007a, Sections 6.3.2.2 and 6.3.2.3). The environmental transport pathways identified in the interaction matrix in Figure 2.3.10-7, and explicitly included in the biosphere model for the volcanic ash exposure scenario, are listed in Table 2.3.10-2. The conceptual representation of the transport of radionuclides among environmental media and the resulting exposure to the RMEI are displayed in Figure 2.3.10-8. The typical activities that may lead to radiation exposure are summarized in Table 2.3.10-4.

2.3.10.2.4 Radioactive Decay and Ingrowth in the Biosphere

BDCFs were calculated for all radionuclides identified in the radionuclide screening analysis (SNL 2007c) (Section 2.3.7.4.1.2). Those radionuclides are considered primary radionuclides in the biosphere model (Table 2.3.10-5). Radioactive decay products of these radionuclides were also considered in the model (FEP 3.1.01.01.0A). In the radionuclide screening analysis (SNL 2007c), two additional radionuclides were included (^{245}Cm and ^{241}Pu) not because of their direct dose contribution but to include them in the TSPA model as predecessors (sources) of ^{241}Am.

Decay products of primary radionuclides with half-lives greater than 180 days were classified as long-lived; those with half-lives of less than 180 days were classified as short-lived (Table 2.3.10-5). The 180 day half-life cut-off was selected because it is comparable with the crop and animal growing cycle in the biosphere (SNL 2007a, Section 6.3.1.4). The same value can also be selected in the RESRAD model (Yu et al. 2001). (RESRAD is a computer model designed to estimate radiation doses and risks from residual radioactive materials. It is widely used for the evaluation of radioactively contaminated sites.) Short-lived radionuclides in each decay chain were considered to be in secular equilibrium with the long-lived parent in all environmental media included in the biosphere model; that is, the activity concentration of decay products in those media is the same as that of their parent radionuclide. This modeling assumption was reasonable because the primary radionuclides have long half-lives and, even if the secular equilibrium with their decay products were perturbed during radionuclide transfer, a new equilibrium would be reached in less than 1 year because the half-lives of most decay products are much less than 180 days (Table 2.3.10-5) (SNL 2007a, Sections 6.3.1.4 and 6.3.5). This modeling assumption did not result in under-representation of risk, because the activity of the decay products would be highest when in equilibrium with the long-lived parent radionuclides (SNL 2007a, Section 6.3.1.4). The dose contribution of short-lived decay products was included in the BDCF for the primary radionuclide through the effective dose coefficients for external exposure, inhalation, and ingestion that were developed for primary radionuclides and used to calculate annual dose (Table 2.3.10-6 to 2.3.10-9) (SNL 2007a, Section 6.3.5).

In addition to assuming that the short-lived decay products build up to equilibrium with their parent primary radionuclide in any environmental media, the biosphere model includes the buildup of the long-lived decay products of primary radionuclides in the surface soil as a result of long-term irrigation (SNL 2007a, Section 6.3.5). The accumulation of activity concentration of these long-lived decay products in the soil was calculated in the surface soil submodel. The transport of these radionuclides from surface soil to the other environmental media, and the subsequent internal and external exposure of the RMEI, were then calculated for each long-lived decay product. The contribution of each long-lived decay product was added to the BDCF for its primary radionuclide. For example, ^{243}Am and ^{239}Pu are primary radionuclides, but ^{243}Am decays to ^{239}Pu, so there are

two sources of ^{239}Pu in the environment: (1) ^{239}Pu that was originally in the groundwater; and (2) ^{239}Pu that was produced in the soil by the decay of ^{243}Am originally present in the groundwater. If groundwater containing both of these primary radionuclides is used for irrigation, the total activity concentration of ^{239}Pu in the soil results from ^{239}Pu in the groundwater and from ^{239}Pu produced in the soil by the decay of ^{243}Am. These two fractions of ^{239}Pu are independently accounted for in the biosphere model. The contribution of ^{239}Pu that would be produced in the soil by a decay of ^{243}Am was included in the BDCF of ^{243}Am (SNL 2007a, Sections 6.3.5 and 6.4.1.2).

^{228}Th, which is a long-lived decay product that was not a primary radionuclide, was considered to be at the same activity concentration in the source as its long-lived parent, ^{232}U, but was tracked in the biosphere model separately from its parent radionuclide. Separate tracking was necessary because ^{228}Th has different environmental transport properties and, therefore, may not be in equilibrium with its parent radionuclides after transport within the biosphere has occurred (SNL 2007a, Section 6.3.5).

2.3.10.2.5 Conceptual Model for the Groundwater Exposure Scenario

The initial source of radionuclides in the reference biosphere for the groundwater exposure scenario are groundwater wells intersecting the contaminant plume (FEP 1.4.07.02.0A). The purpose of the biosphere model for the groundwater exposure scenario is to provide the conversion factors and methods needed to calculate the annual dose to the RMEI from use of groundwater containing radionuclides. The primary model outputs are BDCFs, which are numerically equal to an all-pathway annual dose that the RMEI would receive when exposed to the concentration of a radionuclide in environmental media arising from a unit concentration of the radionuclide in groundwater (1 Bq/m^3). These conversion factors were calculated because the biosphere model was run independently of the TSPA calculations of time-dependent radionuclide concentrations in groundwater. Because the biosphere model output was the annual dose per unit radionuclide concentration in groundwater, the model was insensitive to the source of groundwater (e.g., wells or springs) so long as the use and treatment of water in the reference biosphere remained the same (FEP 2.3.04.01.0A) (SNL 2007a, Section 6.3.1).

BDCFs for the groundwater exposure scenario were calculated based on unit concentrations of radionuclides in groundwater so that they would be constant over time (and thus, independent of the actual radionuclide concentrations calculated by the TSPA model) (SNL 2007a, Section 6.3.1.4). This assumption allows separate and independent calculations of time-dependent radionuclide concentrations in the TSPA model and time-independent BDCFs in the biosphere model. Based on this assumption, BDCFs were calculated in the biosphere model as the annual dose per unit concentrations of radionuclides in groundwater (i.e., Sv/yr per Bq/m^3), and the annual dose was calculated in the TSPA model as the product of the BDCFs and radionuclide concentrations in groundwater (SNL 2007a, Section 6.3.1.6) (Figure 2.3.10-9). The preferred units for the radionuclide concentration in groundwater used in the TSPA model are Ci/m^3, while ERMYN uses Bq/m^3. However, GoldSim, which is used for the TSPA model, is dimensionally-aware and data can be entered and displayed in any units, as long as they are dimensionally consistent.

Because the biosphere model for the groundwater exposure scenario was based on unit concentrations of radionuclides in groundwater, there were few modeling approximations, assumptions, or methods used to model FEPs that were shared with other TSPA model abstractions.

The assumptions and other methods that were common among the biosphere model and other abstractions were consistently implemented. Descriptions of similarities and justifications for differences between the parameter values used in the biosphere model and other abstractions that define sorption coefficients, volcanic tephra properties, and other shared parameters are described in Section 2.3.10.3.

The conceptual and mathematical models for the groundwater exposure scenario were developed in the biosphere model as a series of eight submodels, representing five environmental media (the source of radionuclides, groundwater, was not included as a submodel) and the three exposure pathways described in Section 2.3.10.2.3. Figure 2.3.10-9 shows the interactions among the submodels (i.e., the transfer pathways). In addition to the eight submodels, a separate submodel was included to calculate ^{14}C concentrations in surface soil, air, crops, and animal products. This was done because carbon is a ubiquitous element and because some of the transfer mechanisms for ^{14}C would be different from the other radionuclides considered (SNL 2007a, Section 6.3.1.6).

The special submodel for ^{14}C is not shown in Figure 2.3.10-9 as a separate submodel. In this representation of the biosphere model structure, ^{14}C transport to soil, air, crops, and animal products is included in the submodels representing surface soil, air, plant uptake, and animal uptake submodels, respectively. This is because ^{14}C concentrations in the affected environmental media are subsequently used in the ingestion, inhalation, and external exposure submodels in the same manner as the concentrations of the other radionuclides in those media calculated in the air, plant uptake, and animal uptake submodels.

Surface Soil Submodel—The purpose of the surface soil submodel for the groundwater exposure scenario was to calculate radionuclide concentrations in irrigated surface soil (i.e., the soil layer that is tilled) and in the thin layer of surface soil that could become suspended (FEPs 2.3.02.02.0A and 2.4.09.01.0B). The source of radionuclides in the surface soil would be groundwater used for crop irrigation. Based on agricultural practices in Amargosa Valley, groundwater is the only source of irrigation water considered (FEP 1.4.07.02.0A) (SNL 2007a, Section 6.3.1.6).

Processes included in the model that would result in the removal of radionuclides from the surface soil were radioactive decay, leaching to the deep soil, erosion, and the gaseous release of ^{222}Rn and $^{14}CO_2$ (SNL 2007a, Section 6.3.1.6). Radionuclides leached below the root zone were considered to be unavailable to plants. Although radionuclides eroded from cultivated fields (FEP 2.3.02.03.0A) could be deposited elsewhere in the biosphere, the biosphere model only tracked radionuclides in the surface soil of cultivated fields. This is a conservative estimation of exposure because, in the external exposure and inhalation submodels, the RMEI was considered to be continuously exposed to contaminated irrigated soil at all times while in the biosphere, regardless of whether the RMEI would be in irrigated fields (SNL 2007a, Section 6.3.1.6).

The following modeling assumptions were used in the development of the surface soil submodel. To determine the concentration of radionuclides in soil, cultivated fields and gardens were assumed to be irrigated for up to a thousand years prior to a year for which the annual dose is calculated (SNL 2007a, Section 6.3.1.4; SNL 2007b, Section 6.7). This assumption was based on the analysis of physical and social limitations on agricultural practices, including the evidence of degradation of agricultural land quality in arid regions, as well as socioeconomic characteristics of the Amargosa Valley population (SNL 2007b, Section 6.7). The following factors were considered in the

evaluation: population tenure and mobility, housing, employment, land and groundwater use, quality of soils, business longevity, and the prevalence of home gardens. These factors, combined with the available information about the history of the settlement and agriculture in the region, were used to make assumptions about the value of irrigation duration that would be a reasonable but cautious estimate of this parameter for irrigated land in Amargosa Valley. As a result of long-term irrigation, radionuclides would build up in the soil and their concentration would increase. The radionuclide concentration in the soil was calculated for the surface soil layer (i.e., the tilled soil) as well as for the thin upper layer of the surface soil that can become suspended. The two soil layers were modeled separately because the radionuclide distribution with soil depth may be different in these layers, depending on whether the soil was plowed. The radionuclide concentration in the surface soil was assumed to be uniform due to mixing by plowing. As a result of long-term irrigation, radionuclides would build up in the surface soil and some would reach equilibrium concentrations. Radionuclides with low distribution coefficients, such as ^{99}Tc or ^{129}I, reach equilibrium concentration in the soil quickly. The highly-sorbed radionuclides with high distribution coefficients build up much more slowly in the surface soil. The level of radionuclide equilibrium in the soil depends on the effectiveness of the removal processes and the duration (number of years) of prior irrigation (SNL 2007a, Sections 6.4.1.1 and 6.4.1.2). Such a representation is appropriate for modeling plant root uptake of radionuclides and the external exposure to radionuclides in the soil.

For modeling radionuclide concentrations in a very thin soil layer at the soil surface, the same model was used as that for the entire surface soil thickness. The model considers the rates of radionuclide addition and removal from the defined thickness of soil, which, in the case of the thin layer at the source surface, was equal to the thickness of soil available for resuspension. This was done because there is a possibility that the soil would not be tilled for longer periods (e.g., when the land is used for growing alfalfa, fruit trees, or vines) and, consequently, the distribution in the surface soil layer would not be uniform. Radionuclide concentration in the resuspendable layer of surface soil was first calculated assuming equilibrium conditions. At equilibrium, additions of radionuclides to the surface soil are balanced by their losses from erosion, leaching, and radioactive decay. Then the greater of the two concentrations (i.e., the concentration in the surface soil and the concentration in the soil layer that can be resuspended) was taken to represent radionuclide concentrations in the thin layer at the soil surface that can become resuspended (SNL 2007a, Section 6.4.1.1 and Table 7.4-4). This value was used in calculating human and animal soil ingestion, as well as the concentrations of airborne radionuclides originating from the soil, which are subsequently used to estimate foliar deposition of soil particles and human inhalation exposure.

Based on the modeling assumption of long-term land use and irrigation practices, the average irrigation rate of a variety of field and garden crops grown in Amargosa Valley was used to calculate radionuclide concentrations in soil (SNL 2007a, Section 6.3.1.4). Radionuclide concentration in surface soil was calculated separately for field and garden crops using different average irrigation rates and durations for a variety of crops in those categories. Using the average irrigation rate of field and garden crops was valid because crop rotation occurs in Amargosa Valley (Horak and Carns 1997, Section 1.b). Therefore, it is likely that many types of crops would be grown on the same cultivated plot of land over a time period when the plot is irrigated (SNL 2007a, Section 6.3.1.4).

If groundwater were to be sprayed on crops for irrigation, some radionuclides in the water would be intercepted by crop leaves. Wind and other mechanisms would then displace some of the intercepted

radionuclides onto the soil. The biosphere model conservatively double counts some of those radionuclides by assuming that all radionuclides in irrigation water, including those intercepted by crop surfaces, would reach the soil (SNL 2007a, Section 6.3.1.4). This modeling approximation is reasonable because the portion of radioactive material remaining on plants is predicted to be small (i.e., less than 10%) relative to the amount in irrigation water that would be deposited on the ground (SNL 2007a, Section 7.4.4.1).

Harvesting of crops would result in the removal of radionuclides in those crops from cultivated fields. This loss of radionuclides from cultivated soil as a result of harvesting of crops, which is accounted for in some other biosphere models (e.g., Napier, Strenge et al. 2006, Section 9.2; BIOMASS 2003, p. 339), is not considered in the surface soil submodel because at least some of the radionuclides removed when crops are harvested would be replaced by addition as fertilizer of contaminated manure to cultivated fields in Amargosa Valley. This approach is reasonable because manure is commonly used as fertilizer in Amargosa Valley (Horak and Carns 1997, p. 10). The source of radionuclides in manure would be from ingestion by farm animals of harvested crops, cultivated soil, and water. The contribution from ingestion of water would be low because the animal radionuclide intake from drinking water is low (SNL 2007a, Section 6.13.4.4), so this pathway would not substantially affect the addition of radionuclides in fields by using manure as fertilizer. The amount of radionuclides in manure added to soil would be less than that removed from cultivated fields because some radionuclides ingested by animals would be retained in animal tissues. Also, radionuclides incorporated into crops consumed by people would not be returned to fields (SNL 2007a, Section 6.3.1.4).

Soil in cultivated fields and gardens was divided into two major layers: surface and deep soil. Within the surface soil, a thin resuspendable layer was modelled separately, as described earlier. Radionuclide concentration in the resuspendable layer of surface soil was used to calculate inhalation exposure, foliar deposition of resuspended soil, and soil ingestion by people and animals. In the remaining calculations involving radionuclide concentration in soil, the entire surface soil depth was used (SNL 2007a, Section 6.3.1.6). The depth of the surface soil layer was determined based on tillage (i.e., plowing) depth. Because the surface soil would be tilled periodically, radionuclides were modeled as uniformly distributed through that soil layer where they would be available for root uptake. Although crop roots can penetrate into the deep soil compartment, in the biosphere model all roots were modeled as contained in the surface layer because, generally, 80% to 90% of a plant's roots occur in the upper 60% to 75% of the root zone (BSC 2004c, Section 6.12.2). In addition, radionuclide concentrations in soil would typically decrease with soil depth due to leaching. Accordingly, radionuclide concentrations would be higher in irrigated surface soil (where the plant’s roots are primarily located) than in deep soil (SNL 2007a, Section 6.3.1.4). This approach maximizes root uptake of radionuclides by plants.

The output from the surface soil submodel was used directly in all but the fish and inhalation submodels (Figure 2.3.10-9) because the modeling of many environmental transport and exposure pathways depended in some way on the radionuclide concentration in surface soil (SNL 2007a, Section 6.3.1.6).

Air Submodel—The air submodel was used to estimate radionuclide concentrations in the air (FEP 3.2.10.00.0A). Inputs to the air submodel were the concentrations of radionuclides in groundwater (1 Bq/m^3) and concentrations in surface soil calculated in the surface soil submodel

(Figure 2.3.10-9). Three pathways for the transport of radionuclides into air were considered in this submodel: soil resuspension, release of ^{222}Rn from soil, and the generation of aerosols by evaporative coolers (SNL 2007a, Section 6.3.1.6).

Concentrations of radionuclides in air inhaled by the RMEI would differ substantially depending on the activity and location of the RMEI. Therefore, the reference biosphere was divided into indoor and outdoor environments. In the outdoor environment, the RMEI was considered to be actively disturbing the soil or inactive relative to soil disturbance. In the indoor environment, the RMEI was considered to be either active or inactive (i.e., asleep). Concentrations of radionuclides in air were determined for each environment (SNL 2007a, Section 6.4.2.1).

In the air submodel, all resuspended particles in indoor and outdoor environments were considered to come from irrigated soils. This modeling assumption is reasonable because the most important sources of resuspended particles are human soil-disturbing activities, such as farming. This modeling assumption overestimates radionuclide concentration in the air because some resuspended particles in the biosphere would be from uncultivated areas that would have lower or negligible concentrations of radionuclides originating from the repository (SNL 2007a, Sections 6.3.1.6 and 6.4.2.1).

The air submodel calculated radionuclide concentrations in air around plants separately from concentrations in the RMEI environments. Concentrations of resuspended particles in air are environment-specific, and may be different above fields where crops are growing from concentrations in air inhaled by the RMEI (SNL 2007a, Section 6.3.1.6). In addition, concentrations of radionuclides on soil particles in the air may be different from the corresponding radionuclide concentrations in the surface soil. To account for higher or lower concentrations of radionuclides on soil particles in the air, compared to those on the ground, an environment-specific enhancement factor was included in the air submodel (NCRP 1999, Section 4.2.2).

Two radionuclides considered in the groundwater exposure scenario—^{222}Rn and ^{14}C—could be released from surface soil to air as gases. ^{222}Rn, a decay product of ^{226}Ra, is a radioactive gas that leads to a chain of short-lived progeny. The release of ^{222}Rn from surface soil was considered in the air submodel separately for indoor and outdoor environments (SNL 2007a, Section 6.4.2.3). Release of ^{222}Rn from water was not included because the resulting concentrations in air would be several orders of magnitude lower than concentrations of ^{222}Rn released from soil after many years of irrigation (SNL 2007a, Section 7.4.3.1). ^{14}C would be released from surface soil as radioactive carbon dioxide gas ($^{14}CO_2$). In this form, $^{14}CO_2$ could be taken up by plants during photosynthesis and could also contribute to human inhalation exposure. The effects of atmospheric mixing and dilution on the concentrations of ^{222}Rn and ^{14}C in the air were considered in the air submodel (SNL 2007a, Section 6.3.1.6).

The contribution to radionuclide concentrations in indoor air from operation of evaporative coolers was included in the biosphere model because a large proportion of the Amargosa Valley population uses evaporative coolers (DOE 1997, Table 2.4.2; BSC 2005, Section 6.3.4). Evaporative coolers work by forcing low-humidity outdoor air through wet, porous pads, resulting in evaporation of water and cooling of the incoming air. As water evaporates, some of the contaminants in the water would be released into indoor air. It was considered that evaporative coolers would not cause radionuclides to build up in indoor air because they continually replenish the air in the dwelling, that

radionuclide concentrations in indoor air would be constant on days when coolers were used, and that the contribution of radioactive aerosols to the outdoor environments would be unimportant. These modeling assumptions are reasonable and would not result in underestimation of the risk of inhaling aerosols for the following reasons. Because coolers must be operated with an open window or door to be effective, the large volume of airflow would carry contaminated aerosols out of the buildings and concentrations would not build up substantially indoors. Although some coolers cycle on and off to maintain a relatively constant indoor temperature, the periods when the cooler is off usually would be relatively short, and decreases in radionuclide concentrations during those periods due to decay and air exchange would be small. Also, air containing radionuclides from the use of evaporative coolers that is transferred to outdoor air would be diluted and rapidly dispersed in the outdoor environment (SNL 2007a, Section 6.3.1.4).

The airborne concentrations of radionuclides as resuspended soil particles, gases, and aerosols were the outputs of the air submodel. These concentrations were used in the plant uptake submodel to calculate the concentration of radionuclides in plants from direct deposition of particles on crop leaves and carbon uptake by photosynthesis, and in the inhalation submodel to calculate inhalation exposure to the RMEI (Figure 2.3.10-9) (SNL 2007a, Section 6.3.1.6).

Plant Uptake Submodel—Radionuclide concentrations in plant parts consumed by humans and farm animals were calculated in the plant uptake submodel (FEP 3.3.02.01.0A). Inputs to this submodel were the concentration of radionuclides in groundwater (1 Bq/m^3) and concentrations calculated in the surface soil and air submodels (Figure 2.3.10-9). Three transport pathways were included in this submodel: root uptake, water interception, and dust interception (SNL 2007a, Section 6.3.1.6). The plant uptake submodel did not include radioactive decay following harvest because the radionuclides considered are long-lived and would decay very little during the short time between harvest and consumption of produce and forage (SNL 2007a, Section 6.4.3).

Crops consumed by humans were divided into four types: leafy vegetables, other vegetables, fruits, and grains. Leafy vegetables included lettuce, spinach, cabbage, and other vegetables that have aboveground, edible portions that are directly exposed to contaminated air and sprayed water. Other vegetables included root crops (e.g., carrots and potatoes) and crops with edible parts that are not directly exposed to contaminants (e.g., peas and beans that grow inside pods). Fruits included a variety of products, such as berries, grapes, melons, and apples. Grains included seed crops such as wheat, corn, and barley. Crops consumed by farm animals were also considered in the plant uptake submodel (SNL 2007a, Sections 6.3.1.6 and 6.4.3). Beef cattle and dairy cows were considered to be fed fresh, locally produced forage (e.g., alfalfa); poultry and laying hens were considered to be fed locally produced grain. This is a reasonable modeling approximation because alfalfa and grain are grown in Amargosa Valley and fed to farm animals there (Horak and Carns 1997, pp. 12, 15, and 16). Radionuclide concentrations were calculated separately for each crop type to account for differences in irrigation rates, growing times, and other factors (SNL 2007a, Section 6.3.1.6).

Root uptake of radionuclides by plants was estimated in the plant submodel based on an equilibrium or constant ratio between radionuclide concentrations in soil and crops (SNL 2007a, Section 6.3.1.6). All crop roots were modelled as in the surface soil layer, and concentrations of radionuclides in crops from root uptake were calculated using radionuclide concentrations in surface soil. This modeling approximation was reasonable because most plant roots occur in the surface soil (SNL 2007a, Section 6.3.1.4). Radionuclide concentration in garden soil was used to

calculate root uptake by leafy vegetables, other vegetables, and fruit. For field crops, a different radionuclide concentration in surface soil was used. Grains and animal forage were assumed to belong to the category of field crops.

Direct deposition of radionuclides on plant surfaces was modeled as a continuous process occurring during the growing season, accompanied by the continuous removal of radionuclides by weathering. Two types of direct deposition, interception of sprayed water and deposition of resuspended soil particles, were considered in the plant uptake submodel. The fraction of irrigation water intercepted depends on irrigation practices, which vary by crop type, and plant biomass. The fraction of resuspended particles intercepted would be a function of crop type and biomass. The proportion of radionuclides remaining on crops that would be translocated to the edible portions of plants depends on the type of crop (SNL 2007a, Section 6.3.1.6).

The output of the plant uptake submodel, concentrations of radionuclides in crops, was used as input in the ingestion submodel to calculate the annual dose contribution of consumption of crops to the RMEI's ingestion pathways. The output was also used in the animal uptake submodel to calculate the contribution of feed consumption to radionuclide concentrations in animal products (SNL 2007a, Section 6.3.1.6) (Figure 2.3.10-9).

Animal Uptake Submodel—The animal uptake submodel calculated the concentration of radionuclides in animal products for human consumption (FEPs 2.4.09.02.0A and 3.3.02.02.0A). Inputs to the animal uptake submodel were the concentration of radionuclides in groundwater (1 Bq/m^3) and concentrations in surface soil and animal feed (Figure 2.3.10-9). Four types of animal products (meat, poultry, eggs, and milk) and three environmental transport pathways (ingestion of contaminated crops, groundwater, and soil) were included in this submodel (SNL 2007a, Sections 6.3.1.6 and 6.4.4). The animal products were selected based on a survey of the diet of the residents of Amargosa Valley (DOE 1997). Radionuclide uptake into animals by inhalation was not included because it would have a negligible contribution to the concentration of radionuclides in animal products (SNL 2007a, Section 7.4.5).

The output of the animal uptake submodel, radionuclide concentrations in animal products, was used as input to calculate the contribution from the consumption of animal products in the human ingestion pathway (SNL 2007a, Section 6.3.1.6) (Figure 2.3.10-9).

Fish Uptake Submodel—The fish uptake submodel was used to calculate radionuclide concentrations in farm-raised fish in Amargosa Valley (FEP 3.3.02.03.0A). The biosphere model included fish because a fish farm operated in Amargosa Valley in the 1990s and the potential exists for its reactivation (YMP 1999, Tables 8 and 9). Radionuclide accumulation in fish was considered to be caused exclusively by the use of contaminated groundwater in the fishponds, and the only input to the fish uptake submodel was the concentration of radionuclides in groundwater (1 Bq/m^3) (SNL 2007a, Section 6.3.1.6) (Figure 2.3.10-9).

Radionuclide transfer from water to fish was modeled as a bioaccumulation process based on equilibrium conditions between radionuclide concentrations in water and the edible parts of fish. The bioaccumulation factors used in the fish uptake submodel were developed from measurements taken in natural systems. The bioaccumulation factors measured in those natural systems included the influence of all components of the systems—including water, sediment, and food—on the

accumulation of radionuclides in fish. These bioaccumulation factors are conservative because fish in Amargosa Valley were given commercial feed, which would be uncontaminated because it is not produced locally (SNL 2007a, Section 6.3.1.6).

The output for the fish uptake submodel, radionuclide concentration in fish, was used to calculate the contribution of fish consumption to the human ingestion pathway (SNL 2007a, Section 6.3.1.6) (Figure 2.3.10-9).

^{14}C Submodel—Carbon is an abundant and ubiquitous element that can readily move through the environment as a gas in the form of carbon dioxide. Consequently, some of the environmental transport pathways for ^{14}C would be different from those for radionuclides present in solid form. The transport of carbon in the environment, therefore, was calculated in a separate submodel. The ^{14}C submodel estimated ^{14}C concentrations in surface soil and air; in crops from root uptake and photosynthesis; and in animal products from the ingestion of feed, water, and soil (SNL 2007a, Section 6.3.1.6). Concentrations of ^{14}C in the environmental media, determined using the ^{14}C submodel, are then used in the inhalation, ingestion, and external exposure submodels to calculate annual dose from this radionuclide in the same manner as is done for the other radionuclides.

The concentration of ^{14}C in air was calculated based on the steady-state concentration of ^{14}C in the surface soil, where the rate of gain controlled by the daily irrigation rate was equal to the rate of loss controlled primarily by the gaseous emission loss rate of $^{14}CO_2$ from the soil. In the air, ^{14}C would be subject to mixing due to atmospheric processes, which were modeled using air movement in a mixing cell of defined dimensions. The uptake of ^{14}C by biota was modeled using a specific-activity approach that was based on steady-state conditions among the environmental media involved. The specific-activity approach was used to calculate ^{14}C concentrations in crop and animal products. The bioaccumulation of ^{14}C in fish was assessed using a similar method to that used for other radionuclides. After the media concentrations of ^{14}C were calculated, the dose assessment was carried out using the same approach as was used for other radionuclides (SNL 2007a, Section 6.3.1.6).

External Exposure Submodel—The external exposure submodel estimated the annual dose due to radiation emitted by radioactive materials outside the human body (FEP 3.3.04.03.0A). The only input from other submodels was the concentration of radionuclides in surface soil (Figure 2.3.10-9).

The annual effective dose was calculated for the external exposure pathway. Contaminated materials typically considered in calculations of external exposure doses include soil, air, and water. The biosphere model only calculated exposure to soil. All soil within the reference biosphere was considered to be contaminated, and the RMEI was conservatively considered to be continuously exposed to radionuclides in contaminated surface soil while within the reference biosphere (SNL 2007a, Section 6.3.1.6). External exposure to air (air submersion) and water (water immersion) were not calculated because they would contribute little to the annual dose (SNL 2007a, Section 7.4.8). For example, the dose predicted from water immersion (e.g., during showers, baths, and while swimming) was 1 to 4 orders of magnitude lower (depending on the radionuclide) than that from soil exposure, in part because the RMEI would be directly exposed to water (e.g., while bathing) for a small portion of a day (SNL 2007a, Section 7.4.8.2). Likewise, the predicted dose from air submersion was about 6 orders of magnitude lower than that from exposure to soil, because

radionuclide concentrations in the air would be much lower than those in the soil (SNL 2007a, Section 7.4.8.1). External exposure to radionuclides accumulated on the pads of evaporative coolers, and other external exposure pathways related to operation of evaporative coolers, also would be negligible compared to the annual dose from other sources of exposure (SNL 2007a, Appendix D). External exposure from other media (FEP 3.3.03.01 0A) (e.g., building material, furniture, and clothing) would be possible, but none of those materials are produced in Amargosa Valley using groundwater. Thus, external exposure to all media except soil would be insignificant because the RMEI was conservatively modeled to be exposed to surface soil at all times while in the reference biosphere (SNL 2007a, Section 6.3.1.6).

The external exposure submodel considered indoor and outdoor external exposure to radionuclides in the soil. For outdoor exposures, radiation doses depended on radionuclide concentrations in the soil, the duration of exposure, and the dose coefficients used to convert exposure to dose. For indoor exposures, the shielding effect of buildings was also considered (SNL 2007a, Section 6.3.1.6). To calculate external exposure while the RMEI was outdoors actively disturbing the soil surface, the radionuclide concentration in soil used to grow field crops was used. For the other environments, the radionuclide concentration in garden soil was used (SNL 2007a, Section 6.4.7.1).

The output of the external exposure submodel—the annual dose from external exposure—contributed to the all-pathway dose, which was used to calculate BDCFs (SNL 2007a, Section 6.3.1.6) (Figure 2.3.10-9).

Inhalation Submodel—The purpose of the inhalation submodel was to calculate radiation doses due to the inhalation of radionuclides (FEP 3.3.04.02.0A). The 50-year committed effective dose resulting from annual intake of radionuclides by inhalation was estimated for this pathway. Three sources of contamination were considered: resuspended particles, gaseous emissions from the soil, and aerosols generated by evaporative coolers (SNL 2007a, Section 6.3.1.6). Concentrations of radionuclides in air from these sources were provided by the air submodel (SNL 2007a, Section 6.3.1.6) (Figure 2.3.10-9).

In addition to radionuclide concentrations in the air, estimates of inhalation doses depended on the duration of inhalation exposure, breathing rates, and dose coefficients. Breathing rates and exposure times differ among activities, occupations, work locations, and other human factors. To account for these differences, breathing rates and exposure times were developed separately for each receptor environment (SNL 2007a, Section 6.3.1.6). Analogous to the external exposure submodel, the radionuclide concentration in the soil inhaled by the RMEI while outdoors and involved in soil disturbing activities was that typical of areas where alfalfa and other field crops are grown. Inhalation exposure in the other environments was assumed to occur on garden soil (SNL 2007a, Section 6.4.8.1).

The output of the inhalation submodel—the annual inhalation dose—contributed to the all-pathway dose, which was used to calculate BDCFs (SNL 2007a, Section 6.3.1.6) (Figure 2.3.10-9).

Ingestion Submodel—The ingestion submodel was used to calculate radiation doses due to the ingestion of radionuclides (FEPs 3.3.01.00.0A and 3.3.04.01.0A). The 50-year committed effective dose resulting from the annual intake of radionuclides by ingestion was estimated for this pathway (SNL 2007a, Section 6.3.1.6). Inputs to the ingestion submodel were radionuclide

concentrations in the groundwater and the outputs from the surface soil, plant uptake, animal uptake, and fish uptake submodels (SNL 2007a, Section 6.3.1.6) (Figure 2.3.10-9).

The ingestion submodel determined exposure to the RMEI from ingesting drinking water, four types of crops (leafy vegetables, other vegetables, fruits, and grains), four types of animal products (meat, poultry, milk, and eggs), freshwater fish, and soil. The radionuclide concentrations in these media were combined with corresponding consumption rates and dose coefficients to produce ingestion doses (SNL 2007a, Section 6.3.1.6). Consumption rates used in the ingestion submodel were based on the estimated rate of consumption of locally produced foods by the people who reside in Amargosa Valley (BSC 2005, Section 6.4).

The output of the ingestion submodel—the annual ingestion dose—contributed to the all-pathway dose, which was used to calculate BDCFs (SNL 2007a, Section 6.3.1.6) (Figure 2.3.10-9).

BDCFs and Biosphere Model Results—The all-pathway dose for the groundwater exposure scenario was the sum of the radionuclide-specific annual doses from the external, inhalation, and ingestion exposure pathways (FEP 3.3.05.01.0A and 3.3.08.00.0A). The all-pathway dose was expressed in terms of the total effective dose from annual intake and external exposure. For the purposes of assessing doses to the RMEI, the total effective dose was the sum of the effective dose for external exposures and the committed effective dose for internal exposures. The resulting BDCFs are numerically equal to the all-pathway annual dose to the RMEI from a unit activity concentration in the groundwater. The concentration of each radionuclide in the groundwater as a function of time was calculated in the saturated zone abstraction models (Section 2.3.9), and the total annual dose was the sum of the products of the radionuclide-specific BDCFs and the time-dependent activity concentrations of radionuclides in 3,000 acre-feet of groundwater, consistent with 10 CFR 63.331 (SNL 2007a, Section 6.4.10.4) (Figure 2.3.10-9). The entire domestic and agricultural water supply of the hypothetical community, including the two liters of water per day that the RMEI drinks, is drawn from the same 3,000 acre-feet of annual water demand.

2.3.10.2.6 Conceptual Model for the Volcanic Ash Exposure Scenario

The source of radionuclides for the volcanic ash exposure scenario would be particles of radioactive waste associated with tephra from a volcanic eruption through the repository host horizon (FEP 1.2.04.07.0A). In an eruptive event, airborne tephra and radionuclides could be transported into the biosphere. Tephra and radionuclides also could be transported into the biosphere by aeolian and fluvial processes after an eruption ceases (SNL 2007a, Sections 6.3.2 and 6.5). These depositional and erosional processes, and corresponding changes in tephra depth and radionuclide concentrations, were modeled as described in Section 2.3.11.

The biosphere model evaluates human exposure after initial deposition of tephra at, or redistribution to, the location of the community that includes the RMEI, following an eruption. Separate dose factors were developed to evaluate the consequences of exposure to airborne radionuclides during the eruptive phase. These factors were developed separately from the biosphere model because the dose for the eruptive phase must be calculated based on daily exposure, whereas the dose for the post-eruptive phase is calculated based on annual exposure (SNL 2007a, Section 6.3).

To evaluate exposure after initial deposition or redistribution of tephra, the biosphere model calculated BDCFs that represented the annual dose to the RMEI that would result from a unit activity concentration in the resuspendable layer of soil (Bq/kg) and on the ground surface (1 Bq/m^2), depending on the exposure pathway. The calculation of annual dose following an eruption is more complicated than the product of BDCFs and activity concentrations required for the groundwater exposure scenario. Exposure following a volcanic eruption would be influenced by the level of airborne particulates in addition to the concentration of radionuclides deposited in the surface soil. The dose from inhalation of resuspended particles would change over time because the radionuclide concentration in the air would decrease following an eruption as the concentration of resuspended particles decreases (SNL 2007a, Section 6.3.2). In the biosphere model, the entire activity associated with volcanic tephra, as quantified by the source terms, is treated as available for further transport in the biosphere and intake by the RMEI, without regard to the tephra particle size. This is because the biosphere model for the volcanic ash exposure scenario does not include any corrections for the fraction of radioactivity in the source terms that is available for environmental transport and exposure of the RMEI (SNL 2007a, Sections 6.3.2 and 6.5). This assumption is especially conservative for the evaluation of inhalation dose because only the smallest volcanic ash particles could become resuspended and, subsequently, inhaled.

Volcanic BDCFs consist of three BDCF components for each primary radionuclide. The first component accounts for exposure to sources external to the body, for ingestion of radionuclides, and for inhalation of radon decay products. This component is numerically equal to the annual dose to the RMEI from these exposure pathways per unit of areal radionuclide concentration in the soil (Sv/yr per Bq/m^2). The second and third BDCF components, called the short-term and the long-term inhalation BDCF components, account for inhaling airborne particulates. The short-term inhalation component is numerically equal to the early-time incremental increase in the inhalation dose (over and above the long-term inhalation dose described by the long-term inhalation BDCF component) during the first year following a volcanic eruption per unit of radionuclide concentration in the soil layer that can become resuspended (Sv/yer per Bq/kg). This term is used together with the time function, representing the decrease of the airborne particulate concentration with time, to calculate the short-term increase in inhalation exposure due to elevated levels of airborne particulate matter after a volcanic eruption, relative to the conditions existing before and long after an eruption. With time, mass loading returns to the pre-eruption level. These conditions are described by the long-term inhalation BDCF, which accounts for inhalation of resuspended particulates under nominal conditions (i.e., when the mass loading is not elevated as the result of volcanic eruption). This component is numerically equal to the annual dose to the RMEI from inhaling particulates at the nominal concentration in the air, per unit of radionuclide concentration in the soil that can be resuspended (Sv/yer per Bq/kg) (SNL 2007a, Sections 6.3.2 and 6.12.2).

Because the biosphere model for the volcanic ash exposure scenario was based on unit concentrations of radionuclides in soil mixed with volcanic tephra, there were few modeling approximations, assumptions, or methods used to model FEPs that were shared with other TSPA model abstractions. Those assumptions and other methods that were common among the biosphere model and other abstractions were consistently implemented. Descriptions of similarities and justifications for differences between the parameter values used in the biosphere model and other abstractions that define tephra characteristics, soil types, and other shared parameters are described in Section 2.3.10.3.2.

The conceptual model for the volcanic ash exposure scenario was divided into seven submodels (Figure 2.3.10-10) that represented the four environmental media (soil, air, plants, and animals) and three exposure pathways (external, inhalation, and ingestion) included in this scenario (Section 2.3.10.2.3). The biosphere model for the volcanic ash scenario does not include the fish uptake submodel and the ^{14}C submodel. The fish uptake submodel is not included because the water is not a source of radionuclides in the biosphere for this scenario. ^{14}C is not included because this radionuclide is not defined to be a significant contributor to exposure in the TSPA volcanic eruption modeling case. The submodels, and the pathways of radionuclide transport among them, were selected based on the interaction matrix in Figure 2.3.10-7 and the FEPs applicable to this scenario. Because many radionuclide transfer mechanisms were the same in the groundwater and volcanic ash exposure scenarios, the submodels were similar (SNL 2007a, Section 6.3.2). The following description of the volcanic ash conceptual model focuses on the differences between the two scenarios.

Surface Soil Submodel—The surface soil submodel for the volcanic ash exposure scenario differed from the surface soil submodel for the groundwater exposure scenario. This is because the areal radionuclide concentration in the surface soil and the radionuclide concentration in the resuspendable soil layer are the source terms for the biosphere model for the volcanic ash exposure scenario. These concentrations did not have to be calculated in the biosphere model, because they are calculated in the tephra redistribution model (Section 2.3.11.4). The only function of the soil submodel was to convert areal radionuclide concentration to mass radionuclide concentration in the surface soil, which was used in the other submodels. A volcanic eruption would spread tephra over a large area, while irrigation would deposit radionuclides only on the relatively small farming area. Also, radionuclides would not accumulate in the surface soil following an eruption because they would not be continuously added to the environment. Losses of radionuclides from the soil by erosion and other surficial processes were considered in the modeling of tephra redistribution (Section 2.3.11); therefore, these processes were not included in the calculations of BDCFs for the volcanic ash exposure scenario. Because mixing of soil and tephra would differ between cultivated and noncultivated lands, and because the radiation exposure would differ between those areas, radionuclide concentrations in soil on cultivated and noncultivated areas were treated separately in the model (SNL 2007a, Section 6.3.2.6). Radionuclide concentrations in cultivated soil were calculated by using the areal radionuclide concentration source. For noncultivated soil, radionuclide concentration in the resuspendable soil layer was used.

The concentration of radionuclides in cultivated soil was used to calculate concentrations of radionuclides in crops and animal products. It was also used for inadvertent soil ingestion by the RMEI because most soil ingested by humans would be from consuming incompletely washed crops (SNL 2007a, Section 6.3.2.6). Volcanic tephra was modeled as uniformly mixed into cultivated soil, and the resulting mixture was assumed to have the characteristics (e.g., bulk density) of that soil. These modeling assumptions were reasonable because the predicted depth of tephra deposits 18 km south of the repository was much less than the tillage depth of soil (SNL 2007a, Appendix G). The predicted ash depths were based on the ash plume model, as described in Section 2.3.11.4.

The concentration of radionuclides in noncultivated soil was used to calculate inhalation and external exposure. This was done because most soil in the reference biosphere would not be cultivated. Using radionuclide concentrations in the resuspendable layer of noncultivated soil to

calculate inhalation and external exposure is a conservative approach because the concentrations in uncultivated soil would be higher than in cultivated soil for the volcanic ash exposure scenario. Because uncultivated lands would not be disturbed by agricultural activities, volcanic tephra, especially that deposited on the interchannel divides, would not mix quickly with surface soil and would remain on or near the soil surface. The interchannel divides constitute the inactive portion of the Fortymile Wash alluvial fan and receive contaminated tephra only through primary deposition from the eruption. In the channels, mixing of contaminated volcanic tephra with uncontaminated channel sediments would occur (see Section 2.3.11.4 for the description and treatment of the Fortymile Wash alluvial fan area, i.e., the location of the RMEI, in the tephra redistribution model).

Air Submodel—The air submodel calculated radionuclide concentrations in air resulting from two transport mechanisms: resuspension of ash and soil particles and exhalation of ^{222}Rn from deposited volcanic tephra. The methods used to determine the airborne concentrations of radionuclides were similar to those used for the groundwater exposure scenario, including use of a microenvironmental modeling approach to calculate concentrations in indoor and outdoor environments (SNL 2007a, Section 6.3.2.6).

Concentrations of resuspended particles in air would be higher than normal for some time after a volcanic eruption, because there would be more unconsolidated, fine particles on the soil surface that would be readily resuspended by wind, human activity, or other disturbances. Over time, the tephra would erode, become mixed into the soil, buried, or otherwise stabilized and unavailable for resuspension. In the biosphere model, resuspended particle concentrations were considered to return to levels experienced before the eruption within tens of years or less, and this process was quantified by the mass loading time function (Section 2.3.10.3.2.2) (SNL 2007a, Sections 6.3.2.4 and 6.3.2.6) (BSC 2006, Section 6.4). This modeling assumption was based on measurements of changes in the concentrations of resuspended particles in air after the eruption of Mount St. Helens and other volcanoes (BSC 2006, Sections 6.3 and 6.4).

The evaluation of ^{222}Rn exhalation for the volcanic ash exposure scenario differed from that used for the groundwater exposure scenario. Because tephra thickness was expected to be relatively thin, and the radon emanation coefficient for tephra may be higher than that for soil, it was assumed that all ^{222}Rn created by decay in the tephra–soil layer was considered to be released to the atmosphere, where it would decay and contribute to the inhalation dose (SNL 2007a, Section 6.3.2.4). Unlike the groundwater exposure scenario, the indoor ^{222}Rn concentration in air was considered to be the same as the outdoor concentration because there would be little or no volcanic tephra under or in existing buildings. Even if new buildings were built on land where tephra had been deposited, infiltration of ^{222}Rn from the ground into indoor spaces would be limited because the thin layer of tephra would likely be removed or mixed with surface soil during construction. Because all ^{222}Rn from outdoor soil was considered to be released, it was not necessary to include an additional source of indoor ^{222}Rn (SNL 2007a, Section 6.5.2.2).

Plant Uptake Submodel—Two transfer pathways were considered in the plant uptake submodel to calculate radionuclide concentrations in plants consumed by humans and farm animals: root uptake from soil and foliar uptake from intercepted resuspended radionuclides. Except for the absence of direct deposition of irrigation water on crop leaves, radionuclide transfer mechanisms from soil to plants and from particulates to plants were the same as those used in the groundwater

exposure scenario. The crop types also were the same in both scenarios (SNL 2007a, Section 6.3.2.6).

Animal Uptake Submodel—The animal uptake submodel considered two pathways for the accumulation of radionuclides in animal products: ingestion of feed and soil by farm animals. This submodel was the same as that used for the groundwater exposure scenario, except the removal of the transfer pathway for ingesting contaminated water (SNL 2007a, Section 6.3.2.6). Inhalation of resuspended ash by animals was not included in the animal uptake submodel because this pathway would have a negligible influence on the concentrations of radionuclides in animal products (SNL 2007a, Section 7.4.5).

External Exposure Submodel—The external exposure submodel evaluated radiation exposure from contaminated volcanic tephra deposited at the location of the hypothetical community that includes the RMEI. The deposited activity consisted of the initial tephra fallout on the interchannel divides and the alluvial redistribution in the channels. The annual effective dose from this pathway was calculated as the product of the radionuclide concentrations in the soil, exposure times by the RMEI, building shielding factors, and the dose coefficients for external exposure to contaminated soil surface. Unlike the groundwater exposure scenario, where soil contamination could be deep, volcanic tephra and associated radionuclides could be distributed on or near the soil surface. Thus, the source for external exposure could be a thin layer of noncultivated soil and tephra mixture on the ground surface. This modeling assumption could overestimate the external exposure from the areas categorized as the distributary channels, where contaminated volcanic tephra would be mixed throughout, and diluted by, the uncontaminated material transported in the channels during fluvial events. Because it is expected that the interchannel divides will occupy a larger area than the distributary channels, and because there is considerably more noncultivated land than cultivated land in Amargosa Valley (BSC 2006, Section 6.2; SNL 2007d, Section 6.5.4), this assumption was reasonably conservative. The effects of radiation attenuation in the soil and volcanic tephra were conservatively not considered (SNL 2007a, Section 6.3.2.4).

Because radionuclides were considered to be in a thin layer on the soil surface, external exposure does not depend on the thickness of the contaminated soil layer (SNL 2007a, Sections 6.3.2.6 and 6.5.5). As in the groundwater exposure scenario, external exposure to other media, such as air and water, were not considered in the external exposure submodel because they would contribute little to the overall external dose to the RMEI (SNL 2007a, Section 7.4.8).

Inhalation Submodel—The inhalation dose was calculated as the committed effective dose for the 50-year commitment period resulting from annual intake of radionuclides by inhalation. Two sources of radionuclides in air were considered; resuspended particles and ^{222}Rn gas. The inhalation dose was the sum of the dose from both sources (SNL 2007a, Section 6.3.2.6).

Two components of exposure to resuspended particles in the air were considered in the inhalation submodel. The first component represented the incremental increase in inhalation exposure over the nominal level due to elevated postvolcanic, time-dependent concentrations of resuspended particles. The second represented inhalation exposure to time-independent, nominal resuspended particle concentrations that would occur after tephra deposits have stabilized. Annual inhalation exposure was calculated separately for the short-term elevated component and for the long-term component from stabilized airborne concentrations (SNL 2007a, Section 6.5.6.1). The total dose

from resuspension of contaminated particles was considered to be the sum of the long-term, nominal dose and the short-term incremental dose increase after a volcanic eruption. The change in the annual inhalation dose during the period when resuspended particle concentrations in air would be decreasing was modeled as exponential in time (BSC 2006, Section 6.4).

Ingestion Submodel—The ingestion exposure pathway for the volcanic ash exposure scenario was the same as that for the groundwater exposure scenario, except that only 9 of the 11 media were included: four crop types, four types of animal products, and soil. Ingestion of groundwater was not included because deposition of volcanic tephra on the ground surface would not affect the concentration of radionuclides in groundwater. Ingestion of fish was not included because deposition of tephra on fish ponds would have a very short term and, therefore, a negligible effect on BDCFs (SNL 2007a, Appendix E). Inputs to the ingestion submodel were the radionuclide concentrations in foodstuffs and the soil. These media concentrations, when combined with the corresponding consumption rates and dose coefficients, were used to produce ingestion doses (SNL 2007a, Section 6.3.2.6).

BDCFs and Biosphere Model Results—The all-pathway dose for the volcanic ash exposure scenario was the sum of the radionuclide-specific annual doses from the external, inhalation, and ingestion exposure pathways. The all-pathway dose was expressed in terms of total effective dose. The BDCF components (Sv/yr per Bq/kg or Sv/yr per Bq/m^3, depending on the pathway) were numerically equal to the pathway dose from a unit activity concentration in the soil mixed with volcanic tephra. The calculation of radionuclide concentrations in the mixture of soil and volcanic tephra was modeled as described in Section 2.3.11. The total dose was calculated as the sum of the products of the radionuclide-specific BDCFs, considering changes in airborne particle concentrations with time and the time-dependent concentrations of radionuclides in the soil mixed with volcanic tephra for the radionuclides in the TSPA model (SNL 2007a, Section 6.3.2.6) (Figure 2.3.10-10).

2.3.10.3 Data and Data Uncertainty

[NUREG-1804, Section 2.2.1.3.13.3: AC 2, AC 3(1) to (4); Section 2.2.1.3.14.3: AC 2, AC 3(1) to (4)]

The mathematical representations of the biosphere radionuclide transport processes and exposure pathways in the reference biosphere were constructed based in part on a review of calculations in other biosphere models, including primarily GENII (Napier, Peloquin et al. 1988; Leigh et al. 1993; Napier, Strenge et al. 2006); RESRAD (Yu et al. 2001); and NCRP-129 (NCRP 1999). For most submodels of the biosphere model, applicable methods were selected from the other models and modified, if necessary, to appropriately model the conditions of the Yucca Mountain region and meet the requirements of proposed 10 CFR Part 63 (SNL 2007a, Sections 6.4, 6.5, and 7.3). This approach was reasonable because the radiological assessment methods that were used to construct the biosphere model are mature and widely used by the scientific community, and also because there are few differences in the methods used in modeling the biosphere processes and their resulting predictions. Distributions of the input parameters that were represented by the probability functions were stochastically sampled in the biosphere model. Input parameter values were developed from site-specific data and surveys, reviews of distributions used in other models, data from analogue sites, and other information contained in applicable publications. The bounds of parameter distributions were selected to ensure that risk, as measured by annual dose, would not be

underestimated, as well as to incorporate the range of reasonable variation and uncertainty in environmental parameters and the range of reasonable variation and uncertainty about the average of parameters that represent dietary and lifestyle characteristics of the RMEI (SNL 2007a, Section 6.6.3; BSC 2005, Section 6).

The biosphere model parameters, their values, probability distributions, and their sources are listed in Table 2.3.10-10. The following sections describe the data and parameters that were used in the biosphere model to calculate BDCFs for the groundwater and volcanic ash exposure scenarios. Uncertainty associated with those data and parameters is characterized, and propagation of that uncertainty through the biosphere model is described. This section also includes descriptions of the mathematical methods used to estimate radionuclide concentrations in environmental media and exposures to those media, so that the data and parameters can be put into the context of their use in the biosphere model. Separate descriptions are provided for each exposure scenario.

In developing the biosphere model, data from Yucca Mountain and the surrounding region have been used, uncertainties and variabilities in parameter values have been accounted for, and the technical bases for parameter ranges have been described, as required by proposed 10 CFR 63.114(a)(1) through (a)(3).

2.3.10.3.1 Groundwater Exposure Scenario

The mathematical model for the groundwater exposure scenario was developed in eight submodels that represent five environmental media (soil, air, plants, farm animals, and fish) and three receptor exposure pathways (external, inhalation, and ingestion exposure) (Figure 2.3.10-9) (SNL 2007a, Section 6.4). In addition, a separate submodel was included to calculate potential ^{14}C concentrations in soil, air, plants, and animals. The data and parameters used to calculate BDCFs for the groundwater exposure scenario are described below for each submodel.

2.3.10.3.1.1 Surface Soil Submodel

The surface soil submodel calculated the radionuclide concentrations in the surface soil, and in the resuspendable layer of surface soil, resulting from the use of groundwater for irrigation. Radionuclide transport and accumulation in surface soil was modeled with consideration of soil properties in the Yucca Mountain region (FEP 2.3.02.01.0A). Radionuclide concentrations in the surface soil were calculated based on the unit activity concentration of radionuclides in groundwater (i.e., 1 Bq/m^3); the annual irrigation rate of crops; irrigation duration; loss by radioactive decay, leaching, and erosion; and soil characteristics. The radionuclide concentrations in the resuspendable layer of surface soil were calculated for equilibrium conditions (i.e., the rate of addition from irrigation water was equal to the rate of loss from radioactive decay, leaching, and erosion). If the equilibrium concentration in the resuspendable soil layer was greater than the radionuclide concentration in the entire layer of the surface soil, the equilibrium concentration was used in the calculations for the pathways involving the resuspendable soil layer. Otherwise, the radionuclide concentration in the surface soil was used for all pathways involving the soil (i.e., the resuspendable layer and the entire surface soil thickness). This method was used to ensure that, regardless of whether the surface soil was mixed by plowing or not, the doses to the receptor are not underrepresented (SNL 2007a, Section 6.4.1).

As discussed in Section 2.3.10.2.4, short-lived radionuclides (half-lives less than 180 days) were considered to be in secular equilibrium with the parent primary radionuclides. Long-lived radionuclides produced by the decay of primary radionuclides in the soil were treated numerically similar to primary radionuclides, but the rate of their addition to the system was from decay of primary radionuclide in the soil rather than application of groundwater (SNL 2007a, Section 6.4.1.2).

Irrigation Rate—The annual irrigation rate for field and garden crops, which was used to calculate the addition of radionuclides into the surface soil, was calculated from the annual irrigation rates of 26 representative garden crops, commercial crops, and horticultural plants grown in the Yucca Mountain region. These crops are representative of the four crop types consumed by humans and locally produced forage considered in the biosphere model (BSC 2004c, Section 6.5). This was done to account for uncertainty in the types of crops that would be grown on a plot of land over a long period. Irrigation rates were determined by calculating evapotranspiration, effective precipitation, and overwatering rates for representative crops using the methods developed by the Food and Agriculture Organization of the United Nations (Allen et al. 1998; Doorenbos and Pruitt 1977).

Information on climate and the crop growing season used to calculate irrigation rates was consistent with the conditions in the region surrounding Yucca Mountain. Weather data (average monthly precipitation, temperature, humidity, wind speed, and solar radiation) collected in northern Amargosa Valley were used for the present-day climatic conditions (FEP 2.3.11.01.0A). Crop growing seasons were defined primarily from site-specific and analogue site information in publications of the U.S. Department of Agriculture Cooperative Extension Service and Agricultural Statistics for southern Nye County (BSC 2004c, Section 4.1.4).

Information on water salinity was used to calculate the amount of irrigation water that must be applied in addition to the amount necessary for the crop growth to prevent detrimental salt buildup for representative crops (i.e., the overwatering rate) consistent with present practices. Water salinity was obtained from measurements of electrical conductivity of groundwater pumped from a well drilled for the Nye County Early Warning Drilling Program at the southwest corner of the Nevada Test Site (BSC 2004c, Section 4.1.7).

Uncertainty in irrigation rates was primarily due to lack of data regarding water management practices in Amargosa Valley (i.e., excessive underwatering or overwatering) and the crops a farmer would choose to grow. Variation in irrigation rates was primarily from differences in water use, season length among crops, and yearly variation in climate (BSC 2004c, Section 6.5.2). Variation among crops and uncertainty about which crops would be grown were accounted for by using the irrigation requirements of 26 plants to develop a distribution of irrigation rates. Selection of plants was based on an evaluation of those currently grown in southern Nye County, national patterns of food consumption, and variation in the growing season and growth form (i.e., shape, annual or perennial, location on plant of edible portion) of commonly grown and consumed crops. Because the same plants can be grown under the range of arid to semi-arid climatic conditions, one set of representative crops was used for all this range of climate states (BSC 2004c, Appendix A). To account for other sources of variation and uncertainty, maximum and minimum irrigation rates were selected that encompass reasonable variation in the effects of values of season length, temperature, overwatering, and underwatering.

Leaching Rate—Leaching was included in the surface soil submodel to account for the residence time of radionuclides in the surface soil and their transport in solution to deeper soil (SNL 2007a, Section 6.4.1). The leaching rate was calculated as a function of the overwatering rate, element-specific solid–liquid distribution coefficients, and soil properties (e.g., bulk density, soil porosity, and soil moisture content) (SNL 2007a, Section 6.4.1.3).

In the current arid conditions at Yucca Mountain, leaching occurs primarily when irrigation water is added to flush accumulated salts from the surface soil in order to maintain plant productivity. The average overwatering rate estimated for the surface soil for the present-day climate was 0.079 m/yr, with a range of 0.009 to 0.275 m/yr (BSC 2004c, Table 6.9-2). This distribution was calculated using the methods developed by the Food and Agriculture Organization of the United Nations (Allen et al. 1998; Doorenbos and Pruitt 1977) and data on climate, salinity, and crop characteristics described above for irrigation rates. The minimum and maximum values were selected to encompass variation and uncertainty in crop growing seasons, climate, and water management practices (BSC 2004c, Section 6.9). The distribution of the overwatering rate for the resuspendable layer of soil was calculated based on the overwatering rate of the surface soil and the proportion of annual irrigation retained in that layer.

The values of distribution (i.e., sorption) coefficients used in the biosphere model were developed from information by Sheppard, M.I. and Thibault (1990, Tables A-1 and A-2). To be consistent with the soil conditions in Amargosa Valley, and not underestimate radionuclide concentrations in soil, the highest average coefficient (and associated standard deviation) reported for sandy or sandy loam soils was selected. Because of the large amount of variation measured for distribution coefficients, the selected distributions for some radionuclides ranged over several orders of magnitude (SNL 2007b, Section 6.3). The distribution coefficients used to calculate BDCFs differed from the sorption coefficients used to model the transport of radionuclides through the saturated and unsaturated zones (Sections 2.3.8 and 2.3.9). This was done because the sorptive properties of the media in the geosphere (e.g., tuffaceous rocks and alluvium) differ from those of the surface soil in the biosphere. These differences are due to the different adsorbing properties of these media as well as differences in aqueous chemical conditions in these media.

Erosion Rate—Soil erosion accounts for the loss of deposited radionuclides from irrigated lands by wind and water erosion. The rate of soil loss from erosion is dependent on soil characteristics, land use, and stewardship. To incorporate these influences, the minimum soil erosion rate used in the model was selected based on the soil loss by erosion on noncultivated cropland in Nevada. The average surface soil loss rate for such croplands is about 0.2 kg/m^2 per year (SNL 2007b, Section 6.4). The upper limit of the erosion rate was selected as 5 tons per acre per year (1.1 kg/m^2 per year) and was based on the average values of sheet, rill, and wind erosion for cultivated and non-cultivated cropland and for pastureland for Nevada with consideration of tolerance factor for the Amargosa Valley soils (USDA 2004). This range for the annual erosion rate of agricultural land is consistent with estimates of annual wind erosion on pastureland and cropland in Nevada (USDA 2000, Tables 10 and 11; SNL 2007b, Section 6.4).

Soil Characteristics—To calculate concentrations of radionuclides in the surface soil, the bulk density, volumetric water content, and depth of surface soil were also required. A distribution of soil bulk density of 1.3 to 1.7 g/cm^3 was used (SNL 2007b, Section 6.2). This distribution was developed from descriptions of the soils in Amargosa Valley that were published by the U.S.

Department of Agriculture (USDA 2004). The distribution of water-holding capacity ranged from 0.15 to 0.28 (unitless), and was selected from the range of typical values for the common soil texture in Amargosa Valley (sandy loam) (SNL 2007b, Section 6.6). A distribution of surface soil depth of 5 to 30 cm was developed, based on typical tillage depths for conventional and soil conservation tilling methods (i.e., shallow plowing to prevent erosion) (BSC 2004c, Section 6.10).

2.3.10.3.1.2 Air Submodel

The air submodel calculates the concentrations of radionuclides in air resulting from three transport pathways: soil resuspension, the generation of aerosols by evaporative coolers, and release of ^{222}Rn from soil (SNL 2007a, Section 6.4.2).

Soil Resuspension—Separate distributions of radionuclide concentrations in air resulting from resuspension of soil particles were developed for the environment around crops and for environments where exposure to the RMEI would occur (SNL 2007a, Section 6.4.2.1).

Airborne radionuclide concentrations that may be directly deposited on plants were calculated as the product of radionuclide concentrations in cultivated soil and atmospheric mass loading (i.e., the mass concentration in air of resuspended particles) in the environment around plants (SNL 2007a, Section 6.4.2). Mass loading in agricultural fields and gardens during the latter part of the growing season was estimated to range from 0.025 to 0.200 mg/m^3, similar to or higher than concentrations reported by the U.S. Environmental Protection Agency (EPA) from stationary monitoring sites in rural, agricultural areas in arid to semiarid regions of the western United States (BSC 2006, Section 6.2.5). Static measurements from those monitoring sites were used because the measurements would have been influenced by resuspended dust from agricultural fields and agricultural activities in the general vicinity of monitoring stations. To account for uncertainty about differences between the environment around crops in Amargosa Valley and the locations where monitoring stations were located, it was assumed that the modal and maximum values of the mass loading distribution for crops were about twice that reported at the monitoring stations in arid and semiarid locations. Higher modal and maximum values were not considered, primarily because there are few soil-disturbing activities that occur late in the growing season and because the crops typically grown in Amargosa Valley, such as alfalfa and other hay, cover most of the soil surface when mature, thereby reducing resuspension (BSC 2006, Section 5.1).

To account for variation and uncertainty in the characteristics of the RMEI and concentrations of radionuclides in air throughout the biosphere, the biosphere model used a microenvironmental modeling approach to calculate inhalation exposure (this method was also used to calculate external exposure). Microenvironmental models are commonly used to evaluate exposure to particulate matter and other contaminants (Duan 1982; Mage 1985; Klepeis 1999). The total exposure environment (i.e., the reference biosphere) was divided into segments, or environments (described below), that would have different levels of inhalation or external exposure. Radionuclide concentrations in air, time spent in each environment, and intake rates or exposure factors (e.g., breathing rates and shielding factors) were determined for each environment, and total airborne exposure was calculated as the sum of exposure in all environments (SNL 2007a, Section 6.4.8). Using this method, estimates of mass loading could be clearly associated with the types of surface-disturbing activities expected at the location of the RMEI (BSC 2006, Section 6.1),

and consideration of the expected duration of those activities could be incorporated into estimates of exposure times (BSC 2005, Section 6.3.2).

Five environments associated with different human activities were considered in the biosphere model. These mutually exclusive environments represented behavioral and environmental combinations for which the RMEI could receive a substantially different rate of exposure via inhalation or external exposure (BSC 2005, Section 6.2).

1. **Active Outdoors**—This environment encompassed potentially contaminated locations outdoors where the RMEI would conduct activities that would resuspend soil, including dust-generating activities while working (e.g., plowing, excavating, livestock operations), driving on unpaved roads, and performing other outdoor recreational activities (e.g., gardening, landscaping, riding horses, riding motorbikes, and walking on uncompacted soil). Average annual mass loading in this environment was estimated to range from 1.0 to 10.0 mg/m^3. This range was selected based on the experimental site-specific data and on analogue data and published measurements of personal exposure to resuspended dust during soil-disturbing activities, such as farming (e.g., Nieuwenhuijsen, Kruize et al. 1998, Nieuwenhuijsen, Noderer et al. 1999). To account for uncertainty in the applicability of these analogue data to the current conditions in Amargosa Valley and the types of activities conducted by the RMEI, the selected distribution of annual average mass loading in the active outdoor environment varied over an order of magnitude and encompassed applicable average airborne particulate concentrations for activities evaluated in the published studies (BSC 2006, Section 6.2.1). It was estimated that an average of 20% of time spent outdoors in contaminated area not working is spent conducting dust-generating activities, and that local outdoor workers spend an average of 50% of their work time conducting dust generating activities (BSC 2005). The remainder of the time spent outdoors was spent in the inactive outdoors environment described below.

2. **Inactive Outdoors**—This environment included outdoor locations within potentially contaminated areas where the RMEI is not conducting soil-disturbing activities. In this environment, the RMEI would spend time outdoors engaged in activities that would not resuspend soil (e.g., sitting, swimming, walking on turf or compacted/covered surfaces, driving on paved roads, barbecuing, and equipment maintenance) in areas where radionuclides may be present. This environment also included time spent commuting within the contaminated area because the major roads in Amargosa Valley are paved. The distribution of average annual mass loading in the inactive outdoor environment ranged from 0.025 to 0.100 mg/m^3. This distribution was developed from annual average airborne particulate concentrations measured at 21 static air-quality monitoring stations located in rural, agricultural settings in arid to semiarid environments. These data were obtained from the EPA Office of Air and Radiation AirData (Ambrose 2002a; Ambrose 2002b). The data were used because the measurements were taken at stationary, outdoor sites and therefore would be representative of mass loading that would be experienced by a person in a rural agricultural setting such as Amargosa Valley who is outdoors and not conducting activities that resuspend substantial amounts of dust (BSC 2006, Section 6.2.2).

3. **Active Indoors**—This environment included indoor locations in areas that may contain radionuclides where the RMEI would spend time active, including working and recreating. The mass loading distribution for this environment ranged from 0.060 to 0.175 mg/m^3. This distribution was based on published measurements of static and personnel exposure taken indoors while people were active (BSC 2006, Section 6.2.3).

4. **Inactive Indoors**—This environment included locations where the RMEI would spend time sleeping indoors in areas that may contain radionuclides. The mass loading distribution selected for this environment was lower than that for other environments and ranged from 0.010 to 0.050 mg/m^3. This distribution was based on measurements taken indoors while people were sleeping or inactive (BSC 2006, Section 6.2.4).

5. **Away from Potentially Contaminated Area**—This environment encompassed locations that would not contain radionuclides, including commuting routes to work and work locations outside of contaminated areas. No mass loading estimate was required for this environment (BSC 2006, Section 6.1).

Because the individual protection standards in proposed 10 CFR 63.311 and 63.321 are expressed in terms of the annual dose limit for the RMEI, the biosphere model calculates BDCFs as the annual dose (per unit concentration of radionuclides in the source media). To correctly calculate the annual inhalation dose, the mass loading distributions associated with the environments described above must be representative of the average annual concentrations of resuspended particles in air while the RMEI would be in an environment. Those distributions of average annual concentrations do not include unusually high concentrations that occur during such infrequent, short-duration events as dust storms, or unusually low concentrations that occur after recent precipitation, or when the wind speed is low (BSC 2006, Section 6.1.2).

To calculate the inhalation exposure in each environment, radionuclide concentrations in air were calculated as the product of radionuclide concentrations in resuspendable soil layer associated with that environment, an environment-specific enhancement factor, and mass loading in each environment (SNL 2007a, Section 6.4.2). The enhancement factor was the ratio of the activity concentration per unit mass in resuspended particles to the activity concentration in surface soil for a radionuclide. This parameter was included to account for differences in activity concentrations between soil and resuspended particles. Distributions of enhancement factors used in the biosphere model ranged from 0.4 to 1.5 for active outdoors environment, when soil is being disturbed, and from 2 to 7 for other environments (SNL 2007b, Section 6.5). These distributions were selected from measurements of enhancement factors taken over disturbed and undisturbed soil containing radionuclides, and from consideration of radionuclide enhancement as a result of particle size selective resuspension of soil particles (SNL 2007b, Section 6.5.3).

To evaluate the influence on mass loading of a climate ranging from arid to semi-arid, annual average concentrations of particulate matter in air at rural, agricultural sites in the western United States were compared among sites with different amounts of precipitation and snowfall (BSC 2006, Section 6.1.3). Rural, agricultural sites were selected to ensure that the level of human activity and the surface-disturbing conditions at the sites were consistent with the conditions in the Yucca Mountain region. Over 20 sites included in the analysis had a total annual precipitation of less than 10 in (0.25 m). Some of these arid sites are within or along the northern edge of the Mojave Desert

and have vegetation consistent with that found in the Yucca Mountain region (e.g., Moapa, Nevada; Bishop, California; Corcoran, California). Most of the other sites also are in areas with sparse native vegetation (BSC 2006, Section 6.1.3). Although the analyzed data from 97 rural agricultural sites had a large degree of scatter, they indicated that there was a weak inverse relationship between the total suspended particulate concentration in air and the annual precipitation over a range of precipitation from 5 to 50 in (0.13 to 1.3 m). This relationship is not as discernible for arid and semi-arid sites, i.e., for the sites with the annual precipitation of about 20 in. (0.51 m) or less. The mass loading levels at the sites with annual precipitation less than 20 in. (0.51 m) does not seem to depend strongly on precipitation. Based on this analysis, it was concluded that annual average concentrations of resuspended particles are not expected to be affected by the range of precipitation associated with the arid to semi-arid range of climatic conditions.

Evaporative Cooler Operation—The concentration of radionuclides in indoor air resulting from the operation of evaporative coolers was calculated as a function of the concentration of radionuclides in groundwater, the rate at which water evaporates from coolers while in operation, the rate of air flow, and the fraction of radionuclides in the water that transfers to the air. This calculation was based on evaporative cooler operation and the conservation of radioactivity (i.e., activity transferred to air is equal to the loss of activity from water) (SNL 2007a, Section 6.4.2.2).

The distribution of the airflow rate used for evaporative coolers in the biosphere model ranged from 1,700 to 10,200 m^3/hr. This distribution encompassed the typical flow rates of window- and roof-mounted coolers used in manufactured and other homes. The distribution of water evaporation rates used in the biosphere model had a geometric mean of 17 L/hr and a geometric standard deviation of 1.7 L/hr. This distribution was calculated from measurements of water use of residential coolers. A correlation coefficient of 0.8 between these two parameters was used to account for the positive correlation between the airflow and water use rates of evaporative coolers (BSC 2004d, Section 6.5.2).

The fraction of radionuclide concentration in the water used in the evaporative cooler that would be transferred to indoor air during the cooler operation is an important parameter that affects the concentration in air of radioactive aerosols generated by evaporative coolers. A search of the scientific literature did not find environmental assessments that considered the transport of contaminants through the evaporative cooler. Therefore, a uniform distribution, ranging from a minimum possible value of 0 to a maximum possible value of 1, was assumed to account for variability and uncertainty in this parameter (BSC 2004d, Section 6.5.2). This distribution is very conservative because it assumes that, on average, 50% of radioactive contaminants would be transferred from the water to the indoor air. In a properly operated and maintained cooler, the dissolved radioactive species would precipitate out inside the unit during water evaporation and the water vapor introduced into the indoor air would be essentially mineral free. The subsequent contamination of the cooler air could occur when the air flowing through the cooler pads liberates small particles of the solids left behind after evaporation, especially if a cooler is poorly maintained (BSC 2004d, Section 6.5). However, this process is believed to account for much less than 50% of contaminant transfer from water to air. Alternatively, the indoor air could become contaminated if water carry-over occurred through the gaps between the cooler pad fibers or through the thin spots in the pads, with the subsequent water evaporation outside the cooler (BSC 2004d, Section 6.5). Since this effect results in a loss in cooler performance, the coolers are designed to prevent it.

BDCFs for radionuclides with an atomic number less than that of actinium are not strongly influenced by the value of the transfer fraction for evaporative coolers, because the contribution to the BDCFs from this pathway is only 3.5% or less. For the remaining radionuclides (atomic number 89 or more), inhalation of radioactive aerosols generated by evaporative coolers may contribute, on average, up to 36% to the BDCF value (Table 2.3.10-11; SNL 2007a, Table 6.13-1). However, considering the conservative value of the evaporative cooler water transfer fraction, these contributions are likely to represent bounding conditions. Using the full range of possible values for the distribution of the evaporative cooler transfer fraction reasonably captures the range of uncertainty with a midpoint that is conservative.

^{222}Rn Exhalation from Surface Soil—Concentrations of ^{222}Rn were calculated separately for indoor and outdoor air. The radon level outdoors was estimated from the calculated concentration of ^{226}Ra in the surface soil and the relationship between the concentration of ^{226}Ra in the soil and the corresponding concentration of ^{222}Rn in the air. This relationship is called the release factor. A release factor of 0.25 Bq/m^3 per Bq/kg was used in the biosphere model, based on a global average value of the concentration ratio of ^{222}Rn activity in air to ^{226}Ra in soil (SNL 2007a, Section 6.4.2.3; BSC 2004d, Section 6.6.1). Based on a U.S. Geological Survey assessment (EPA 2007), the geologic radon potential of southern Nevada is low to moderate. In addition, outdoor radon concentrations would likely be lower than those calculated based on the release factor. This is because the proportion of irrigated areas relative to the available land area is relatively small in the Yucca Mountain region and, therefore, atmospheric mixing with uncontaminated air would cause dilution of outdoor radon concentrations. Therefore, using the average value did not result in an underestimation of risk.

The method for calculating the concentration of ^{222}Rn in indoor air was developed for a single-story house built on contaminated soil, assuming equilibrium conditions between the rate of ^{222}Rn entry into the house and the rate of removal. The main sources of indoor ^{222}Rn would be outdoor air and the soil beneath the house. This assumption did not result in an underestimation of risk, because it is unlikely that all houses would be built on soil that was subject to long-term irrigation and had a significant ^{226}Ra buildup. The indoor radon concentration was calculated as a function of the concentration of radon in outdoor air, flux density of radon from soil beneath the house, the fraction of that radon that would enter a home, home ventilation rate, and interior wall height (SNL 2007a, Section 6.4.2.3). The concentration of radon in outdoor air and the flux density of radon from soil were calculated based on the predicted concentration of ^{226}Ra in soil. The fraction of ^{222}Rn that would enter a home (range of 0.1 to 0.25) was selected from measurements taken in homes with concrete foundations. This distribution is likely to overestimate the fraction of ^{222}Rn that would enter a house because mobile homes usually have a gap between the soil and floor that would allow some ^{222}Rn to dissipate before reaching the dwelling (BSC 2004d, Section 6.6.2). Distributions of the wall height (range of 2.1 to 2.7 m) and ventilation rate were based on conditions in manufactured homes (BSC 2004d, Section 6.6.2). Because ventilation rates differ substantially when evaporative coolers are off (0.35 to 2.9 air exchanges per hour) and when they are operated (1 to 30 exchanges per hour), the ^{222}Rn concentration in indoor air was calculated separately for periods when coolers would be on and off (SNL 2007a, Section 6.4.2.3; BSC 2004d, Section 6.6.2).

2.3.10.3.1.3 Plant Uptake Submodel

The plant uptake submodel calculates the concentrations of radionuclides in edible portions of plants from three independent and simultaneous transport mechanisms: root uptake, water interception, and dust interception. Concentrations were calculated for four types of food consumed by the RMEI (leafy vegetables, other vegetables, fruits, and grains) and two types consumed by farm animals (forage and grain). The locally grown grains consumed by the people in the community and farm animals were considered to be identical (SNL 2007a, Section 6.3.1.6).

Many of the input parameters in the plant uptake submodel vary substantially among crops (e.g., irrigation rates and growing season length). To ensure that variation among crops was included in those parameter distributions, and that the results of this submodel were consistent with current conditions in Amargosa Valley, a set of representative crops was selected for each crop type. Five to seven representative crops were selected for leafy vegetables, root vegetables, and fruits. Crops grown in gardens, orchards, and fields in Amargosa Valley were selected (Horak and Carns 1997; USDA 1999a, Tables 2, 41, 42, and 50; Mills et al. n.d.). Fewer representative crops were selected for grains and cattle forage, because there is less diversity in the types of field crops that are grown in the region (BSC 2004c, Appendix A). Distributions of the input parameters were then developed that incorporated the values for each crop within a crop type, along with uncertainty about environmental factors that influence the parameters (BSC 2004c, Section 6). The same representative crops could be grown in a range of arid to semi-arid climate states (Antonelli et al. 1998; USDA 1999b, Tables 2, 41, 42, and 50; Washington State University Cooperative Extension 2002).

Root Uptake—The concentration of radionuclides in edible portions of crops due to uptake through roots was calculated as the product of radionuclide concentrations in soil, a radionuclide-specific soil-to-plant transfer factor for each crop type, and the dry-to-wet ratio of foodstuffs within each crop type (SNL 2007a, Section 6.4.3.1).

The soil-to-plant transfer factor was the ratio of the activity concentration of a radionuclide in dry edible parts of plants to the activity concentration in dry soil. Measurements of transfer factors vary widely, mainly because of differences among soils, crops, and environmental conditions. Transfer factors used in the biosphere model were selected from published information (Wang et al. 1993; IAEA 1994; Kennedy and Strenge 1992). Determination of soil-to-plant transfer factors included consideration of site-specific soil characteristics and the crops typically grown in Amargosa Valley. Truncated lognormal probability distribution functions that included relevant transfer factors reported in the reviewed publications were used (BSC 2004d, Section 6.2.1). There is a negative correlation between distribution coefficients and transfer factors because elements that preferentially bind to solids in the soil (i.e., have high distribution coefficients) have limited mobility and availability for plant uptake, while elements with low distribution coefficients are preferentially present in liquid and, thus, can be taken up by plant roots (BIOMASS 2003, pp. 193 to 197). To account for this effect, a correlation of –0.8 between distribution coefficients and transfer factors was included in the model (BSC 2004d, Section 6.2.1.5). This value was within the range reported in the literature (Davis et al. 1993, p. 234; Karlsson et al. 2001, p. 37; Sheppard, S.C. and Sheppard 1989, p. 653).

The dry-to-wet-weight ratio is a measure of the ratio of dry mass to wet mass of edible foodstuffs. Distributions of this ratio for human foodstuffs and grains were developed from measurements of water content of foods reported in the *Composition of Foods Raw, Processed, Prepared, USDA Nutrient Database for Standard Reference, Release 14* (USDA 2002). Distributions of this ratio for cattle forage were developed from measurements reported in NUREG/CR-3332, *Radiological Assessment, A Textbook on Environmental Dose Analysis* (Till and Meyer 1983; BSC 2004c, Section 6.2).

Deposition of Irrigation Water—The calculation of radionuclide concentrations in crops resulting from irrigation water sprayed on plants incorporated the processes of deposition, interception, translocation, and retention (SNL 2007a, Section 6.4.3.2). The deposition rate of radionuclides initially sprayed on crops was calculated as the product of their concentrations in groundwater, daily irrigation rates per crop type, and the fraction of irrigation applied using overhead methods. Average daily irrigation rates over the growing season were determined by considering seasonal irrigation requirements of representative crops and the duration of the crop growing season (BSC 2004c, Section 6.8). Average daily irrigation rates per crop type for the present-day climate ranged from 4.6 to 7.7 mm/day. Distributions of this parameter included variation and uncertainty related to crop characteristics, climate, and water management practices (BSC 2004c, Section 6.8).

The fraction of irrigation applied using overhead methods was included in the calculation of radionuclide concentrations in crops resulting from irrigation water sprayed on plants because some crops, such as fruit trees and some vegetables, may not be irrigated using overhead spray methods. Information from the Washington State University Cooperative Extension Service was used to determine methods commonly used to irrigate commercial and garden crops in arid and semiarid regions (Washington State University Cooperative Extension 2002). Data collected on irrigation methods in Amargosa Valley were used to determine methods commonly used to irrigate grains and cattle forage (BSC 2004c, Section 6.3). Average values of the distributions of this parameter were 0.75 (with standard deviation of 0.1) for vegetables and 0.5 (with standard deviation of 0.1) for fruits. Because most field crops in Amargosa Valley are irrigated using center pivot or rolling sprinklers, the average fraction of overhead irrigation for grains and cattle forage was 0.9 (with standard deviation of 0.05). These distributions account for uncertainty and variation in crops grown and irrigation methods used in gardens and agricultural fields (BSC 2004c, Section 6.3).

The fraction of radionuclide deposition rate from overhead irrigation that would be intercepted by plants was estimated using an empirical formula derived by Hoffman et al. (1989). This empirical formula calculates the water interception fraction as a function of crop biomass, the amount and intensity of irrigation, and empirical constants that vary among radionuclides with different charges and particle sizes. Because there was no information available to calculate radionuclide-specific constants for most radionuclides, and because radionuclides in the groundwater may be present in different chemical forms (e.g., have different ionic charges) or as suspended particles, one set of empirical constants was used in the biosphere model for all radionuclides. To ensure that interception of radionuclides by plants was not underestimated, the constants used were conservatively derived from experiments involving the radionuclide that had the highest interception fraction (cationic beryllium) (SNL 2007a, Section 6.4.3.2).

Distributions of dry biomass per crop type used in the calculation of the water interception fraction were calculated from estimates of commercial crop yield and foodstuff dry-to-wet ratios reported by the U.S. Department of Agriculture (e.g., USDA 2001; USDA 2002). Biomass of grains, other vegetables, and fruits were divided by a harvest index to convert dry yield to aboveground dry biomass. Harvest index values for grains, other vegetables, and fruits reported by the U.S. Department of Agriculture (Neitsch et al. 2002, Table A-8, pp. 381 to 384) were used to calculate total aboveground biomass. Because there is little variation in dry-to-wet ratios and harvest indices within each crop type, the distributions of dry biomass primarily reflect variation and uncertainty in crop yield (BSC 2004c, Section 6.1).

Distributions of the amount of irrigation applied each time a crop was watered (which were used in the calculation of the interception fraction) were calculated using the irrigation rate methodology described in Section 2.3.10.3.1.1 (BSC 2004c, Section 6.7). The distribution of irrigation intensity (the rate at which water is applied) was developed based on the soil types and irrigation methods in Amargosa Valley (BSC 2004c, Section 6.6). The selected distribution (range of 1.0 to 7.5 cm/hr) included reasonable uncertainty in the types of spray irrigation equipment used in Amargosa Valley (BSC 2004c, Section 6.6.2).

Using the empirical formula of Hoffman et al. (1989) and the parameter distributions described above, interception fractions calculated for the present-day climate ranged from about 0.1 to 1.0; averages per crop type ranged from 0.22 for leafy vegetables to 0.47 for grains (SNL 2007a, Section 6.13.4.3).

The translocation factor included in the water deposition calculation quantified the fraction of radionuclides intercepted by plant surfaces that would be translocated to edible plant parts (SNL 2007a, Section 6.4.3.2). Translocation factors used in the biosphere model were selected based on a review of translocation factors reported in the literature and used in other environmental radiation models (Napier, Peloquin et al. 1988, p. 4.67; Napier, Strenge et al. 2006, Section 9.4.1.6; Kennedy and Strenge 1992, pp. 6.41 to 6.42; Yu et al. 2001, p. D-12). A fixed value of 1.0 was used for leafy vegetables and cattle forage because radionuclides would be deposited directly on the edible plant parts (i.e., the leaves). A distribution ranging from 0.05 to 0.30 was used for other crop types. The upper bound of this distribution is higher than has been used in most other environmental radiation assessments. This high bound was conservatively selected to ensure that radionuclide concentrations in crops resulting from this potentially important transfer process were not underestimated (BSC 2004d, Sections 5.1 and 6.2.2.2).

The calculation of the retention of intercepted radionuclides included a loss component to account for weathering and other field losses. This component was calculated as a function of the weathering half-life and growing time per crop type (SNL 2007a, Section 6.4.3.2). The weathering half-life is the time it takes for the amount of radionuclide deposited on plants to be reduced by 50% in the absence of any additional contamination. A distribution of 5 to 30 days was selected to account for variation among crops and radionuclides and uncertainty in the rate of weathering (BSC 2004d, Section 6.2.2.3). This distribution of weathering half-lives encompasses the range of weathering rates reported in other publications and biosphere models (e.g., Baes et al. 1984, p. 124; IAEA 2001, p. 63). Growing time was selected from information on the growing season of representative crops, as described in the surface soil submodel (Section 2.3.10.3.1.1). Because the calculation of radionuclide concentrations in plants was insensitive to changes in growing times greater than about

50 to 75 days, fixed values of growing time (ranging from 75 days for leafy vegetables to 200 days for grains) were used in the biosphere model (BSC 2004c, Section 6.4).

Deposition of Dust—The calculation of radionuclide concentrations in crops resulting from settling of resuspended soil on plants incorporated the processes of deposition, initial interception, translocation, and retention (as a function of weathering half-life and growing season length) (SNL 2007a, Section 6.4.3.3). This calculation of dust interception used the same input parameter distributions for the translocation factor, weathering half-life, and growing time that were used for the calculation of water interception.

The deposition rate of resuspended soil particles quantified the combined effects of removal of particulates from the atmosphere by several processes (e.g., gravitational settling, diffusion, turbulent transport). The deposition rate was calculated in the biosphere model as a function of radionuclide concentrations in the air around crops (calculated in the air submodel) and the dry deposition velocity. A distribution of deposition velocity (ranging from 3×10^{-4} m/s to 3×10^{-1} m/s) was developed based on variation and uncertainty in wind speeds in Amargosa Valley, surface roughness, and the expected particle size distribution of resuspended particles in fields and gardens (BSC 2004d, Section 6.2.2.1).

The fraction of resuspended soil particles intercepted by plant surfaces was calculated as an exponential function of dry biomass per crop type and an empirical factor that quantified differences in interception among crop types. Distributions of dry biomass per crop type were developed, as described above, for water interception. The empirical factors for leafy vegetables, cattle forage, and grains (2.9) resulted in higher interception fractions per unit biomass than those resulting from the factor used for other crop types (3.6), because the edible parts of leafy vegetables, forage, and grains are directly exposed. These factors were adopted from those used in the GENII biosphere model (Napier, Peloquin et al. 1988, Section 4.7.4; Napier, Strenge et al. 2006, Section 9.4.1.4). Average dust interception fractions ranged from 0.46 for leafy vegetables (the crop type with the lowest biomass) to 0.96 for grains (highest biomass) (SNL 2007a, Section 6.4.3.3 and Table 6.10-1).

2.3.10.3.1.4 Animal Uptake Submodel

Radionuclide concentrations in animal products due to ingestion of the three media considered in the animal uptake submodel (feed, water, and soil) were calculated as the product of the concentration of radionuclides in those media, ingestion rates of the media, and animal-intake to animal-product transfer coefficients. Radionuclide concentrations in feed and soil were calculated in the plant uptake and surface soil submodels, respectively (SNL 2007a, Section 6.4.4).

Consumption rates of feed, water, and soil were developed from a review of published consumption rates of beef cattle, dairy cows, and chickens. Consideration was given to the applicability of the published values of animal consumption to arid and semiarid conditions. Distributions of feed consumption ranged from 29 to 68 kg/day for beef cattle, 50 to 73 kg/day for dairy cows, and 0.12 to 0.4 kg/day for poultry and laying hens. Water consumption rates were 60 L/day for beef cattle, 60 to 100 L/day for dairy cows, and 0.5 L/day for poultry and laying hens. Distributions of soil consumption ranged from 0.4 to 1.0 kg/day for beef cattle, 0.8 to 1.1 kg/day for dairy cows, and 0.01 to 0.03 kg/day for poultry and laying hens (BSC 2004d, Sections 6.3.2 and 7.1.2).

Transfer coefficients represent the amount of radionuclide in 1 kg of animal product as a fraction of the daily intake of that radionuclide (e.g., Bq/kg per Bq/d). These coefficients differ among elements, chemical forms, and animal products, and uncertainty is considerable for most elements. Truncated lognormal distributions of transfer coefficients were used in the biosphere model. These distributions were selected from published compendia of values and reports containing recommendations or applications of coefficients in other biosphere models (e.g., Wang et al. 1993; IAEA 1994; Kennedy and Strenge 1992). To incorporate uncertainty and variation in the transfer coefficients, geometric means and standard deviations were calculated for each element using values reported in the reviewed literature. These distributions had a range of about 1.5 to more than 5 orders of magnitude (BSC 2004d, Section 6.3.3).

2.3.10.3.1.5 Fish Uptake Submodel

The radionuclide concentration in farm-raised fish would result from exposure to groundwater used to fill fishponds, but not from feed, because fish in Amargosa Valley were fed commercial feed, which would be uncontaminated (BSC 2004d, Section 6.4.3). The radionuclide concentration in fish was calculated as the product of radionuclide concentrations in water, a bioaccumulation factor, and a water concentration modifying factor (SNL 2007a, Section 6.4.5).

The bioaccumulation factor is the ratio of the radionuclide concentration in edible portions of fish tissue to that in water. There is a large amount of uncertainty and variation in this bioaccumulation factor, so the element-specific distributions used in the biosphere model ranged over several orders of magnitude (BSC 2004d, Section 6.4.3). All estimates of the bioaccumulation factor available for selection of this parameter distribution were measured in natural systems where the entire natural food chain existing within the system was contaminated; therefore, the bioaccumulation factor bounds estimates of radionuclide accumulation in farm-raised fish (SNL 2007a, Section 6.4.5).

The water concentration modifying factor was included in the calculation of radionuclide concentrations in fish because radionuclide concentrations in water would increase over time as water is added to the fish ponds to replace that lost by evaporation (SNL 2007a, Section 6.4.5). Catfish were raised in Amargosa Valley ponds for at least 1 year (and reached full size in about 2 years), and the ponds were drained each time after fish were harvested (Roe 2002, p. 2). Therefore, distributions of the water concentration modifying factor were developed based on the assumption that radionuclides would accumulate in the ponds for 1 to 2 years (after which fish would be harvested and the ponds drained), and that water would be replaced at a rate equal to the annual evaporation rate for the climate. The water concentration modifying factor was calculated as a function of the depth of the Amargosa Valley fishponds (0.8 to 1.7 m); the annual water evaporation rate (about 2 m/yr); and the length of the fish-raising cycle (1 to 2 years) (BSC 2004d, Section 6.4.3). Site-specific evaporation rates were estimated from a detailed map of surface evaporation rates (Farnsworth et al. 1982, Map 3) as 2.03 m/yr for the present-day climate. The resulting distributions of the water concentration modifying factor ranged from 2.2 to 6.1 (i.e., the radionuclide concentration in pond water would be about 2 to 6 times higher than in groundwater) (BSC 2004d, Sections 6.4.3 and 6.4.5).

2.3.10.3.1.6 ^{14}C Submodel

The ^{14}C submodel included calculations of ^{14}C concentrations in soil and air; in crops from root uptake and photosynthesis; in animal products from the ingestion of feed, water, and soil; and bioaccumulation in fish (SNL 2007a, Section 6.4.6).

The method used to calculate soil concentrations of ^{14}C was the same as that used in the surface soil submodel for other radionuclides, with two exceptions (SNL 2007a, Section 6.4.6.1). First, an additional loss mechanism, gaseous emission loss, was included because ^{14}C is volatile and quickly released from soil as $^{14}CO_2$. The emission rate constant used in the biosphere model was 22 per year (i.e., 6% of ^{14}C in the surface soil would be lost per day), based on rates measured for sandy soils (BSC 2004d, Section 6.7.1). Thus, when continuously irrigated with water containing ^{14}C, concentrations of this radionuclide in surface soils would reach equilibrium within 1 to 2 months, and gaseous emission would be the dominant mechanism for removing ^{14}C from the soil. Second, ^{14}C concentrations in the soil were calculated separately for each crop type based on daily irrigation rates specific to each crop type (versus an average soil concentration for field and garden crops, as was used for other radionuclides). The daily rates were calculated by dividing the annual average irrigation rate for a crop by the number of days in the growing season for that crop (BSC 2004c, Section 6.8). This method was used because ^{14}C is rapidly released from the soil, and, therefore, irrigation must be considered locally and only during the growing season (SNL 2007a, Section 6.4.6.1).

Because ^{14}C is quickly released from the soil as a gas, the concentration of gaseous ^{14}C in air was calculated as a function of the flux density of gaseous ^{14}C from soil and the dilution of the released gas in a mixing cell of defined dimensions (i.e., the volume of air within which gaseous ^{14}C would mix) (SNL 2007a, Section 6.4.6.2). The flux density of gaseous ^{14}C from soil (equal to the rate of application of this radionuclide with the irrigation water as equilibrium conditions would be rapidly established) was calculated as the product of soil concentration of this radionuclide and emission rate constant. Because ^{14}C would only be released from irrigated land, the surface area of the mixing cell was estimated from the size of farms and gardens in Amargosa Valley (SNL 2007a, Section 6.4.6.2). The height of the cell was 2 m for human environments and 1 m for crops. The mixing rate was based on local terrain conditions and the average wind speeds measured in northern Amargosa Valley. This rate differed for human environments and crops, with a lower rate for crops because the wind speed would be slower close to the ground (BSC 2004d, Section 6.7.2).

The concentration of ^{14}C in crops due to photosynthesis was calculated as a function of the fraction of carbon in plants that would be derived from the air and the ratio of the concentrations of ^{14}C and stable carbon in the air (SNL 2007a, Section 6.4.6.3). Based on values used in other biosphere models (Napier, Peloquin et al. 1998, p. 4.88; Napier, Strenge et al. 2006, Section 9.6.2; Yu et al. 2001, p. L-20), the fraction of stable carbon in plants used in the biosphere model was 0.40 for grains and 0.09 for the other crop types (BSC 2004d, Section 6.7.3). Similarly, the concentration of ^{14}C in crops from root uptake was calculated as a function of the fraction of soil-derived carbon in plants and the ratio of the concentrations of ^{14}C and stable carbon in soil. Based on experimental results reported by Sheppard, M.I. et al. (1991), the fractions of carbon in plants derived from air and soil used in the biosphere model were 0.98 and 0.02, respectively (BSC 2004d, Section 6.7.3). Thus, ^{14}C concentrations in crops would be due primarily to uptake from air during photosynthesis.

The concentration of ^{14}C in animal products was derived from estimated concentrations in animal feed, soil, and drinking water. The transfer of ^{14}C from these media to animal products was modeled by calculating the ratio of ^{14}C intake from all animal ingestion pathways to total carbon intake from the same pathways. Multiplication of this ratio by the fraction of stable carbon in the animal product provided the required ^{14}C concentration per unit mass of the product (SNL 2007a, Section 6.4.6.4). Fractions of stable carbon used in the biosphere model varied from 0.07 for milk to 0.24 for beef (BSC 2004d, Section 6.7.4). Because there would be only a small amount of carbon in the soil and water, the primary source of ^{14}C in animal products would be feed.

The bioaccumulation of ^{14}C in fish was calculated in the same manner as for other radionuclides, as a product of radionuclide concentration in fishpond water and the bioaccumulation factor. To calculate radionuclide concentration in pond water, an additional ^{14}C loss mechanism was included. ^{14}C could be lost by emission of $^{14}CO_2$ from the water to the atmosphere. This additional loss mechanism was included in the calculation of the water concentration modifying factor (BSC 2004d, Section 6.4.4).

2.3.10.3.1.7 External Exposure Submodel

External exposure to soil was calculated for each primary radionuclide and long-lived decay product as the product of a radionuclide-specific effective dose coefficient, the concentration of the radionuclide in the soil (from the surface soil submodel), an environment-specific building shielding factor, and the estimated time spent by the RMEI in each of five environments. The total annual external dose (per unit concentration of radionuclides in groundwater) for a primary radionuclide was then calculated as the sum of doses for that radionuclide and its long-lived decay products (SNL 2007a, Section 6.4.7).

Effective dose coefficients were calculated as the weighted sum of dose coefficients for long-lived radionuclides and their short-lived decay products (Section 2.3.10.2.4), with weights being branching fractions of the decay products (Table 2.3.10-5) (SNL 2007a, Section 6.4.7.2). Dose coefficients for soil contaminated to an infinite depth (with respect to attenuation of radiation originating in the soil) reported in *Federal Guidance Report No. 13* (EPA 2002) were used to calculate the external exposure dose for the groundwater exposure scenario (Table 2.3.10-6) (SNL 2007a, Section 6.4.7.2). This choice of dose coefficients was appropriate and realistic because the radiation contributing to external exposure may originate in deep soil due to tilling and downward movement of radionuclides (SNL 2007a, Section 6.3.1.4). The use of dose coefficients for adults from *Federal Guidance Report No. 13* (EPA 2002) is consistent with the requirement of 10 CFR 63.312(e) that the RMEI "is an adult with metabolic and physiological considerations consistent with present knowledge of adults."

The shielding factor was included in the external exposure dose calculation to account for the effects of shielding from radiation (i.e., the reduction of the outdoor dose rate) provided by buildings when the RMEI is indoors (SNL 2007a, Section 6.4.7.1). Shielding factor values for radionuclides included in the biosphere model ranged from zero (for radionuclides that emit no penetrating radiation) to 0.4 (for photon emitters of energy greater than 100 keV) (BSC 2005, Table 6-31). These factors were developed for lightly constructed housing and were consistent with conditions in Amargosa Valley because most residents live in mobile homes (Section 2.3.10.2.2). Shielding

factors were only applied to indoor environments (i.e., the shielding factor for outdoor environments equaled 1.0) (SNL 2007a, Section 6.4.7.1).

As described in the air submodel, a microenvironmental modeling approach was used to evaluate external exposure and inhalation doses (SNL 2007a, Sections 6.4.7 and 6.4.8). The biosphere was divided into five environments, and average exposure time within each environment was calculated (BSC 2005, Section 6.3.2). To support those calculations, the average time spent by Amargosa Valley residents conducting various work and nonwork activities was determined. These determinations were used to develop the 24-hour time budgets for the population groups described below. They were based on a survey of the residents of Amargosa Valley conducted in 2000 (Bureau of the Census 2002, Tables P8, P31, P47, P49, and P50). Information in *Exposure Factors Handbook* (EPA 1997a, Section 15) and associated documentation (Klepeis et al. 1996, Table 6-1) was also used. Uncertainty about the use of these national data was incorporated into the distributions of exposure time.

The average time worked by employed residents of Amargosa Valley 16 years of age or older was calculated as 5.5 hours per day (standard error of 0.3 hour). The average time spent commuting to and from work outside of areas potentially contaminated by use of groundwater for irrigation was 0.5 hours per day (standard error of 0.1 hour). Residents spend, on average, 8.3 hours per day (standard error of 0.1 hour) sleeping and 1.5 hours per day (standard error of 0.2 hour) outdoors while not working, 20% of which would be spent conducting dust-generating activities. Because Amargosa Valley residents likely spend some time outside of the valley shopping, obtaining medical services, participating in recreational activities, and conducting other nonwork activities, it was estimated that residents spend an average of 2.0 hours per day (standard error of 0.4 hour) away from contaminated areas (BSC 2005, Section 6.3.2.1).

To account for variation and uncertainty in the characteristics of the RMEI that influence exposure times, the Amargosa Valley population was divided into four mutually exclusive groups: local outdoor workers, commuters, local indoor workers, and nonworkers; exposure times were calculated for each group (BSC 2005, Sections 6.3.1 and 6.3.2). These four population groups represented the range of behaviors that would most influence the amount of time that people would be exposed to radionuclides through the external exposure and inhalation pathways. Variation among individuals in these exposure pathways would be influenced primarily by the amount of time they would spend indoors and outdoors within contaminated areas, and the amount of time they would spend away from contaminated areas. For adults, variation among these time factors would primarily be a function of occupational characteristics, as people who work outside the contaminated area generally would experience less exposure than people who remain within the area, and people working outdoors would be exposed differently than those remaining indoors. Therefore, the categories were based on work location and occupation. The proportion of the adult Amargosa Valley population in each of the following four groups was based on a survey of the residents of Amargosa Valley conducted in 2000 (Bureau of the Census 2002, Tables P31, P47, and P49).

Local Outdoor Workers—This group included residents who work outdoors and disturb (and, therefore, resuspend) soil that may contain radionuclides. Based on an assumption that this group would include all of 26 adult Amargosa Valley residents identified in the 2000 Census who worked in agriculture, 25% of 7 construction workers, 10% of 8 utility workers, and 10% of 119

miners, an average of 5.5% of adult residents was classified as local outdoor workers, with a range of 2.9% to 8.1%. Only a portion of miners and construction and utility workers were included in this category because there is limited work for those professions in Amargosa Valley; the remainder commute to work in areas outside of Amargosa Valley (BSC 2005, Sections 5.2 and 6.3.1).

Commuters—This group included residents who work outside of areas where radionuclides may be present. An average of 39.2% of the population was classified as commuters (with a range of 33.9% to 44.5%), based on the current conditions in the agricultural region of Amargosa Valley and the proportion of Amargosa Valley residents who stated during the 2000 Census that they commuted 10 minutes or more to work (BSC 2005, Section 6.1.3). That agricultural region is a maximum of about 13 km wide; therefore, residents can drive away from all irrigated fields within 10 minutes (BSC 2005, Section 5.1). Based on the commute time of the employed resident of Amargosa Valley (Bureau of the Census 2002, Table P31), and the estimates described above of time spent in each environment, commuters were estimated to spend an average of 0.3 hours per day active outdoors, 1.4 hours per day inactive outdoors, 6.0 hours per day active indoors, 8.3 hours per day asleep, and 8.0 hours per day away from areas where radionuclides may be present (BSC 2005, Sections 6.3.1 and 6.3.2).

Local Indoor Workers—Local indoor workers were residents who work indoors (or outdoors in enclosed vehicles) in areas that may contain radionuclides. This group was composed of employed adults who were not classified as local outdoor workers or commuters. The proportion of local indoor workers was calculated as a remaining proportion of Amargosa Valley population after subtracting proportions of all other groups. Local indoor workers were estimated to spend an average of 0.3 hours per day active outdoors, 1.3 hours per day inactive outdoors, 12.1 hours per day active indoors, 8.3 hours per day asleep, and 2.0 hours per day away from areas where radionuclides may be present (BSC 2005, Sections 6.3.1 and 6.3.2).

Nonworkers—Nonworkers included residents who were unemployed or otherwise not in the labor force (e.g., retired people). An average of 39.2% of the resident adult population in Amargosa Valley met this criterion in 2000 (with a range of 34.4% to 44.0%). Nonworkers were estimated to spend an average of 0.3 hours per day active outdoors, 1.2 hours per day inactive outdoors, 12.2 hours per day active indoors, 8.3 hours per day asleep, and 2.0 hours per day away from areas where radionuclides may be present (BSC 2005, Sections 6.3.1 and 6.3.2).

To meet the requirement of 10 CFR 63.312(b) that mean values of lifestyle characteristics of the residents of Amargosa Valley be used in the TSPA dose assessments, the average exposure time per environment was calculated in the biosphere model as the average of exposure times per group, weighted by the proportion of the population in each group (SNL 2007a, Section 6.4.7.1). These average exposure times were about 0.5 hours per day in the active outdoor environment, 1.4 hours per day inactive outdoors, 9.4 hours per day active indoors, 8.3 hours per day asleep indoors, and 4.4 hours per day away from areas where radionuclides may be present (SNL 2007a, Section 6.13.5.2.1). These projections are based on a 1997 survey of the people of Amargosa Valley, and are representative of their living style, consistent with 10 CFR 63.312(b).

2.3.10.3.1.8 Inhalation Submodel

The inhalation submodel calculated the annual dose (committed effective dose from annual intake per unit concentration of radionuclides in groundwater) from the inhalation of resuspended soil, aerosols from evaporative coolers, and gaseous emissions of ^{222}Rn and ^{14}C from soil. The total inhalation dose was the sum of the doses resulting from these three exposure pathways (SNL 2007a, Section 6.4.8).

The inhalation dose from the three exposure pathways was calculated similarly for all radionuclides except ^{222}Rn. Dose due to inhalation of radionuclides transferred to air by soil resuspension, generation of aerosols from evaporative coolers, and by gaseous emissions of ^{222}Rn and ^{14}C was the product of radionuclide concentration in air within each of the RMEI environments (calculated in the air submodel), the time spent by the RMEI in each environment, environment-specific breathing rate, and a radionuclide-specific effective dose coefficient. Radionuclide concentration in resuspended soil included contribution from ingrowth of long-lived decay products of primary radionuclides in the soil. The dose for a primary radionuclide was calculated as the sum of doses for that radionuclide and its long-lived decay products (SNL 2007a, Section 6.4.8). The effective dose coefficients for long-lived radionuclides other than ^{222}Rn were developed from inhalation dose coefficients for adults in *Federal Guidance Report No. 13* (EPA 2002), and included the contribution from short-lived decay products (Table 2.3.10-8) (SNL 2007a, Sections 6.3.5, 6.4.8.1, and 6.4.8.5). The use of dose coefficients for adults is consistent with the requirement of 10 CFR 63.312(e) that the RMEI "is an adult with metabolic and physiological considerations consistent with present knowledge of adults."

The same exposure times and population proportions described for the external exposure submodel were used to calculate inhalation exposure. Breathing rates of adults used in the calculations of inhalation exposure were 1.57 m^3/hr for time spent active outdoors, 1.08 m^3/hr while inactive outdoors and active indoors, and 0.39 m^3/hr while sleeping. These breathing rates were developed from information related to the respiratory tract model in *Human Respiratory Tract Model for Radiological Protection* (ICRP 1994a), including the breathing rate and nominal mix of exercise levels for various environments (BSC 2005, Section 6.3.3).

To convert exposure to radon decay products to the committed effective dose, a conversion factor from the International Commission on Radiological Protection Publication 65 (ICRP 1994b, Chapter 6) was used. This conversion factor was modified to allow for incorporation into the calculation of exposure to ^{222}Rn decay products of the environment-specific breathing rates developed for the RMEI (BSC 2005, Section 6.5.4). In addition, an environment-specific equilibrium factor for ^{222}Rn decay products was included in the calculation to account for the degree of equilibrium between a parent radionuclide and its short-lived decay products in different environments. The equilibrium factor is defined as the ratio of the actual potential alpha energy concentration in air to the concentration that would occur if the decay products were in equilibrium with ^{222}Rn (SNL 2007a, Section 6.4.8.4). Based in part on measurements taken in the southwestern United States (Wasiolek and James 1995, Table 2), and on the typical values of this parameter worldwide (UNSCEAR 2000, pp. 103 to 104), equilibrium factors ranging from 0.5 to 0.7 for outdoor environments and 0.3 to 0.5 for indoor environments were used in the calculation of ^{222}Rn exposure (BSC 2004d, Section 6.6.3).

The calculation of inhalation exposure to radionuclides introduced into indoor air from evaporative coolers included factors that quantified the proportion of residences with coolers and the proportion of the year that coolers would be operated. Those factors were also included in the calculation of dose from inhalation of ^{222}Rn because the home ventilation rate would influence the buildup of ^{222}Rn indoors. The proportion of homes with coolers (average equals 0.74) was determined from a survey of Amargosa Valley residents (DOE 1997; BSC 2005, Section 6.3.4.1). The minimum proportion of the year that coolers would be operated was estimated from the average number of days in Amargosa Valley that the daily maximum temperature exceeded 90°F. The maximum proportion of the year that coolers would be operated was based on the average number of days that the daily maximum temperature exceeded 80°F. This distribution ranged from 32% to 46% for the present-day climate. The temperature range of 80°F to 90°F is the range of daily maximum temperatures over which people are likely to turn on their coolers (BSC 2005, Section 6.3.4.2).

2.3.10.3.1.9 Ingestion Submodel

The ingestion submodel calculated the annual dose (committed effective dose from annual intake) from the ingestion of radionuclides in water, locally produced food stuffs, and soil.

Ingestion exposure was calculated for each of 11 media (four crop types, four animal products, fish, water, and soil) as the product of the effective dose coefficient, radionuclide concentration in the medium, and annual consumption rate of the medium (SNL 2007a, Section 6.4.9). The effective dose coefficients were developed from ingestion dose coefficients for adults in *Federal Guidance Report No. 13* (EPA 2002). The dose contribution of short-lived radionuclides was included in the effective dose coefficients for long-lived primary radionuclides (Table 2.3.10-9) (SNL 2007a, Sections 6.3.5 and 6.4.9.6). For ingestion of plants, animal products, and soil, the contribution to ingestion exposure from radioactive decay and ingrowth in surface soil also was included. Total ingestion exposure was calculated as the sum of the dose from the 11 media (SNL 2007a, Section 6.4.9).

The annual consumption rate of water was 2 L/day, or 730 L/yr, as specified in 10 CFR 63.312(d) (BSC 2005, Section 7.1.2.1). The soil ingestion rate was representative of the amount of soil that adults inadvertently ingest (e.g., from dirty hands, from food, while breathing through the mouth) and did not include purposeful soil ingestion. Based on the arid, rural conditions in Amargosa Valley, a distribution of 50 to 200 mg/day of ingested soil was used in the biosphere model (BSC 2005, Section 6.4.3). This distribution was based on an average value of 100 mg/day recommended in the *Exposure Factors Handbook* (EPA 1997b, Section 4.7) for residential and agricultural scenarios and an uncertainty distribution developed by Simon (1998, p. 663) for agricultural scenarios and rural lifestyles (BSC 2005, Section 6.4.3).

Consumption rates of locally produced crops and animal products were based on the 1997 survey of Amargosa Valley residents (DOE 1997). During that survey, residents were asked how often they ate locally produced foods. To develop distributions of annual consumption rates, the information on frequency of consumption from the survey was combined with survey information obtained by the U.S. Department of Agriculture on the amount of each food type eaten by people in the western United States. Statistical uncertainty associated with the Amargosa Valley and U.S. Department of Agriculture surveys was incorporated into the distributions of consumption rates

(BSC 2005, Section 6.4). Lognormal distributions with the following average values and standard errors were used (BSC 2005, Table 7-5):

- Leafy vegetables: average value = 3.78 kg/yr, standard error = 0.88 kg/yr
- Other vegetables: average value = 4.73 kg/yr, standard error = 0.67 kg/yr
- Fruit: average value = 12.68 kg/yr, standard error = 1.36 kg/yr
- Grain: average value = 0.23 kg/yr, standard error = 0.11 kg/yr
- Beef: average value = 2.85 kg/yr, standard error = 0.65 kg/yr
- Poultry: average value = 0.42 kg/yr, standard error = 0.13 kg/yr
- Milk: average value = 4.66 kg/yr, standard error = 1.68 kg/yr
- Eggs: average value = 5.30 kg/yr, standard error = 0.83 kg/yr
- Fish: average value = 0.23 kg/yr, standard error = 0.10 kg/yr.

The 1997 survey is representative of the diet of the people who now reside in Amargosa Valley. The population of Amargosa Valley increased by about 11% from 1997 to 2003 (CRWMS M&O 1997, Table 3-4; BSC 2003, Table 1), but there have been few changes in the agricultural industry in the valley that would have resulted in changes in the amount of locally produced food available to residents. A pistachio processing and packaging facility has been opened since 1997, which has increased the availability of locally produced nuts. However, most of the fields in the valley are still planted in alfalfa and other hay, and there has been no significant switch to the production of other human foodstuffs (BSC 2005, Section 6.4.1). Even if some of the new residents of the community ate substantially more locally produced foods than did those surveyed in 1997, the biosphere model results would not be substantially affected. For example, if the average consumption rate of all locally produced food types was twice that obtained from the 1997 survey (an unreasonably high expectation, which is selected here to document the sensitivity of the model), the BDCF for ^{99}Tc and ^{129}I would increase by an average of only 21% and 18%, respectively, and the BDCF for ^{237}Np would increase by 3% (SNL 2007a, Section 6.13.5.1). These values are within the range of the uncertainty distributions of the BDCFs for these radionuclides (Table 2.3.10-12). Thus, the biosphere model is relatively insensitive to reasonable changes in food consumption rates, and sufficient survey data of the people of Amargosa Valley exist to determine the average consumption rate of locally produced food (SNL 2007a, Section 6.13.5.1).

2.3.10.3.2 Volcanic Ash Exposure Scenario

The mathematical model for the volcanic ash exposure scenario was developed in seven submodels that represent four contaminated media (soil, air, plants, and animals) and three exposure pathways (external, inhalation, and ingestion exposure) (Figure 2.3.10-10) (SNL 2007a, Section 6.5). The data and parameters used to calculate BDCFs for this scenario are described for each submodel in Sections 2.3.10.3.2.1 to 2.3.10.3.2.7. Many of the methods and parameter values used to calculate BDCFs for the volcanic ash exposure scenario were the same as described for the groundwater exposure scenario (SNL 2007a, Section 6.5). The methods and parameters that differ from those used for the groundwater exposure scenario are described in this section, and the parameters that are used exclusively in the model for the volcanic ash exposure scenario are identified in Table 2.3.10-10. Most of the parameters listed in Table 2.3.10-10 that are used in the groundwater scenario model, but not in the volcanic ash scenario model, are those related to the groundwater usage (SNL 2007a, Section 6.6.3.1).

2.3.10.3.2.1 Surface Soil Submodel

The surface soil submodel for the volcanic ash exposure scenario differed from that for the groundwater exposure scenario primarily because a volcanic eruption (and the subsequent tephra redistribution) would disperse contaminated tephra over a large area, while irrigating would contaminate the relatively small farming area. The scenarios also differ because, in the volcanic ash exposure scenario, radionuclides would not accumulate in the surface soil because they are not continuously added to the environment, as is the case for contaminated irrigation water. The source of radionuclides for this scenario is volcanic tephra deposited on the ground surface or redistributed to the location occupied by the community that includes the RMEI. The surface soil in this scenario is a mixture of volcanic tephra and native soil. The concentrations of radioactive waste in the soil, resulting from a volcanic eruption, are calculated outside the biosphere model by the tephra redistribution model (Section 2.3.11.4), and are used as source terms in calculation of the dose to the RMEI from a volcanic eruption.

The biosphere model uses two source terms (SNL 2007a, Section 6.5.1). The two source terms are (1) the radionuclide concentration in the resuspendable layer of soil in units of mass activity concentration (e.g., Bq/kg); and (2) depth-integrated (areal) radionuclide concentration in surface soil in units of surface activity concentration (e.g., Bq/m^2) (SNL 2007a, Section 6.5.1). The depth over which the integrated concentrations are determined is the tillage depth. Radionuclide concentration in the resuspendable layer of soil is used in the inhalation submodel to calculate inhalation dose from exposure to suspended particulates. Areal radionuclide concentration is used in estimates of doses from the remaining exposure pathways included in the model (i.e., ingestion; inhalation of radon decay products, when applicable; and external exposure).

The source term for evaluation of RMEI exposure to radionuclides released from the repository during a volcanic eruption is calculated using two models: ASHPLUME and FAR (Section 2.3.11) (SNL 2007a, Section 6.3.2.1). The ASHPLUME atmospheric tephra dispersal model and the associated computer code calculate tephra and radioactive waste concentrations initially deposited in the Yucca Mountain region, including the area occupied by the community that includes the RMEI. The FAR model and supporting software evaluate the redistribution of that initially deposited volcanic tephra and associated radioactive waste within the Fortymile Wash drainage area, and calculates contaminant transport within the soil. The FAR model segregates the Fortymile Wash alluvial fan into distributary channels and interchannel divides. On interchannel divides, radioactive waste is considered to be deposited only from primary tephra fall. In channels, the initial radionuclide concentration includes the primary fallout as well as the radionuclides redistributed from the upper basin by fluvial processes. Both of these components will be mixed with channel sediments by fluvial scour and redeposition.

The reference biosphere for the volcanic ash scenario is divided into two areas: cultivated land, and noncultivated land (SNL 2007a, Section 6.5.1). Land use is an important factor considered in the surface soil submodel because the radionuclide concentration in surface soil, and, consequently, the concentration of resuspended radionuclides in air, would differ on cultivated and uncultivated lands. On agricultural and other cultivated land (e.g., gardens), volcanic tephra would be uniformly mixed with surface soil during tilling. This mechanical mixing would not occur on uncultivated land, although natural surface processes would cause radionuclide redistribution from the original deposits (e.g., during fluvial episodes), and by migration into the soil.

The source term for the cultivated land is the areal radionuclide concentration in the surface soil (SNL 2007a, Section 6.5.1.1). This quantity is calculated outside the biosphere model by the tephra redistribution model (Figure 2.3.10-3) as a depth-integrated radionuclide concentration (Sections 2.3.11.4.2.3.3 and 2.3.11.4.5.3; SNL 2007a, Section 6.5.1.1). Tilling depth is used in these calculations, consistent with the depth of surface soil in the biosphere model. Areal radionuclide concentrations in the surface soil are converted to radionuclide mass concentrations in the surface soil, similar to the groundwater soil submodel. The radionuclide concentration in a mixture of soil and tephra on cultivated land is used to estimate radionuclide transfers to plant foodstuffs and animal products, and transfers directly to the RMEI by inadvertent soil ingestion. These processes are modeled in the plant, animal, and ingestion submodels, respectively. Most soil-related parameters are considered to be the same as those used for the groundwater scenario (SNL 2007b).

The areal radionuclide concentration in surface soil (i.e., activity integrated to a depth of surface soil), is also used to calculate BDCF contribution from external exposure and from inhalation of radon decay products. This quantity does not depend on the distribution of radionuclides in the surface soil, and is thus independent on the land use (i.e., whether the land is cultivated or not). To calculate the BDCF contributions from these two pathways, it is assumed that the radionuclides are located at the soil surface (SNL 2007a, Section 6.3.2.4, Assumptions 15 and 16).

For noncultivated lands, the assumption of uniform distribution of radionuclide concentration in surface soil is not used. Since the majority of land in the Amargosa Valley is not farmed, but could still be affected by a deposition or redistribution of volcanic tephra, it is assumed that the source of resuspended particulates for calculation of inhalation dose is a thin layer of surface soil, also called the critical thickness, originating in noncultivated land (SNL 2007a, Section 6.5.1.2). The critical thickness is the layer from which particles are resuspended; this is, at most, a few millimeters thick (BSC 2004d, Section 6.8). Radionuclide concentration in this layer, with dimensions of activity per unit mass, is calculated outside the biosphere model by the tephra redistribution model (Section 2.3.11.4) and is the source term for the dose calculations (SNL 2007a, Sections 6.5.1.2 and 6.12.3). The mass radionuclide concentration in the resuspendable layer of soil for noncultivated land is used to calculate the radionuclide concentration in air, which is then used to estimate the inhalation dose.

2.3.10.3.2.2 Air Submodel

The air submodel for the volcanic ash exposure scenario has two components: one accounting for radionuclide concentration in air from resuspension of contaminated soil, and the other one from exhalation of radon gas from contaminated soil (SNL 2007a, Section 6.5.2).

Soil and Ash Resuspension—Radionuclide concentrations in the air were calculated separately for cultivated and noncultivated lands. The concentration of airborne radionuclides associated with cultivated lands was calculated as previously described for the groundwater exposure scenario (Section 2.3.10.3.1.2), but a higher distribution of mass loading representative of postvolcanic conditions was used (range of 0.05 to 0.60 mg/m^3) to account for the increased availability of resuspendable particles in soil following an eruption (BSC 2006, Section 6.3.5). The resulting radionuclide concentration in air was used to calculate the radionuclide activity concentration in crops resulting from deposition of resuspended particles on plant surfaces in the plant uptake submodel. The radionuclide concentration in the air around plants was conservatively

considered to remain high over time, rather than decrease as for the calculation of the inhalation dose described below. This is because the concentration in air around plants is used in the calculation of the ingestion dose, which is not modeled as a function of time (BSC 2006, Section 6.3).

Observations at Mount St. Helens (BSC 2006, Figure 6-9) and other volcanic sites (Gordian et al. 1996; Yano et al. 1990) indicate that concentrations of resuspended particles in air are high following an eruption, and subsequently return to preeruption concentrations within one year or less. This is because ash initially is more readily resuspended than the soil upon which it was deposited. Through time the tephra erodes, becomes mixed into the soil, is buried, or otherwise stabilized. That erosion or stabilization results in a decrease in mass loading, which eventually returns to conditions similar to those measured before the eruption. Because of this change in mass loading through time, the dose resulting from inhalation of resuspended particles following a volcanic eruption was calculated as a function of time (SNL 2007a, Sections 6.3.1.4, 6.5.2.1, and 6.5.8; BSC 2006, Sections 6.3 and 6.4).

Two sets of mass loading distributions and a mass loading time function were developed to model changes over time in the dose resulting from inhalation of resuspended particles (BSC 2006, Sections 6.3 and 6.4). Each mass-loading set had four distributions, one for each of the four RMEI environments where radionuclides could be present (Section 2.3.10.3.1.2). The first set of mass loading distributions was used to calculate the short-term inhalation component of the BDCF. The mass loading values in this set represented the increase in the average concentration of resuspended particulates during the first year after a volcanic eruption relative to the preeruption level. The mass loading time function was then applied to calculate the decrease in the short-term inhalation component for a given year following an eruption. The second set of distributions was representative of conditions after mass loading returned to preeruption levels. This second set of mass loading distributions was used to calculate the long-term inhalation component of the BDCFs, and was the same as that used for the groundwater scenario. To calculate the total dose resulting from inhalation of resuspended particles in a given year, the short-term inhalation dose would be multiplied by the time function for that year and added to the long-term inhalation dose (SNL 2007a, Section 6.5.2.1; BSC 2006, Sections 6.3 and 6.4).

For the active outdoors environment, the average first-year post-eruption mass loading, calculated as the sum of the averages of the short-term and the long-term (nominal) mass loading distributions (BSC 2006, Section 7.1), was 7.3 mg/m^3. The corresponding value for the inactive outdoors environment was 0.16 mg/m^3. The average of the triangular mass loading distribution (BSC 2006, Section 7.1) was calculated as 1/3 of the sum of the mode, the minimum and the maximum values. As discussed in Section 2.3.10.5.2.2, the first year values were recommended to be used for the duration of the first time step in the TSPA model.

Similar to the groundwater exposure scenario, the time spent outdoors was divided between the active and inactive environments. In the active outdoors environment, people would spend their time conducting dust-generating activities, such as plowing, livestock operations, gardening, riding motorbikes, and walking on uncompacted soil or ash. An estimated 50% of time spent working outdoors by the outdoors worker was spent in the active outdoors environment. All the population groups would spend 20% of their time spent outdoors not working in that environment. The remainder of the time outdoors in the contaminated area was spent in the inactive outdoors

environment (i.e., conducting activities that do not actively generate dust, such as walking on pavement or compacted surfaces and driving on paved roads). For the volcanic exposure scenario, time spent in the inactive outdoors environment was longer than that for the groundwater scenario because the commute time in the contaminated area was longer (BSC 2005, Sections 6.3.2.1 and 6.3.2.2).

The parameter distributions representative of mass loading during the first year following a volcanic eruption were developed primarily from concentrations of resuspended particles in air measured before and after the 1980 eruption of Mount St. Helens. Measurements taken following the eruptions of Mount Spurr (Alaska), Mount Sakurajima (Japan), Soufriere Hills (Montserrat), and Cerro Negro (Nicaragua) were also considered to better understand variation and uncertainty in postvolcanic concentrations of resuspended particles (BSC 2006, Section 6.3). Average annual concentrations of resuspended particles in air following those eruptions were no more than twice as high as preeruption levels, and returned to preeruption levels within 1 year or less.

The conditions at the locations where mass loading was measured following the eruption of Mount St. Helens generally were analogous to tephra-deposit thickness and climatic conditions predicted for the area south of Yucca Mountain. Tephra thickness ranged from about 1 to 10 mm at four analogue sites in eastern Washington from which mass loading measurements were considered (BSC 2006, Section 6.3.2.3). This is similar to the thickness of the tephra deposit predicted south of Yucca Mountain if an eruption were to occur (SNL 2007a, Appendix G). For example, tephra depths at the location of the RMEI (18 km from Yucca Mountain, assuming a wind blowing to the south in order to provide a worst-case analysis), were predicted to range from 3.6×10^{-5} to 12.4 cm, based on 100 realizations of the ASHPLUME model (SNL 2007a, Appendix G). Approximately 58% of the predicted depths of deposited tephra were less than 1 cm; 92% were less than 3 cm. Tephra depths at that location under the variable wind conditions would be much lower because the wind at Yucca Mountain blows to the south infrequently.

The climate at the analogue sites in eastern Washington is semi-arid, with the conditions wetter and cooler than the present-day climate in the Yucca Mountain region. Because of the greater annual precipitation and more abundant vegetation, consolidation and removal of tephra at the analogue eastern Washington sites after an eruption would occur faster than that expected at Yucca Mountain under the present-day climatic conditions for the similar fall of tephra (BSC 2006, Section 6.4.3).

There was also uncertainty about comparing measurements of mass loading following eruptions of nonbasaltic volcanoes, such as Mount St. Helens, to basaltic volcanoes of the type typical in the Yucca Mountain region; about the predicted maximum depth of tephra deposits at the location of the RMEI; and about climate and the influence of redistribution of tephra from aeolian and fluvial processes on mass loading (BSC 2006, Section 6.3.2.3). To account for these sources of uncertainty (i.e., uncertainty related to the climatic conditions and uncertainty related to the type of volcanic eruption) and to not underestimate the risk to the RMEI, the maximum values selected for the mass loading distributions were higher than those indicated from the analogue measurements. For example, a maximum increase in the average annual mass loading of 3 mg/m^3 was selected for the active outdoor environment, and was added to the long-term mass loading distribution having a maximum value of 6 mg/m^3 to calculate mass loading in that environment the first year following an eruption. The resulting maximum was comparable to the highest mass loading of about 10 mg/m^3 measured over actively disturbed tephra deposits at Mount St. Helens and on the island of

Montserrat (BSC 2006, Section 6.3.1). Similarly, although data from Mount St. Helens and other eruptions indicated that average annual mass loading outdoors during the year following an eruption would be no more than twice as high as those prior to an eruption, a maximum average annual value of mass loading 3 times greater than nominal conditions was selected for the inactive outdoor environment (BSC 2006, Section 6.3.2). Similar distributions were used for indoor environments. Increasing the maximum values of mass loading distributions accounted for sources of uncertainty associated with analogue data, and ensured that the influence of tephra-deposit thickness on mass loading was incorporated in the biosphere model (BSC 2006, Sections 6.3.1.2, 6.3.2.3, 6.3.3.2, and 6.3.4.2).

The mass loading time function quantified the decrease in mass loading and the associated inhalation dose following an eruption (SNL 2007a, Section 6.5.2.1). An exponential time function, $e^{-\lambda t}$, was used, with λ representing the mass loading decrease rate constant (1/yr) and t equal to time (years) (BSC 2006, Section 6.4). To account for uncertainty about how tephra-deposit thickness would influence the rate at which mass loading would decrease following an eruption, initially separate distributions of the mass loading decrease constant were developed for thin (less than 10 mm) and thick (greater than or equal to 10 mm) deposits (BSC 2006, Section 6.4.3). The distinction between thick and thin deposits was made based on the availability of analogue data for deposits less than 10 mm. The maximum value of the mass loading decrease rate constant (i.e., fastest rate of decrease) for thin deposits was similar to or lower than (i.e., slower rate of decrease) that measured following the eruptions of Mount St. Helens, Mount Spurr, and Mount Sakurajima. Lower (i.e., slower) modal and minimum rates of the distribution of the mass loading decrease rate constant were selected to account for uncertainty about the influence of the climate, differences in particle size distributions between analogue eruptions and those predicted from Yucca Mountain, and the effects of aeolian and fluvial redistribution of tephra into northern Amargosa Valley. If the tephra thickness is greater than 10 mm, it is expected that the mass loading will decrease more slowly than for the thinner tephra deposits. However, no data were available on the rate of change in mass loading in areas having tephra deposits thicker than 10 mm.

For a contaminated layer depth of less than 10 mm, the mass loading decrease rate constant was represented by a triangular probability distribution function with a mode of 0.33/yr, a minimum of 0.2/yr, and a maximum of 2.0/yr. For a contaminated layer depth of 10 mm or more, the mass loading decrease constant was represented by a triangular distribution with a mode of 0.20/yr, a minimum of 0.125/yr, and a maximum of 1.0/yr, which would result in the mass loading decrease rates being lower than those measured following Mount St. Helens and other eruptions (BSC 2006, Section 6.4.3). These lower (i.e., slower) rates were selected to account for the additional uncertainty in the effects of an initial tephra deposit greater than those measured at analogue sites. The maximum of the distribution was equal to the half of that for the thin tephra layer, and the mode was equal to the minimum of the distribution for the thin tephra. The minimum value would result in mass loading more than an order of magnitude higher than for a decay rate constant of 2.0 per year. Therefore, this rate reasonably bounds uncertainty in the effects of differences in conditions between analogue sites and the Yucca Mountain region, including the effects of an initial tephra deposit deeper than 1 cm.

As noted in Section 2.3.10.3.2.1, the tephra redistribution model considered the interchannel divides separately from the distributary channels that carry redistributed tephra. These areas could have a different thickness of tephra, or tephra mixed with soil, and thus different mass loading

decrease rate constants. However, because the thickness of the redistributed tephra in the channels is likely to be greater than the threshold depth of 10 mm, it was reasonable to always use the mass decrease rate constant for the thicker contaminated layer.

The enhancement factors (Section 2.3.10.3.1.2) used in the volcanic ash exposure scenario for the active outdoor environment (range of 0.9 to 9.4) were, in general, higher than that used for the groundwater exposure scenario to account for the resuspension of radionuclides associated with the waste particles, which are denser than the particles of soil. The enhancement factors for other environments were generally lower than those used in the groundwater exposure scenario (SNL 2007b, Table 6-2[a]). These distributions were developed from measurements of enhancement factors taken over disturbed and undisturbed soil containing radionuclides (SNL 2007b, Section 6.5.2.3).

Exhalation of ^{222}Rn from Soil and Tephra—^{222}Rn concentrations in indoor and outdoor air were calculated using the relationship between the concentration of ^{226}Ra in surface soil (containing contaminated tephra), ^{222}Rn flux density from soil, and ^{222}Rn concentration in the air. An assumption was made that all ^{222}Rn produced from decay of ^{226}Ra in contaminated tephra would be released into the air because the predicted tephra layers are relatively thin (SNL 2007a, Section 6.3.2.4, Assumption 15 and Section 6.5.2.2). The assumption of a complete release of ^{222}Rn produced by decay of ^{226}Ra in the tephra or in the contaminated soil involves assuming that the radon emanation coefficient is equal to unity, and that there are no losses during radon transport in soil. The typical radon emanation coefficient values are much less than 1.0. For instance, a default coefficient for soil used in the RESRAD calculation is 0.25 (Yu et al. 2001, Table B-1). The complete exhalation of ^{222}Rn assumed in the biosphere model accounts for the possible differences in the radon emanation properties of contaminated media (soil versus volcanic tephra) and the geometry involved in radon transport in soil (volume versus surface contamination). A ratio of ^{222}Rn concentrations in air to the flux density of ^{222}Rn from soil of 300 Bq/m^3 per Bq/(m^{2}s) was used in the biosphere model. This ratio was based on measurements of flux densities for dry soil relative to concentrations of ^{222}Rn in air (BSC 2004d, Section 6.6.1). Indoor ^{222}Rn concentrations for the volcanic tephra exposure scenario were considered to be the same as outdoor concentrations because there would be very little volcanic tephra indoors compared with the outdoor sources (SNL 2007a, Section 6.5.2.2).

2.3.10.3.2.3 Plant Uptake Submodel

Two transfer pathways were considered in this submodel to calculate radionuclide concentrations in plants consumed by humans and farm animals following an eruptive event through the repository: root uptake from soil and foliar uptake from intercepted resuspended matter. The methods and parameters used to evaluate these transfer pathways in the volcanic ash exposure scenario were the same as those used in the groundwater exposure scenario (Section 2.3.10.3.1.3) because the processes and associated parameter values would not be substantially affected by the shallow tephra deposits predicted to occur south of Yucca Mountain (SNL 2007a, Section 6.5.3; BSC 2004c, Section 6; BSC 2004d, Section 6.2).

2.3.10.3.2.4 Animal Uptake Submodel

The animal uptake submodel considered two pathways for the accumulation of radionuclides in animal products: ingestion of feed and soil. The methods and input parameters used to calculate radionuclide concentrations in animal products were the same as those used for the groundwater exposure scenario, because the processes and associated parameter values would not be substantially affected by the shallow tephra deposits predicted to occur south of Yucca Mountain (Section 2.3.10.3.1.4) (SNL 2007a, Section 6.5.4; BSC 2004d, Section 6.3).

2.3.10.3.2.5 External Exposure Submodel

The methods used to calculate external exposure to radionuclides associated with volcanic tephra were the same as those described in Section 2.3.10.3.1.7, but the effective dose coefficients, distributions of population proportion, and exposure times were different than those used for the groundwater exposure scenario. Dose coefficients for exposure to a contaminated ground surface from *Federal Guidance Report No. 13* (EPA 2002) were used to calculate external exposure to tephra (Table 2.3.10-6) (SNL 2007a, Section 6.5.5.2). These coefficients were selected based on the assumption that, regardless of the predicted thickness of the tephra, radionuclides would be located on the soil surface (SNL 2007a, Section 6.3.2.4, Assumption 16).

Population proportions and exposure times differed from those used for the groundwater exposure scenario because radionuclides could be spread over a larger area following an eruption than would occur as a result of using groundwater for irrigation (BSC 2005, Section 5.1). Because of uncertainty about where tephra from an eruption at Yucca Mountain would fall, the ranges of the distributions for commuters and local indoor and outdoor workers were greater than those for the groundwater exposure scenario. In addition, it was assumed that Amargosa Valley residents who commute 35 minutes or less (versus 10 minutes for the groundwater exposure scenario) would work within areas containing radionuclides from a volcanic eruption at Yucca Mountain. This assumption was based on the likely distribution of tephra following an eruption and the location of centers of employment surrounding the Yucca Mountain region (BSC 2005, Section 5.1). Based on this assumption and data from the 2000 Census (Bureau of the Census 2002, Tables P31, P47, and P49), an average of 12.5% of the population were classified as commuters (range of 4.9% to 16.3%), 5.5% as local outdoor workers (range of 2.9% to 10.7%) and 39.2% as nonworkers (range of 34.4% to 44.0%). The biosphere model calculated the percentage of local indoor workers as the remainder of the population (BSC 2005, Section 6.3.1).

The only differences between exposure times used for the volcanic ash exposure scenario and those from the groundwater exposure scenario were an increase in time spent in the inactive outdoor environment and a decrease in time spent away from the contaminated environment for the volcanic ash exposure scenario. These different exposure times were used because radionuclides would be more widespread, and commute times within the area containing radionuclides would be longer for the volcanic ash exposure scenario (BSC 2005, Sections 6.3.1 and 6.3.2). The average exposure times per environment, weighted by the proportion of the population in each group, were about 0.5 hours per day in the active outdoor environment, 1.6 hours per day inactive outdoors, 10.9 hours per day active indoors, 8.3 hours per day asleep indoors, and 2.7 hours per day away from the area containing radionuclides (SNL 2007a, Section 6.14.5.1).

2.3.10.3.2.6 Inhalation Submodel

Three components of the annual inhalation dose per unit concentration of radionuclides in soil containing contaminated volcanic tephra were calculated. The first component accounted only for the consequences of exposure to resuspended particles at nominal, preeruption concentrations. The second component accounted for the consequences of an incremental increase in inhalation exposure resulting from high concentrations of resuspended particles in air in the first year after an eruption. This component was combined with a function of time to calculate the increase in the inhalation dose in any year after an eruption. The third component was for external exposure, ingestion, and inhalation of radon decay products (SNL 2007a, Section 6.5.6). Population proportions and exposure times used in the calculations were the same as those described in Section 2.3.10.3.2.5 for external exposure (BSC 2005, Sections 6.3.1 and 6.3.2). Other input parameters (dose coefficients, breathing rates, ^{222}Rn equilibrium factor) were the same as those used in the groundwater exposure scenario (Section 2.3.10.3.1.8) (BSC 2005, Sections 6.3.3 and 6.5.3.1; BSC 2004d, Section 6.6.3).

2.3.10.3.2.7 Ingestion Submodel

Ingestion exposure was calculated using the radionuclide concentrations in food stuffs calculated in the plant uptake and animal uptake submodels for the volcanic ash exposure scenario, and the effective dose coefficients and consumption rates described for the groundwater exposure scenario (Section 2.3.10.3.1.9). The methods used to evaluate these exposure pathways in the volcanic ash exposure scenario were the same as those used in the groundwater exposure scenario (SNL 2007a, Section 6.5.7).

2.3.10.4 Model Uncertainty

[NUREG-1804, Section 2.2.1.3.13.3: AC 4; Section 2.2.1.3.14.3: AC 4]

Uncertainty associated with the results of the biosphere model relates to decisions about the inclusion or exclusion of potential pathways in the conceptual model, the use of simplified analytical methods, and representation of parameter values by distributions (SNL 2007a, Section 6.6). Uncertainty in data and model input parameters is described in Section 2.3.10.3. The following two sections describe the uncertainty associated with the conceptual model, including a description of alternative conceptual models, and the mathematical model. The influence of that uncertainty on the resulting range of BDCFs generated by the biosphere model is described in Section 2.3.10.5 (see also SNL 2007a).

2.3.10.4.1 Conceptual Model Uncertainty

The following considerations contributed to the uncertainty associated with the biosphere conceptual model that is described in Section 2.3.10.2 (SNL 2007a, Section 6.6).

Human Receptor—The definitions of the RMEI and reference biosphere in proposed 10 CFR Part 63 substantially reduced uncertainty about the dietary and lifestyle characteristics of the receptor and the selection of environmental transfer and exposure pathways that are applicable to that receptor (SNL 2007a, Sections 6.1.1, 6.1.2 and 6.6.1). Uncertainty about the site-specific

information used to characterize the behavior and other attributes of the RMEI was incorporated into the associated parameter distributions, as described in Section 2.3.10.3.

Environmental Transport of Radionuclides—Interaction matrices (Figures 2.3.10-5 and 2.3.10-7) were used to identify pathways of radionuclide transfer among biosphere model components (environmental media). Important radionuclide transfer mechanisms were considered during development of the biosphere model. The only transfer mechanisms identified in the matrix that were excluded from the model were those shown to have a negligible influence on model results (SNL 2007a, Sections 6.6.1 and 7.4). Therefore, there was little resulting uncertainty due to selection of radionuclide transfer mechanisms in the biosphere model (SNL 2007a, Section 6.6.1).

Consideration of Human Exposure Pathways—Potentially applicable exposure pathways were considered during development of the conceptual model (SNL 2007a, Sections 6.3.1 and 6.3.2). All of those pathways were included in the model, except for those that were shown to have a negligible influence on the model results. For example, water immersion was excluded because the dose for typical exposure times would either be much less than the dose from exposure to contaminated soil, or it would have a negligible contribution to the BDCF (depending on the radionuclide) (SNL 2007a, Section 7.4.8.2). Likewise, air submersion was not included because the dose would be about 5 to 6 orders of magnitude lower than that from soil exposure (SNL 2007a, Section 7.4.8.1). Therefore, decisions regarding inclusion or exclusion of exposure pathways had little effect on uncertainty in the biosphere model results (SNL 2007a, Section 6.3).

Future Conditions—10 CFR 63.305(b) states that the U.S. Department of Energy (DOE) "should not project changes in society, the biosphere (other than climate), human biology, or increases or decreases of human knowledge or technology." Therefore, uncertainty due to changes in the lifestyle and biology of the RMEI, or conditions in the biosphere other than climate, were not considered in the biosphere model (SNL 2007a, Section 6.6.1). The analysis of the BDCF values, while all climate-dependent model parameters were allowed to vary, indicated that BDCF values for the glacial transition and monsoon climates were consistently lower than the corresponding values for the present-day climate (SNL 2007a, Section 6.11.2). The BDCFs for the future climates states were lower than the present-day BDCFs by up to about 25%. If only those climate-dependent parameters that are not affected by human activities are allowed to vary, the differences between the BDCFs for the present-day and the future climate states are negligible.

Alternative Conceptual Models—Because the RMEI and reference biosphere are clearly defined by regulation in 10 CFR 63.312 and proposed 10 CFR 63.305, respectively, and because the biosphere model included all important transfer pathways and exposure pathways, no alternative conceptual models at the system level were identified that could be utilized in place of the biosphere model (SNL 2007a, Section 6.6.1). Other published biosphere system models used in dose assessments are fundamentally the same as the biosphere model in their conceptual approach, which demonstrates that the basic methods of biosphere modeling are similar and generally accepted by the scientific community and regulatory agencies (SNL 2007a, Section 7.2).

Seven alternative conceptual models were identified that apply to the methods used to model specific environmental transport or exposure processes. Conceptual and numerical comparisons of the methods selected in the biosphere model and the alternative methods were made to evaluate the effects of those alternative conceptual models on the results of the biosphere model and the

evaluation of repository performance, and to ensure that all alternative conceptual models that are important to radiation dose assessment have been considered (SNL 2007a, Sections 6.3.3 and 7.4). The evaluation included several criteria, such as consistency with the available data and scientific understanding of the modeled processes, applicability of a model to the conditions in the Yucca Mountain region, representation of the uncertainty, and whether the alternative model could result in an underestimation of the risk to the RMEI. The mathematical model uncertainty was evaluated by comparison of biosphere model results to the results from alternative models at the process or submodel levels. The following alternative conceptual models were evaluated:

1. **Radon Release from Soil (Air Submodel)**—The biosphere conceptual model for radon was based on a radon release factor for radium-contaminated soil. An alternative conceptual model relies on modeling radon transport in the soil and the atmosphere (Yu et al. 2001, Appendix C). The radon release factors calculated by the alternative model are 33% (volcanic ash exposure scenario) to 40% (groundwater exposure scenario) less than those calculated using the biosphere model (SNL 2007a, Section 7.4.3.1. A higher release factor results in a higher BDCF for ^{226}Ra and does not result in underrepresentation of the dose to the RMEI. Because the difference is small relative to more than an order-of-magnitude range of variation in the BDCF for ^{226}Ra (Section 2.3.10.5.1.1), exclusion of this alternative model would have little effect on the biosphere model results or the evaluation of repository performance. The method based on a radon release factor for radium-contaminated soil was selected because it required fewer parameters. The more complex alternative model would yield lower BDCFs, and did not produce results sufficiently different to warrant its implementation (SNL 2007a, Section 7.3.2.2).

2. **Evaporative Cooler Operation (Air Submodel)**—The conceptual model for evaporative coolers selected for implementation in the biosphere model was based on the mechanical operation of evaporative coolers and considered the generation of aerosols, as air is forced through a wet, porous surface. This model uses a very conservative assumption that the fraction of radionuclides in the water transferred to the cooling airflow is, on average, 50%. An alternative conceptual model would be to calculate radionuclide concentrations in air based on differences in absolute humidity between indoor and outdoor air caused by the operation of evaporative coolers. For a given radionuclide release fraction, the alternative model produced radionuclide concentrations in air that were higher by a factor of 2. This, for example, would result in an increase in the BDCF for ^{237}Np of about 34%, and an increase in the BDCF of ^{129}I and ^{99}Tc of 3% or less (SNL 2007a, Section 6.13.4.2.1). These changes in BDCFs are small compared to the approximately order-of-magnitude variation in BDCFs (Section 2.3.10.5.1.1). ^{99}Tc, ^{129}I, and ^{237}Np were chosen in this example because they are significant contributors to the dose to the RMEI (Section 2.4). The method used in the biosphere model was selected because there was less uncertainty in defining the operating parameters of evaporative coolers, such as air flow rate and water evaporation rate, than was required to quantify temporal variation in absolute humidity (SNL 2007a, Section 7.4.3.2). In addition, the process of radionuclide transport in the alternative model involves the water carry-over, which the evaporative coolers are designed to prevent (Section 2.3.10.3.1.2). The method selected for the biosphere model could thus

be used to better represent site-specific conditions and, because of the conservative choice of parameter value, was unlikely to underestimate the risk to the RMEI.

3. **Direct Deposition of Irrigated Water (Plant Uptake Submodel)**—The biosphere model considers radionuclides in irrigation water to be directly translocated into edible plant parts with accumulation and weathering occurring during the entire growing period. An alternative conceptual model would be to consider this process in two steps: movement of deposited radionuclides from external plant surfaces into the plant tissues, and movement of radionuclides from plant tissues into edible parts of the crop. This alternative conceptual model applies weathering to contaminants that remain on external plant surfaces, and also considers food-processing losses (BIOMASS 2003, Section C3.5.4.3). A numerical comparison was made using input values described in Section 2.3.10.3 for the biosphere model, when possible, and using default values for the alternative model when necessary. The alternative model would result in an estimated concentration of radionuclides in plants due to water interception that is two times higher than that predicted by the biosphere model (SNL 2007a, Section 7.4.4.1). This would result in an increase of 12% in the BDCF for ^{129}I, 7% for ^{99}Tc, and 2% for ^{237}Np (SNL 2007a, Section 6.13.4.3). These changes are small relative to the approximately order-of-magnitude variation in BDCFs. The alternative model uses parameters that are not commonly used in environmental transport modeling and are, thus, difficult to quantify. In addition, the alternative model was developed for a temperate climate and implies infrequent irrigation episodes, which are inappropriate for the arid or semiarid conditions at Yucca Mountain (SNL 2007a, Sections 7.3.3.2 and 7.4.4.1).

4. **Direct Deposition of Airborne Particulates (Plant Uptake Submodel)**—In the biosphere model, resuspended soil deposited on crop leaves was treated in the same manner as intercepted irrigation water. Some other published biosphere models (BIOMASS 2003, Section C3.5.4.3) use a soil contamination factor to quantify external contamination of crops. Differences between the biosphere model and this alternative conceptual model were evaluated using the input values described in Section 2.3.10.3 for comparable parameters, and default data from the alternative conceptual model when comparable parameters were not available. The radionuclide concentrations in crops calculated by the alternative model were about 50% lower than those predicted by the biosphere model for all crop types except leafy vegetables. The radionuclide concentration in leafy vegetables was predicted by the alternative conceptual model to be an order of magnitude lower. This difference was because the biosphere model used a high translocation factor for leafy vegetables and forage, whereas the analogous factor in the alternative model was high only for forage. Because leafy vegetables and forage have similar growth forms (i.e., the consumed portion of the plant is aboveground and directly exposed), the same high translocation factor should be used for both. The biosphere model, therefore, was selected because it produces more accurate results (SNL 2007a, Sections 6.3.3, 7.3.3.3, and 7.4.4.3).

5. **Animal Product Contamination (Animal Uptake Submodel)**—The biosphere model calculated radionuclide concentrations in animal products resulting from the consumption of water, soil, and feed. Some environmental radiation models include an

additional transfer pathway: inhalation of radionuclides in air by animals (e.g., BIOMASS 2003, Section C3.5.4.3). These transport pathways were compared numerically to determine their relative importance. It was concluded that the contribution from inhalation of contaminated dust would be about 5 orders of magnitude lower than total concentrations. Therefore, the animal uptake submodel included soil ingestion by farm animals but omitted inhalation of dust (SNL 2007a, Sections 6.3.3, 7.3.4, and 7.4.5).

6. **^{14}C Concentrations in Crops (^{14}C Submodel)**—The methods used in the biosphere model to calculate ^{14}C concentrations in crops were based on experimental results of the release of $^{14}CO_2$ gas from soil (Sheppard et al. 1991; Yu et al. 2001, Section L.3). The biosphere model includes two pathways of ^{14}C transport to plants: direct root uptake and uptake of $^{14}CO_2$ gas into plants during photosynthesis, and six RMEI exposure pathways: external exposure to and ingestion of ^{14}C in soil, inhalation of $^{14}CO_2$ gas, inhalation of ^{14}C in soil particulates, and ingestion of ^{14}C in crops and animal products. At least one alternative biosphere model (Napier, Strenge et al. 2006, p. 4.89) used different methods to calculate ^{14}C concentrations in crops. This alternative model considers uptake into plants only from roots, and uses a very low removal rate of carbon from soil because it does not account for gaseous release of $^{14}CO_2$. The method used by the biosphere model was chosen because it more realistically considers uptake of $^{14}CO_2$ gas into plants, resulting in higher plant concentrations (SNL 2007a, Sections 6.3.3, 7.3.6, and 7.4.7). An additional alternative model for calculating concentrations of ^{14}C in plant and animal products was also proposed (BIOMASS 2000, Appendix A), but was not considered because the default parameter values necessary to run the model have not been developed by the authors of the BIOMASS model and were unavailable (SNL 2007a, Section 7.3.6).

7. **Environment-Specific Inhalation Submodel (Inhalation Submodel)**—In the biosphere model, inhalation exposure was treated as a function of environment and human activity because many of the input parameters (mass loading, breathing rate, exposure time) would be influenced by human activities. Similar models, called microenvironmental models, have been used to assess exposure to particulate matter and other contaminants (Duan 1982; Mage 1985; Klepeis 1999). An alternative method that is commonly used in risk assessments is to use a single value or distribution that is representative of the entire range of people, conditions, and times being modeled. These methods produce the same results if average values used in the biosphere model for each environment are used for the alternative method. The method used in the biosphere model better incorporates variation and uncertainty in input parameters (SNL 2007a, Sections 6.3.3, 7.3.8, and 7.4.9), which is especially important for parameters that vary greatly over the range of conditions being modeled, such as mass loading, which may vary from less than 0.1 mg/m^3 while sleeping to more than 10 mg/m^3 while actively disturbing soil (BSC 2006, Section 6.2).

Based on the conceptual and numerical evaluations summarized above, the methods used in the biosphere model were considered more consistent with available data and scientific understanding than the methods associated with the excluded alternative conceptual models. The alternative models may have resulted in underestimation of risk, were not as applicable to the conditions in the

Yucca Mountain region, or did not adequately incorporate parameter uncertainty (SNL 2007a, Section 7.4). Because the effects of the alternative conceptual models on the biosphere model results were small relative to the total variation of BDCFs, screening of those alternatives did not have an important influence on the evaluation of waste isolation and repository performance and did not affect model uncertainty (SNL 2007a, Sections 6.6.1 and 7.4).

2.3.10.4.2 Mathematical Model Uncertainty

The mathematical implementation of the biosphere model involved calculations of concentrations of radionuclides in environmental media and exposure to the RMEI that would result from a unit concentration of radionuclides in groundwater and soil mixed with volcanic tephra. The biosphere model included the transfer pathways, environmental media, and exposure pathways identified in the conceptual model (Section 2.3.10.2) (SNL 2007a, Sections 6.3.1 and 6.3.2). The biosphere model also included the disposition of the FEPs included in the biosphere model (SNL 2007a, Sections 6.3.4 and 6.7.1).

The mathematical representations of transport and exposure pathways used in the biosphere model were developed from a review of applicable methods in numerous biosphere and radiological assessment models (SNL 2007a, Section 6.6.2). Appropriate methods were chosen from among those reviewed and, if necessary, adapted to match site-specific conditions, the requirements of proposed 10 CFR Part 63, and the needs of the TSPA (SNL 2007a, Sections 6.4, 6.5, 6.6.2, 7.1, and 7.3). For the few processes for which no appropriate method had been previously used (e.g., increase in radionuclide concentrations in fishponds as a result of water evaporation and transfer of radionuclides from water to air during the operation of evaporative coolers), new methods were developed (SNL 2007a, Sections 6.4, 6.5, 6.6.2, 7.3.2.3, and 7.3.5).

The mathematical implementation of these individual transport and exposure pathways in the biosphere model was validated by comparing the computational methods used in the biosphere model to the methods of five published biosphere and radiological assessment models: GENII (Napier, Peloquin et al. 1988; Leigh et al. 1993; Napier, Strenge et al. 2006), BIOMASS ERB2A (BIOMASS 2003), EPRI–Yucca Mountain (EPRI 2002; EPRI 2004), RESRAD (Yu et al. 2001), and NCRP-129 (NCRP 1999). The five validation models were selected because they are commonly used and available, and they are representative of the range of methods used to calculate environmental transport of radionuclides and exposure to radionuclides. Additional models were reviewed but not included in the validation because their methods are similar to those used in the validation models, are not applicable to the Yucca Mountain, or are not commonly used (SNL 2007a, Section 7.1).

To validate the biosphere model, the process-level methods and calculations used in each submodel were compared to the analogous methods and calculations in the validation models (SNL 2007a, Section 7.3). For each environmental transport process or exposure pathway, the comparison focused first on the core part of the submodels, i.e., how a given process is represented conceptually and mathematically in the biosphere model and in the validation models.

Representations of the following processes were evaluated and compared (SNL 2007a, Table 7.3-1):

- Radionuclide buildup in soil as a result of irrigation with contaminated water
- Individual processes that remove radionuclides from the surface soil
- Resuspension of soil
- Radon release from radium contaminated soil
- Radionuclide buildup in indoor air from the operation of evaporative coolers
- Crop contamination due to root uptake
- Direct deposition on crop leaf surfaces due to interception of irrigation water
- Irrigation deposition rate
- Interception fraction of irrigation
- Direct deposition on leaf surfaces due to interception of resuspended soil
- Dust deposition rate
- Interception fraction for resuspended soil
- Animal product contamination due to animal feed
- Animal product contamination due to drinking water
- Animal product contamination due to soil ingestion
- Animal product contamination due to dust inhalation
- Fish contamination due to fishpond water
- ^{14}C special submodel for soil contamination
- ^{14}C special submodel for air contamination
- ^{14}C special submodel for plant contamination
- ^{14}C special submodel for animal product contamination
- External exposure to contaminated soil
- Inhalation dose
- Water ingestion
- Crop ingestion
- Animal product ingestion
- Fish ingestion
- Soil ingestion.

For the vast majority of the processes and pathways, their representations from the published models were mathematically equivalent to those used in the biosphere model, and resulted in approximately the same numerical values (SNL 2007a, Section 7.3). Therefore, there was little uncertainty in the mathematical model of a given process or pathway. For a few process or pathways models, the mathematical representations from the validation models were not equivalent to the one used in the biosphere model. (Most of these models were determined to be alternative conceptual models.) For these models, additional evaluations were conducted that explored the appropriateness of the models for the site-specific conditions, whether the model predictions were consistent with the cautious approach to dose assessment used in the biosphere model, whether the model formulation was supported by the available input parameters, and, finally, how the model results compared with those of the biosphere model. If the methods were numerically the same, or resulted in differences of a factor of 2 or less, it was concluded that there was little uncertainty in the mathematical model of a given process and the methods and calculations were considered validated with no further justification (SNL 2007a, Section 7.1.2). A factor of 2 was chosen because that level of difference in the results of a calculation within a submodel is small relative to the total variation

in BDCFs (Sections 2.3.10.5.1.1 and 2.3.10.5.2.1) (SNL 2007a, Sections 7.1.1, 7.1.2, and 7.1.3). If the methods in one or more of the validation models resulted in a difference of a factor of greater than 2 (in the output of a calculation or submodel), the method that resulted in the least mathematical uncertainty, that best matched the site-specific conditions, and that did not underestimate risk was selected for use in the biosphere model (SNL 2007a, Section 7.1.2). Uncertainty associated with the selected methods was evaluated to ensure that those methods did not result in underestimation of the risk predicted by other models.

As noted above, few of the mathematical methods used by the validation models resulted in a difference of a factor of more than 2 in the results of a calculation, and, in those instances, additional justification for selecting a given method was provided (SNL 2007a, Section 7.4). However, the exclusion of these alternative approaches was primarily based on the advantages of the methods chosen for the biosphere model with regard to the representation of a given process and their relevance, especially from the perspective of site-specificity, rather than the numerical comparisons. In most cases, the results of the process modeling were not significantly affected by the choice of the alternative conceptual model. All potentially significant alternative models identified in the five validation modes have been addressed in Section 2.3.10.4.1. Because the validation models were not significantly different from the biosphere model, it was concluded that the methods used in the biosphere model are well documented and accepted by the scientific community, and that the results are consistent with output from other process-level models (SNL 2007a, Sections 7.3 and 7.4). The differing methods were not incorporated into the biosphere model because they may have resulted in underestimation of risk, were not as applicable to the conditions in the Yucca Mountain region, or did not adequately incorporate parameter uncertainty (SNL 2007a, Section 7.3). Based on the comparisons conducted for model validation, and the information provided elsewhere in Section 2.3.10, it is concluded that there is little uncertainty associated with the mathematical methods used in the biosphere model to calculate BDCFs and that adequate technical basis for the biosphere model has been provided, as required by proposed 10 CFR 63.114(a)(7) (SNL 2007a, Sections 6.6.2, 7.3, and 7.4).

2.3.10.5 Abstraction

[NUREG-1804, Section 2.2.1.3.13.3: AC 5; Section 2.2.1.3.14.3: AC 3(6), AC 5]

The results of the biosphere model in the form of BDCFs, rather than as an abstraction of those results, were directly incorporated into the TSPA. Uncertainty in the supporting data was propagated into the BDCFs for each exposure scenario, as described in Sections 2.3.10.5.1.1 and 2.3.10.5.2.1. The BDCFs were developed and provided to the TSPA as 1,000 correlated sets, each consisting of the BDCF values for individual radionuclides of interest. The BDCFs calculated by the biosphere model for the groundwater and volcanic ash exposure scenarios are described in Sections 2.3.10.5.1 and 2.3.10.5.2, respectively. Those sections also describe the important exposure pathways and input parameters for selected radionuclides, and the methods that were used in the TSPA model to calculate the total annual dose for evaluation of compliance with the individual protection standard (proposed 10 CFR 63.311) and the individual protection standard for human intrusion (proposed 10 CFR 63.321). The results of the biosphere model were directly used in the TSPA model without further abstraction.

Confidence that the results of the biosphere model are consistent with other detailed process-level models of biosphere transport and receptor exposure was gained as follows. First, to validate the

biosphere model, the calculations used in each submodel to represent individual environmental transport and exposure pathways and processes were compared to those used in five other process-level models of biosphere transport and receptor exposure (Section 2.3.10.4.2). The results of the process-level calculations used in those other models were the same, or similar, to the results obtained using the biosphere model (SNL 2007a, Sections 7.3 and 7.4). Second, to verify GoldSim implementation, the results of the biosphere model for representative radionuclides (^{239}Pu, ^{226}Ra, ^{232}Th, and ^{14}C) were compared with the results of spreadsheet calculations—based on equations used in the biosphere mathematical model—and the results were identical (SNL 2007a, Section 6.10).

2.3.10.5.1 Groundwater Exposure Scenario

2.3.10.5.1.1 Biosphere Dose Conversion Factors

The BDCFs for each radionuclide were calculated in 1,000 realizations of the biosphere model, using parameter values described in Section 2.3.10.3. These BDCFs incorporated variation and uncertainty in current conditions at Yucca Mountain. The BDCFs for the mean present-day climate were used in the TSPA model for all climate states expected during the 10,000 year period following repository closure, and for the period beyond 10,000 years within the period of geologic stability prescribed by proposed 10 CFR 63.311 and 63.321 (SNL 2007a, Section 6.11.3). Such an approach is reasonably conservative for the dose assessment and is appropriate for wetter climate conditions.

Consideration of Climate Change—10 CFR 63.305(b) provides that:

> DOE should not project changes in society, the biosphere (other than climate), human biology, or increases or decreases of human knowledge or technology. In all analyses done to demonstrate compliance with this part, DOE must assume that all of those factors remain constant as they are at the time of license application submission.

In contrast to the direction not to project changes in society, the biosphere, human biology, or human knowledge or technology, proposed 10 CFR 63.305(c) directs the DOE to vary factors related to climate. Because BDCFs are a function of climate factors that depend on human activities and those that do not, the effect of climate change (FEP 1.3.01.00.0A) on BDCFs for the groundwater exposure scenario needed to be evaluated from the perspective of these two requirements. Under wetter climatic conditions, agricultural activities in the region around the Yucca Mountain site would rely less on irrigation using well water, and the contribution to the RMEI dose from contaminated food and some other pathways would presumably be lowered or perhaps eliminated (70 FR 49014, p. 49,023).

To investigate the effect of the climate change on the BDCFs, the biosphere model was constructed with a range of climates from arid to semi-arid (SNL 2007a, Section 6.11.1.2.2). The modeling of the climate in the arid to semi-arid range is addressed in the biosphere model through model input parameters. The conceptual and mathematical structures of the biosphere model remain the same. The influence of the climate-dependent parameters on the BDCFs was evaluated by determining correlations between the BDCFs and the climate-dependent parameters that were allowed to vary over the range of values characteristic for the present-day and future climate states (monsoon and

glacial transition climates). The results of this analysis indicated that almost all the climate-dependent parameters that have influence on the BDCFs involve human actions and are related to the amount of water usage for irrigation and for evaporative cooling. There was practically no correlation between the BDCFs and climate-related parameters that could be considered independent of human activities (SNL 2007a, Section 6.11.1.2.2). This finding was important because of the 10 CFR 63.305(b) and proposed 10 CFR 63.305(c) requirements to vary in the performance assessment the factors that are related to climate but to keep the factors related to the society constant.

The magnitude of the effect that climate change would have on the BDCFs, if the whole set of climate-dependent parameters were allowed to vary with climate, was also evaluated and the BDCFs for the present-day, monsoon, and glacial transition climates were compared (SNL 2007a, Table 6.11-12). The BDCFs for the future climates states were lower than the present-day BDCFs by 3% to about 25%.

The climate-related factors that have the largest effect on the BDCFs depend on human activities, and the BDCFs are relatively insensitive to other climate-dependent factors that are independent of human activities. Furthermore, the BDCFs for the future climate, which is predicted to be cooler and wetter than the present-day climate (BSC 2004a), are lower than the corresponding present-day climate BDCFs and would result in lower doses to the RMEI. Therefore, using the present-day climate BDCFs represents a suitable balance between the requirements of 10 CFR 63.305(b) and proposed 10 CFR 63.305(c), meets the requirements of 10 CFR 63.305(a) and (b), and is appropriate for the assessment of doses to the RMEI for the 10,000 year period following repository closure and for the period beyond 10,000 years, within the period of geologic stability prescribed by proposed 10 CFR 63.311 and 63.321 (SNL 2007a, Section 6.11.3).

Modeling Results—For the groundwater exposure scenario, 1,000 sets of BDCFs were calculated for 1,000 realizations of the biosphere model (SNL 2007a, Section 6.11). For each realization, the same radionuclide-independent input parameter values were used to calculate BDCFs for all radionuclides, thereby capturing the inherent correlation among radionuclides within each set of BDCFs. The results were stored in a two-dimensional array containing the BDCFs for all primary radionuclides and for all model realizations. The sets of BDCFs were sampled randomly within the TSPA model to propagate uncertainty from the biosphere model into the TSPA dose calculations. Therefore, the results of the biosphere model, rather than an abstraction of those results, were incorporated into the TSPA model (SNL 2007a, Section 6.11.3). The summary statistics for the BDCFs for the groundwater exposure scenario are presented in Table 2.3.10-12.

BDCFs generally were lowest for radionuclides with low atomic numbers and increased with increasing atomic number (Figure 2.3.10-11). The lowest average BDCF was for ^{99}Tc; the highest BDCFs were for ^{226}Ra. The difference between the lowest and highest BDCFs was over 4 orders of magnitude. The total range of variation in BDCFs for most radionuclides was about 1 to 2 orders of magnitude. Among the primary radionuclides, ^{79}Se had the greatest range, extending over about 2.6 orders of magnitude, and the range for ^{228}Ra is only 0.4 orders of magnitude (a factor of about 2.6). The range from the 5th to the 95th percentile was much narrower, spanning from a factor of 1.6 for ^{228}Ra to about a factor of 13.4 for ^{79}Se (Figure 2.3.10-11) (SNL 2007a, Section 6.13.1).

Ingestion of water was the dominant exposure pathway for several radionuclides, including ^{99}Tc, and ^{129}I. The relative importance of other exposure pathways varied among radionuclides (Table 2.3.10-11). Ingestion of crops (primarily leafy vegetables and fruits) and animal products (milk and eggs) were important pathways for ^{99}Tc and ^{129}I. For all radionuclides with the mass number equal to or greater than 89 (i.e., isotopes of actinium and heavier elements), inhalation of particulate matter and aerosols generated by evaporative coolers were important pathways (Table 2.3.10-11) (SNL 2007a, Section 6.13.2).

Correlation coefficients between BDCFs and stochastically sampled input parameters were calculated to identify the parameters that have the greatest influence on the results of the biosphere model (Table 2.3.10-13). Because the ingestion rate of water was constant at 2.0 L per day, as required by 10 CFR 63.312(d), no parameters related to this exposure pathway appear in this analysis (SNL 2007a, Section 6.13.3). The following is a summary of the important exposure pathways and input parameters for the radionuclides that are likely to contribute substantially to the annual dose calculated to demonstrate compliance with the postclosure individual protection standard.

^{99}Tc—Consumption of water contributed 42% of the average BDCF for ^{99}Tc. The remainder was from consumption of crops (about 17%) and animal products (about 39%, including fish) (Table 2.3.10-11; SNL 2007a, Table 6.13-1). Because the water ingestion contribution to BDCFs was fixed, variation in the BDCF for this radionuclide was almost entirely from the food ingestion exposure pathways. Mean contributions from inhalation and external exposure were about 1 and 4 orders of magnitude lower, respectively, than that from ingestion (SNL 2007a, Figure 6.13-7). Root uptake was the most important pathway of ^{99}Tc transport to crops, contributing on average about two-thirds of the ^{99}Tc concentration in crops; deposition of irrigation water contributed one-third (SNL 2007a, Section 6.13.4.3). 89% or more of the ^{99}Tc concentration in animal products was from consumption of feed (SNL 2007a, Section 6.13.4.4).

The relative contribution from ingestion of crops and animal products generally was higher for the products with the largest consumption rates (e.g., leafy vegetables and fruit: see Section 2.3.10.3.1.9). However, those consumption rates had little influence on the variation in BDCFs. For example, doubling the average consumption rate of locally produced foods (with all other parameter values held constant) increased the BDCF for ^{99}Tc by about 21% (SNL 2007a, Section 6.13.5.1).

The model input parameters having the highest correlations with BDCFs for ^{99}Tc were the overwatering rate, transfer factors, transfer coefficients, and distribution coefficient (Table 2.3.10-13) (SNL 2007a, Section 6.13.3). The overwatering rate and distribution coefficient controlled the rate of removal of ^{99}Tc from surface soil by leaching. The transfer factors and transfer coefficients influenced the bioaccumulation of ^{99}Tc in crops and animal products, respectively. The values of most of these parameters spanned several orders of magnitude, but individually did not cause large changes to the model results. For example, order-of-magnitude changes in each of these parameter values resulted in changes in the BDCF for ^{99}Tc of about a factor of 2 or less (SNL 2007a, Figures 6.13-14, 6.13-25, and 6.13-29).

^{129}I—Drinking of water contributed 60% to the average BDCF for ^{129}I. Because of the large contribution from this fixed model component, the distribution of BDCFs for ^{129}I is relatively

narrow (Figure 2.3.10-11). Much of the remaining contribution was from ingestion of animal products (28%) with smaller amounts from consumption of crops (6%) and fish (5%) (Table 2.3.10-11; SNL 2007a, Table 6.13-1). Mean contributions from inhalation and external exposure were about 3 orders of magnitude lower than contributions from ingestion and did not influence the variation in the BDCF of ^{129}I (Table 2.3.10-11) (SNL 2007a, Figure 6.13-7).

Similar to ^{99}Tc, the overwatering rate and transfer coefficient were strongly correlated with the BDCF for ^{129}I. The weathering half-life was also an important contributor to the BDCF uncertainty. The parameters that quantified the transfer of this radionuclide to crops, particularly those consumed by animals, and to animal products from other environmental media, also were important (Table 2.3.10-13) (SNL 2007a, Section 6.13.3).

In contrast to ^{99}Tc, deposition of irrigation water was the most important pathway of ^{129}I transport to crops, contributing an average of about 78% of its concentration in crops. Concentrations in meat and milk were primarily from feed consumption. About 64% of the ^{129}I concentration in poultry and eggs was from feed consumption, and about 26% was from soil consumption (SNL 2007a, Sections 6.13.4.3 and 6.13.4.4).

^{234}U—Ingestion of water and inhalation were the dominant exposure pathways for this radionuclide, with inhalation of particulate matter contributing 22% of the average BDCF. The contribution from inhalation of aerosols from evaporative coolers was 23%; the contribution from drinking water was 44%. Ingestion of food contributed about 10% (Table 2.3.10-11) (SNL 2007a, Section 6.13.2).

Variation in the distribution coefficient accounted for a significant fraction of the variance in the BDCF for ^{234}U. This parameter controlled the level of radionuclide concentration in the soil, and thus had a direct effect on the dose from inhalation of particulate matter. The distribution coefficient had an exceptionally large range for uranium, spanning six orders of magnitude from the 1st to 99th percentile. Even though ingestion of locally grown food is not a major pathway for ^{234}U (Table 2.3.10-11; SNL 2007a, Table 6.13-3), the BDCF for this radionuclide was correlated with soil-to-plant transfer factors. This was due to the correlation between distribution coefficients and transfer factors used in the biosphere model. The BDCF for ^{234}U is also correlated with the parameters used in calculation of inhalation exposure from evaporative coolers and parameters that influenced the level of activity concentration of this radionuclide in surface soil, such as the erosion rate and the overwatering rate (Table 2.3.10-13) (SNL 2007a, Section 6.13.3).

Mass loading and the enhancement factor for the active outdoor environment also were correlated with the BDCF for ^{234}U (Table 2.3.10-13). These parameters were correlated only for the active outdoor environment because the majority of the dose for actinides from inhalation of particulate matter occurred in that environment (SNL 2007a, Section 6.13.5.2.1).

^{237}Np—For ^{237}Np, inhalation of aerosols from evaporative coolers was the most important exposure pathway, accounting for 36% of the BDCF contribution. This was the highest contribution from this pathway of all the primary radionuclides. Inhalation was the most important exposure pathway overall, with inhalation of particulate matter contributing additional 21% of the BDCF. Water consumption accounted for 29% of the average BDCF. Ingestion of food contributed

about 7%; external exposure also contributed about 7% of the BDCF (Table 2.3.10-11) (SNL 2007a, Section 6.13.2).

The highest BDCF correlation coefficient for ^{237}Np was for the evaporative cooler water transfer fraction; evaporative cooler water usage rate was also an important contributor to the BDCF uncertainty. The BDCF for ^{237}Np was correlated with the parameters that control radionuclide concentration in the soil, such as the distribution coefficient, overwatering rate, and irrigation duration, and also with the parameters that control radionuclide concentration in the air, such as the mass loading and the enhancement factor for the active outdoor environment (Table 2.3.10-13) (SNL 2007a, Section 6.13.3).

^{239}Pu—Inhalation of particulate matter was the most important pathway for ^{239}Pu, accounting for about 51% of the average BDCF. Inhalation of aerosols generated by evaporative coolers contributed 25%, followed by consumption of water, with 19% contribution. Consumption of locally produced foods accounted for only about 5%, and external exposure was negligible (Table 2.3.10-11) (SNL 2007a, Section 6.13.2).

Because the water ingestion pathway contribution to BDCFs was fixed, the uncertainty in the BDCF for ^{239}Pu was primarily from variation in the air and inhalation submodels input parameters. The highest correlation coefficients for the BDCFs were with the distribution coefficient and the evaporative cooler water transfer fraction. The dose from inhalation of particulate matter for this and all other radionuclides would accrue primarily in the active outdoor environment, because the concentration of resuspended radionuclides in air would be much higher there than in other environments. Thus, the model input parameters that were used to calculate doses from this pathway, such as mass loading and the enhancement factor in the active outdoor environments, activity budgets, and some population proportions, were correlated with the BDCF for ^{239}Pu. The BDCF calculated for the mass loading in the active outdoor environment at the maximum of the distribution (and keeping all other parameter values constant) was 48% greater than the average BDCF for ^{239}Pu (SNL 2007a, Section 6.13.4.2.2). The BDCF for this radionuclide was also correlated with parameters that control its rate of accumulation and loss from soil (distribution coefficient, soil erosion rate, and irrigation duration) (Table 2.3.10-13) (SNL 2007a, Section 6.13.3).

2.3.10.5.1.2 Individual Protection Standards Dose Calculations—Groundwater Exposure Scenario

To evaluate compliance with the requirements of proposed 10 CFR 63.311 for the individual protection standard after permanent closure, and proposed 10 CFR 63.321 for the individual protection standard for human intrusion, the total annual dose from exposure to radionuclides in groundwater was calculated in the TSPA model as the sum of the products of radionuclide-specific BDCFs and time-dependent activity concentrations of radionuclides in the groundwater at the accessible environment:

$$D_{total}(t) = \sum_i BDCF_i \cdot Cw_i(t) \qquad \text{(Eq. 2.3.10-1)}$$

where

$D_{total}(t)$ = time-dependent total annual dose to the RMEI resulting from the release of radionuclides from the repository; this includes contributions from all radionuclides considered in the TSPA model (Sv/yr)

$BDCF_i$ = biosphere dose conversion factor for radionuclide *i* (Sv/yr per Bq/m^3)

$Cw_i(t)$ = time dependent activity concentration of radionuclide *i* in the groundwater (Bq/m^3).

This equation was based on the linear relationship between radionuclide concentrations in groundwater and the resulting doses. The calculation of the total dose in the TSPA model used the set of BDCFs for the present-day climate state (SNL 2007a, Sections 6.4.10.4 and 6.11.3).

2.3.10.5.2 Volcanic Ash Exposure Scenario

2.3.10.5.2.1 Biosphere Dose Conversion Factors

As noted previously, the results of the biosphere model were directly used in the TSPA model without further abstraction. For the volcanic ash exposure scenario, the biosphere model produced three BDCF components for each radionuclide. The first component accounted for exposure to sources external to the body, ingestion, and inhalation of radon decay products. The second and third BDCF components accounted for inhaling airborne particulates. The short-term inhalation component represented inhalation exposure during the first year following a volcanic eruption. This term was used together with the time function, as described in Section 2.3.10.3.2.2, to calculate short-term increase in inhalation exposure, due to elevated levels of airborne particulate matter, after a volcanic eruption, relative to the conditions existing before and long after an eruption. With time, mass loading would return to the preeruption level. These conditions were described by the long-term inhalation component, which represented exposure from inhalation of resuspended particulates under nominal conditions (i.e., when the mass loading was not elevated as the result of volcanic eruption) (Section 2.3.10.2.6) (SNL 2007a, Section 6.12.3). For each realization of the model, the same radionuclide-independent input parameter values were used to calculate BDCFs for all radionuclides, thereby capturing the inherent correlation in BDCFs among radionuclides. The results of the BDCF calculations were stored as a two dimensional array containing 1,000 rows: one for each model realization. Each row contained the complete set of three BDCF components for all primary radionuclides. The sets of BDCFs were randomly sampled in the TSPA model to calculate the total expected annual dose. Therefore, the direct results of the biosphere model, rather than an abstraction of those results, were incorporated into the TSPA model (SNL 2007a, Section 6.12.3). The mean values of the three BDCF components are listed in Table 2.3.10-14.

The BDCF components for inhalation of airborne particulates (long term and short term inhalation) were calculated using a different source term (1 Bq/kg) than that used to generate the BDCF component accounting for external exposure, ingestion, and inhalation of radon decay products (1 Bq/m^2). To evaluate the relative significance of the exposure pathways arising from the volcanic releases of the radionuclides, an assumption about the depth distribution of radionuclides in the soil was made. This assumption is not used in the TSPA model; it was made to facilitate pathway

comparison for all the exposure pathways included in the BDCF components for the volcanic ash exposure scenario. It was assumed that the distribution of radionuclide concentration in the surface soil was uniform (SNL 2007a, Section 6.14.2). Such an assumption was appropriate for the agricultural land, where the surface soil would be mixed by plowing. For the undisturbed soil, the radionuclide concentration would generally be greater at the soil surface, especially immediately after the fallout. However, with time, the diffusion processes would cause downward migration of the radionuclides through the soil profile. This process is modelled by the FAR tephra redistribution model, as described in Section 2.3.11.4. The percent pathway contributions under such conditions are provided in Table 2.3.10-15. The dominant pathways for almost all radionuclides are inhalation and external exposure. ^{99}Tc, ^{129}I, and ^{210}Pb are the only radionuclides with a significant contribution from the ingestion of contaminated food products and soil. For most of the radionuclides with the atomic number of 89 or greater, inhalation of particulates accounts for the majority of the dose. External exposure is the most important pathway for several radionuclides, including ^{90}Sr, ^{126}Sn, ^{137}Cs, ^{228}Ra, ^{228}Th, ^{235}U, and ^{238}U.

Variability in the BDCF component for ingestion, inhalation of radon decay products, and external exposure differed greatly among radionuclides (Figure 2.3.10-12). Radionuclides that had a large contribution from external exposure (Table 2.3.10-14) had a very small BDCF range. For example, this BDCF component varied only by a factor of 1.3 for ^{137}Cs. Variation in external exposure was low because the radionuclide concentration in soil did not vary in the biosphere model for the volcanic ash exposure scenario (it was the source term for this model). The modeling of processes that result in transport, deposition, and redistribution of radionuclides released from the repository during a volcanic eruption to the location of the RMEI is described in Section 2.3.11.4. Variability in the ingestion, inhalation of radon decay products, and external exposure BDCF component for some other radionuclides was much greater (Figure 2.3.10-12). For example, for ^{239}Pu, this component varied by a factor of about 10 from the 5th to the 95th percentile and by a factor of about 72 over the entire range (SNL 2007a, Section 6.14.1).

The only radionuclide-specific input parameter used in the calculation of the short-term and long-term inhalation components was the inhalation dose coefficient. Because this parameter was treated as a fixed value, variation in these BDCF components was the same for all radionuclides (Figures 2.3.10-13 and 2.3.10-14). The short-term inhalation component varied by a factor of 6.4 from the 5th to the 95th percentile, and by a factor of 23 over the entire range. The corresponding values for the long-term inhalation component were factors of 6.7 and 29 respectively (SNL 2007a, Section 6.14.1).

Table 2.3.10-16 lists the input parameters that were correlated with the BDCF component for ingestion, inhalation of radon decay products, and external exposure for the radionuclides. Table 2.3.10-17 lists the input parameters that were correlated with the short-term and long-term inhalation BDCF components. The correlation results in that table were the same for all radionuclides, because the stochastically sampled parameters that were used to calculate these BDCF components were radionuclide independent (SNL 2007a, Section 6.14.3). The following is a summary of the important exposure pathways and input parameters for the radionuclides that are either likely to contribute to the annual dose calculated to demonstrate compliance with the postclosure individual protection standards, or have distinct exposure pathways, unlike the other radionuclides.

^{90}Sr—The pathway contributions for ^{90}Sr were diverse, with about 79% of the total BDCF (for the conditions specified above) from external exposure, 14% from ingestion of crops, and 6% from ingestion of animal products (Table 2.3.10-15) (SNL 2007a, Table 6.14-2). Over 97% of the concentration of ^{90}Sr in crops was from root uptake. About 96% of the concentration in meat and milk, and 65% in poultry and eggs, was from feed consumption, with the remainder from consumption of soil (SNL 2007a, Sections 6.14.4.3 and 6.14.4.4).

The ^{90}Sr BDCF component for ingestion, inhalation of radon decay products, and external exposure was strongly correlated with soil-to-plant transfer factors. The BDCF for ^{90}Sr also had a relatively strong negative correlation with surface soil depth, which was used to calculate the radionuclide concentration in cultivated soil, and with the distribution coefficient. The distribution coefficient was included in the mathematical model for the volcanic ash exposure scenario only to control the correlation among transfer factors (Table 2.3.10-16). The parameters that had the greatest influence on variation in the inhalation BDCF components for ^{90}Sr were the same as those described below for actinides (SNL 2007a, Section 6.14.3).

^{137}Cs—Almost 99% of the dose from this radionuclide was from external exposure (Table 2.3.10-15) (SNL 2007a, Table 6.14-2). Because the concentration of radionuclides in soil was constant in the biosphere model, variation in this pathway was only influenced by the duration and conditions of exposure to contaminated soil. Thus, the parameters having the highest correlation coefficients for ^{137}Cs were those that influence the population-weighted time spent in the potentially contaminated environments, such as the proportion of outdoor workers and commuters in the population and the exposure times by nonworkers and indoor workers (Table 2.3.10-16). Although consumption of crops was an unimportant pathway for ^{137}Cs, soil-to-crop transfer factors, soil depth, and the distribution coefficient were correlated with the BDCF component for ingestion, inhalation of radon decay products, and external exposure. This was because the variation in those input parameters was large relative to variation in the input parameters used to calculate external exposure (SNL 2007a, Section 6.14.3).

Plutonium Isotopes and ^{241}Am—The dose for isotopes of plutonium and for ^{241}Am for this exposure scenario was almost exclusively from inhalation of particulate matter (short-term and long-term inhalation) (Table 2.3.10-15) (SNL 2007a, Table 6.14-2). 75% or more of that inhalation dose was accrued in the active outdoor environment (SNL 2007a, Section 6.14.5.1), and air mass loading and the enhancement factor in that environment were strongly correlated with the inhalation BDCF components (Table 2.3.10-17). An increase in mass loading in the active outdoor environment resulted in almost a proportional increase in the inhalation BDCF components (SNL 2007a, Section 6.14.4.2). The proportion of outdoor workers in the population and the time spent outdoors by nonworkers and indoor workers (the largest population groups) were also correlated with the inhalation BDCF components (Table 2.3.10-17) (SNL 2007a, Section 6.14.3).

2.3.10.5.2.2 Individual Protection Standard Dose Calculations—Volcanic Ash Exposure Scenario

The following expression, which combines the source terms (calculated in the TSPA model) and the BDCFs (provided by the biosphere model), was used to calculate the annual dose to the RMEI from a volcanic eruption, conditional upon an eruption occurring (SNL 2007a, Section 6.12.3):

$$D_{allpathway,i}(t,T) = BDCF_{ext,ing,Rn,i}Cs_i(t) + (BDCF_{inh,v,i}f(t-T) + BDCF_{inh,p,i})Cs_{mc,i}(t) \quad \text{(Eq. 2.3.10-2)}$$

where

$D_{all\ pathway,\ i}\ (t,T)$ = all-pathway annual dose for primary radionuclide i at time t (yr) after the repository closure, conditional on a volcanic eruption at time T (yr) (Sv/yr)

$BDCF_{ext,ing,Rn,i}$ = BDCF component for external exposure, ingestion, and inhalation of radon decay products for primary radionuclide i (Sv/yr per Bq/m^2)

$Cs_i(t)$ = areal radionuclide concentration in a specified depth of surface soil at time t (yr) after the repository closure (Bq/m^2) calculated in the TSPA model

$BDCF_{inh,v,i}$ = BDCF component representing the average inhalation exposure in excess of the long-term inhalation exposure in the first year after a volcanic eruption; used in calculation of short-term inhalation exposure at post eruption level of mass loading above nominal mass loading for primary radionuclide i (Sv/yr per Bq/kg)

$BDCF_{inh,p,i}$ = BDCF component for long-term inhalation at nominal level of mass loading for primary radionuclide i (Sv/yr per Bq/kg)

$f(t–T)$ = decay function describing the reduction of the annual average mass loading with time at time t-T following a volcanic eruption

$Cs_{mc,i}(t)$ = activity concentration of radionuclide i per unit mass of soil in the resuspendable layer of surface soil (critical thickness) at time t (yr) after the repository closure calculated in the TSPA model (Bq/kg).

The time-dependent areal radionuclide concentration in surface soil, $Cs_i(t)$, represents radionuclide activity integrated over the tillage depth. The tillage depth is a stochastic biosphere model parameter

that was also provided as input to the TSPA model to allow calculation of soil depth-integrated radionuclide concentration per unit surface area of the soil (SNL 2007a, Section 6.12.3).

The time-dependent radionuclide activity concentration per unit mass, $Cs_{mc,i}(t)$, was calculated by averaging mass radionuclide concentration over the depth of the resuspendable layer of soil (critical thickness). The critical depth (i.e., the depth of surface soil layer that is available for resuspension), was represented by the uniform distribution, with a minimum of 0.001 m (1 mm) and a maximum of 0.003 m (3 mm) (SNL 2007a, Section 6.12.3).

Both source terms used in the calculation of doses (Equation 2.3.10-2) (i.e., the areal radionuclide concentration in surface soil, $Cs_i(t)$) and the mass radionuclide concentration in the resuspendable soil layer, $Cs_{mc,i}(t)$, were calculated in the TSPA model by weighting the appropriate radionuclide concentrations by the respective expected areas of the distributary channels and the interchannel divides at the location of the RMEI (SNL 2007a, Section 6.12.3). The radioactive waste mass concentration in the resuspendable layer of soil, $Cs_{mc,i}(t)$, was determined from the results of the ASHPLUME and FAR models. These models produced the results in terms of contaminant concentration in soil per unit volume. The concentration per unit volume was converted to concentration per unit mass by dividing it by the density of the resuspendable layer, ρ_c. In the interchannel divides, the density of the resuspendable layer, ρ_c, can be calculated from the known tephra thickness, d_a, and density, ρ_a, and surface soil density, ρ_s, as (SNL 2007a, Section 6.12.3)

$$\rho_c = \frac{d_a\rho_a + (d_c - d_a)\rho_s}{d_c} \quad \text{when } d_a < d_c \text{ and} \qquad \text{(Eq. 2.3.10-3)}$$

$$\rho_c = \rho_a \quad \text{when } d_a \geq d_c$$

where

ρ_c = bulk density of resuspendable layer of surface soil, including volcanic tephra (kg/m^3)

d_c = thickness of resuspendable soil layer; i.e., the critical thickness (m)

d_a = thickness of initial tephra layer (m)

ρ_a = bulk density of volcanic tephra (kg/m^3)

ρ_s = bulk density of the surface soil (without tephra) (kg/m^3).

The TSPA model kept track of the radionuclide activity concentration per unit mass of waste, and apportioned the correct activity of each radionuclide to the known waste concentration in the surface soil. In the channels, where the tephra is mixed with soil and diluted, the density of resuspendable layer, ρ_c, was approximated by the density of soil, ρ_s (SNL 2007a, Section 6.12.3).

Because of the anticipated decrease in airborne particulate concentration over time, the dose from inhalation of airborne particulates was a function of time after a volcanic eruption. This was

accomplished by multiplying the BDCF component representing the first year dose from inhalation of particulates, $BDCF_{inh,v,i}$, by the mass loading decrease function. The term $BDCF_{inh,v,i}$ represented inhalation exposure in excess of the nominal, steady-state (i.e., at pre-eruption mass loading levels) inhalation exposure (SNL 2007a, Section 6.12.3). The function of time, $f(t\text{-}T)$, in Equation 2.3.10-2, thus accounted for the reduction of mass loading in the years immediately following volcanic eruption (occurring at time T). Mass loading was assumed to decrease exponentially with time after the eruption ($t > T$) as (SNL 2007a, Section 6.12.3)

$$f(t - T) = e^{-\lambda(t - T)} \qquad \text{(Eq. 2.3.10-4)}$$

where

λ = mass loading decrease rate constant (1/yr)

T = time of a volcanic eruption (yr); $t–T = 0$ represents the first year after a volcanic eruption.

The mass loading decrease rate constant (λ in Equation 2.3.10-4) depends on the tephra thickness, and was initially developed for two tephra thicknesses less than 10 mm and equal to or greater than 10 mm. As described in Section 2.3.10.3.2.2, it was recommended that the mass loading decrease rate constant for the thicker tephra be used in the TSPA model at all times (SNL 2007a, Section 6.12.3).

In the TSPA model, calculations of the expected dose to the RMEI are carried out in a series of time steps. The mass loading decrease function is thus calculated for every time step. The value of the mass loading decrease function for a given time step was that for the time beginning that time step, to ensure that the annual dose for the first year in a time step is not systematically underestimated. For example, in the case of the first time step after an eruption, $t–T = 0$, representing the first year after a volcanic eruption, would be used to calculate $f(t–T)$ (Equation 2.3.10-4) for the entire duration of the first time step.

The total annual conditional dose at time $t–T$ after a volcanic eruption, and time t after repository closure, was then calculated as the sum of all-pathway doses for individual primary radionuclides included in the TSPA model, including their decay products (SNL 2007a, Section 6.12.3):

$$D_{total}(t, T) = \sum_{i} D_{allpathway,\,i}(t, T) \qquad \text{(Eq. 2.3.10-5)}$$

where

$D_{total}(t,T)$ = total annual dose from all radionuclides at time $t–T$ after a volcanic release of radionuclides from the repository at time t after repository closure (Sv/yr)

$D_{all\ pathway,i}\ (t,T)$ = all-pathway annual dose for primary radionuclide *i* at time *t*–*T* after a volcanic release of radionuclides from the repository at time *t* after repository closure (Sv/yr).

2.3.10.6 Conclusions

The biosphere model simulates the features and processes that contribute to the transport of radionuclides within the reference biosphere and the dose received by the RMEI. Because the biosphere model only addresses features and processes in the accessible environment outside of the repository system boundary, it provides no information regarding the capability of the natural or engineered barriers to reduce or prevent the flow of water or the movement of radionuclides at Yucca Mountain.

The biosphere model considers two modes of radionuclide release from the repository: in groundwater drawn from wells and in volcanic tephra deposited in the reference biosphere by a volcanic eruption through the repository. For each of these release modes, an exposure scenario is developed and the BDCFs are calculated. The BDCFs calculated for the groundwater exposure scenario are applied to the TSPA scenarios and cases that consider radionuclide release to groundwater. The BDCFs for the volcanic ash exposure scenario are applied in the TSPA model to the volcanic eruption modeling case of the igneous scenario class. The biosphere model provides BDCFs to the TSPA model for use in calculating annual dose to the RMEI.

The biosphere modeling component is the final component of the TSPA model, and is designed to incorporate the characteristics and physical processes of the biosphere into an analysis of potential doses resulting from radionuclide releases from the repository at Yucca Mountain. The characteristics of the environment that may affect pathways of radionuclide transport were incorporated in the biosphere model through the construction of conceptual and mathematical models of the reference biosphere, as well as through model parameters that characterize climate, soil, communities, agriculture, and other conditions in the region surrounding the Yucca Mountain site (Section 2.3.10.2.1). The characteristics of the population of the Town of Amargosa Valley were manifested in the biosphere model through consideration and representation of the exposure pathways of the RMEI, and through model parameters that characterize the lifestyle, diet, and metabolic and physiological considerations of the RMEI (Section 2.3.10.2.2). The parameters that quantify the diet and living style of the RMEI were developed based on information from surveys of the people who reside in Amargosa Valley.

Processes important to environmental transport pathways for radionuclides are simulated in the biosphere model for both the groundwater exposure scenario and the volcanic ash exposure scenario (Sections 2.3.10.2.3 and 2.3.10.2.4). These include radioactive decay, radionuclide transport in water, soil and air, uptake by crops consumed by animals or humans, and uptake by animals or farm-raised fish. Transport of ^{14}C, a gaseous radionuclide, and ^{222}Rn and its decay products, were also included. These processes result in contamination of environmental media in the reference biosphere, and the dose to the RMEI by inhalation, ingestion, and external exposure. The BDCFs calculated by the biosphere model represent the all-pathway annual dose for the groundwater exposure scenario (Section 2.3.10.5.1) and the volcanic ash exposure scenario per unit radionuclide concentration in the contaminated source media (groundwater and soil) (Section 2.3.10.5.2).

For the groundwater exposure scenario, the sets of BDCFs for the present-day climate state were calculated for 1,000 realizations of the model. For each model realization, the same radionuclide-independent input parameter values were used to calculate BDCFs, capturing the inherent correlation among all radionuclides in the set. The results of each realization were stored as rows in the two-dimensional array containing the BDCFs for all primary radionuclides and all biosphere model realizations. Each row was populated by a different set of BDCFs. The rows from this array were sampled randomly within the TSPA model to propagate uncertainty from the biosphere model into the TSPA dose calculations, and to calculate the annual dose to the RMEI for present-day climate state. Therefore, the results of the process-level biosphere model were incorporated into the TSPA model without further abstraction (Section 2.3.10.5).

For the volcanic ash exposure scenario, the model produced three BDCF components for each radionuclide accounting for (1) ingestion, inhalation of radon decay products, and external exposure; (2) short-term inhalation of particulate matter; and (3) long-term inhalation of particulate matter. For each model realization, the same radionuclide-independent input parameter values were used to calculate BDCFs, capturing the inherent correlation among radionuclides. The results of each of the 1,000 realizations were stored as a row in a two-dimensional array containing a complete set of the BDCF components for all primary radionuclides. The array rows were sampled by the TSPA model to calculate the expected annual dose to the RMEI. Therefore, the results of the process-level biosphere model were incorporated into the TSPA model without further abstraction (Section 2.3.10.5).

Uncertainties Associated with the Biosphere Model—Uncertainties associated with the biosphere model are derived from uncertainty and variability in the data and parameters used to represent the characteristics of the biosphere, and from the models used to simulate transport and exposure pathways. The uncertainties associated with data are described in Section 2.3.10.3; the uncertainties associated with the models are described in Section 2.3.10.4.

The BDCFs displayed a total variation of about 1 to 2 orders of magnitude for most radionuclides (Section 2.3.10.5.1.1). The range from the 5th to the 95th percentile was much narrower. To evaluate mathematical model uncertainty in the biosphere model, the calculations were compared to results obtained from other biosphere models. In most cases, the results were the same or similar. The differences resulting from the alternative models were small relative to the total variability in BDCFs (Section 2.3.10.4.1).

The uncertainty attributed to input parameters and model uncertainty have a direct effect on the predicted dose to the RMEI. This is because the annual dose to the RMEI from groundwater contamination is calculated as a product of the BDCFs and the radionuclide concentration in the groundwater. The dose from soil contamination in the volcanic eruption modeling case is also a linear function of the BDCFs with the correction for the decrease of mass loading with time. However, compared to the broad range of other uncertainties incorporated in the TSPA model for the Yucca Mountain system, the uncertainty in the BDCFs is small and not significant (Section 2.4.2).

Conservatisms in Models Used to Assess Biosphere Transport and Exposure—The biosphere submodels incorporate conservative assumptions concerning the conceptual model, mathematical model, and the model parameters. The general philosophy applied to biosphere modeling was to

use a cautious but reasonable approach that would not result in underestimation of risk to the RMEI. This approach is reflected in the selection of the models, at the process level, and the model parameters and their distributions. The biosphere model uses hundreds of input parameters. Many model parameters were developed based on site specific information and, thus, reflect environmental and societal conditions in the region surrounding Yucca Mountain. However, many parameters, especially those concerning the environmental transport of radionuclides, were developed using natural analogues or generic data. The decisions made in the development of these parameters necessarily involved making choices concerning the treatment of uncertainties. Consistent with the cautious but reasonable approach, these choices were made so as to ensure that the parameter values are defensible and do not underestimate the risk to the RMEI. Some conservatisms used in the biosphere model are presented below:

- Surface soil within the reference biosphere was considered to be subject to long-term irrigation. The dose to the RMEI at time t was calculated assuming that the soil was irrigated for a defined period of time prior to time t, resulting in a buildup of radionuclides in the soil. The irrigation duration for all agricultural soils, assumed to be up to 1,000 years for fields and up to 250 year for home gardens, was conservative with regard to the present-day characteristics of the Yucca Mountain region.

- For the groundwater exposure scenario, all resuspended particles in indoor and outdoor environments were considered to originate from soils irrigated with contaminated groundwater. This assumption was conservative because, currently, only about 9% of the land in Amargosa Valley is irrigated, and some resuspended particles in the biosphere would originate from uncultivated soil with lower or negligible concentrations of radionuclides.

- For evaluation of external exposure, the RMEI was conservatively assumed to be continuously exposed to radionuclides in surface soil, although even if the radionuclide releases from the repository occurred, most of the land in the Amargosa Valley would not be affected.

- Groundwater was assumed to be the source for all water needs, including drinking water, irrigation, and other domestic uses.

- Farm animals were assumed to be raised using only contaminated feed and water.

- No credit was taken for water treatment and for removal of radionuclides from food by food washing and processing.

- Soil inadvertently ingested by the RMEI and by farm animals was assumed to originate from contaminated land.

- Consumption of aquatic food was included in the model despite the fact that the aquaculture farm, which was located in the Amargosa Valley during the food consumption survey, is no longer in operation. Furthermore, the radionuclide uptake into aquatic food was modeled using bioaccumulation factors. In the Amargosa Valley, fish were raised using commercial feed, which was not produced locally and thus was unlikely

to be contaminated. Therefore, using bioaccumulation factors is conservative and provides an upper bound analysis.

- The model for evaluating the activity of aerosols generated by evaporative coolers uses a conservative assumption that the fraction of radionuclides in the water transferred to the cooling airflow is, on average, 50%. In a properly operated and maintained cooler, the dissolved radioactive species would precipitate out during water evaporation inside the cooling unit and the water vapor introduced into the indoor air would be essentially mineral-free. The subsequent contamination of the cooler air could potentially occur when the air flowing through the cooler pads liberates small particles of solids left there by water evaporation, especially if a cooler is poorly maintained. However, this process is believed to account for much less than 50% of the contaminant transfer from the water to the indoor air.

- The calculation of radon concentration in the atmosphere for both exposure scenarios is based on the radon release factor from radium-contaminated soil. This factor represents the activity concentration of radon in the air per unit of radium activity concentration in the soil or per unit radon flux density from the soil, depending on the exposure scenario. The values of the radon release factors are based on the global averages and for the conditions where the radon exhalation occurs from very large surfaces. The contaminated surfaces in the reference biosphere are much smaller in extent, and some mixing and dilution of radon and its decay product concentrations in air with the uncontaminated air would be expected.

- All radon from radium-contaminated volcanic tephra is assumed to be released into the air, where it would mix and be available for inhalation. In the tephra-soil mixture, no credit was taken for the fractional emanation of radon from the grains of contaminated soil, and for the subsequent loss of radon from soil gas during transport through the soil before the exhalation from the soil.

- For the evaluation of external exposure under the groundwater exposure scenario, the soil is assumed to be contaminated to an infinite depth, regardless of the actual depth of the contaminated soil layer. For the volcanic ash exposure scenario, all radionuclides were assumed to remain on the ground surface and no credit was taken for radiation attenuation by the soil.

- The biosphere model used the worst-case dose coefficients for internal intakes. The conservative values were used because of uncertainty in the final chemical/physical form of the radionuclides supplied to the biosphere from groundwater and the uncertainty in the subsequent evolution of the chemical/physical form in the biosphere. In addition, the dose coefficients were calculated for the commitment period of 50 years, which for the radionuclides with the long effective half-lives in the body will overestimate the average life-time dose.

Summary of Interface Between TSPA Model Abstractions and Process Models—As shown in Figures 2.3.10-2 and 2.3.10-3, the TSPA model incorporates BDCFs calculated by the biosphere model in calculating annual dose to the RMEI. Therefore, the model abstractions described in

Section 2.3.10.5 are explicitly part of the TSPA model. As described in Section 2.4.4, the TSPA model has been checked and verified to ensure that submodels, including the use of BDCFs from the biosphere model, have been implemented correctly. Coupling between submodels in the TSPA model was examined by verifying that the information generated by one submodel is fed correctly to successive submodels. In addition, it confirmed that this information does not exceed the range of applicability of the submodel.

Summary of Key Output Parameters Provided to the TSPA Model—The biosphere model provides BDCFs for the groundwater exposure scenario to support calculation of annual dose to the RMEI for the TSPA modeling scenarios and cases that result in radionuclide release to the groundwater. BDCFs include all potential pathways of radionuclide transport and exposure. BDCFs for all primary radionuclides and all biosphere model realizations are provided to the TSPA model, which randomly samples these inputs to propagate uncertainty from the biosphere model into TSPA dose calculations.

The biosphere model also supports the calculation of the annual dose to the RMEI for TSPA volcanic eruption modeling case by providing BDCFs for the volcanic ash exposure scenario. For this exposure scenario, three BDCF components are developed for each radionuclide (ingestion, inhalation of radon decay products, and external exposure; short-term inhalation of particulate matter; and long-term inhalation of particulate matter). BDCF components for all primary radionuclides and all biosphere model realizations are provided to the TSPA for use in calculating the expected annual dose to the RMEI while allowing propagation of uncertainty from the biosphere model into the TSPA model.

2.3.10.7 General References

70 FR 49014. Public Health and Environmental Radiation Protection Standards for Yucca Mountain, NV.

Allen, R.G.; Pereira, L.S.; Raes, D.; and Smith, M. 1998. *Crop Evapotranspiration, Guidelines for Computing Crop Water Requirements.* FAO Irrigation and Drainage Paper 56. Rome, Italy: Food and Agriculture Organization of the United Nations. TIC: 245062.

Altman, W.D.; Donnelly, J.P.; and Kennedy, J.E. 1988. *Qualification of Existing Data for High-Level Nuclear Waste Repositories: Generic Technical Position*. NUREG-1298. Washington, D.C.: U.S. Nuclear Regulatory Commission. TIC: 200652.

Ambrose, V. 2002a. "AQS System AMP450 + AMP 380 ASCII Text & Report Files." E-mail from V. Ambrose (EPA) to K. Rautenstrauch, September 6, 2002, with attachment ACC: MOL.20020923.0190; MOL.20020923.0196.

Ambrose, V. 2002b. "Site/Monitor Information." E-mail from V. Ambrose (EPA) to T. Wirth, September 17, 2002, with attachment. ACC: MOL.20020923.0191; MOL.20020923.0196.

Antonelli, A.L.; Byther, R.S.; Collman, S.J.; Thornton, R.E.; and Van Denburgh, R. 1998. *Home Gardens*. EB0422. Pullman, Washington: Washington State University, Cooperative Extension, College of Agriculture & Home Economics. TIC: 251823.

Baes, C.F., III; Sharp, R.D.; Sjoreen, A.L.; and Shor, R.W. 1984. *A Review and Analysis of Parameters for Assessing Transport of Environmentally Released Radionuclides through Agriculture*. ORNL-5786. Oak Ridge, Tennessee: Oak Ridge National Laboratory. ACC: NNA.19870731.0041.

BIOMASS (Biosphere Modelling and Assessment) 2000. *Example Reference Biosphere 2A: Agricultural Well, Constant Biosphere.* Draft TECDOC. BIOMASS/T1/WD08. Vienna, Austria: International Atomic Energy Agency, Division of Radiation and Waste Safety. TIC: 249456.

BIOMASS 2003. *"Reference Biospheres" for Solid Radioactive Waste Disposal, Report of BIOMASS Theme 1 of the BIOsphere Modelling and ASSessment (BIOMASS) Programme, Part of the IAEA Coordinated Research Project on Biosphere Modelling and Assessment (BIOMASS)*. IAEA-BIOMASS-6. Vienna, Austria: International Atomic Energy Agency, Waste Safety Section. TIC: 255411.

BSC (Bechtel SAIC Company) 2003. *Yucca Mountain Project Summary of Socioeconomic Data Analyses Conducted in Support of the Radiological Monitoring Program, During FY 2003*. TDR-MGR-EV-000040 REV 00. Las Vegas, Nevada: Bechtel SAIC Company. ACC: DOC.20031203.0003.

BSC 2004a. *Future Climate Analysis.* ANL-NBS-GS-000008 REV 01. Las Vegas, Nevada: Bechtel SAIC Company. ACC: DOC.20040908.0005.

BSC 2004b. *Yucca Mountain Site Description.* TDR-CRW-GS-000001 REV 02 ICN 01. Two volumes. Las Vegas, Nevada: Bechtel SAIC Company. ACC: DOC.20040504.0008.

BSC 2004c. *Agricultural and Environmental Input Parameters for the Biosphere Model.* ANL-MGR-MD-000006 REV 02. Las Vegas, Nevada: Bechtel SAIC Company. ACC: DOC.20040915.0007.

BSC 2004d. *Environmental Transport Input Parameters for the Biosphere Model.* ANL-MGR-MD-000007 REV 02. Las Vegas, Nevada: Bechtel SAIC Company. ACC: DOC.20040913.0003.

BSC 2005. *Characteristics of the Receptor for the Biosphere Model*. ANL-MGR-MD-000005 REV 04. Las Vegas, Nevada: Bechtel SAIC Company. ACC: DOC.20050405.0005.

BSC 2006. *Inhalation Exposure Input Parameters for the Biosphere Model*. ANL-MGR-MD-000001 REV 04. Las Vegas, Nevada: Bechtel SAIC Company. ACC: DOC.20060605.0011.

Bureau of the Census 2002. "2000 Summary File 3 (SF 3) Sample Data, Amargosa Valley CCD, Nye County, Nevada." Washington, D.C.: U.S. Department of Commerce, Bureau of the Census. Accessed August 28, 2002. TIC: 253098. http://factfinder.census.gov/servlet/DTTable?_ts=48597952130

CRWMS M&O (Civilian Radioactive Waste Management System Management and Operating Contractor) 1997. *Yucca Mountain Site Characterization Project Summary of Socioeconomic Data Analyses Conducted in Support of the Radiological Monitoring Program First Quarter 1996 to First Quarter 1997*. Las Vegas, Nevada: CRWMS M&O. ACC: MOL.19971117.0460.

CRWMS M&O 1999a. *Evaluation of Soils in the Northern Amargosa Valley.* B00000000-01717-5705-00084 REV 00. Las Vegas, Nevada: CRWMS M&O. ACC: MOL.19990224.0268.

CRWMS M&O 1999b. *Environmental Baseline File for Biological Resources.* B00000000-01717-5700-00009 REV 00. Las Vegas, Nevada: CRWMS M&O. ACC: MOL.19990302.0181; MOL.19990330.0560.

Davis, P.A; Zach, R.; Stephens, M.E.; Amiro, B.D.; Bird, G.A.; Reid, J.A.K.; Sheppard, M.I.; Sheppard, S.C.; and Stephenson, M. 1993. *The Disposal of Canada's Nuclear Fuel Waste: The Biosphere Model, BIOTRAC, for Postclosure Assessment.* AECL-10720. Pinawa, Manitoba, Canada: Atomic Energy of Canada Limited. TIC: 244741.

DOE (U.S. Department of Energy) 1997. *The 1997 "Biosphere" Food Consumption Survey Summary Findings and Technical Documentation.* Las Vegas, Nevada: U.S. Department of Energy, Office of Civilian Radioactive Waste Management. ACC: MOL.19981021.0301.

DOE 2002. *Final Environmental Impact Statement for a Geologic Repository for the Disposal of Spent Nuclear Fuel and High-Level Radioactive Waste at Yucca Mountain, Nye County, Nevada*. DOE/EIS-0250. Washington, D.C.: U.S. Department of Energy, Office of Civilian Radioactive Waste Management. ACC: MOL.20020524.0314 through MOL.20020524.0320.

Doorenbos, J. and Pruitt, W.O. 1977. *Crop Water Requirements.* FAO Irrigation and Drainage Paper 24. Rome, Italy: Food and Agriculture Organization of the United Nations. TIC: 245199.

Duan, N. 1982. "Models for Human Exposure to Air Pollution." *Environment International*, *8*, 305–309. New York, New York: Pergamon Press. TIC: 250558.

Eckerman, K.F. and Ryman, J.C. 1993. *External Exposure to Radionuclides in Air, Water, and Soil, Exposure-to-Dose Coefficients for General Application, Based on the 1987 Federal Radiation Protection Guidance.* EPA 402-R-93-081. Federal Guidance Report No. 12. Washington, D.C.: U.S. Environmental Protection Agency, Office of Radiation and Indoor Air. TIC: 225472.

EPA (U.S. Environmental Protection Agency) 1997a. *Activity Factors.* Volume III of *Exposure Factors Handbook.* EPA/600/P-95/002Fc. Washington, D.C.: U.S. Environmental Protection Agency. TIC: 241062.

EPA 1997b. *General Factors*. Volume I of *Exposure Factors Handbook*. EPA/600/P-95/002Fa. Washington, D.C.: U.S. Environmental Protection Agency. TIC: 241060.

EPA 1999. *Cancer Risk Coefficients for Environmental Exposure to Radionuclides.* EPA 402-R-99-001. Federal Guidance Report No. 13. CD Supplement. Washington, D.C.: U.S.

Environmental Protection Agency, Office of Radiation and Indoor Air. ACC: MOL.20020312.0287.

EPA 2002. *Federal Guidance Report 13, CD Supplement, Cancer Risk Coefficients for Environmental Exposure to Radionuclides, EPA.* EPA-402-C-99-001, Rev. 1. Washington, D.C.: U.S. Environmental Protection Agency. ACC: MOL.20051013.0016.

EPA 2007. "EPA Map of Radon Zones." Washington, D.C.: U.S. Environmental Protection Agency. Accessed May 8, 2007. ACC: LLR.20070518.0158.

EPRI (Electric Power Research Institute) 2002. *Evaluation of the Proposed High-Level Radioactive Waste Repository at Yucca Mountain Using Total System Performance Assessment, Phase 6.* EPRI TR-1003031. Palo Alto, California: Electric Power Research Institute. TIC: 252239.

EPRI 2004. *Potential Igneous Processes Relevant to the Yucca Mountain Repository: Extrusive-Release Scenario.* EPRI TR-1008169. Palo Alto, California: Electric Power Research Institute. TIC: 256654.

Farnsworth, R. K.; Thompson, E.S.; and Peck, E.L. 1982. *Evaporation Atlas for the Contiguous 48 United States.* NOAA Technical Report NWS 33. Washington, D.C.: National Oceanic and Atmospheric Administration. ACC: MOL.19950105.0024 through MOL.19950104.0028.

Firestone, R.B. 1998. *Table of the Isotopes.* Chu, S.Y.F. and Baglin, C.M., eds. 8th Edition: 1998 Update. New York, New York: Wiley-Interscience. TIC: 259100.

Gordian, M.E.; Ozkaynak, H.; Xue, J.; Morris, S.S.; and Spengler, J.D. 1996. "Particulate Air Pollution and Respiratory Disease in Anchorage, Alaska." *Environmental Health Perspectives*, *104* (3), 290–297. Research Park Triangle, North Carolina: National Institute of Environmental Health Sciences, National Institutes of Health. TIC: 250157.

Hoffman, F.O.; Frank, M.L.; Blaylock, B.G.; von Bernuth, R.D.; Deming, E.J.; Graham, R.V.; Mohrbacher, D.A.; and Waters, A.E. 1989. *Pasture Grass Interception and Retention of ^{131}I, ^{7}Be, and Insoluble Microspheres Deposited in Rain.* ORNL-6542. Oak Ridge, Tennessee: Oak Ridge National Laboratory. TIC: 237241.

Horak, C. and Carns, D. 1997. *Amargosa Focus Group Report.* Biosphere Study. Las Vegas, Nevada: University of Nevada, Las Vegas. TIC: 241712.

IAEA (International Atomic Energy Agency) 1994. *Handbook of Parameter Values for the Prediction of Radionuclide Transfer in Temperate Environments*. Technical Reports Series No. 364. Vienna, Austria: International Atomic Energy Agency. TIC: 232035.

IAEA 2001. *Generic Models for Use in Assessing the Impact of Discharges of Radioactive Substances to the Environment*. Safety Reports Series No. 19. Vienna, Austria: International Atomic Energy Agency. TIC: 251295.

ICRP (International Commission on Radiological Protection) 1975. *Report of the Task Group on Reference Man: A Report Prepared by a Task Group of Committee 2 of the International Commission on Radiological Protection*. ICRP Number 23. Tarrytown, New York: Elsevier. ACC: MOL.20000516.0124.

ICRP 1991. *1990 Recommendations of the International Commission on Radiological Protection*. Volume 21, Nos. 1–3 of *Annals of the ICRP*. ICRP Publication 60. New York, New York: Pergamon Press. TIC: 235864.

ICRP 1994a. *Human Respiratory Tract Model for Radiological Protection.* Volume 24, Nos. 1–3 of *Annals of the ICRP.* Smith, H., ed. ICRP Publication 66. New York, New York: Pergamon. TIC: 249223.

ICRP 1994b. *Protection Against Radon-222 at Home and at Work.* Volume 23, No. 2 of *Annals of the ICRP.* ICRP Publication 65. New York, New York: Pergamon Press. TIC: 236754.

Karlsson, S.; Bergström, U.; and Meili, M. 2001. *Models for Dose Assessments, Models Adapted to the SFR-Area, Sweden.* SKB TR-01-04. Stockholm, Sweden: Svensk Kärnbränsleförsörjning A.B. TIC: 252806.

Kennedy, W.E., Jr. and Strenge, D.L. 1992. *Technical Basis for Translating Contamination Levels to Annual Total Effective Dose Equivalent*. Volume 1 of *Residual Radioactive Contamination from Decommissioning*. NUREG/CR-5512. Washington, D.C.: U.S. Nuclear Regulatory Commission. ACC: MOL.20010721.0030.

Klepeis, N.E. 1999. "An Introduction to the Indirect Exposure Assessment Approach: Modeling Human Exposure Using Microenvironmental Measurements and the Recent National Human Activity Pattern Survey." *Environmental Health Perspectives*, *107* (Supplement 2), 365–374. Research Triangle Park, North Carolina: National Institute of Environmental Health Sciences, National Institutes of Health. TIC: 250567.

Klepeis, N.E.; Tsang, A.M.; and Behar, J.V. 1996. *Analysis of the National Human Activity Pattern Survey (NHAPS) Respondents from a Standpoint of Exposure Assessment, Percentage of Time Spent, Duration, and Frequency of Occurrence for Selected Microenvironments by Gender, Age, Time-of-Day, Day-of-Week, Season, and U.S. Census Region, Final Report*. EPA/600/R-96/074. Washington, D.C.: U.S. Environmental Protection Agency, Office of Research and Development. TIC: 252656.

Leigh, C.D.; Thompson, B.M.; Campbell, J.E.; Longsine, D.E.; Kennedy, R.A.; and Napier, B.A. 1993. *User's Guide for GENII-S: A Code for Statistical and Deterministic Simulations of Radiation Doses to Humans from Radionuclides in the Environment.* SAND91-0561. Albuquerque, New Mexico: Sandia National Laboratories. ACC: MOL.20010721.0031.

Lide, D.R. and Frederikse, H.P.R., eds. 1997. *CRC Handbook of Chemistry and Physics.* 78th Edition. Boca Raton, Florida: CRC Press. TIC: 243741.

Mage, D.T. 1985. "Concepts of Human Exposure Assessment for Airborne Particulate Matter." *Environment International*, *11*, 407–412. New York, New York: Pergamon Press. TIC: 250582.

Mills, L.; Morris, B.; Roberts, A.; Robinson, M. L.; Hammond, B.; and Mandekic, J. n.d. *Beginning Gardening in the Desert.* Pahrump, Nevada: Southern Nye County Cooperative Extension. TIC: 243450.

Napier, B.A.; Peloquin, R.A.; Strenge, D.L.; and Ramsdell, J.V. 1988. *Conceptual Representation*. Volume 1 of *GENII—The Hanford Environmental Radiation Dosimetry Software System*. PNL-6584. Richland, Washington: Pacific Northwest Laboratory. TIC: 252237.

Napier, B.A.; Strenge, D.L.; Ramsdell, J.V., Jr.; Eslinger, P.W.; and Fosmire, C. 2006. *GENII Version 2 Software Design Document*. PNNL-14584, Rev. 1. Richland, Washington: Pacific Northwest National Laboratory. ACC: MOL.20060815.0035.

NCRP (National Council on Radiation Protection and Measurements) 1999. *Recommended Screening Limits for Contaminated Surface Soil and Review of Factors Relevant to Site-Specific Studies*. NCRP Report No. 129. Bethesda, Maryland: National Council on Radiation Protection and Measurements. TIC: 250396.

Neitsch, S.L.; Arnold, J.G.; Kiniry, J.R.; Srinivasan, R.; and Williams, J.R. 2002. "Land Cover/Plant Growth Database." *Soil and Water Assessment Tool User's Manual, Version 2000.* 356–385. College Station, Texas: Texas Water Resources Institute. TIC: 254059.

Nieuwenhuijsen, M.J.; Kruize, H.; and Schenker, M.B. 1998. "Exposure to Dust and Its Particle Size Distribution in California Agriculture." *American Industrial Hygiene Association Journal*, *59*, 34–38. Fairfax, Virginia: American Industrial Hygiene Association. TIC: 248134.

Nieuwenhuijsen, M.J.; Noderer, K.S.; Schenker, M.B.; Vallyathan, V.; and Olenchock, S. 1999. "Personal Exposure to Dust, Endotoxin and Crystalline Silica in California Agriculture." *Annals of Occupational Hygiene*, *43* (1), 35–42. Oxford, England: Elsevier. TIC: 248271.

Rasmuson, K.E. 2004. "Summary of 2004 Agricultural Activities, Businesses, and Community Services and Organizations in Amargosa Valley." Interoffice memorandum from K.E. Rasmuson (BSC) to K.R. Rautenstrauch (BSC), May 20, 2004, 0520041667, with enclosures. ACC: MOL.20040519.0033.

Roe, L.K. 2002. "Summary of RDA Investigation ID: 4/10/02 Fish Farming in Amargosa Valley." Interoffice memorandum from L.K. Roe (BSC) to File, November 5, 2002, 1105024986, with attachment. ACC: MOL.20021107.0091; MOL.20020821.0002.

Sheppard, M.I.; Sheppard, S.C.; and Amiro, B.D. 1991. "Mobility and Plant Uptake of Inorganic ^{14}C and ^{14}C-Labelled PCB in Soils of High and Low Retention." *Health Physics*, *61* (4), 481–492. New York, New York: Pergamon Press. TIC: 252687.

Sheppard, M.I. and Thibault, D.H. 1990. "Default Soil Solid/Liquid Partition Coefficients, K_ds, for Four Major Soil Types: A Compendium." *Health Physics*, *59* (4), 471–482. New York, New York: Pergamon Press. TIC: 249329.

Sheppard, S.C. and Sheppard, M.I. 1989. "Impact of Correlations on Stochastic Estimates of Soil Contamination and Plant Uptake." *Health Physics*, *57* (4), 653-657. New York, New York: Pergamon Press. TIC: 253545.

Simon, S.L. 1998. "Soil Ingestion by Humans: A Review of History, Data, and Etiology with Application to Risk Assessment of Radioactively Contaminated Soil." *Health Physics*, *74* (6), 647–672. Baltimore, Maryland: Williams & Wilkins. TIC: 253001.

SNL (Sandia National Laboratories) 2007a. *Biosphere Model Report*. MDL-MGR-MD-000001 REV 02. Las Vegas, Nevada: Sandia National Laboratories. ACC: DOC.20070830.0007.

SNL 2007b. *Soil-Related Input Parameters for the Biosphere Model*. ANL-NBS-MD-000009 REV 03 ADD 01. Las Vegas, Nevada: Sandia National Laboratories. ACC: DOC.20070927.0004.

SNL 2007c. *Radionuclide Screening.* ANL-WIS-MD-000006 REV 02. Las Vegas, Nevada: Sandia National Laboratories. ACC: DOC.20070326.0003.

SNL 2007d. *Redistribution of Tephra and Waste by Geomorphic Processes Following a Potential Volcanic Eruption at Yucca Mountain, Nevada*. MDL-MGR-GS-000006 REV 00. Las Vegas, Nevada: Sandia National Laboratories. ACC: DOC.20071220.0004.

SNL 2008. *Total System Performance Assessment Model/Analysis for the License Application.* MDL-WIS-PA-000005 REV 00 ADD 01. Las Vegas, Nevada: Sandia National Laboratories. ACC: DOC.20080312.0001.

Till, J.E. and Meyer, H.R. 1983. *Radiological Assessment, A Textbook on Environmental Dose Analysis*. NUREG/CR-3332. Washington, D.C.: U.S. Nuclear Regulatory Commission. TIC: 223809.

UNSCEAR (United Nations Scientific Committee on the Effects of Atomic Radiation) 2000. *Sources and Effects of Ionizing Radiation, United Nations Scientific Committee on the Effects of Atomic Radiation, UNSCEAR 2000 Report to the General Assembly, with Scientific Annexes.* Two volumes. New York, New York: United Nations. TIC: 249863.

USDA (U.S. Department of Agriculture) 1999a. *1997 Census of Agriculture, Nevada State and County Data*. Geographic Area Series Part 28, Volume 1. AC97-A-28. Washington, D.C.: U.S. Department of Agriculture, National Agricultural Statistics Service. TIC: 246010.

USDA 1999b. *1997 Census of Agriculture, Washington State and County Data*. Geographic Area Series Part 47, Volume 1. AC97-A-47. Washington, D.C.: U.S. Department of Agriculture, National Agricultural Statistics Service. TIC: 252668.

USDA 2000. *Summary Report, 1997 National Resources Inventory (Revised December 2000).* Washington, D.C.: U.S. Department of Agriculture. TIC: 253006.

USDA 2001. *Agricultural Statistics 2001.* Washington, D.C.: U.S. Government Printing Office. TIC: 252544.

USDA 2002. *Composition of Foods Raw, Processed, Prepared, USDA Nutrient Database for Standard Reference, Release 14.* Washington, D.C.: U.S. Department of Agriculture, Agricultural Research Service, Nutrient Data Laboratory. TIC: 252893.

USDA 2004. *Soil Survey of Nye County, Nevada, Southwest Part*. Two parts. Washington, D.C.: U.S. Department of Agriculture. ACC: MOL.20050614.0146.

Wang, Y.-Y.; Biwer, B.M.; and Yu, C. 1993. *A Compilation of Radionuclide Transfer Factors for the Plant, Meat, Milk, and Aquatic Food Pathways and the Suggested Default Values for the RESRAD Code*. ANL/EAIS/TM-103. Argonne, Illinois: Argonne National Laboratory. TIC: 232998.

Wasiolek, P.T. and James, A.C. 1995. "Outdoor Radon Dose Conversion Coefficient in South-Western and South-Eastern United States." *Radiation Protection Dosimetry*, *59* (4), 269–278. Ashford, Kent, England: Nuclear Technology Publishing. TIC: 254339.

Washington State University Cooperative Extension 2002. *Vegetable Gardening*. C146. Spokane, Washington: Washington State University Cooperative Extension. TIC: 251733.

Yano, E.; Yokoyama, Y.; Higashi, H.; Nishii, S.; Maeda, K.; and Koizumi, A. 1990. "Health Effects of Volcanic Ash: A Repeat Study." *Archives of Environmental Health*, *45* (6), 367–373. Washington, D.C.: Heldref Publications. TIC: 250162.

YMP (Yucca Mountain Site Characterization Project) 1999. *Yucca Mountain Site Characterization Project: Summary of Socioeconomic Data Analyses Conducted in Support of the Radiological Monitoring Program, April 1998 to April 1999.* North Las Vegas, Nevada: Yucca Mountain Site Characterization Office. ACC: MOL.19991021.0188.

Yu, C.; Zielen, A.J.; Cheng, J.-J.; LePoire, D.J.; Gnanapragasam, E.; Kamboj, S.; Arnish, J.; Wallo, A., III.; Williams, W.A.; and Peterson, H. 2001. *User's Manual for RESRAD Version 6.* ANL/EAD-4. Argonne, Illinois: Argonne National Laboratory. TIC: 252702.

Table 2.3.10-1. Biosphere-Related Features, Events, and Processes Included in the Total System Performance Assessment

LA FEP Number and Name	FEP Description	Summary of Technical Basis/Approach for FEP Inclusion
1.2.04.07.0A Ashfall	Finely divided waste particles may be carried up a volcanic vent and deposited on the land surface from an ash cloud.	Volcanic tephra is the initial source of contamination for the eruption case of the volcanic scenario (Section 2.3.10.2.6). Tephra characteristics and depth were considered in development of the input parameters for the surface soil and air submodels (Section 2.3.10.3.2).
1.3.01.00.0A Climate change	Climate change may affect the long-term performance of the repository. This includes the effects of long-term change in global climate (e.g., glacial/interglacial cycles) and shorter-term change in regional and local climate. Climate is typically characterized by temporal variations in precipitation and temperature.	The effect of climate change on the BDCFs was evaluated from the perspective of the factors that are related to the human society, which 10 CFR 63.305(b) directs DOE not to vary in its performance assessments, and those factors that are independent of human activities, which proposed 10 CFR 63.305(c) requires to vary. A conclusion was reached that the present-day climate BDCFs are appropriate for the assessment of doses to the RMEI for the entire period of geologic stability (Section 2.3.10.5.1.1).
1.4.07.01.0A Water management activities	Water management is accomplished through a combination of dams, reservoirs, canals, pipelines, and collection and storage facilities. Water management activities could have a major influence on the behavior and transport of contaminants in the biosphere.	Water management activities conducted in the Yucca Mountain region (e.g., irrigation and fish farming) were incorporated throughout the conceptual and mathematical model and considered in the development of parameter values for the plant uptake and fish uptake submodels (Sections 2.3.10.2 and 2.3.10.3.1).
1.4.07.02.0A Wells	One or more wells drilled for human use (e.g., drinking water, bathing) or agricultural use (e.g., irrigation, animal watering) may intersect the contaminant plume.	A well is the source of groundwater for domestic and agricultural uses in the groundwater exposure scenario (Section 2.3.10.2.5).
2.3.02.01.0A Soil type	Soil type is determined by many different factors (e.g., formative process, geology, climate, vegetation, land use). The physical and chemical attributes of the surficial soils (such as organic matter content and pH) may influence the mobility of radionuclides.	This feature was included through the consideration of the soil characteristics in the reference biosphere in the development of parameter values for the surface soil, plant uptake, and ^{14}C submodels (Section 2.3.10.3).
2.3.02.02.0A Radionuclide accumulation in soils	Radionuclide accumulation in soils may occur as a result of upwelling of contaminated groundwater (leaching, evaporation at discharge location), deposition of contaminated water or particulates (irrigation water, runoff), and/or atmospheric deposition.	Accumulation of radionuclides in soil from deposition of irrigation water and volcanic tephra was modeled in the surface soil submodel (Section 2.3.10.2).

Table 2.3.10-1. Biosphere-Related Features, Events, and Processes Included in the Total System Performance Assessment (Continued)

LA FEP Number and Name	FEP Description	Summary of Technical Basis/Approach for FEP Inclusion
2.3.02.03.0A Soil and sediment transport in the biosphere	Contaminated sediments can be transported to and through the biosphere by surface runoff and fluvial processes, and, to a lesser extent, by aeolian processes and bioturbation. Sediment transport and redistribution may cause concentration or dilution of radionuclides in the biosphere.	Soil and sediment transport via erosion were included in the surface soil and air submodels (Section 2.3.10.2).
2.3.04.01.0A Surface water transport and mixing	Radionuclides released from an underground repository might enter the biosphere through discharge of deep groundwater into a lake or river. Transport and mixing within the surface water bodies affects the subsequent behavior and transport of radionuclides in the biosphere. Transport and mixing includes dilution, sedimentation, aeration, streamflow, and river meander.	The groundwater scenario implicitly included water transport because the model could accommodate the use of any water containing radionuclides, regardless of the origin, if the reference biosphere, water-use practices, and characteristics of the RMEI remain unchanged. The model did not consider mixing of contaminated and uncontaminated water (Section 2.3.10.2.5).
2.3.11.01.0A Precipitation	Precipitation is an important control on the amount of infiltration, flow in the unsaturated zone, seepage into the repository and groundwater recharge. It transports solutes with it as it flows downward through the subsurface or escapes as runoff. Precipitation influences agricultural practices of the receptor. The amount of precipitation depends on climate.	Levels of precipitation consistent with current knowledge of the reference biosphere were considered in the development of input parameter distributions for the surface soil, plant uptake, and ^{14}C submodels (Section 2.3.10.3).
2.3.13.01.0A Biosphere characteristics	The principal components, conditions, or characteristics of the biosphere system can influence radionuclide transport and affect the long-term performance of the disposal system. These include the characteristics of the reference biosphere, such as climate, soils and microbes, flora and fauna, and their influences on human activities.	The principal components, conditions, and characteristics of the reference biosphere that influence radionuclide transport were represented in the conceptual and mathematical models (Section 2.3.10.2). Current knowledge of the conditions in the reference biosphere was considered in the development of parameter distributions for all submodels (Section 2.3.10.3).
2.3.13.02.0A Radionuclide alteration during biosphere transport	Once in the biosphere, radionuclides may be transported and transferred through and between different compartments of the biosphere. Temporally and spatially dependent physical and chemical environments in the biosphere may lead to alteration of both the physical and chemical properties of the radionuclides as they move through or between the different compartments of the biosphere. These alterations could consequently control exposure to the human population.	Changes in the physical and chemical form of radionuclides during transfer among biosphere components were incorporated throughout the conceptual and mathematical models. This FEP was also implicitly incorporated through the use of radionuclide-specific transfer factors in the plant uptake and animal uptake submodels (Sections 2.3.10.2 and 2.3.10.3).

Table 2.3.10-1. Biosphere-Related Features, Events, and Processes Included in the Total System Performance Assessment (Continued)

LA FEP Number and Name	FEP Description	Summary of Technical Basis/Approach for FEP Inclusion
2.4.01.00.0A Human characteristics (physiology, metabolism)	This FEP addresses human characteristics. These include physiology, metabolism, and variability among individual humans.	Metabolic and physiologic considerations consistent with present knowledge of adults, as per 10 CFR 63.312(e), were used in the development of parameter distributions for the external exposure, inhalation, and ingestion submodels (Sections 2.3.10.2 and 2.3.10.3).
2.4.04.01.0A Human lifestyle	Human lifestyle, including everyday household activities and leisure activities, will influence the critical exposure pathways to humans.	Activities representative of the living style of the residents of the Town of Amargosa Valley were incorporated throughout the conceptual and mathematical model (Section 2.3.10.2). The living style of Amargosa Valley residents was considered in the development of parameter distributions for the air, external exposure, inhalation, and ingestion submodels (Section 2.3.10.3).
2.4.07.00.0A Dwellings	This FEP addresses human dwellings and the ways in which dwellings might affect human exposures. Exposure pathways might be influenced by building materials and location.	Characteristics of dwellings representative of the living style of the residents of the Town of Amargosa Valley were considered in the development of input parameters for the air, external exposure, and inhalation submodels (Sections 2.3.10.2 and 2.3.10.3).
2.4.08.00.0A Wild and natural land and water use	Human uses of wild and natural lands (forests, bush, coastlines) and water (lakes, rivers, oceans) may affect the long-term performance of the repository. Wild and natural land use will be primarily controlled by natural factors (topography, climate, etc.).	Wild and natural land and water use (e.g., use of natural lands, ingestion of game animals) of the residents of the Town of Amargosa Valley was incorporated into the air, external exposure, and ingestion submodels (Section 2.3.10.2). These lifestyle characteristics were considered in the development of parameters for those submodels (Section 2.3.10.3).
2.4.09.01.0B Agricultural land use and irrigation	Agricultural areas exist near Yucca Mountain, particularly in the direction of groundwater flow. Current practices include irrigation, plowing, fertilization, crop storage, and soil modification and amendment. Existing practices may play a significant role in determining exposure pathways and dose.	Agricultural land use and irrigation practices of the residents of the Town of Amargosa Valley were incorporated into the soil, air, plant uptake, animal uptake, ^{14}C, and fish uptake submodels (Section 2.3.10.2). These practices were considered in the development of parameters for those submodels (Section 2.3.10.3).
2.4.09.02.0A Animal farms and fisheries	Domestic livestock or fish could become contaminated through the intake of contaminated feed, water, or soil. Such contamination could then enter the food chain.	Animal farms and fisheries practices of the residents of the Town of Amargosa Valley were incorporated into the animal uptake and fish uptake submodels (Section 2.3.10.2). These practices were considered in the development of parameters for those submodels (Section 2.3.10.3).

Table 2.3.10-1. Biosphere-Related Features, Events, and Processes Included in the Total System Performance Assessment (Continued)

LA FEP Number and Name	FEP Description	Summary of Technical Basis/Approach for FEP Inclusion
2.4.10.00.0A Urban and industrial land and water use	Urban and industrial uses of land and water (industry, urban development, earthworks, energy production, etc.) may affect the long-term performance of the repository. Urban and industrial land use will be controlled by both natural factors (topography, climate, etc.) and human factors (economics, population density, etc.).	Land and water use in urban and industrial settings of the residents of the Town of Amargosa Valley were incorporated into the soil, air, ^{14}C, external exposure, inhalation, and ingestion submodels (Section 2.3.10.2). These lifestyle characteristics were considered in the development of parameters for those submodels (Section 2.3.10.3).
3.1.01.01.0A Radioactive decay and ingrowth	Radioactivity is the spontaneous disintegration of an unstable atomic nucleus that results in the emission of subatomic particles. Radioactive species (isotopes) of a given element are known as radionuclides. Radioactive decay of the fuel in the repository changes the radionuclide content in the fuel with time and generates heat. Radionuclide quantities in the system at any time are the result of the radioactive decay and the ingrowth of decay products as a consequence of that decay. Over a 10,000 year performance period, these processes will produce decay products that need to be considered in order to adequately evaluate the release and transport of radionuclides to the accessible environment.	Radioactive decay and ingrowth in soil was included in the surface soil submodel. In addition, the calculation of effective dose coefficients and effective dose conversion factors included dose contributions from the decay products of primary radionuclides (Section 2.3.10.2.4).
3.2.10.00.0A Atmospheric transport of contaminants	Atmospheric transport includes radiotoxic and chemotoxic species in the air as gas, vapor, particulates, or aerosol. Transport processes include wind, plowing and irrigation, degassing, saltation, and precipitation.	The processes of atmospheric transport of radionuclides from resuspension of soil and ash particles, gaseous emission of radionuclides from soil, and generation of aerosols from evaporative coolers were included in the air and ^{14}C submodels (Section 2.3.10.2).
3.3.01.00.0A Contaminated drinking water, foodstuffs, and drugs	This FEP addresses human diet and fluid intake. Consumption of food, water, soil, drugs, etc. will affect human exposure to radionuclides. Other influences include filtration of water, dilution of diet with uncontaminated food, and food preparation techniques.	Consumption of contaminated water and soil and consumption of locally produced crops, animal products, and fish were included in the ingestion submodel (Section 2.3.10.2). Consumption rates were based on the diet of the residents of the Town of Amargosa Valley and the requirements of 10 CFR 63.312 (Section 2.3.10.3.1.9).

Table 2.3.10-1. Biosphere-Related Features, Events, and Processes Included in the Total System Performance Assessment (Continued)

LA FEP Number and Name	FEP Description	Summary of Technical Basis/Approach for FEP Inclusion
3.3.02.01.0A Plant uptake	Uptake and accumulation of contaminants by plants could affect potential exposure pathways. Plant uptake from contaminated soils and irrigation water is possible. Particulate deposition onto plant surfaces is also possible. These plants may be used as feed for livestock and/or consumed directly by humans.	The process of plant uptake of radionuclides was included in the plant uptake and ^{14}C submodels (Section 2.3.10.2).
3.3.02.02.0A Animal uptake	Livestock may accumulate radionuclides as a result of ingestion (water, feed, and soil/sediment) and inhalation (aerosols and particulates). Depending on the livestock, they may be used for human consumption directly, or their produce (milk, eggs, etc.) may be consumed.	The animal uptake submodel included the process of radionuclide uptake by farm animals (Section 2.3.10.2).
3.3.02.03.0A Fish uptake	Uptake and bioaccumulation of contaminants in aquatic organisms could affect potential exposure pathways.	The fish uptake submodel included the bioaccumulation of radionuclides in fish (Section 2.3.10.3).
3.3.03.01.0A Contaminated nonfood products and exposure	Contaminants may be concentrated in various products: clothing (e.g., hides, leather, linen, wool); furniture (e.g., wood, metal); building materials (e.g., stone, clay for bricks, wood, dung); fuel (e.g., peat), tobacco, pets.	The external exposure submodel bounded exposure to the few nonfood products produced in Amargosa Valley that may contain radionuclides by assuming that the RMEI would be exposed to contaminated soil at all times while in the biosphere (Section 2.3.10.2).
3.3.04.01.0A Ingestion	Ingestion is human exposure to repository-derived radionuclides through eating contaminated foodstuffs or drinking contaminated water.	The ingestion submodel included ingestion of contaminated food, drinking water, and soil (Section 2.3.10.2).
3.3.04.02.0A Inhalation	Inhalation pathways for repository-derived radionuclides should be considered. Two possible pathways are: inhalation of gases and vapors emanating directly from the ground after transport through the far field; and inhalation of suspended, contaminated particulate matter (e.g., decay products of radon, dust, smoke, pollen, and soil particles).	The inhalation submodel includes inhalation of gaseous ^{14}C and radon decay products from radon exhalation from the ground, contaminated resuspended particles, and contaminated aerosols from evaporative coolers (Section 2.3.10.2).
3.3.04.03.0A External exposure	External exposure is human exposure to repository-derived radionuclides by contact, use, or exposure to contaminated materials.	The external exposure submodel included external exposure to contaminated materials (Section 2.3.10.2).

Table 2.3.10-1. Biosphere-Related Features, Events, and Processes Included in the Total System Performance Assessment (Continued)

LA FEP Number and Name	FEP Description	Summary of Technical Basis/Approach for FEP Inclusion
3.3.05.01.0A Radiation doses	The radiation dose is calculated from exposure rates (external, inhalation, and ingestion) and dose coefficients. The latter are based upon radiation type, human metabolism, metabolism of the element of concern in the human body, and duration of exposure.	Calculation of the predicted annual dose as required by proposed 10 CFR 63.311 for a unit activity concentration of a radionuclide (i.e., BDCF) was conducted in the external exposure, inhalation, and ingestion submodels (Sections 2.3.10.2 and 2.3.10.5).
3.3.08.00.0A Radon and radon decay product exposure	This FEP addresses human exposure to radon and radon decay products. ^{226}Ra occurs in nuclear fuel waste and it gives rise to ^{222}Rn gas, the radioactive decay products of which can result in radiation doses to humans upon inhalation.	Concentrations of ^{222}Rn and ^{222}Rn decay products were calculated in the air submodel. Exposure to ^{222}Rn and decay products was included in the inhalation submodel (Section 2.3.10.2).

Table 2.3.10-2. Transport Pathways Explicitly Included in the Groundwater and Volcanic Ash Exposure Scenarios

Transport Pathway	Groundwater	Volcanic
Radionuclide accumulation in soil from irrigation with water	X	
Radionuclide accumulation in soil from deposition and redistribution of volcanic tephra		X
Removal of radionuclides from soil by leaching	X	
Removal of radionuclides from soil by erosion	X	
Resuspension of soil	X	X
Deposition of resuspended soil on crops	X	X
Deposition of irrigation water on crops	X	
Translocation of radionuclides to the edible tissues of crops	X	X
Postdeposition retention by crops (including weathering processes)	X	X
Radionuclide uptake by crops through the roots	X	X
Release of gaseous radionuclides (^{222}Rn, $^{14}CO_2$) from the soil	X	
Absorption of $^{14}CO_2$ by crops from the atmosphere	X	
Radionuclide uptake by animals through consumption of feed, water, and soil, followed by transfer to animal products	X	X
Radionuclide transfer from water to air via evaporative coolers	X	
Radionuclide transfer from water to fish	X	

Source: SNL 2007a, Sections 6.3, 6.4, and 6.5.

Table 2.3.10-3. Exposure Pathways for the Groundwater Exposure Scenario

Environmental Medium	Exposure Mode	Exposure Pathway	Examples of Typical Activities
Water	Ingestion	Water intake	Drinking water and water-based beverages; water used in food preparation
Soil	Ingestion	Inadvertent soil ingestion	Recreational activities, occupational activities, gardening, consumption of fresh fruits and vegetables
Soil	External	External radiation exposure	Time spent on or near soil containing radionuclides
Air	Inhalation	Breathing resuspended particles, gases (^{222}Rn and progeny, $^{14}CO_2$), and aerosols from evaporative coolers	Outdoor activities, including soil-disturbing activities related to work and recreation; domestic activities, including sleeping
Plants	Ingestion	Consumption of locally produced crops (leafy vegetables, other vegetables, fruit, and grain)	Eating crops
Animals	Ingestion	Consumption of locally produced animal products (meat, poultry, milk, and eggs)	Eating animal products
Fish	Ingestion	Consumption of locally produced freshwater fish	Eating fish

Source; SNL 2007a, Table 6.3-1.

Table 2.3.10-4. Exposure Pathways for the Volcanic Ash Exposure Scenario

Environmental Medium	Exposure Mode	Exposure Pathways	Examples of Typical Activities
Soil	Ingestion	Inadvertent soil ingestion	Recreational activities, occupational activities, gardening, consumption of fresh fruit and vegetables
Soil	External	External radiation exposure	Activities on or near soil containing radionuclides
Air	Inhalation	Breathing of airborne particulates, breathing of gases (^{222}Rn and progeny)	Outdoor activities, including soil-disturbing activities related to work and recreation. Domestic activities, including sleeping
Plants	Ingestion	Consumption of locally produced crops, including leafy vegetables, other vegetables, fruit, and grain	Eating and drinking plant materials
Animals	Ingestion	Consumption of locally produced animal products, including meat, poultry, milk, and eggs	Eating and drinking animal products

Source: SNL 2007a, Table 6.3-3.

Table 2.3.10-5. Radionuclides of Interest and Their Decay Products

Primary Radionuclide		Decay Product [b] (Branching Fraction if not 100%, Half-Life)	Terminal Nuclide	
Radionuclide [a]	Half-life (yr) [b]		Nuclide	Half-life (yr) [b,c]
^{14}C	5730	—	^{14}N	*
^{36}Cl	3.01×10^{5}	—	^{36}Ar (1.9%) ^{36}S (98.1%)	* *
^{79}Se	1.13×10^{6c}	—	^{79}Br	*
^{90}Sr D	29.12	^{90}Y (64.0 hours)	^{90}Zr	*
^{99}Tc	2.13×10^{5}	—	^{99}Ru	*
^{126}Sn D	1.0×10^{5}	^{126m}Sb (19.0 minutes) ^{126}Sb (14%, 12.4 days)	^{126}Te	*
^{129}I	1.57×10^{7}	—	^{129}Xe	*
^{135}Cs	2.3×10^{6}	—	^{135}Ba	*
^{137}Cs D	30.0	^{137m}Ba (94.6%, 2.552 minutes)	^{137}Ba	*
^{242}Pu	3.763×10^{5}	—	^{238}U	4.468×10^{9}
^{238}U D	4.468×10^{9}	^{234}Th (24.10 days) ^{234m}Pa (99.80%, 1.17 minutes) ^{234}Pa (0.33%, 6.7 hours)[d]	^{234}U	2.445×10^{5}
^{238}Pu	87.74	—	^{234}U	2.445×10^{5}
^{234}U	2.445×10^{5}	—	^{230}Th	7.7×10^{4}
^{230}Th	7.7×10^{4}	—	^{226}Ra	1.60×10^{3}
^{226}Ra	1.60×10^{3}	^{222}Rn (3.8235 days) ^{218}Po (3.05 minutes) ^{214}Pb (99.98%, 26.8 minutes) ^{218}At (0.02%, 2 seconds) ^{214}Bi (19.9 minutes) ^{214}Po (99.98%, 1.64×10^{-4} second) ^{210}Tl (0.02%, 1.3 minutes)	^{210}Pb	2.23×10^{1}
^{210}Pb	22.3	^{210}Bi (5.012 days) ^{210}Po (138.38 days)	^{206}Pb	*
^{240}Pu	6.537×10^{3}	—	^{236}U	2.3415×10^{7}
^{236}U	2.3415×10^{7}	—	^{232}Th	1.405×10^{10}
^{232}Th	1.405×10^{10}	—	^{228}Ra	5.75
^{228}Ra	5.75	^{228}Ac (6.13 hours)	^{228}Th	1.9131
^{232}U	72	—	^{228}Th	1.9131

Table 2.3.10-5. Radionuclides of Interest and Their Decay Products (Continued)

Primary Radionuclide		Decay Product [b] (Branching Fraction if not 100%, Half-Life)	Terminal Nuclide	
Radionuclide [a]	Half-life (yr) [b]		Nuclide	Half-life (yr) [b,c]
^{228}Th[e]	1.9131	^{224}Ra (3.66 days) ^{220}Rn (55.6 seconds) ^{216}Po (0.15 second) ^{212}Pb (10.64 hours) ^{212}Bi (60.55 minutes) ^{212}Po (64.07%, 0.305 microsecond) ^{208}Tl (35.93%, 3.07 minutes)	^{208}Pb	*
^{243}Am	7.38×10^{3}	^{239}Np (2.355 days)	^{239}Pu	2.406×10^{4}
^{239}Pu	2.4065×10^{4}	—	^{235}U	7.038×10^{8}
^{235}U	7.038×10^{8}	^{231}Th (25.52 hours)	^{231}Pa	3.276×10^{4}
^{231}Pa	3.276×10^{4}	—	^{227}Ac	2.1773×10^{1}
^{227}Ac	21.773	^{227}Th (98.62%, 18.718 days) ^{223}Fr (1.38%, 21.8 minutes) ^{223}Ra (11.434 days) ^{219}Rn (3.96 seconds) ^{215}Po (1.78 milliseconds) ^{211}Pb (36.1 minutes) ^{211}Bi (2.14 minutes) ^{207}Tl (99.72%, 4.77 minutes) ^{211}Po (0.28%, 0.516 seconds)	^{207}Pb	*
^{241}Am	432.2	—	^{237}Np	2.14×10^{6}
^{237}Np	2.14×10^{6}	^{233}Pa (27.0 days)	^{233}U	1.585×10^{5}
^{233}U	1.585×10^{5}	—	^{229}Th	7.34×10^{3}
^{229}Th	7.34×10^{3}	^{225}Ra (14.8 days) ^{225}Ac (10.0 days) ^{221}Fr (4.8 minutes) ^{217}At (32.3 milliseconds) ^{213}Bi (45.65 minutes) ^{213}Po (97.84%, 4.2 microseconds) ^{209}Tl (2.16%, 2.2 minutes) ^{209}Pb (3.253 hours)	^{209}Bi	*

NOTE: [a]"D" indicates that the radionuclide is treated in the model together with the short-lived ($T_{1/2}$ less than 180 days) decay products.
[b]Eckerman and Ryman 1993, Table A.1; Lide and Frederikse 1997, p. 11-125, was used for ^{210}Tl; Firestone 1998, was used for ^{79}Se half-life.
[c]A "*" denotes a stable nuclide.
[d]The sum of branching fractions for ^{234}Pa and ^{234m}Pa (decay products of ^{234}Th) is greater than one because a fraction of ^{234}Pa undergoes decay to ^{234}Pa. Both of these radionuclides then decay to ^{234}U.
[e]^{228}Th is a long-lived decay product of ^{228}Ra and in the biosphere model it is treated the same as a primary radionuclide.

Source: SNL 2007a, Table 6.3-7.

Table 2.3.10-6. Dose Coefficients and Effective Dose Coefficients for Exposure to Soil Contaminated to an Infinite Depth

Primary Radionuclide[a]	Decay Product[b] (Branching Fraction if not 100%, Half-Life)	Dose coefficient[c] (Sv/s/(Bq/m^3))	Effective Dose Coefficient (Sv/s/(Bq/m^3))
^{14}C	—	5.90×10^{-23}	5.90×10^{-23}
^{36}Cl	—	1.33×10^{-20}	1.33×10^{-20}
^{79}Se	—	8.21×10^{-23}	8.21×10^{-23}
^{90}Sr D	^{90}Y (64.0 hours)	3.46×10^{-21} 2.15×10^{-19}	2.18×10^{-19}
^{99}Tc	—	5.81×10^{-22}	5.81×10^{-22}
^{126}Sn D	^{126m}Sb (19.0 minutes) ^{126}Sb (14%, 12.4 days)	6.97×10^{-19} 4.67×10^{-17} 8.60×10^{-17}	5.94×10^{-17}
^{129}I	—	5.14×10^{-20}	5.14×10^{-20}
^{135}Cs	—	1.72×10^{-22}	1.72×10^{-22}
^{137}Cs D	^{137m}Ba (94.6%, 2.552 minutes)	4.47×10^{-21} 1.81×10^{-17}	1.71×10^{-17}
^{242}Pu	—	5.32×10^{-22}	5.32×10^{-22}
^{238}U D	^{234}Th (24.10 days) ^{234m}Pa (99.80%, 1.17 minutes) ^{234}Pa (0.33%, 6.7 hours)	4.27×10^{-22} 1.14×10^{-19} 5.28×10^{-19} 5.83×10^{-17}	8.34×10^{-19}
^{238}Pu	—	6.25×10^{-22}	6.25×10^{-22}
^{234}U	—	1.84×10^{-21}	1.84×10^{-21}
^{230}Th	—	5.73×10^{-21}	5.73×10^{-21}
^{226}Ra D	^{222}Rn (3.8235 days) ^{218}Po (3.05 minutes) ^{214}Pb (99.98%, 26.8 minutes) ^{218}At (0.02%, 2 seconds) ^{214}Bi (19.9 minutes) ^{214}Po (99.98%, 1.64×10^{-4} second) ^{210}Tl (0.02%, 1.3 minutes)	1.56×10^{-19} 1.17×10^{-20} 2.85×10^{-22} 6.65×10^{-18} 2.61×10^{-20} 4.99×10^{-17} 2.59×10^{-21} 0	5.67×10^{-17}
^{210}Pb D	^{210}Bi (5.012 days) ^{210}Po (138.38 days)	1.06×10^{-20} 2.92×10^{-20} 2.64×10^{-22}	4.01×10^{-20}
^{240}Pu	—	6.03×10^{-22}	6.03×10^{-22}
^{236}U	—	9.53×10^{-22}	9.53×10^{-22}
^{232}Th	—	2.44×10^{-21}	2.44×10^{-21}

Table 2.3.10-6. Dose Coefficients and Effective Dose Coefficients for Exposure to Soil Contaminated to an Infinite Depth (Continued)

Primary Radionuclide[a]	Decay Product[b] (Branching Fraction if not 100%, Half-Life)	Dose coefficient[c] (Sv/s/(Bq/m^3))	Effective Dose Coefficient (Sv/s/(Bq/m^3))
^{228}Ra D	^{228}Ac (6.13 hours)	0 3.03×10^{-17}	3.03×10^{-17}
^{232}U	—	4.25×10^{-21}	4.25×10^{-21}
^{228}Th D[d]	^{224}Ra (3.66 days) ^{220}Rn (55.6 seconds) ^{216}Po (0.15 seconds) ^{212}Pb (10.64 hours) ^{212}Bi (60.55 minutes) ^{212}Po (64.07%, 0.305 microsecond) ^{208}Tl (35.93%, 3.07 minutes)	3.85×10^{-20} 2.53×10^{-19} 1.15×10^{-20} 5.26×10^{-22} 3.46×10^{-18} 5.96×10^{-18} 0 1.17×10^{-16}	5.18×10^{-17}
^{243}Am D	^{239}Np (2.355 days)	6.66×10^{-19} 3.69×10^{-18}	4.36×10^{-18}
^{239}Pu	—	1.41×10^{-21}	1.41×10^{-21}
^{235}U D	^{231}Th (25.52 hours)	3.53×10^{-18} 1.72×10^{-19}	3.70×10^{-18}
^{231}Pa	—	9.44×10^{-19}	9.44×10^{-19}
^{227}Ac D	^{227}Th (98.62%, 18.718 days) ^{223}Fr (1.38%, 21.8 minutes) ^{223}Ra (11.434 days) ^{219}Rn (3.96 seconds) ^{215}Po (1.78 milliseconds) ^{211}Pb (36.1 minutes) ^{211}Bi (2.14 minutes) ^{207}Tl (99.72%, 4.77 minutes) ^{211}Po (0.28%, 0.516 second)	2.40×10^{-21} 2.57×10^{-18} 9.71×10^{-19} 2.96×10^{-18} 1.53×10^{-18} 5.06×10^{-21} 1.56×10^{-18} 1.27×10^{-18} 1.23×10^{-19} 2.40×10^{-19}	1.00×10^{-17}
^{241}Am	—	1.99×10^{-19}	1.99×10^{-19}
^{237}Np D	^{233}Pa (27.0 days)	3.73×10^{-19} 5.04×10^{-18}	5.41×10^{-18}
^{233}U	—	6.77×10^{-21}	6.77×10^{-21}

Table 2.3.10-6. Dose Coefficients and Effective Dose Coefficients for Exposure to Soil Contaminated to an Infinite Depth (Continued)

Primary Radionuclide[a]	Decay Product[b] (Branching Fraction if not 100%, Half-Life)	Dose coefficient[c] (Sv/s/(Bq/m^3))	Effective Dose Coefficient (Sv/s/(Bq/m^3))
^{229}Th		1.55×10^{-18}	7.92×10^{-18}
	^{225}Ra (14.8 days)	4.63×10^{-20}	
	^{225}Ac (10.0 days)	3.09×10^{-19}	
	^{221}Fr (4.8 minutes)	7.56×10^{-19}	
	^{217}At (32.3 milliseconds)	8.86×10^{-21}	
	^{213}Bi (45.65 minutes)	3.83×10^{-18}	
	^{213}Po (97.84%, 4.2 microseconds)	0	
	^{209}Ti (2.16%, 2.2 minutes)	6.56×10^{-17}	
	^{209}Pb (3.253 hours)	4.04×10^{-21}	

NOTE: [a]A "D" indicates that the radionuclide is treated with its short-lived (less than 180 days) decay products.
[b]Half-lives and branching fractions were taken from Table 2.3.10-5.
[c]Dose coefficient source: EPA 2002.
[d]^{228}Th is a long-lived decay product of 228Ra and in the biosphere model it is treated the same as a primary radionuclide.

Source: SNL 2007a, Table 6.4-4.

Table 2.3.10-7. Dose Coefficients and Effective Dose Coefficients for Exposure to Contaminated Ground Surface

Primary Radionuclide[a]	Decay Product[b] (Branching Fraction if not 100%, Half-Life)	Dose coefficient[c] (Sv/s/(Bq/m^2))	Effective Dose Coefficient (Sv/s/(Bq/m^2))
^{90}Sr D	^{90}Y (64.0 hours)	1.64×10^{-18} 1.10×10^{-16}	1.12×10^{-16}
^{99}Tc	—	6.49×10^{-20}	6.49×10^{-20}
^{126}Sn D	^{126m}Sb (19.0 minutes) ^{126}Sb (14%, 12.4 days)	4.83×10^{-17} 1.54×10^{-15} 2.71×10^{-15}	1.97×10^{-15}
^{137}Cs D	^{137m}Ba (94.6%, 2.552 minutes)	2.99×10^{-18} 5.78×10^{-16}	5.50×10^{-16}
^{242}Pu	—	4.98×10^{-19}	4.98×10^{-19}
^{238}U D	^{234}Th (24.10 days) ^{234m}Pa (99.80%, 1.17 minutes) ^{234}Pa (0.33%, 6.7 hours)	4.24×10^{-19} 7.50×10^{-18} 1.08×10^{-16} 1.80×10^{-15}	1.22×10^{-16}
^{238}Pu	—	6.26×10^{-19}	6.26×10^{-19}
^{234}U	—	5.86×10^{-19}	5.86×10^{-19}
^{230}Th	—	6.37×10^{-19}	6.37×10^{-19}
^{226}Ra D	^{222}Rn (3.8235 days) ^{218}Po (3.05 minutes) ^{214}Pb (99.98%, 26.8 minutes) ^{218}At (0.02%, 2 seconds) ^{214}Bi (19.9 minutes) ^{214}Po (99.98%, 1.64×10^{-4} second) ^{210}Tl (0.02%, 1.3 minutes)	6.11×10^{-18} 3.82×10^{-19} 8.64×10^{-21} 2.40×10^{-16} 3.65×10^{-18} 1.44×10^{-15} 7.91×10^{-20} 0	1.69×10^{-15}
^{210}Pb D	^{210}Bi (5.012 days) ^{210}Po (138.38 days)	2.13×10^{-18} 3.51×10^{-17} 8.07×10^{-21}	3.72×10^{-17}
^{240}Pu	—	6.01×10^{-19}	6.01×10^{-19}
^{236}U	—	5.03×10^{-19}	5.03×10^{-19}
^{232}Th	—	4.55×10^{-19}	4.55×10^{-19}
^{228}Ra D	^{228}Ac (6.13 hours)	0 9.38×10^{-16}	9.38×10^{-16}
^{232}U	—	8.08×10^{-19}	8.08×10^{-19}

Table 2.3.10-7. Dose Coefficients and Effective Dose Coefficients for Exposure to Contaminated Ground Surface (Continued)

Primary Radionuclide[a]	Decay Product[b] (Branching Fraction if not 100%, Half-Life)	Dose coefficient[c] (Sv/s/(Bq/m^2))	Effective Dose Coefficient (Sv/s/(Bq/m^2))
^{228}Th D[d]	 ^{224}Ra (3.66 days) ^{220}Rn (55.6 seconds) ^{216}Po (0.15 second) ^{212}Pb (10.64 hours) ^{212}Bi (60.55 minutes) ^{212}Po (64.07%, 0.305 microsecond) ^{208}Tl (35.93%, 3.07 minutes)	2.13×10^{-18} 9.15×10^{-18} 3.69×10^{-19} 1.61×10^{-20} 1.35×10^{-16} 2.25×10^{-16} 0 2.97×10^{-15}	1.44×10^{-15}
^{243}AmD	 ^{239}Np (2.355 days)	4.80×10^{-17} 1.54×10^{-16}	2.02×10^{-16}
^{239}Pu	—	2.84×10^{-19}	2.84×10^{-19}
^{235}U D	 ^{231}Th (25.52 hours)	1.40×10^{-16} 1.56×10^{-17}	1.56×10^{-16}
^{231}Pa	—	3.78×10^{-17}	3.78×10^{-17}
^{227}Ac D	 ^{227}Th (98.62%, 18.718 days) ^{223}Fr (1.38%, 21.8 minutes) ^{223}Ra (11.434 days) ^{219}Rn (3.96 seconds) ^{215}Po (1.78 milliseconds) ^{211}Pb (36.1 minutes) ^{211}Bi (2.14 minutes) ^{207}Tl (99.72%, 4.77 minutes) ^{211}Po (0.28%, 0.516 seconds)	1.41×10^{-19} 9.81×10^{-17} 7.76×10^{-17} 1.21×10^{-16} 5.28×10^{-17} 1.68×10^{-19} 9.49×10^{-17} 4.40×10^{-17} 5.56×10^{-17} 7.41×10^{-18}	4.66×10^{-16}
^{241}Am	—	2.33×10^{-17}	2.33×10^{-17}
^{237}Np D	 ^{233}Pa (27.0 days)	2.52×10^{-17} 1.86×10^{-16}	2.11×10^{-16}
^{233}U	—	6.00×10^{-19}	6.00×10^{-19}

Table 2.3.10-7. Dose Coefficients and Effective Dose Coefficients for Exposure to Contaminated Ground Surface (Continued)

Primary Radionuclide[a]	Decay Product[b] (Branching Fraction if not 100%, Half-Life)	Dose coefficient[c] (Sv/s/(Bq/m^2))	Effective Dose Coefficient (Sv/s/(Bq/m^2))
^{229}Th D		7.90×10^{-17}	3.46×10^{-16}
	^{225}Ra (14.8 days)	1.07×10^{-17}	
	^{225}Ac (10.0 days)	1.47×10^{-17}	
	^{221}Fr (4.8 minutes)	2.84×10^{-17}	
	^{217}At (32.3 milliseconds)	2.92×10^{-19}	
	^{213}Bi (45.65 minutes)	1.68×10^{-16}	
	^{213}Po (97.84%, 4.2 microseconds)	0	
	^{209}Tl (2.16%, 2.2 minutes)	1.92×10^{-15}	
	^{209}Pb (3.253 hours)	3.19×10^{-18}	

NOTE: [a]A "D" after a radionuclide symbol denotes that the radionuclide is treated together with the short-lived (less than 180 days) decay product.
[b]Half-lives and branching fractions were taken from Table 2.3.10-5.
[c]Dose coefficients source: EPA 2002.
[d]^{228}Th is a long-lived decay product of ^{228}Ra and in the biosphere model it is treated the same as a primary radionuclide.

Source: SNL 2007a, Table 6.5-1.

Table 2.3.10-8. Dose Coefficients and Effective Dose Coefficients for Inhalation

Primary Radionuclide[a]	Absorption Type	Decay Product[b] (Branching Fraction if not 100%, Half-Life)	Dose Coefficient[c] (Sv/Bq)	Effective Dose Coefficient (Sv/Bq)
^{14}C	(CO_2)	—	6.24×10^{-12}	6.24×10^{-12}
	S	—	5.73×10^{-9}	5.73×10^{-9}
^{36}Cl	S	—	3.80×10^{-8}	3.80×10^{-8}
^{79}Se	S	—	6.77×10^{-9}	6.77×10^{-9}
^{90}Sr D	S S	^{90}Y (64.0 hours)	1.57×10^{-7} 1.50×10^{-9}	1.59×10^{-7}
^{99}Tc	S	—	1.33×10^{-8}	1.33×10^{-8}
^{126}Sn D	S S S	Sb-126m (19.0 minutes) Sb-126 (14%, 12.4 day)	1.55×10^{-7} 1.96×10^{-11} 3.24×10^{-9}	1.55×10^{-7}
^{129}I	F	—	3.59×10^{-8}	3.59×10^{-8}
^{135}Cs	S	—	8.53×10^{-9}	8.53×10^{-9}
^{137}Cs D	S —	Ba-137m (94.6%, 2.552 minutes)	3.92×10^{-8} 0	3.92×10^{-8}
^{242}Pu	F	—	1.13×10^{-4}	1.13×10^{-4}
^{238}U D	S S — S	^{234}Th (24.10 days) ^{234m}Pa (99.80%, 1.17 minutes) ^{234}Pa (0.33%, 6.7 hours)	8.04×10^{-6} 7.69×10^{-9} 0 4.16×10^{-10}	8.05×10^{-6}
^{238}Pu	F	—	1.08×10^{-4}	1.08×10^{-4}
^{234}U	S	—	9.40×10^{-6}	9.40×10^{-6}
^{230}Th	F	—	1.02×10^{-4}	1.02×10^{-4}
^{226}Ra D	S — — S — S — —	^{222}Rn (3.8235 days) ^{218}Po (3.05 minutes) ^{214}Pb (99.98%, 26.8 minutes) ^{218}At (0.02%, 2 seconds) ^{214}Bi (19.9 minutes) ^{214}Po (99.98%, 1.64×10^{-4} second) ^{210}Tl (0.02%, 1.3 minutes)	9.51×10^{-6} 0[d] 0 1.47×10^{-8} 0 1.54×10^{-8} 0 0	9.54×10^{-6}
^{210}Pb D	S S S	^{210}Bi (5.012 days) ^{210}Po (138.38 days)	5.61×10^{-6} 1.33×10^{-7} 4.27×10^{-6}	1.00×10^{-5}
^{240}Pu	F	—	1.19×10^{-4}	1.19×10^{-4}
^{236}U	S	—	8.74×10^{-6}	8.74×10^{-6}
^{232}Th	F	—	1.10×10^{-4}	1.10×10^{-4}

Table 2.3.10-8. Dose Coefficients and Effective Dose Coefficients for Inhalation (Continued)

Primary Radionuclide[a]	Absorption Type	Decay Product[b] (Branching Fraction if not 100%, Half-Life)	Dose Coefficient[c] (Sv/Bq)	Effective Dose Coefficient (Sv/Bq)
^{228}Ra D[e]	S S	^{228}Ac (6.13 hours)	1.60×10^{-5} 1.46×10^{-8}	1.60×10^{-5}
^{232}U	S	—	3.70×10^{-5}	3.70×10^{-5}
^{228}Th D	S S — — S S — —	^{224}Ra (3.66 days) ^{220}Rn (55.6 seconds) ^{216}Po (0.15 second) ^{212}Pb (10.64 hours) ^{212}Bi (60.55 minutes) ^{212}Po (64.07%, 0.305 microsecond) ^{208}Tl (35.93%, 3.07 minutes)	3.97×10^{-5} 3.36×10^{-6} 0 0 1.90×10^{-7} 3.32×10^{-8} 0 0	4.33×10^{-5}
^{243}Am D	F S	^{239}Np (2.355 days)	9.57×10^{-5} 1.03×10^{-9}	9.57×10^{-5}
^{239}Pu	F	—	1.19×10^{-4}	1.19×10^{-4}
^{235}U D	S S	^{231}Th (25.52 hours)	8.47×10^{-6} 3.34×10^{-10}	8.47×10^{-6}
^{234}Pa	F	—	2.30×10^{-4}	2.30×10^{-4}
^{227}Ac D	F S S S — — S — — —	^{227}Th (98.62%, 18.718 days) ^{223}Fr (1.38%, 21.8 minutes) ^{223}Ra (11.434 days) ^{219}Rn (3.96 seconds) ^{215}Po (1.78 milliseconds) ^{211}Pb (36.1 minutes) ^{211}Bi (2.14 minutes) ^{207}Tl (99.72%, 4.77 minutes) ^{211}Po (0.28%, 0.516 second)	1.56×10^{-4} 1.04×10^{-5} 1.21×10^{-8} 8.68×10^{-6} 0 0 1.20×10^{-8} 0 0 0	1.75×10^{-4}
^{241}Am	F	—	9.64×10^{-5}	9.64×10^{-5}
^{237}Np D	F S	^{233}Pa (27.0 days)	4.97×10^{-5} 3.86×10^{-9}	4.97×10^{-5}
^{233}U	S	—	9.59×10^{-6}	9.59×10^{-6}

Table 2.3.10-8. Dose Coefficients and Effective Dose Coefficients for Inhalation (Continued)

Primary Radionuclide[a]	Absorption Type	Decay Product[b] (Branching Fraction if not 100%, Half-Life)	Dose Coefficient[c] (Sv/Bq)	Effective Dose Coefficient (Sv/Bq)
^{229}Th D	F		2.39×10^{-4}	2.55×10^{-4}
	S	^{225}Ra (14.8 days)	7.73×10^{-6}	
	S	^{225}Ac (10.0 days)	8.49×10^{-6}	
	—	^{221}Fr (4.8 minutes)	0	
	—	^{217}At (32.3 milliseconds)	0	
	S	^{213}Bi (45.65 minutes)	3.20×10^{-8}	
	—	^{213}Po (97.84%, 4.2 microseconds)	0	
	—	^{209}Tl (2.16%, 2.2 minutes)	0	
	S	^{209}Pb (3.253 hours)	6.10×10^{-11}	

NOTE: [a]A "D" indicates that the radionuclide is treated with its short-lived (less than 180 days) decay products.
[b]Half-lives and branching fractions were taken from Table 2.3.10-5.
[c]Dose coefficient source: EPA 2002.
[d]Dose coefficient for inhalation of short-lived decay products of ^{222}Rn (alpha emitters) is calculated separately and is equal to 6.62×10^{-9} Sv/Bq (BSC 2005, Section 6.5.4).
[e]^{228}Th is a long-lived decay product of ^{228}Ra and in the biosphere model it is treated the same as a primary radionuclide.

Source: SNL 2007a, Table 6.4-5.

Table 2.3.10-9. Dose Coefficients and Effective Dose Coefficients for Ingestion

Primary Radionuclide[a]	Fractional Uptake to Blood[c]	Decay Product[b] (Branching Fraction if not 100%, Half-Life)	Dose Coefficient[c] (Sv/Bq)	Effective Dose Coefficient (Sv/Bq)
^{14}C	1.0	—	5.81×10^{-10}	5.81×10^{-10}
^{36}Cl	1.0	—	9.29×10^{-10}	9.29×10^{-10}
^{79}Se	8×10^{-1}	—	2.89×10^{-9}	2.89×10^{-9}
^{90}Sr D	3×10^{-1} 1×10^{-4}	^{90}Y (64.0 hours)	2.77×10^{-8} 2.69×10^{-9}	3.04×10^{-8}
^{99}Tc	5×10^{-1}	—	6.42×10^{-10}	6.42×10^{-10}
^{126}Sn D	2×10^{-2} 1×10^{-1} 1×10^{-1}	^{126m}Sb (19.0 minutes) ^{126}Sb (14%, 12.4 days)	4.77×10^{-9} 3.60×10^{-11} 2.46×10^{-9}	5.15×10^{-9}
^{129}I	1.0	—	1.06×10^{-7}	1.06×10^{-7}
^{135}Cs	1.0	—	2.00×10^{-9}	2.00×10^{-9}
^{137}Cs D	1.0 —	^{137m} Ba (94.6%, 2.552 minutes)	1.36×10^{-8} 0	1.36×10^{-8}
^{242}Pu	5×10^{-4}	—	2.38×10^{-7}	2.38×10^{-7}
^{238}U D	2×10^{-2} 5×10^{-4} — 5×10^{-4}	^{234}Th (24.10 days) ^{234m}Pa (99.80%, 1.17 minutes) ^{234}Pa (0.33%, 6.7 hours)	4.45×10^{-8} 3.40×10^{-9} 0 5.24×10^{-10}	4.79×10^{-8}
^{238}Pu	5×10^{-4}	—	2.28×10^{-7}	2.28×10^{-7}
^{234}U	2×10^{-2}	—	4.95×10^{-8}	4.95×10^{-8}
^{230}Th	5×10^{-4}	—	2.14×10^{-7}	2.14×10^{-7}
^{226}Ra D	2×10^{-1} — — 2×10^{-1} — 5×10^{-2} — —	^{222}Rn (3.8235 days) ^{218}Po (3.05 minutes) ^{214}Pb (99.98%, 26.8 minutes) ^{218}At (0.02%, 2 seconds) ^{214}Bi (19.9 minutes) ^{214}Po (99.98%, 1.64×10^{-4} second) ^{210}Tl (0.02%, 1.3 minutes)	2.80×10^{-7} 0 0 1.39×10^{-10} 0 1.12×10^{-10} 0 0	2.80×10^{-7}
^{210}Pb D	2×10^{-1} 5×10^{-2} 5×10^{-1}	^{210}Bi (5.012 days) ^{210}Po (138.38 days)	6.96×10^{-7} 1.31×10^{-9} 1.21×10^{-6}	1.91×10^{-6}
^{240}Pu	5×10^{-4}	—	2.51×10^{-7}	2.51×10^{-7}
^{236}U	2×10^{-2}	—	4.69×10^{-8}	4.69×10^{-8}
^{232}Th	5×10^{-4}	—	2.31×10^{-7}	2.31×10^{-7}

Table 2.3.10-9. Dose Coefficients and Effective Dose Coefficients for Ingestion (Continued)

Primary Radionuclide[a]	Fractional Uptake to Blood[c]	Decay Product[b] (Branching Fraction if not 100%, Half-Life)	Dose Coefficient[c] (Sv/Bq)	Effective Dose Coefficient (Sv/Bq)
^{228}Ra D	2×10^{-1} 5×10^{-4}	^{228}Ac (6.13 hours)	6.97×10^{-7} 4.01×10^{-10}	6.97×10^{-7}
^{232}U	2×10^{-2}	—	3.36×10^{-7}	3.36×10^{-7}
^{228}Th D[d]	5×10^{-4} 2×10^{-1} — — 2×10^{-1} 5×10^{-2} — —	^{224}Ra (3.66 days) ^{220}Rn (55.6 seconds) ^{216}Po (0.15 seconds) ^{212}Pb (10.64 hours) ^{212}Bi (60.55 minutes) ^{212}Po (64.07%, 0.305 microseconds) ^{208}Tl (35.93%, 3.07 minutes)	7.20×10^{-8} 6.45×10^{-8} 0 0 5.98×10^{-9} 2.59×10^{-10} 0 0	1.43×10^{-7}
^{243}Am D	5×10^{-4} 5×10^{-4}	^{239}Np (2.355 days)	2.03×10^{-7} 7.99×10^{-10}	2.04×10^{-7}
^{239}Pu	5×10^{-4}	—	2.51×10^{-7}	2.51×10^{-7}
^{235}U D	2×10^{-2} 5×10^{-4}	^{231}Th (25.52 hours)	4.67×10^{-8} 3.36×10^{-10}	4.70×10^{-8}
^{231}Pa	5×10^{-4}	—	4.79×10^{-7}	4.79×10^{-7}
^{227}Ac D	5×10^{-4} 5×10^{-4} 1.0 2×10^{-1} — — 2×10^{-1} — — —	^{227}Th (98.62%, 18.718 days) ^{223}Fr (1.38%, 21.8 minutes) ^{223}Ra (11.434 days) ^{219}Rn (3.96 seconds) ^{215}Po (1.78 milliseconds) ^{211}Pb (36.1 minutes) ^{211}Bi (2.14 minutes) ^{207}Tl (99.72%, 4.77 minutes) ^{211}Po (0.28%, 0.516 second)	3.23×10^{-7} 9.02×10^{-9} 2.36×10^{-9} 1.04×10^{-7} 0 0 1.78×10^{-10} 0 0 0	4.36×10^{-7}
^{241}Am	5×10^{-4}	—	2.04×10^{-7}	2.04×10^{-7}
^{237}Np D	5×10^{-4} 5×10^{-4}	^{233}Pa (27.0 days)	1.07×10^{-7} 8.78×10^{-10}	1.08×10^{-7}
^{233}U	2×10^{-2}	—	5.13×10^{-8}	5.13×10^{-8}

Table 2.3.10-9. Dose Coefficients and Effective Dose Coefficients for Ingestion (Continued)

Primary Radionuclide[a]	Fractional Uptake to Blood[c]	Decay Product[b] (Branching Fraction if not 100%, Half-Life)	Dose Coefficient[c] (Sv/Bq)	Effective Dose Coefficient (Sv/Bq)
^{229}Th D	5×10^{-4} 2×10^{-1} 5×10^{-4} — — 5×10^{-2} — — 2×10^{-1}	 ^{225}Ra (14.8 days) ^{225}Ac (10.0 days) ^{221}Fr (4.8 minutes) ^{217}At (32.3 milliseconds) ^{213}Bi (45.65 minutes) ^{213}Po (97.84%, 4.2 microseconds) ^{209}Tl (2.16%, 2.2 minutes) ^{209}Pb (3.253 hours)	5.00×10^{-7} 9.95×10^{-8} 3.85×10^{-8} 0 0 1.98×10^{-10} 0 0 5.67×10^{-11}	6.38×10^{-7}

NOTE: [a]A "D" after a radionuclide symbol denotes that the radionuclide is treated together with the short-lived (less than 180 days) decay products.
[b]Half-lives and branching fractions were taken from Table 2.3.10-5.
[c]EPA 2002.
[d]^{228}Th is a long-lived decay product of ^{228}Ra and in the biosphere model it is treated the same as a primary radionuclide.

Source: SNL 2007a, Table 6.4-6.

Table 2.3.10-10. Summary of Biosphere Model Input Parameters

Submodel	Parameter Name	Distribution Type	Units	Mean, Mode, Average[a]	SD/SE[a]	Min.[b]	Max.[b]	Reference/Notes[c]
Surface Soil Sections 2.3.10.3.1.1 and 2.3.10.3.2.1	Radionuclide concentration in groundwater	Fixed	Bq/m^3	1	—	—	—	Unit activity concentration – used as a source term for the groundwater BDCF
	Annual average irrigation rate, garden crops, present-day climate	Normal	m/yr	0.91	0.09	0.69	1.13	SNL 2007a, Section 6.4.1.1
	Annual average irrigation rate, field crops, present-day climate	Normal	m/yr	1.78	0.14	1.41	2.14	SNL 2007a, Section 6.4.1.1
	Irrigation duration, garden crops	Triangular	year	25	—	25	250	SNL 2007b
	Irrigation duration, field crops	Triangular	year	100	—	100	1,000	SNL 2007b
	Radionuclide half-life	Fixed	year	See Table 2.3.10-5	—	—	—	SNL 2007a, Table 6.3-7
	Surface soil erosion rate	Triangular	$kg/(m^2 \cdot yr)$	0.2 (mode)	—	0.2	1.1	SNL 2007b
	Soil bulk density	Triangular	kg/m^3	1,500 (mean and mode)	—	1,300	1,700	SNL 2007b
	Surface soil depth (equal to tillage depth)	Uniform	m	0.25	—	0.05	0.30	BSC 2004c
	Depth of resuspendable soil layer	Uniform	m	0.002	—	0.001	0.003	BSC 2004d

Table 2.3.10-10. Summary of Biosphere Model Input Parameters (Continued)

Submodel	Parameter Name		Distribution Type	Units	Mean, Mode, Average[a]	SD/SE[a]	Min.[b]	Max.[b]	Reference/Notes[c]
Surface Soil (continued)	Soil solid-liquid distribution coefficient	Carbon	Lognormal	L/kg	1.8×10^{1}	6.0×10^{0}	5.3×10^{-1}	6.2×10^{2}	SNL 2007b, Lognormal distributions of distribution coefficients are given in terms of geometric mean and standard deviation. Distribution coefficients are correlated with the soil-to-plant transfer factors. The correlation coefficient is –0.8.
		Chlorine			1.4×10^{-1}	6.0×10^{0}	1.3×10^{3}	1.4×10^{1}	
		Selenium			1.5×10^{2}	6.0×10^{0}	4.4×10^{0}	5.1×10^{3}	
		Strontium			2.0×10^{1}	5.5×10^{0}	7.2×10^{-1}	5.6×10^{2}	
		Technetium			1.4×10^{-1}	6.0×10^{0}	1.3×10^{-3}	1.4×10^{1}	
		Tin			4.5×10^{2}	6.0×10^{0}	1.3×10^{1}	1.5×10^{4}	
		Iodine			4.5×10^{0}	7.4×10^{0}	8.9×10^{-2}	2.3×10^{2}	
		Cesium			4.4×10^{3}	3.7×10^{0}	1.6×10^{2}	1.3×10^{5}	
		Lead			1.6×10^{4}	4.1×10^{0}	1.0×10^{3}	2.5×10^{5}	
		Radium			3.6×10^{4}	2.2×10^{1}	8.3×10^{1}	1.6×10^{7}	
		Actinium			1.5×10^{3}	6.0×10^{0}	4.3×10^{1}	5.0×10^{4}	
		Thorium			3.0×10^{3}	8.2×10^{0}	4.9×10^{1}	1.8×10^{5}	
		Protactinium			1.8×10^{3}	6.0×10^{0}	5.3×10^{1}	6.2×10^{4}	
		Uranium			3.3×10^{1}	2.5×10^{1}	6.3×10^{1}	1.8×10^{4}	
		Neptunium			2.5×10^{1}	3.3×10^{0}	2.3×10^{0}	2.6×10^{2}	
		Plutonium			1.2×10^{3}	3.3×10^{0}	1.2×10^{2}	1.3×10^{4}	
		Americium			2.0×10^{3}	1.4×10^{1}	1.2×10^{1}	3.3×10^{5}	

Table 2.3.10-10. Summary of Biosphere Model Input Parameters (Continued)

Submodel	Parameter Name		Distribution Type	Units	Mean, Mode, Average[a]	SD/SE[a]	Min.[b]	Max.[b]	Reference/Notes[c]
Surface Soil (continued)	Overwatering rate, present-day climate		Cumulative	m/yr	0.079		0.009 0.030 0.045 0.077 0.129 0.233 0.275	0% 19% 38% 57% 76% 95% 100%	BSC 2004c
	Volumetric water content		Uniform	—	0.20	—	0.15	0.28	SNL 2007b
	Radionuclide concentration in tephra-soil mixture deposited on ground surface		Fixed	Bq/m^2	1	—	—	—	Unit areal activity concentration – a source term for the volcanic ash scenario.
	Radionuclide concentration in resuspendable layer of soil		Fixed	Bq/kg	1	—	—	—	Unit mass activity concentration – a source term for the volcanic ash scenario.
Air Sections 2.3.10.3.1.2 and 2.3.10.3.2.2	Mas loading for crops	Nominal	Triangular	mg/m^3	0.12	—	0.025	0.200	BSC 2006
		Post-volcanic			0.24	—	0.050	0.600	
	Mass loading for receptor environments at nominal conditions	Active outdoors	Triangular	mg/m^3	3.00	—	1.000	10.000	BSC 2006, Used for the groundwater scenario and for the long-term inhalation component for the volcanic ash scenario.
		Inactive outdoors			0.06	—	0.025	0.100	
		Active indoors			0.10	—	0.060	0.175	
		Asleep indoors			0.03	—	0.010	0.050	

Table 2.3.10-10. Summary of Biosphere Model Input Parameters (Continued)

Submodel	Parameter Name		Distribution Type	Units	Mean, Mode, Average[a]	SD/SE[a]	Min.[b]	Max.[b]	Reference/Notes[c]
Air (continued)	Mass loading for receptor environments at post-volcanic condition	Active outdoors	Triangular	mg/m^3	3.0	—	0.000	5.000	BSC 2006, Used for short-term inhalation component for the volcanic ash scenario.
		Inactive outdoors			0.06	—	0.025	0.200	
		Active indoors			0.10	—	0.060	0.175	
		Asleep indoors			0.03	—	0.010	0.050	
	Mass loading function $f(t) = S_0 e^{-\lambda t}$, λ = decrease rate constant λ for all tephra depths		Triangular	1/yr	0.20	—	0.125	1.0	BSC 2006, This decay function is used in the TSPA model.
	Enhancement factor groundwater scenario	Active outdoors	Triangular	—	1 (mode)	—	0.4	1.5	SNL 2007b
		Inactive outdoors			4 mode)	—	2	7	
		Active indoors							
		Asleep indoors							
	Enhancement factor volcanic scenario	Active outdoors	Lognormal	—	2.9 (GM)	1.8 (GSD)	0.9	9.4	
		Inactive outdoors			1.2 (GM)	2.0 (GSD)	0.3	4.6	
		Active indoors							
		Asleep indoors							
	Fraction of radionuclides transferred in evaporative cooler from water into air		Uniform	—	0.5	—	0	1	BSC 2004d

Table 2.3.10-10. Summary of Biosphere Model Input Parameters (Continued)

Submodel	Parameter Name		Distribution Type	Units	Mean, Mode, Average[a]	SD/SE[a]	Min.[b]	Max.[b]	Reference/Notes[c]
Air (continued)	Water evaporation (use) rate of evaporative cooler		Lognormal	L/hr	17 (GM)	1.7 (GSD)	—	—	BSC 2004d, Airflow rate is correlated with water evaporative rate (correlation coefficient = 0.8).
	Air flow rate of evaporative cooler		Cumulative	m^3/hr	8300 (median)	—	1700 8300 10200	0% 50% 100%	
	Radon release factor		Fixed	$(Bq/m^3)/(Bq/kg)$	0.25	—	—	—	BSC 2004d
	Interior wall height		Cumulative	m	2.3 (median)	—	2.1 2.3 2.7	0% 50% 100%	BSC 2004d
	House ventilation rate	Cooler off	Lognormal	1/hr	1 (AM)	1.1 (ASD)	0.35	2.9	BSC 2004d
		Cooler on	Uniform		15.5	—	1	30	
	Fraction of radon from soil entering into the house		Uniform	—	0.175	—	0.10	0.25	BSC 2004d
	Ratio of ^{222}Rn concentration in air to flux density from soil		Fixed	$(Bq/m^3)/(Bq/m^2 \cdot s)$	300	—	—	—	BSC 2004d
Plant Sections 2.3.10.3.1.3 and 2.3.10.3.2.3	Soil-to-plant transfer factor for leafy vegetables	Chlorine	Lognormal	$(Bq/kg_{plant})/(Bq/kg_{soil})$	6.4×10^{1}	2.0	1.1×10^{1}	3.8×10^{2}	BSC 2004d, Transfer factors are given in terms of geometric mean and geometric standard deviation.
		Selenium			4.6×10^{-2}	3.8	1.4×10^{-3}	1.4×10^{0}	
		Strontium			1.7×10^{0}	2.0	2.9×10^{-1}	1.0×10^{1}	
		Technetium			4.6×10^{1}	2.6	3.8×10^{0}	5.5×10^{2}	
		Tin			3.8×10^{-2}	2.0	6.4×10^{-3}	2.3×10^{-1}	
		Iodine			2.6×10^{-2}	9.9	7.2×10^{-5}	9.7×10^{0}	

Table 2.3.10-10. Summary of Biosphere Model Input Parameters (Continued)

Submodel	Parameter Name		Distribution Type	Units	Mean, Mode, Average[a]	SD/SE[a]	Min.[b]	Max.[b]	Reference/Notes[c]
Plant (continued)	Soil-to-plant transfer factor for leafy vegetables (continued)	Cesium	Lognormal	$(Bq/kg_{plant})/(Bq/kg_{soil})$	8.5×10^{-2}	2.5	7.7×10^{-3}	9.4×10^{-1}	
		Lead			1.5×10^{-2}	4.6	3.0×10^{-4}	7.7×10^{-1}	
		Radium			6.8×10^{-2}	2.7	5.1×10^{-3}	9.2×10^{-1}	
		Actinium			4.3×10^{-3}	2.0	7.2×10^{-4}	2.6×10^{-2}	
		Thorium			4.3×10^{-3}	2.8	3.2×10^{-4}	5.9×10^{-2}	
		Protactinium			4.6×10^{-3}	3.8	1.4×10^{-4}	1.4×10^{-1}	
		Uranium			1.1×10^{-2}	2.0	1.8×10^{-3}	6.6×10^{-2}	
		Neptunium			5.9×10^{-2}	4.4	1.3×10^{-3}	2.6×10^{0}	
		Plutonium			2.9×10^{-4}	2.0	4.9×10^{-5}	1.7×10^{-3}	
		Americium			1.2×10^{-3}	2.5	1.2×10^{-4}	1.3×10^{-2}	
	Soil-to-plant transfer factor for other vegetables	Chlorine	Lognormal	$(Bq/kg_{plant})/(Bq/kg_{soil})$	6.4×10^{1}	2.0	1.1×10^{1}	3.8×10^{2}	BSC 2004d, Transfer factors are given in terms of geometric mean and geometric standard deviation.
		Selenium			4.6×10^{-2}	3.8	1.4×10^{-3}	1.4×10^{0}	
		Strontium			7.9×10^{-1}	2.0	1.4×10^{-1}	4.5×10^{0}	
		Technetium			4.4×10^{0}	3.7	1.5×10^{-1}	1.2×10^{2}	
		Tin			1.5×10^{-2}	3.6	5.3×10^{-4}	4.0×10^{-1}	
		Iodine			3.2×10^{-2}	4.4	7.0×10^{-4}	1.5×10^{0}	
		Cesium			5.0×10^{-2}	2.0	8.4×10^{-3}	3.0×10^{-1}	
		Lead			9.0×10^{-3}	3.1	5.0×10^{-4}	1.6×10^{-1}	
		Radium			1.2×10^{-2}	5.3	1.6×10^{-4}	8.6×10^{-1}	
		Actinium			1.1×10^{-3}	4.9	1.8×10^{-5}	6.6×10^{-2}	
		Thorium			4.4×10^{-4}	5.6	5.3×10^{-6}	3.6×10^{-2}	

Table 2.3.10-10. Summary of Biosphere Model Input Parameters (Continued)

Submodel	Parameter Name		Distribution Type	Units	Mean, Mode, Average[a]	SD/SE[a]	Min.[b]	Max.[b]	Reference/Notes[c]
Plant (continued)	Soil-to-plant transfer factor for other vegetables (continued)	Protactinium	Lognormal	$(Bq/kg_{plant})/(Bq/kg_{soil})$	1.1×10^{-3}	10.0	3.0×10^{-6}	4.3×10^{-1}	
		Uranium			6.0×10^{-3}	2.8	4.2×10^{-4}	8.5×10^{-2}	
		Neptunium			3.1×10^{-2}	4.9	5.0×10^{-4}	1.9×10^{0}	BSC 2004d
		Plutonium			1.9×10^{-4}	2.0	3.3×10^{-5}	1.1×10^{-3}	
		Americium			4.0×10^{-4}	2.6	3.5×10^{-5}	4.6×10^{-3}	
	Soil-to-plant transfer factor for fruit	Chlorine	Lognormal	$(Bq/kg_{plant})/(Bq/kg_{soil})$	6.4×10^{1}	2.0	1.1×10^{1}	3.8×10^{2}	BSC 2004d, Transfer factors are given in terms of geometric mean and geometric standard deviation.
		Selenium			4.6×10^{-2}	3.8	1.4×10^{-3}	1.4×10^{0}	
		Strontium			2.9×10^{-1}	2.3	3.6×10^{-2}	2.4×10^{0}	
		Technetium			4.3×10^{0}	4.6	8.7×10^{-2}	2.1×10^{2}	
		Tin			1.5×10^{-2}	3.6	5.3×10^{-4}	4.0×10^{-1}	
		Iodine			5.7×10^{-2}	2.8	4.1×10^{-3}	7.9×10^{-1}	
		Cesium			5.6×10^{-2}	2.8	3.8×10^{-3}	8.1×10^{-1}	
		Lead			1.2×10^{-2}	3.3	5.8×10^{-4}	2.6×10^{-1}	
		Radium			7.3×10^{-3}	4.3	1.6×10^{-4}	3.2×10^{-1}	
		Actinium			8.5×10^{-4}	3.4	3.7×10^{-5}	2.0×10^{-2}	
		Thorium			2.9×10^{-4}	4.9	4.8×10^{-6}	1.7×10^{-2}	
		Protactinium			1.1×10^{-3}	10.0	3.0×10^{-6}	4.3×10^{-1}	
		Uranium			6.3×10^{-3}	2.9	3.9×10^{-4}	1.0×10^{-1}	
		Neptunium			3.4×10^{-2}	6.9	2.3×10^{-4}	5.0×10^{0}	

Table 2.3.10-10. Summary of Biosphere Model Input Parameters (Continued)

Submodel	Parameter Name		Distribution Type	Units	Mean, Mode, Average[a]	SD/SE[a]	Min.[b]	Max.[b]	Reference/Notes[c]
Plant (continued)	Soil-to-plant transfer factor for fruit (continued)	Plutonium	Lognormal	$(Bq/kg_{plant})/(Bq/kg_{soil})$	1.8×10^{-4}	3.4	7.8×10^{-6}	4.2×10^{-3}	
		Americium			5.4×10^{-4}	2.3	6.5×10^{-5}	4.5×10^{-3}	
	Soil-to-plant transfer factor for grain	Chlorine	Lognormal	$(Bq/kg_{plant})/(Bq/kg_{soil})$	2.4×10^{1}	8.4	1.0×10^{-1}	5.8×10^{3}	BSC 2004d, Transfer factors are given in terms of geometric mean and geometric standard deviation.
		Selenium			2.9×10^{-2}	2.0	4.8×10^{-3}	1.7×10^{-1}	
		Strontium			1.7×10^{-1}	2.0	2.8×10^{-2}	1.0×10^{0}	
		Technetium			1.6×10^{0}	4.3	3.8×10^{-2}	6.8×10^{1}	
		Tin			9.2×10^{-3}	2.0	1.5×10^{-3}	5.5×10^{-2}	
		Iodine			2.5×10^{-2}	10.0	6.6×10^{-5}	9.4×10^{0}	
		Cesium			2.0×10^{-2}	2.2	2.7×10^{-3}	1.6×10^{-1}	
		Lead			5.5×10^{-3}	2.1	8.2×10^{-4}	3.8×10^{-2}	
		Radium			3.1×10^{-3}	4.0	8.8×10^{-5}	1.1×10^{-1}	
		Actinium			5.4×10^{-4}	2.9	3.6×10^{-5}	8.0×10^{-3}	
		Thorium			1.7×10^{-4}	5.2	2.4×10^{-6}	1.2×10^{-2}	
		Protactinium			9.5×10^{-4}	7.2	5.9×10^{-6}	1.5×10^{-1}	
		Uranium			1.1×10^{-3}	3.6	4.1×10^{-5}	3.1×10^{-2}	
		Neptunium			4.4×10^{-3}	6.9	3.1×10^{-5}	6.3×10^{-1}	
		Plutonium			1.9×10^{-5}	4.2	4.8×10^{-7}	7.8×10^{-4}	
		Americium			7.5×10^{-5}	3.2	3.8×10^{-6}	1.5×10^{-3}	

Table 2.3.10-10. Summary of Biosphere Model Input Parameters (Continued)

Submodel	Parameter Name		Distribution Type	Units	Mean, Mode, Average[a]	SD/SE[a]	Min.[b]	Max.[b]	Reference/Notes[c]
Plant (continued)	Soil-to-plant transfer factor for forage	Chlorine	Lognormal	(Bq/kg_{plant})/(Bq/kg_{soil})	7.5×10^{1}	2.0	1.3×10^{1}	4.5×10^{2}	BSC 2004d, Transfer factors are given in terms of geometric mean and geometric standard deviation.
		Selenium			1.5×10^{-1}	5.5	1.9×10^{-3}	1.3×10^{1}	
		Strontium			2.1×10^{0}	2.1	3.2×10^{-1}	1.3×10^{1}	
		Technetium			2.7×10^{1}	2.7	2.1×10^{0}	3.5×10^{2}	
		Tin			1.6×10^{-1}	5.8	1.7×10^{-3}	1.5×10^{1}	
		Iodine			4.0×10^{-2}	10.0	1.1×10^{-4}	1.5×10^{1}	
		Cesium			1.3×10^{-1}	3.3	6.3×10^{-3}	2.8×10^{0}	
		Lead			1.8×10^{-2}	7.0	1.2×10^{-4}	2.8×10^{0}	
		Radium			8.2×10^{-2}	3.0	4.9×10^{-3}	1.4×10^{0}	
		Actinium			1.7×10^{-2}	5.4	2.2×10^{-4}	1.3×10^{0}	
		Thorium			1.0×10^{-2}	4.2	2.5×10^{-4}	3.9×10^{-1}	
		Protactinium			1.9×10^{-2}	6.7	1.4×10^{-4}	2.5×10^{0}	
		Uranium			1.7×10^{-2}	6.1	1.6×10^{-4}	1.9×10^{0}	
		Neptunium			5.8×10^{-2}	5.6	6.8×10^{-4}	4.9×10^{0}	
		Plutonium			1.0×10^{-3}	10.0	2.7×10^{-6}	3.9×10^{-1}	
		Americium			2.1×10^{-3}	10.0	5.5×10^{-6}	7.9×10^{-1}	

Table 2.3.10-10. Summary of Biosphere Model Input Parameters (Continued)

Submodel	Parameter Name		Distribution Type	Units	Mean, Mode, Average[a]	SD/SE[a]	Min.[b]	Max.[b]	Reference/Notes[c]
Plant (continued)	Dry-to-wet weight ratio	Leafy vegetables	Cumulative	kg_{dry}/kg_{wet}	0.070	—	0.041 0.054 0.06 0.078 0.081 0.084 0.093	0% 17% 33% 50% 67% 83% 100%	BSC 2004c
		Other vegetables			0.103	—	0.035 0.063 0.078 0.08 0.103 0.122 0.24	0% 17% 33% 50% 67% 83% 100%	
		Fruit			0.120	—	0.062 0.084 0.102 0.155 0.194	0% 25% 50% 75% 100%	
		Grain			0.903	—	0.891 0.896 0.906 0.918	0% 33% 67% 100%	
		Forage			0.220	—	0.182 0.227 0.238	0% 75% 100%	

Table 2.3.10-10. Summary of Biosphere Model Input Parameters (Continued)

Submodel	Parameter Name		Distribution Type	Units	Mean, Mode, Average[a]	SD/SE[a]	Min.[b]	Max.[b]	Reference/Notes[c]
Plant (continued)	Translocation factor	Leafy vegetables	Fixed	—	1.0	—	—	—	BSC 2004d
		Other vegetables	Cumulative	—	0.1	—	0.05 0.10 0.30	0% 50% 100%	
		Fruit							
		Grain							
		Forage	Fixed	—	1.0	—	—	—	
	Fraction of overhead irrigation	Leafy vegetables	Normal	—	0.75	0.10	0.49	1.0	BSC 2004c
		Other vegetables			0.75	0.10	0.49	1.0	
		Fruit			0.50	0.10	0.24	1.0	
		Grain			0.90	0.05	0.77	1.0	
		Forage			0.90	0.05	0.77	1.0	
	Weathering half-life		Cumulative	day	14	—	5 14 30	0% 50% 100%	BSC 2004d
	Crop growing time, present-day climate	Leafy vegetables	Fixed	day	75	—	—	—	BSC 2004c
		Other vegetables			80	—	—	—	
		Fruit			160	—	—	—	
		Grain			200	—	—	—	
		Forage			75	—	—	—	

Table 2.3.10-10. Summary of Biosphere Model Input Parameters (Continued)

Submodel	Parameter Name		Distribution Type	Units	Mean, Mode, Average[a]	SD/SE[a]	Min.[b]	Max.[b]	Reference/Notes[c]
Plant (continued)	Crop wet yield	Leafy vegetables	Cumulative	kg/m^2	3.30	—	1.08 1.46 1.78 2.01 2.98 3.25 3.83 7.79 7.85	0% 5% 20% 35% 50% 65% 80% 95% 100%	BSC 2004c
		Other vegetables			4.13	—	2.8 3.37 3.56 3.64 4.92 5.15 6.61	0% 5% 28% 51% 72% 95% 100%	
		Fruit			2.75	—	0.73 1.51 2.67 2.92 3.00 3.63 6.89	0% 5% 28% 51% 72% 95% 100%	
		Grain			0.59	—	0.27 0.28 0.44 0.54 1.1 1.22	0% 5% 35% 65% 95% 100%	
		Forage			2.14	—	0.69 1.02 1.87 5.78 6.28	0% 5% 73% 95% 100%	

Table 2.3.10-10. Summary of Biosphere Model Input Parameters (Continued)

Submodel	Parameter Name		Distribution Type	Units	Mean, Mode, Average[a]	SD/SE[a]	Min.[b]	Max.[b]	Reference/Notes[c]
Plant (continued)	Crop dry biomass	Leafy vegetation	Cumulative	kg/m^2	0.21	—	0.10 0.13 0.14 0.15 0.16 0.18 0.30 0.42 0.50	0% 5% 20% 35% 50% 65% 80% 95% 100%	BSC 2004c
		Other vegetation			0.43	—	0.30 0.40 0.41 0.43 0.44 0.46 0.60	0% 5% 28% 51% 73% 95% 100%	
		Fruit			0.62	—	0.10 0.56 0.60 0.65 0.68 1.30	0% 5% 35% 65% 95% 100%	
		Grain			1.13	—	0.50 0.61 0.74 1.20 1.97 2.20	0% 5% 35% 65% 95% 100%	
		Forage			0.48	—	0.10 0.23 0.34 1.38 1.50	0% 5% 73% 95% 100%	

Table 2.3.10-10. Summary of Biosphere Model Input Parameters (Continued)

Submodel	Parameter Name		Distribution Type	Units	Mean, Mode, Average[a]	SD/SE[a]	Min.[b]	Max.[b]	Reference/Notes[c]
Plant (continued)	Daily irrigation rate, present-day climate	Leafy vegetables	Cumulative	mm/d	5.41	—	4.00 5.11 5.19 5.21 5.38 5.48 6.00 7.08	0% 5% 20% 35% 50% 80% 95% 100%	BSC 2004c
		Other vegetables			7.71	—	5.00 6.07 6.65 6.93 7.67 8.36 9.03 9.26 10.93	0% 5% 20% 35% 50% 65% 80% 95% 100%	
		Fruit			7.41	—	4.00 5.40 7.02 7.59 8.38 8.67 10.23	0% 5% 28% 51% 72% 95% 100%	
		Grain			4.64	—	3.00 3.44 3.58 3.87 7.69 9.07	0% 5% 35% 65% 95% 100%	

Table 2.3.10-10. Summary of Biosphere Model Input Parameters (Continued)

Submodel	Parameter Name		Distribution Type	Units	Mean, Mode, Average[a]	SD/SE[a]	Min.[b]	Max.[b]	Reference/Notes[c]
Plant (continued)	Daily irrigation rate, present-day climate (continued)	Forage	Cumulative	mm/d	6.55	—	5.00 5.85 6.18 9.02 10.64	0% 5% 73% 95% 100%	
	Irrigation amount per application, present-day climate	Leafy vegetables	Cumulative	mm	14.7	—	6.0 7.5 8.4 10.0 10.9 20.8 22.0 23.5 27.7	0% 5% 20% 35% 50% 65% 80% 95% 100%	BSC 2004c
		Other vegetables			26.0	—	8.0 9.1 18.9 19.8 21.2 33.3 34.8 44.7 52.7	0% 5% 20% 35% 50% 65% 80% 95% 100%	
		Fruit			33.9	—	5.0 6.0 30.3 35.4 48.4 49.4 58.3	0% 5% 28% 51% 72% 95% 100%	

Table 2.3.10-10. Summary of Biosphere Model Input Parameters (Continued)

Submodel	Parameter Name		Distribution Type	Units	Mean, Mode, Average[a]	SD/SE[a]	Min.[b]	Max.[b]	Reference/Notes[c]
Plant (continued)	Irrigation amount per application, present-day climate (continued)	Grain	Cumulative	mm	56.7	—	43.0 48.6 50.1 50.4 77.9 91.9	0% 5% 35% 65% 95% 100%	
		Forage			57.8	—	50.0 56.3 57.6 60.0 71.0	0% 5% 72% 95% 100%	
	Irrigation intensity		Uniform	cm/hr	4.25	—	1.0	7.5	BSC 2004c
	Dry deposition velocity		Cumulative	m/s	8×10^{-3}	—	3×10^{-4} 1×10^{-3} 8×10^{-3} 3×10^{-2} 3×10^{-1}	0% 16% 50% 84% 100%	DTN: MO0406SPAETPBM.002BSC 2004d
Animal Sections 2.3.10.3.1.4 and 2.3.10.3.2.4	Animal product transfer coefficients for meat	Chlorine	Lognormal	d/kg	4.6×10^{-2}	2.0	7.7×10^{-3}	2.7×10^{-1}	BSC 2004d, Transfer coefficients are given in terms of geometric mean and geometric standard deviation.
		Selenium			8.8×10^{-2}	5.8	9.6×10^{-4}	8.0×10^{0}	
		Strontium			1.4×10^{-3}	4.4	3.1×10^{-5}	6.2×10^{-2}	
		Technetium			1.1×10^{-3}	7.2	6.9×10^{-6}	1.8×10^{-1}	
		Tin			1.9×10^{-2}	4.6	3.8×10^{-4}	9.9×10^{-1}	
		Iodine			1.0×10^{-2}	2.8	6.8×10^{-4}	1.5×10^{-1}	
		Cesium			2.4×10^{-2}	2.6	2.1×10^{-3}	2.7×10^{-1}	
		Lead			6.3×10^{-4}	2.6	5.4×10^{-5}	7.5×10^{-3}	

Table 2.3.10-10. Summary of Biosphere Model Input Parameters (Continued)

Submodel	Parameter Name		Distribution Type	Units	Mean, Mode, Average[a]	SD/SE[a]	Min.[b]	Max.[b]	Reference/Notes[c]
Animal (continued)	Animal product transfer coefficients for meat (continued)	Radium	Lognormal	d/kg	8.1×10^{-4}	2.1	1.1×10^{-4}	5.7×10^{-3}	
		Actinium			7.9×10^{-5}	8.2	3.5×10^{-7}	1.8×10^{-2}	
		Thorium			1.1×10^{-4}	10.0	2.8×10^{-7}	4.0×10^{-2}	
		Protactinium			6.6×10^{-5}	10.0	1.8×10^{-7}	2.5×10^{-2}	
		Uranium			4.8×10^{-4}	3.0	2.9×10^{-5}	7.8×10^{-3}	
		Neptunium			3.4×10^{-4}	8.8	1.3×10^{-6}	9.0×10^{-2}	
		Plutonium			1.3×10^{-5}	10.0	3.3×10^{-8}	4.7×10^{-3}	
		Americium			3.4×10^{-5}	9.0	1.2×10^{-7}	9.9×10^{-3}	
	Animal product transfer coefficients for milk	Chlorine	Lognormal	d/L	1.8×10^{-2}	2.0	2.9×10^{-3}	1.0×10^{-1}	BSC 2004d, Transfer coefficients are given in terms of geometric mean and geometric standard deviation.
		Selenium			5.7×10^{-3}	2.5	5.5×10^{-4}	6.0×10^{-2}	
		Strontium			1.7×10^{-3}	2.0	2.8×10^{-4}	1.0×10^{-2}	
		Technetium			2.1×10^{-3}	6.0	2.0×10^{-5}	2.1×10^{-1}	
		Tin			1.1×10^{-3}	2.0	1.8×10^{-4}	6.3×10^{-3}	
		Iodine			9.1×10^{-3}	2.0	1.5×10^{-3}	5.4×10^{-2}	
		Cesium			7.7×10^{-3}	2.0	1.3×10^{-3}	4.6×10^{-2}	
		Lead			1.7×10^{-4}	3.0	1.0×10^{-5}	2.9×10^{-3}	
		Radium			5.8×10^{-4}	2.0	1.0×10^{-4}	3.4×10^{-3}	
		Actinium			7.6×10^{-6}	4.1	2.0×10^{-7}	2.9×10^{-4}	
		Thorium			4.4×10^{-6}	2.0	7.4×10^{-7}	2.6×10^{-5}	
		Protactinium			4.4×10^{-6}	2.0	7.4×10^{-7}	2.6×10^{-5}	

Table 2.3.10-10. Summary of Biosphere Model Input Parameters (Continued)

Submodel	Parameter Name		Distribution Type	Units	Mean, Mode, Average[a]	SD/SE[a]	Min.[b]	Max.[b]	Reference/Notes[c]
Animal (continued)	Animal product transfer coefficients for milk (continued)	Uranium	Lognormal	d/L	4.9×10^{-4}	2.0	8.1×10^{-5}	2.9×10^{-3}	
		Neptunium			6.3×10^{-6}	2.0	1.0×10^{-6}	3.9×10^{-5}	
		Plutonium			2.3×10^{-7}	7.7	1.2×10^{-9}	4.4×10^{-5}	
		Americium			1.6×10^{-6}	4.2	3.9×10^{-8}	6.3×10^{-5}	
	Animal product transfer coefficients for poultry	Chlorine	Lognormal	d/kg	3.0×10^{-2}	2.0	5.0×10^{-3}	1.8×10^{-1}	BSC 2004d, Transfer coefficients are given in terms of geometric mean and geometric standard deviation.
		Selenium			5.1×10^{0}	3.6	1.9×10^{-1}	1.4×10^{2}	
		Strontium			3.1×10^{-2}	5.8	3.4×10^{-4}	2.9×10^{0}	
		Technetium			6.3×10^{-2}	10.0	1.7×10^{-4}	2.4×10^{1}	
		Tin			3.5×10^{-2}	10.0	9.4×10^{-5}	1.3×10^{1}	
		Iodine			5.5×10^{-2}	9.7	1.6×10^{-4}	1.9×10^{1}	
		Cesium			2.6×10^{0}	9.8	7.2×10^{-3}	9.3×10^{2}	
		Lead			2.5×10^{-2}	10.0	6.6×10^{-5}	9.3×10^{0}	
		Radium			1.7×10^{-2}	10.0	4.4×10^{-5}	6.3×10^{0}	
		Actinium			4.0×10^{-3}	2.0	6.7×10^{-4}	2.4×10^{-2}	
		Thorium			5.9×10^{-3}	8.0	2.7×10^{-5}	1.3×10^{0}	
		Protactinium			3.0×10^{-3}	2.0	5.1×10^{-4}	1.8×10^{-2}	
		Uranium			2.4×10^{-1}	10.0	6.5×10^{-4}	9.2×10^{1}	
		Neptunium			3.6×10^{-3}	2.0	6.0×10^{-4}	2.1×10^{-2}	
		Plutonium			1.2×10^{-3}	10.0	3.2×10^{-6}	4.6×10^{-1}	
		Americium			1.8×10^{-3}	10.0	4.8×10^{-6}	6.7×10^{-1}	

Table 2.3.10-10. Summary of Biosphere Model Input Parameters (Continued)

Submodel	Parameter Name		Distribution Type	Units	Mean, Mode, Average[a]	SD/SE[a]	Min.[b]	Max.[b]	Reference/Notes[c]
Animal (continued)	Animal product transfer coefficients for eggs	Chlorine	Lognormal	d/kg	4.4×10^{-2}	10.0	1.2×10^{-4}	1.7×10^{1}	BSC 2004d, Transfer coefficients are given in terms of geometric mean and geometric standard deviation.
		Selenium			7.3×10^{0}	2.0	1.2×10^{0}	4.4×10^{1}	
		Strontium			2.7×10^{-1}	2.0	4.5×10^{-2}	1.6×10^{0}	
		Technetium			2.4×10^{0}	2.0	4.0×10^{-1}	1.4×10^{1}	
		Tin			8.7×10^{-2}	10.0	2.3×10^{-4}	3.3×10^{1}	
		Iodine			2.6×10^{0}	2.0	4.4×10^{-1}	1.6×10^{1}	
		Cesium			3.5×10^{-1}	5.8	3.7×10^{-3}	3.3×10^{1}	
		Lead			5.6×10^{-2}	10.0	1.5×10^{-4}	2.1×10^{1}	
		Radium			3.9×10^{-4}	10.0	1.0×10^{-6}	1.5×10^{-1}	
		Actinium			2.9×10^{-3}	2.3	3.4×10^{-4}	2.5×10^{-2}	
		Thorium			3.5×10^{-3}	7.3	2.0×10^{-5}	5.9×10^{-1}	
		Protactinium			2.0×10^{-3}	2.0	3.4×10^{-4}	1.2×10^{-2}	
		Uranium			6.3×10^{-1}	2.5	6.0×10^{-2}	6.7×10^{0}	
		Neptunium			3.4×10^{-3}	2.4	3.4×10^{-4}	3.3×10^{-2}	
		Plutonium			1.7×10^{-3}	7.4	9.7×10^{-6}	2.9×10^{-1}	
		Americium			4.9×10^{-3}	2.0	8.2×10^{-4}	2.9×10^{-2}	
	Animal consumption rate of feed	Meat	Uniform	kg/d	48.5	—	29	68	BSC 2004d
		Milk			61.5	—	50	73	
		Poultry			0.26	—	0.12	0.40	
		Eggs			0.26	—	0.12	0.40	

Table 2.3.10-10. Summary of Biosphere Model Input Parameters (Continued)

Submodel	Parameter Name		Distribution Type	Units	Mean, Mode, Average[a]	SD/SE[a]	Min.[b]	Max.[b]	Reference/Notes[c]
Animal (continued)	Animal consumption rate of water	Meat	Fixed	L/d	60	—	—	—	BSC 2004d
		Milk	Uniform		80	—	60	100	
		Poultry	Fixed		0.5	—	—	—	
		Eggs	Fixed		0.5	—	—	—	
	Animal consumption rate of soil	Meat	Uniform	kg/d	0.7	—	0.4	1.0	BSC 2004d
		Milk			0.95	—	0.8	1.1	
		Poultry			0.02	—	0.01	0.03	
		Eggs			0.02	—	0.01	0.03	
Fish Section 2.3.10.3.1.5	Bioaccumulation factor	Carbon	Lognormal	L/kg	4.6×10^{3}	3.2	2.3×10^{2}	9.2×10^{4}	BSC 2004d, Bioaccumulation factors are given in terms of geometric mean and geometric standard deviation.
		Chlorine			2.2×10^{2}	5.6	2.6×10^{0}	1.9×10^{4}	
		Selenium			2.3×10^{2}	2.0	3.9×10^{1}	1.4×10^{3}	
		Strontium			4.6×10^{1}	2.0	7.8×10^{0}	2.8×10^{2}	
		Technetium			2.0×10^{1}	2.0	3.3×10^{0}	1.2×10^{2}	
		Tin			2.5×10^{3}	2.0	4.2×10^{2}	1.5×10^{4}	
		Iodine			4.5×10^{1}	2.6	3.8×10^{0}	5.3×10^{2}	
		Cesium			3.5×10^{3}	2.2	4.7×10^{2}	2.5×10^{4}	
		Lead			2.9×10^{2}	2.5	2.7×10^{1}	3.1×10^{3}	
		Radium			6.7×10^{1}	2.2	9.2×10^{0}	5.0×10^{2}	
		Actinium			2.9×10^{1}	3.0	1.7×10^{0}	5.0×10^{2}	
		Thorium			1.1×10^{2}	2.5	1.0×10^{1}	1.2×10^{3}	

Table 2.3.10-10. Summary of Biosphere Model Input Parameters (Continued)

Submodel	Parameter Name		Distribution Type	Units	Mean, Mode, Average[a]	SD/SE[a]	Min.[b]	Max.[b]	Reference/Notes[c]
Fish (continued)	Bioaccumulation factor (continued)	Protactinium	Lognormal	L/kg	1.2×10^{1}	2.0	2.0×10^{0}	7.1×10^{1}	
		Uranium			1.4×10^{1}	3.0	8.4×10^{-1}	2.3×10^{2}	
		Neptunium			3.0×10^{1}	2.9	1.9×10^{0}	4.7×10^{2}	
		Plutonium			4.1×10^{1}	4.7	7.9×10^{-1}	2.2×10^{3}	
		Americium			5.2×10^{1}	2.3	5.8×10^{0}	4.6×10^{2}	
	Modifying factor for present-day climate	Carbon	Fixed	—	1	—	—	—	BSC 2004d
		Other elements	Uniform	—	4.15	—	2.2	6.1	
^{14}C Section 2.3.10.3.1.6	^{14}C emission rate		Fixed	1/yr	22	—	—	—	BSC 2004d
	Typical field size		Fixed	m^2	2.295×10^{6}	—	—	—	SNL 2007a, Section 6.4.6.2
	Typical garden size		Fixed	m^2	2000	—	—	—	SNL 2007a, Section 6.4.6.2
	Annual average wind speed	For inhalation (at 2 m)	Uniform	m/s	2.45	—	2.1	2.8	BSC 2004d
		For crops (at 1 m)			1.9	—	1.5	2.3	
	^{14}C mixing height	For inhalation	Fixed	m	2	—	—	—	BSC 2004d
		For crops			1	—	—	—	
	Fraction of air-derived C in plants		Fixed	—	0.98	—	—	—	
	Fraction of soil-derived C in plants		Fixed	—	0.02	—	—	—	

Table 2.3.10-10. Summary of Biosphere Model Input Parameters (Continued)

Submodel	Parameter Name		Distribution Type	Units	Mean, Mode, Average[a]	SD/SE[a]	Min.[b]	Max.[b]	Reference/Notes[c]
^{14}C (continued)	Fraction of stable C in plant	Leafy vegetables	Fixed	—	0.09	—	—	—	BSC 2004d
		Other vegetables			0.09	—	—	—	
		Fruit			0.09	—	—	—	
		Grain			0.40	—	—	—	
		Forage			0.09	—	—	—	
	Fraction of stable C in soil		Fixed	—	0.03	—	—	—	
	Concentration of stable C in air		Fixed	kg/m^3	1.8×10^{-4}	—	—	—	
	Concentration of stable C in water		Fixed	kg/L	2×10^{-5}	—	—	—	
	Fraction of stable C in animal product	Meat	Fixed	—	0.24	—	—	—	
		Milk			0.07	—	—	—	
		Poultry			0.20	—	—	—	
		Eggs			0.15	—	—	—	
External Exposure Sections 2.3.10.3.1.7 and 2.3.10.3.2.5	Population proportion for groundwater scenario	Outdoor workers	Uniform	%	5.5	2.6	2.9	8.1	BSC 2005, Table 6-5
		Indoor workers[d]			16.1[d]	—	—	—	
		Commuters			39.2	5.3	33.9	44.5	
		Nonworkers			39.2	4.8	34.4	44.0	

Table 2.3.10-10. Summary of Biosphere Model Input Parameters (Continued)

Submodel	Parameter Name			Distribution Type	Units	Mean, Mode, Average[a]	SD/SE[a]	Min.[b]	Max.[b]	Reference/Notes[c]
External Exposure (continued)	Population proportion for volcanic ash scenario		Outdoor workers	Uniform	%	5.5	2.6	2.9	10.7	
			Indoor workers[d]			42.8[d]	—	—	—	
			Commuters			12.5	3.8	4.9	16.3	
			Nonworkers			39.2	4.8	34.4	44.0	
	For GW	Exposure time for outdoor workers	Active outdoors	Lognormal	hr/d	3.1	0.2	2.6	3.7	BSC 2005, Time spent active indoors is calculated in the submodel as 24 h/d minus the sum of times in the other four environments.
			Inactive outdoors			4.0	0.3	3.3	4.8	
			Active indoors[d]			6.6[d]	—	—	—	
			Asleep indoors			8.3	0.1	8.0	8.6	
			Away			2.0	0.4	1.2	3.3	
		Exposure time for indoor workers	Active outdoors	Lognormal	hr/d	0.3	0.1	0.1	0.7	
			Inactive outdoors			1.3	0.2	0.9	1.9	
			Active indoors[d]			12.1[d]	—	—	—	
			Asleep indoors			8.3	0.1	8.0	8.6	
			Away			2.0	0.4	1.2	3.3	
		Exposure time for commuters	Active outdoors	Lognormal	hr/d	0.3	0.1	0.1	0.7	
			Inactive outdoors			1.4	0.2	1.0	2.0	

Table 2.3.10-10. Summary of Biosphere Model Input Parameters (Continued)

Submodel	Parameter Name			Distribution Type	Units	Mean, Mode, Average[a]	SD/SE[a]	Min.[b]	Max.[b]	Reference/Notes[c]
External Exposure (continued)	For GW	Exposure time for commuters (continued)	Active indoors[d]	Lognormal	hr/d	6.0[d]	—	—	—	
			Asleep indoors			8.3	0.1	8.0	8.6	
			Away			8.0	0.5	6.8	9.4	
		Exposure time for nonworkers	Active outdoors	Lognormal	hr/d	0.3	0.1	0.1	0.7	
			Inactive outdoors			1.2	0.2	0.8	1.8	
			Active indoors[d]			12.2[d]	—	—	—	
			Asleep indoors			8.3	0.1	8.0	8.6	
			Away			2.0	0.4	1.2	3.3	
	For VA	Exposure time for outdoor workers	Active outdoors	Lognormal	hr/d	3.1	0.2	2.6	3.7	BSC 2005, Time spent active indoors is calculated in the submodel as 24 h/d minus the sum of times in the other four environments.
			Inactive outdoors			4.2	0.3	3.5	5.0	
			Active indoors[d]			6.4[d]	—	—	—	
			Asleep indoors			8.3	0.1	8.0	8.6	
			Away			2.0	0.4	1.2	3.3	
		Exposure time for indoor workers	Active outdoors	Lognormal	hr/d	0.3	0.1	0.1	0.7	
			Inactive outdoors			1.5	0.2	1.1	2.1	

Table 2.3.10-10. Summary of Biosphere Model Input Parameters (Continued)

Submodel	Parameter Name			Distribution Type	Units	Mean, Mode, Average[a]	SD/SE[a]	Min.[b]	Max.[b]	Reference/Notes[c]
External Exposure (continued)	For VA	Exposure time for indoor workers (continued)	Active indoors[d]	Lognormal	hr/d	11.9[d]	—	—	—	
			Asleep indoors			8.3	0.1	8.0	8.6	
			Away			2.0	0.4	1.2	3.3	
		Exposure time for commuters	Active outdoors	Lognormal	hr/d	0.3	0.1	0.1	0.7	BSC 2005
			Inactive outdoors			2.0	0.2	1.5	2.6	
			Active indoors[d]			5.1[d]	—	—	—	
			Asleep indoors			8.3	0.1	8.0	8.6	
			Away			8.3	0.6	6.9	10.0	
	For VA	Exposure time for non workers	Active outdoors	Lognormal	hr/d	0.3	0.1	0.1	0.7	
			Inactive outdoors			1.2	0.2	0.8	1.8	
			Active indoors[d]			12.2[d]	—	—	—	
			Asleep indoors			8.3	0.1	8.0	8.6	
			Away			2.0	0.4	1.2	3.3	
	Building shielding factor		^{14}C	Fixed	—	0.2	—	—	—	BSC 2005
			^{36}Cl			0.4	—	—	—	
			^{79}Se			0.1	—	—	—	
			^{90}Sr			0.4	—	—	—	
			^{99}Tc			0.2	—	—	—	
			^{126}Sn			0.4	—	—	—	

Table 2.3.10-10. Summary of Biosphere Model Input Parameters (Continued)

Submodel	Parameter Name		Distribution Type	Units	Mean, Mode, Average[a]	SD/SE[a]	Min.[b]	Max.[b]	Reference/Notes[c]
External Exposure (continued)	Building shielding factor (continued)	^{129}I	Fixed	—	0.1	—	—	—	
		^{135}Cs			0.1	—	—	—	
		^{137}Cs			0.4	—	—	—	
		^{242}Pu			0.1	—	—	—	
		^{238}U			0.4	—	—	—	
		^{238}Pu			0.1	—	—	—	
		^{234}U			0.2	—	—	—	
		^{230}Th			0.3	—	—	—	
		^{226}Ra	Fixed	—	0.4	—	—	—	
		^{210}Pb			0.4	—	—	—	
		^{240}Pu			0.1	—	—	—	
		^{236}U			0.1	—	—	—	
		^{232}Th			0.2	—	—	—	
		^{228}Ra			0.4	—	—	—	
		^{232}U			0.3	—	—	—	
		^{228}Th			0.4	—	—	—	
		^{243}Am			0.4	—	—	—	
		^{239}Pu			0.3	—	—	—	
		^{235}U	Fixed	—	0.4	—	—	—	BSC 2005
		^{231}Pa			0.4	—	—	—	

Table 2.3.10-10. Summary of Biosphere Model Input Parameters (Continued)

Submodel	Parameter Name		Distribution Type	Units	Mean, Mode, Average[a]	SD/SE[a]	Min.[b]	Max.[b]	Reference/Notes[c]
External Exposure (continued)	Building shielding factor (continued)	^{227}Ac	Fixed	—	0.4	—	—	—	
		^{241}Am			0.2	—	—	—	
		^{237}Np			0.4	—	—	—	
		^{233}U			0.4	—	—	—	
		^{229}Th			0.4	—	—	—	
	Dose coefficient for exposure to soil contaminated to an infinite depth		Fixed	(Sv/yr)/(Bq/m^3)	See Table 2.3.10-6	—	—	—	SNL 2007a, Table 6.4-4
	Dose coefficient for exposure to contaminated ground surface		Fixed	(Sv/yr)/(Bq/m^2)	See Table 2.3.10-7	—	—	—	SNL 2007a, Table 6.4-4
	Branching fraction		Fixed	—	See Table 2.3.10-5	—	—	—	SNL 2007a, Table 6.3-7
Inhalation Sections 2.3.10.3.1.8 and 2.3.10.3.2.6	Breathing rate	Active outdoors	Fixed	m^3/hr	1.57	—	—	—	BSC 2005
		Inactive outdoors			1.08	—	—	—	
		Active indoors			1.08	—	—	—	
		Asleep indoors			0.39	—	—	—	
		Away from area			1.08	—	—	—	
	Dose coefficients for inhalation		Fixed	Sv/Bq	See Table 2.3.10-8	—	—	—	SNL 2007a, Table 6.4-5

Table 2.3.10-10. Summary of Biosphere Model Input Parameters (Continued)

Submodel	Parameter Name		Distribution Type	Units	Mean, Mode, Average[a]	SD/SE[a]	Min.[b]	Max.[b]	Reference/Notes[c]
Inhalation (continued)	Fraction of houses with evaporative coolers		Binomial	—	0.738	Sample size = 187	—	—	BSC 2005
	Evaporative cooler use factor, present-day climate		Uniform	—	0.39	—	0.32	0.46	
	Equilibrium factor for ^{222}Rn decay products	Outdoors	Uniform	—	0.6	—	0.5	0.7	BSC 2004d
		Indoors	Uniform	—	0.4	—	0.3	0.5	
	Dose conversion factor for inhalation of ^{222}Rn decay products		Fixed	Sv/Bq	6.62×10^{-9}	—	—	—	BSC 2005
Ingestion	Consumption rate of water		Fixed	L/d	2	—	—	—	Required by 10 CFR 63.312.
Sections 2.3.10.3.1.9 and 2.3.10.3.2.7	Consumption rate of locally produced crop foodstuffs	Leafy vegetables	Lognormal	kg/yr	3.78	0.88	—	—	DTN: MO0407SPACRBSM.002BSC 2005, Lognormal distributions are given in terms of arithmetic mean and standard deviation.
		Other vegetables			4.73	0.67	—	—	
		Fruit			12.68	1.36	—	—	
		Grain			0.23	0.11	—	—	
	Consumption rate of locally produced animal products	Meat	Lognormal	kg/yr	2.85	0.65	—	—	
		Milk			4.66	1.68	—	—	
		Poultry			0.42	0.13	—	—	
		Eggs			5.30	0.83	—	—	
	Consumption rate of locally produced fish		Lognormal	kg/yr	0.23	0.10	—	—	

Table 2.3.10-10. Summary of Biosphere Model Input Parameters (Continued)

Submodel	Parameter Name	Distribution Type	Units	Mean, Mode, Average[a]	SD/SE[a]	Min.[b]	Max.[b]	Reference/Notes[c]
Ingestion (continued)	Inadvertent soil ingestion rate	Cumulative	mg/d	100	—	50 100 200	0% 50% 100%	BSC 2005
	Dose coefficients for ingestion	Fixed	Sv/Bq	See Table 2.3.10-9	—	—	—	SNL 2007a, Table 6.4-6

NOTE: [a]The "Mean, Mode, Average" column represents the value for a fixed distribution, the mean for a normal or lognormal distribution, the mode for a triangular distribution, or the average value for distributions that do not require a mean, mode, or average, such as uniform distribution or cumulative distribution, in which values in this column are taken from the sources listed below or calculated as the 50th-percentile value. Data in this column were used in model verification and model validation. "SD/SE" represents the standard deviation or standard error for the described input distribution, such as normal distribution and lognormal distribution. However, for the transfer factors, transfer coefficients, and distribution coefficients the "Mean, Mode, Average" represents the geometric mean and SD/SE represents geometric standard deviation for their lognormal distributions.
[b]"Min." represents the lower bounding value, and "Max." represents the upper bounding value for most distribution types, except for cumulative distributions, in which the "Min." column is the value, and the "Max." column is the corresponding accumulative percentage.
[c]In some instances, the representative or mean values, which are not used as inputs but provide additional information about the parameter distribution, may not be included in the output DTNs and instead were obtained from the source report. Analysis output data are provided in Section 7 of the reports.
[d]Within the block of parameters, this parameter is the dependent variable whose expected value and distribution is determined by the defined distribution of the remaining parameters in the block and the necessary boundary conditions (such as 24 hours per day, percentage total having to be 100 percent).
AM = arithmetic mean; ASD = arithmetic standard deviation; GM = geometric mean; GSD = geometric standard deviation; GW = groundwater exposure scenario; SD = standard deviation, SE = standard error; TSPA = total system performance assessment; VA = volcanic ash exposure scenario.

Table 2.3.10-11. Average Percent Contribution of Exposure Pathways to Groundwater Biosphere Dose Conversion Factors

Radionuclide	External Exposure	Inhalation			Ingestion										
		Particulates	Aerosols	Radon	Water	Leafy Vegetables	Other Vegetables	Fruit	Grain	Meat	Milk	Poultry	Eggs	Fish	Soil
^{14}C	—	—	0.6	—	22.0	0.1	0.2	0.4	0.6	7.2	3.4	0.6	5.6	59.4	—
^{36}Cl	—	—	0.9	—	8.4	2.1	3.1	10.3	3.5	29.0	22.5	0.1	11.1	9.0	—
^{79}Se	—	0.1	0.1	—	8.7	0.4	0.2	0.7	0.1	70.0	3.5	1.0	11.7	3.2	0.2
^{90}Sr	1.0	0.2	0.9	—	64.7	5.9	3.3	5.5	0.8	4.7	5.7	0.1	2.1	4.9	0.4
^{99}Tc	—	0.1	2.3	—	41.7	8.8	1.7	6.2	0.7	6.0	18.3	0.2	12.6	1.4	—
^{126}Sn	93.4	0.1	0.1	—	0.9	—	—	—	—	1.6	0.1	—	0.1	3.6	—
^{129}I	—	—	0.1	—	60.1	2.6	0.7	2.5	0.5	5.8	8.5	0.2	13.2	5.4	0.3
^{135}Cs	—	0.3	0.1	—	10.1	0.7	0.3	1.2	0.2	11.1	6.3	6.0	4.4	58.6	0.8
^{137}Cs	35.2	0.1	0.1	—	7.6	0.4	0.1	0.5	0.1	3.7	2.1	2.9	2.2	44.4	0.5
^{210}Pb	—	2.2	0.7	—	50.8	2.7	0.6	2.4	0.3	0.6	0.4	0.2	6.6	28.0	4.2
^{226}Ra	11.2	2.6	0.5	73.7	5.4	0.6	0.2	0.9	0.2	0.5	0.5	0.1	1.6	0.6	1.3
^{228}Ra	5.9	16.6	3.5	—	56.3	2.8	0.6	2.3	0.3	0.6	0.9	0.1	—	6.5	3.4
^{227}Ac	1.6	42.3	26.4	—	24.5	1.1	0.3	0.9	0.1	0.1	—	—	—	1.6	1.1
^{228}Th	3.6	25.0	27.0	—	33.1	1.4	0.3	1.2	0.2	0.2	—	—	0.1	7.1	0.8
^{229}Th	2.3	52.8	19.5	—	18.1	0.9	0.2	0.7	0.1	0.2	—	—	0.1	3.9	1.2
^{230}Th	1.4	50.8	18.5	8.4	14.4	0.7	0.2	0.6	0.1	0.3	0.1	—	0.2	3.1	1.0
^{232}Th	30.1	41.7	11.7	—	9.1	1.0	0.4	0.9	0.2	0.6	0.7	—	0.1	1.9	1.6

Table 2.3.10-11. Average Percent Contribution of Exposure Pathways to Groundwater Biosphere Dose Conversion Factors (Continued)

Radionuclide	External Exposure	Inhalation			Ingestion										
		Particulates	Aerosols	Radon	Water	Leafy Vegetables	Other Vegetables	Fruit	Grain	Meat	Milk	Poultry	Eggs	Fish	Soil
^{231}Pa	2.5	61.3	18.6	—	14.3	0.7	0.2	0.7	0.1	0.2	—	—	—	0.3	1.0
^{232}U	23.0	14.4	12.1	—	40.7	1.8	0.4	1.5	0.2	0.2	0.3	0.5	2.8	1.2	0.9
^{233}U	0.3	26.2	21.0	—	41.8	1.8	0.4	1.6	0.2	0.3	0.4	0.6	3.3	1.3	0.9
^{234}U	0.0	22.0	22.6	0.1	44.1	1.9	0.5	1.7	0.2	0.3	0.4	0.6	3.4	1.3	0.9
^{235}U	17.5	18.9	17.7	—	36.5	1.6	0.4	1.4	0.2	0.2	0.4	0.5	2.8	1.1	0.7
^{236}U	0.0	21.6	22.4	—	44.7	1.9	0.5	1.7	0.2	0.3	0.5	0.6	3.5	1.3	0.9
^{238}U	4.7	19.4	20.1	—	44.5	1.9	0.5	1.7	0.2	0.3	0.5	0.6	3.5	1.3	0.9
^{237}Np	7.4	21.1	35.7	—	28.8	1.4	0.5	2.0	0.2	0.7	—	—	—	1.9	0.3
^{238}Pu	—	43.8	27.9	—	21.9	1.0	0.2	0.8	0.1	—	—	—	—	3.2	1.0
^{239}Pu	—	50.5	24.5	—	19.2	0.9	0.2	0.7	0.1	—	—	—	—	2.8	0.9
^{240}Pu	—	50.4	24.6	—	19.3	0.9	0.2	0.7	0.1	—	—	—	—	2.8	0.9
^{242}Pu	—	50.6	24.5	—	19.2	0.9	0.2	0.7	0.1	—	—	—	—	2.8	0.9
^{241}Am	0.1	54.6	22.7	—	17.9	0.9	0.2	0.7	0.1	0.1	—	—	—	1.7	1.1
^{243}Am	3.5	54.1	21.2	—	16.8	0.8	0.2	0.7	0.1	0.1	—	—	—	1.6	1.0

NOTE: Pathway contributions of less than 0.05% are not shown.
Aerosols = aerosols generated by evaporative coolers; particulates = suspended soil particles; radon = radon decay products.

Source: SNL 2007a, Table 6.13-1.

Table 2.3.10-12. Summary Statistics for the Groundwater Biosphere Dose Conversion Factors (Sv/yr per Bq/m^3)

Radionuclide	Mean	Standard Deviation	Minimum	5th Percentile	50th Percentile	95th Percentile	Maximum
^{14}C	1.9×10^{-9}	1.9×10^{-9}	7.2×10^{-10}	8.3×10^{-10}	1.4×10^{-9}	5.1×10^{-9}	2.6×10^{-8}
^{36}Cl	8.1×10^{-9}	1.4×10^{-8}	1.3×10^{-9}	1.9×10^{-9}	4.9×10^{-9}	2.3×10^{-8}	3.0×10^{-7}
^{79}Se	2.4×10^{-8}	7.5×10^{-8}	3.6×10^{-9}	5.0×10^{-9}	1.0×10^{-8}	6.8×10^{-8}	1.5×10^{-6}
^{90}Sr	3.4×10^{-8}	6.6×10^{-9}	2.5×10^{-8}	2.7×10^{-8}	3.3×10^{-8}	4.6×10^{-8}	8.6×10^{-8}
^{99}Tc	1.1×10^{-9}	1.3×10^{-9}	5.3×10^{-10}	6.0×10^{-10}	8.5×10^{-10}	2.4×10^{-9}	2.8×10^{-8}
^{126}Sn	4.3×10^{-7}	2.4×10^{-7}	8.9×10^{-8}	1.6×10^{-7}	3.7×10^{-7}	8.8×10^{-7}	1.7×10^{-6}
^{129}I	1.3×10^{-7}	5.3×10^{-8}	8.6×10^{-8}	9.4×10^{-8}	1.2×10^{-7}	1.9×10^{-7}	1.1×10^{-6}
^{135}Cs	1.5×10^{-8}	1.0×10^{-8}	3.1×10^{-9}	5.0×10^{-9}	1.2×10^{-8}	3.5×10^{-8}	8.5×10^{-8}
^{137}Cs	1.3×10^{-7}	6.3×10^{-8}	3.9×10^{-8}	6.2×10^{-8}	1.1×10^{-7}	2.6×10^{-7}	4.6×10^{-7}
^{210}Pb	2.7×10^{-6}	1.1×10^{-6}	1.6×10^{-6}	1.8×10^{-6}	2.4×10^{-6}	5.2×10^{-6}	1.3×10^{-5}
^{226}Ra	3.8×10^{-6}	2.2×10^{-6}	8.8×10^{-7}	1.5×10^{-6}	3.2×10^{-6}	7.6×10^{-6}	1.8×10^{-5}
^{228}Ra	9.0×10^{-7}	1.4×10^{-7}	6.1×10^{-7}	7.1×10^{-7}	8.8×10^{-7}	1.2×10^{-6}	1.5×10^{-6}
^{227}Ac	1.3×10^{-6}	5.3×10^{-7}	4.1×10^{-7}	6.2×10^{-7}	1.2×10^{-6}	2.3×10^{-6}	4.3×10^{-6}
^{228}Th	3.1×10^{-7}	8.6×10^{-8}	1.4×10^{-7}	1.9×10^{-7}	3.1×10^{-7}	4.7×10^{-7}	8.0×10^{-7}
^{229}Th	2.6×10^{-6}	1.0×10^{-6}	7.4×10^{-7}	1.3×10^{-6}	2.4×10^{-6}	4.6×10^{-6}	8.1×10^{-6}
^{230}Th	1.1×10^{-6}	4.3×10^{-7}	2.7×10^{-7}	5.3×10^{-7}	1.0×10^{-6}	1.9×10^{-6}	3.3×10^{-6}
^{232}Th	1.9×10^{-6}	7.3×10^{-7}	5.1×10^{-7}	9.0×10^{-7}	1.7×10^{-6}	3.2×10^{-6}	5.3×10^{-6}
^{231}Pa	2.4×10^{-6}	1.0×10^{-6}	6.6×10^{-7}	1.2×10^{-6}	2.3×10^{-6}	4.4×10^{-6}	8.6×10^{-6}
^{232}U	6.0×10^{-7}	2.2×10^{-7}	2.9×10^{-7}	3.5×10^{-7}	5.6×10^{-7}	1.0×10^{-6}	1.9×10^{-6}
^{233}U	9.0×10^{-8}	3.4×10^{-8}	4.1×10^{-8}	5.1×10^{-8}	8.1×10^{-8}	1.5×10^{-7}	3.1×10^{-7}
^{234}U	8.2×10^{-8}	2.8×10^{-8}	4.0×10^{-8}	4.9×10^{-8}	7.5×10^{-8}	1.3×10^{-7}	2.2×10^{-7}
^{235}U	9.4×10^{-8}	3.7×10^{-8}	3.9×10^{-8}	4.9×10^{-8}	8.5×10^{-8}	1.6×10^{-7}	3.0×10^{-7}
^{236}U	7.7×10^{-8}	2.6×10^{-8}	3.7×10^{-8}	4.6×10^{-8}	7.0×10^{-8}	1.3×10^{-7}	2.0×10^{-7}
^{238}U	7.9×10^{-8}	2.6×10^{-8}	3.8×10^{-8}	4.7×10^{-8}	7.2×10^{-8}	1.3×10^{-7}	2.1×10^{-7}
^{237}Np	2.7×10^{-7}	9.7×10^{-8}	1.1×10^{-7}	1.4×10^{-7}	2.6×10^{-7}	4.5×10^{-7}	8.0×10^{-7}
^{238}Pu	7.6×10^{-7}	2.8×10^{-7}	2.6×10^{-7}	4.0×10^{-7}	7.2×10^{-7}	1.3×10^{-6}	2.1×10^{-6}
^{239}Pu	9.5×10^{-7}	3.4×10^{-7}	3.5×10^{-7}	5.2×10^{-7}	9.0×10^{-7}	1.6×10^{-6}	2.9×10^{-6}
^{240}Pu	9.5×10^{-7}	3.3×10^{-7}	3.5×10^{-7}	5.2×10^{-7}	9.0×10^{-7}	1.6×10^{-6}	2.9×10^{-6}

Table 2.3.10-12. Summary Statistics for the Groundwater Biosphere Dose Conversion Factors (Sv/yr per Bq/m^3) (Continued)

Radionuclide	Mean	Standard Deviation	Minimum	5th Percentile	50th Percentile	95th Percentile	Maximum
^{242}Pu	9.1×10^{-7}	3.2×10^{-7}	3.3×10^{-7}	4.9×10^{-7}	8.6×10^{-7}	1.5×10^{-6}	2.8×10^{-6}
^{241}Am	8.3×10^{-7}	4.0×10^{-7}	2.2×10^{-7}	3.8×10^{-7}	7.5×10^{-7}	1.6×10^{-6}	3.3×10^{-6}
^{243}Am	8.9×10^{-7}	4.10×10^{-7}	2.2×10^{-7}	4.1×10^{-7}	8.0×10^{-7}	1.70×10^{-6}	3.4×10^{-6}

NOTE: The statistics presented in this table are based on 1,000 realizations of the biosphere model. The values presented in this table are graphically displayed in Figure 2.3.10-11.
The TSPA model uses pCi/L as groundwater activity concentration units and rem as units of dose. The following conversion factors can be used to make the necessary conversions from the SI units used in the biosphere model: 1 Ci = 3.7×10^{10} Bq; 1 L = 10^{-3} m^3; 1 rem = 10^{-2} Sv. To calculate the BDCFs in units of rem/y per pCi/L, the BDCF value in Sv/yr per Bq/m^3 should be multiplied by 3.7×10^3.

Source: SNL 2007a, Section 6.11.2.

Table 2.3.10-13. Rank Correlation Coefficients for Biosphere Model Input Parameters and Groundwater Biosphere Dose Conversion Factors for the Present-Day Climate

Submodel	Parameter	^{99}Tc	^{129}I	^{234}U	^{237}Np	^{239}Pu
Soil Submodel	Distribution coefficient	–0.139	0.110	0.647	0.291	0.454
	Overwatering rate	–0.630	–0.266	–0.157	–0.351	—
	Erosion rate	—	—	—	—	–0.267
	Surface soil depth	—	—	—	–0.107	–0.123
	Irrigation duration, fields	—	—	—	—	0.185
	Irrigation duration, gardens	—	—	—	0.155	—
Air Submodel	Enhancement factor, active outdoors	—	—	0.138	0.120	0.190
	Enhancement factor, active indoors	—	—	—	—	0.170
	Evaporative cooler transfer fraction	—	—	0.448	0.605	0.426
	Evaporative cooler water usage	—	—	—	0.147	0.101
	Mass loading, active outdoors	—	—	0.118	0.146	0.351
Plant Submodel	Crop dry biomass, forage	—	0.142	—	—	—
	Crop wet yield, forage	—	–0.192	—	—	—
	Dry-to-wet weight ratio, fruit	0.128	—	—	—	—
	Irrigation application, cattle forage	–0.106	—	—	—	—
	Irrigation intensity	—	–0.173	—	—	—
	Daily irrigation rate, other vegetables	—	—	—	—	0.103
	Transfer factor, cattle forage	0.173	—	–0.507	–0.242	–0.354
	Transfer factor, fruit	0.174	—	–0.510	–0.166	–0.373
	Transfer factor, grain	0.176	—	–0.504	–0.234	–0.334
	Transfer factor, leafy vegetables	0.193	—	–0.480	–0.234	–0.357
	Transfer factor, other vegetables	0.139	—	–0.485	–0.247	–0.348
	Translocation factor	—	0.199	—	—	—
	Weathering half-life	0.100	0.320	—	—	—
Animal Submodel	Transfer coefficient, eggs	0.172	0.275	—	—	—
	Transfer coefficient, meat	0.197	0.201	—	—	—
	Transfer coefficient, milk	0.302	0.204	—	—	—
Fish Submodel	Bioaccumulation factor	—	0.225	—	—	0.117

Table 2.3.10-13. Rank Correlation Coefficients for Biosphere Model Input Parameters and Groundwater Biosphere Dose Conversion Factors for the Present-Day Climate (Continued)

Submodel	Parameter	^{99}Tc	^{129}I	^{234}U	^{237}Np	^{239}Pu
Ingestion Submodel	Consumption rate, eggs	—	0.102	—	—	—
	Consumption rate, fish	—	0.103	—	—	—
Inhalation and External Exposure Submodels	Time active outdoors, nonworkers	—	—	—	0.118	0.104

NOTE: Only parameters with rank correlation coefficients having an absolute value of 0.100 or greater are shown.

Source: SNL 2007a, Table 6.13-3.

Table 2.3.10-14. Components of Volcanic Biosphere Dose Conversion Factors, Average Values

Radionuclide	Inhalation Component (Sv/yr per Bq/kg)		Ingestion, Radon, and External Exposure Component (Sv/yr per Bq/m^2)
	Short-Term	Long-Term	
^{90}Sr	5.3×10^{-10}	8.2×10^{-10}	1.8×10^{-9}
^{99}Tc	4.5×10^{-11}	6.8×10^{-11}	2.7×10^{-10}
^{126}Sn	5.2×10^{-10}	8.0×10^{-10}	2.5×10^{-8}
^{129}I	1.2×10^{-10}	1.8×10^{-10}	1.3×10^{-9}
^{137}Cs	1.3×10^{-10}	2.0×10^{-10}	7.2×10^{-9}
^{210}Pb	3.4×10^{-8}	5.2×10^{-8}	2.3×10^{-9}
^{226}Ra	3.2×10^{-8}	4.9×10^{-8}	3.3×10^{-8}
^{228}Ra	5.4×10^{-8}	8.2×10^{-8}	1.3×10^{-8}
^{227}Ac	5.9×10^{-7}	9.0×10^{-7}	6.2×10^{-9}
^{228}Th	1.4×10^{-7}	2.2×10^{-7}	1.9×10^{-8}
^{229}Th	8.5×10^{-7}	1.3×10^{-6}	4.7×10^{-9}
^{230}Th	3.4×10^{-7}	5.2×10^{-7}	8.5×10^{-11}
^{232}Th	3.7×10^{-7}	5.7×10^{-7}	8.8×10^{-11}
^{231}Pa	7.7×10^{-7}	1.2×10^{-6}	7.1×10^{-10}
^{232}U	1.2×10^{-7}	1.9×10^{-7}	3.8×10^{-10}
^{233}U	3.2×10^{-8}	4.9×10^{-8}	6.5×10^{-11}
^{234}U	3.1×10^{-8}	4.8×10^{-8}	6.0×10^{-11}
^{235}U	2.8×10^{-8}	4.4×10^{-8}	2.1×10^{-9}
^{236}U	2.9×10^{-8}	4.5×10^{-8}	5.5×10^{-11}
^{238}U	2.7×10^{-8}	4.1×10^{-8}	1.6×10^{-9}
^{237}Np	1.7×10^{-7}	2.6×10^{-7}	3.0×10^{-9}
^{238}Pu	3.6×10^{-7}	5.6×10^{-7}	7.8×10^{-11}
^{239}Pu	4.0×10^{-7}	6.1×10^{-7}	8.5×10^{-11}
^{240}Pu	4.0×10^{-7}	6.1×10^{-7}	8.5×10^{-11}
^{242}Pu	3.8×10^{-7}	5.8×10^{-7}	8.0×10^{-11}
^{241}Am	3.2×10^{-7}	5.0×10^{-7}	2.5×10^{-10}

Table 2.3.10-14. Components of Volcanic Biosphere Dose Conversion Factors, Average Values (Continued)

Radionuclide	Inhalation Component (Sv/yr per Bq/kg)		Ingestion, Radon, and External Exposure Component (Sv/yr per Bq/m^2)
	Short-Term	Long-Term	
^{243}Am	3.2×10^{-7}	4.9×10^{-7}	2.7×10^{-9}

NOTE: The uncertainty in the BDCF components is graphically displayed in Figures 2.3.10-12 to 2.3.10-14. Some the TSPA model components may use US customary units for the quantities of dose and for the deposition of radioactive waste on, and concentration in, the soil. The following conversion factors can be used to make the necessary conversions from the SI units used in the biosphere model: 1 Ci = 3.7×10^{10} Bq; 1 cm^2 = 10^{-4} m^2; 1 g = 10^{-3} kg; 1 rem = 10^{-2} Sv.

Source: SNL 2007a, Section 6.12.2.

Table 2.3.10-15.Average Percent Exposure Pathway Contributions to the Annual Dose for the Volcanic Ash Exposure Scenario Assuming Uniform Radionuclide Concentration in Surface Soil

Radionuclide	External Exposure	Inhalation			Ingestion								
		Short Term	Long Term	Radon Decay Products	Leafy Vegetables	Other Vegetables	Fruit	Grain	Meat	Milk	Poultry	Eggs	Soil
^{90}Sr	79.2	0.1	0.2	0.0	4.9	3.7	5.0	0.4	2.2	2.8	0.0	1.1	0.3
^{99}Tc	0.2	0.1	0.1	0.0	22.9	5.0	19.0	1.2	9.6	22.2	0.3	19.4	0.0
^{126}Sn	99.8	0.0	0.0	0.0	0.0	0.0	0.0	0.0	0.1	0.0	0.0	0.0	0.0
^{129}I	8.2	0.0	0.1	0.0	3.0	1.8	6.1	2.1	9.6	14.2	0.9	52.3	1.7
^{137}Cs	98.8	0.0	0.0	0.0	0.0	0.0	0.1	0.0	0.3	0.2	0.2	0.2	0.0
^{210}Pb	17.8	6.0	9.2	0.0	7.9	3.5	14.9	0.9	1.7	1.1	0.6	22.6	13.9
^{226}Ra	65.3	0.5	0.7	32.8	0.2	0.1	0.2	0.0	0.0	0.0	0.0	0.0	0.2
^{228}Ra	90.8	1.9	3.0	0.0	1.0	0.6	1.1	0.1	0.2	0.3	0.0	0.0	1.0
^{227}Ac	45.2	21.1	32.5	0.0	0.2	0.1	0.2	0.0	0.0	0.0	0.0	0.0	0.6
^{228}Th	91.1	3.4	5.2	0.0	0.0	0.0	0.0	0.0	0.0	0.0	0.0	0.0	0.1
^{229}Th	29.6	27.1	41.7	0.0	0.3	0.1	0.2	0.0	0.1	0.0	0.0	0.0	0.8
^{230}Th	0.2	38.6	59.4	0.0	0.3	0.1	0.3	0.0	0.1	0.0	0.0	0.1	1.0
^{232}Th	0.1	38.6	59.4	0.0	0.3	0.1	0.3	0.0	0.1	0.0	0.0	0.1	1.0
^{231}Pa	4.8	36.6	56.3	0.0	0.3	0.2	0.7	0.1	0.1	0.0	0.0	0.0	0.9
^{232}U	0.4	31.4	48.3	0.0	1.3	0.6	2.3	0.1	0.4	0.5	1.9	9.1	3.5
^{233}U	1.7	33.8	52.0	0.0	0.8	0.4	1.5	0.1	0.3	0.3	1.2	5.7	2.2

Table 2.3.10-15. Average Percent Exposure Pathway Contributions to the Annual Dose for the Volcanic Ash Exposure Scenario Assuming Uniform Radionuclide Concentration in Surface Soil (Continued)

Radionuclide	External Exposure	Inhalation			Ingestion								
		Short Term	Long Term	Radon Decay Products	Leafy Vegetables	Other Vegetables	Fruit	Grain	Meat	Milk	Poultry	Eggs	Soil
^{234}U	1.0	34.1	52.4	0.0	0.8	0.4	1.5	0.1	0.3	0.3	1.2	5.7	2.2
^{235}U	83.5	5.7	8.7	0.0	0.1	0.1	0.3	0.0	0.0	0.1	0.2	1.0	0.4
^{236}U	0.6	34.1	52.5	0.0	0.8	0.4	1.5	0.1	0.3	0.4	1.2	5.8	2.3
^{238}U	80.5	6.6	10.2	0.0	0.2	0.1	0.3	0.0	0.1	0.1	0.3	1.3	0.5
^{237}Np	54.4	15.9	24.5	0.0	0.6	0.5	3.4	0.1	0.3	0.0	0.0	0.0	0.4
^{238}Pu	0.1	38.7	59.5	0.0	0.3	0.1	0.3	0.0	0.0	0.0	0.0	0.0	1.0
^{239}Pu	0.1	38.7	59.6	0.0	0.3	0.1	0.3	0.0	0.0	0.0	0.0	0.0	1.0
^{240}Pu	0.1	38.7	59.6	0.0	0.3	0.1	0.3	0.0	0.0	0.0	0.0	0.0	1.0
^{242}Pu	0.1	38.7	59.6	0.0	0.3	0.1	0.3	0.0	0.0	0.0	0.0	0.0	1.0
^{241}Am	4.4	37.0	57.0	0.0	0.3	0.1	0.3	0.0	0.0	0.0	0.0	0.0	1.0
^{243}Am	39.7	23.4	35.9	0.0	0.2	0.0	0.2	0.0	0.0	0.0	0.0	0.0	0.6

Source: SNL 2007a, Table 6.14-1.

Table 2.3.10-16. Rank Correlation Coefficients for Biosphere Model Input Parameters and the Volcanic Ash Scenario Biosphere Dose Conversion Factor Component for External Exposure, Ingestion, and Inhalation of Radon Decay Products

Submodel	Parameter	^{90}Sr	^{137}Cs
Soil Submodel	Distribution coefficient	–0.682	–0.217
	Surface soil depth	–0.539	–0.192
	Surface soil density	–0.116	—
Plant Submodel	Transfer factor for leafy vegetables	0.652	0.179
	Transfer factor for other vegetables	0.603	0.162
	Transfer factor for fruit	0.616	0.183
	Transfer factor for grain	0.547	0.199
	Transfer factor for cattle forage	0.632	0.207
	Deposition velocity	—	0.100
Animal Submodel	Transfer coefficient for meat	0.113	—
	Transfer coefficient for poultry	—	0.160
External Exposure Submodel	Population fraction, outdoor workers	—	0.375
	Population fraction, commuters	—	–0.312
	Time spent active outdoors, nonworkers	—	0.150
	Time spent active outdoors, indoor workers	—	0.155
	Time spent inactive outdoors, indoor workers	—	0.288
	Time spent inactive outdoors, nonworkers	—	0.218
	Time spent away, indoor workers	—	–0.342
	Time spent away, nonworkers	—	–0.324
	Time spent away, commuters	—	–0.102

NOTE: Only parameters with correlation coefficients having an absolute value of 0.100 or greater are shown.

Source: SNL 2007a, Table 6.14-3.

Table 2.3.10-17. Rank Correlation Coefficients for the Input Parameters and Inhalation BDCF Components

Radionuclide	Parameter	Rank Correlation Coefficient
Short-Term Inhalation Component	Enhancement factor, active outdoors environment	0.712
	Ash mass loading, active outdoors environment	0.562
	Enhancement factor, active indoor environment	0.276
	Population proportion, outdoor workers	0.222
	Time spent active outdoors, indoor workers	0.143
	Time spent active outdoors, nonworkers	0.159
Long-Term Inhalation Component	Enhancement factor, active outdoors environment	0.702
	Mass loading, active outdoors environment	0.555
	Population proportion, outdoor workers	0.241
	Time spent active outdoors, indoor workers	0.162
	Enhancement factor, active indoor environment	0.179
	Time spent active outdoors, nonworkers	0.173

NOTE: Only parameters with correlation coefficients having an absolute values of 0.100 or greater are shown.

Source: SNL 2007a, Table 6.14-4.

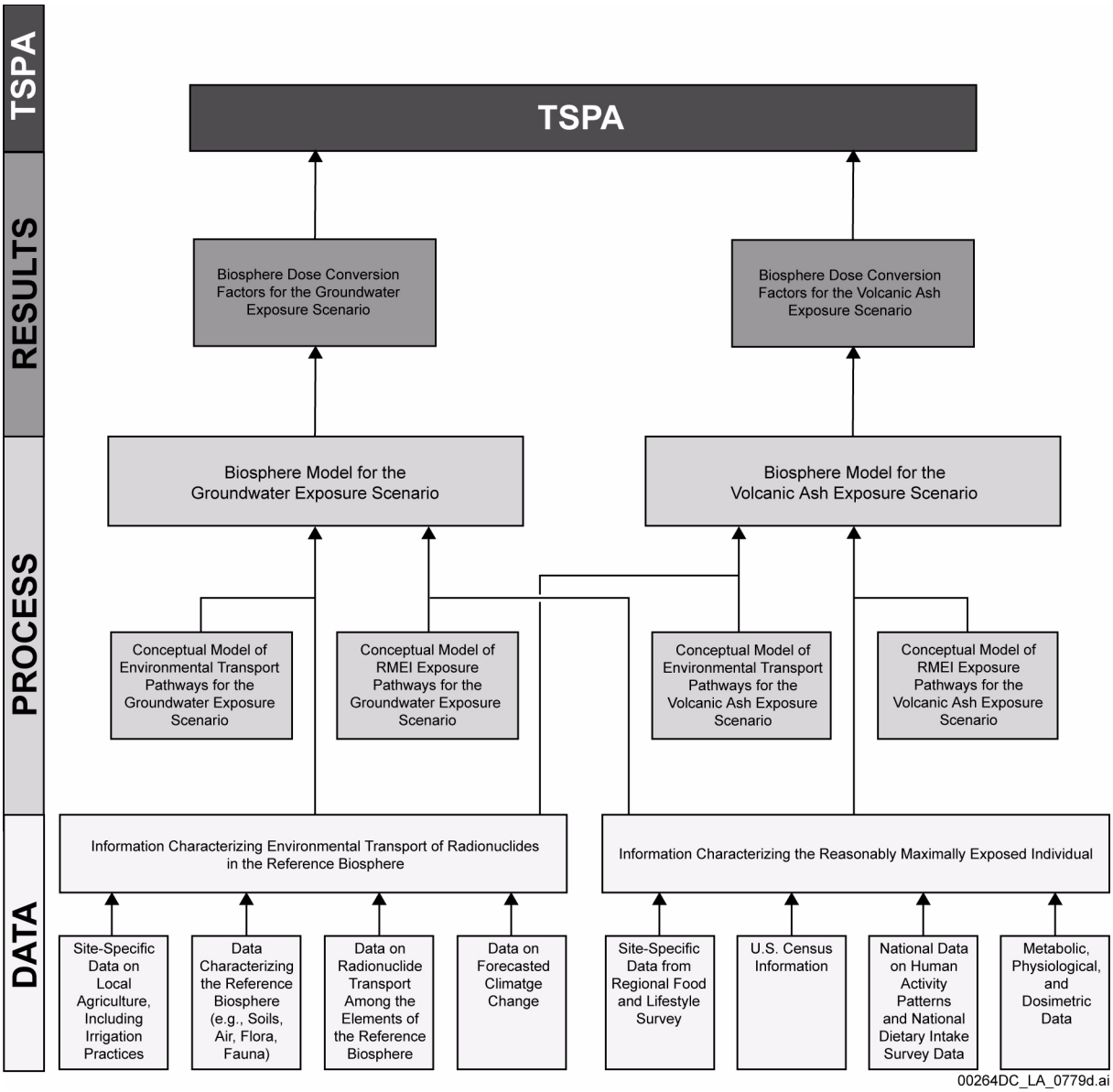

Figure 2.3.10-1. Information Flow Showing Data, Process Level, and Biosphere Dose Conversion Factors Used in the TSPA Model

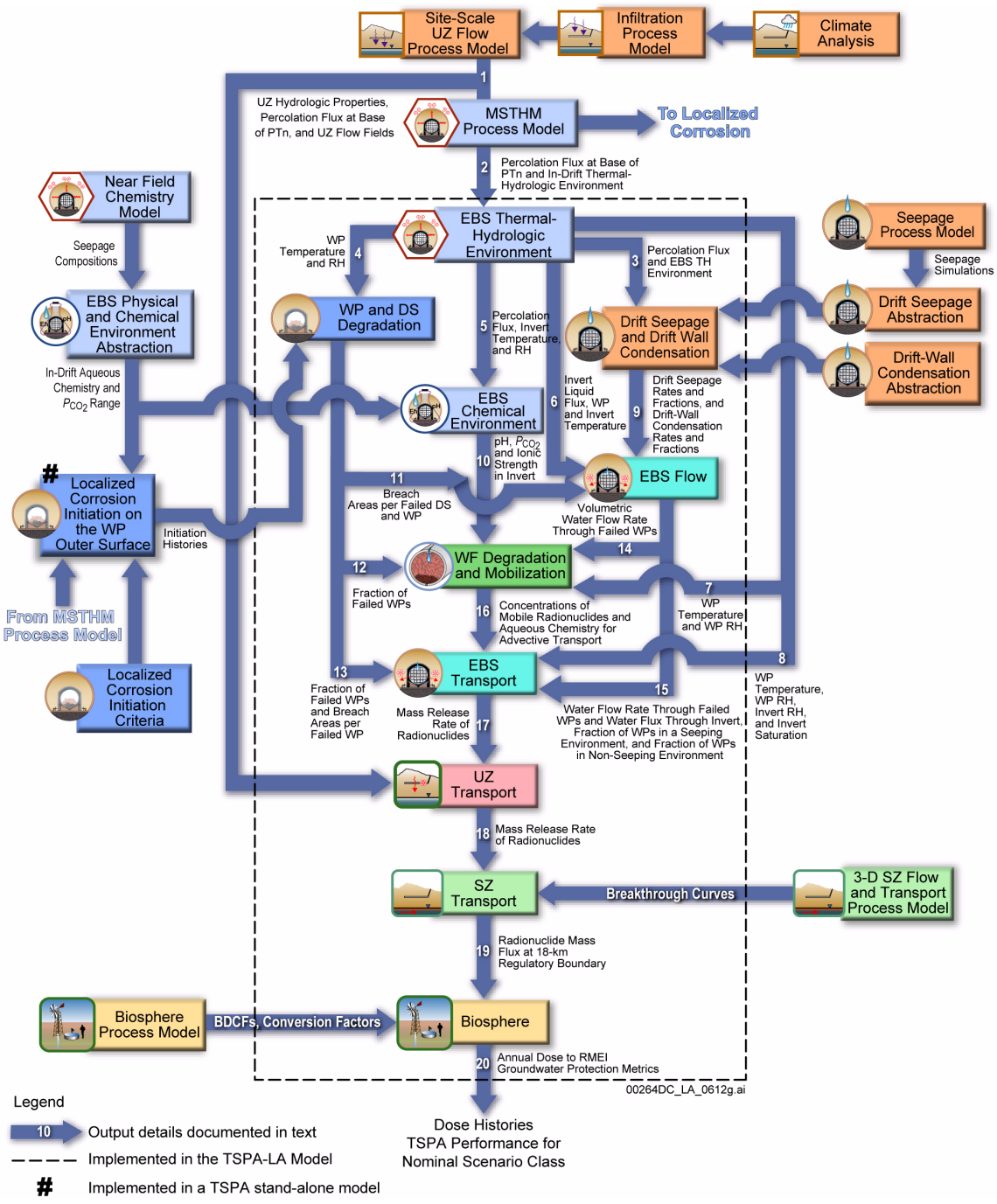

Figure 2.3.10-2. Information Transfer among the Principal Model Components of the TSPA Nominal Scenario Class Model

NOTE: For details about outputs and information transfer shown on this figure, see Section 2.4.2.3.2.1. Although this figure represents the nominal scenario class, it is applicable to all scenario classes and modeling cases where groundwater is the source of the biosphere exposure.
DS = drip shield; EBS = Engineered Barrier System; LC = localized corrosion; PA = performance assessment; RH = relative humidity; SZ = saturated zone; TH = thermal-hydrologic; THC = thermal-hydrologic-chemical; UZ = unsaturated zone; WF = waste form; WP = waste package.

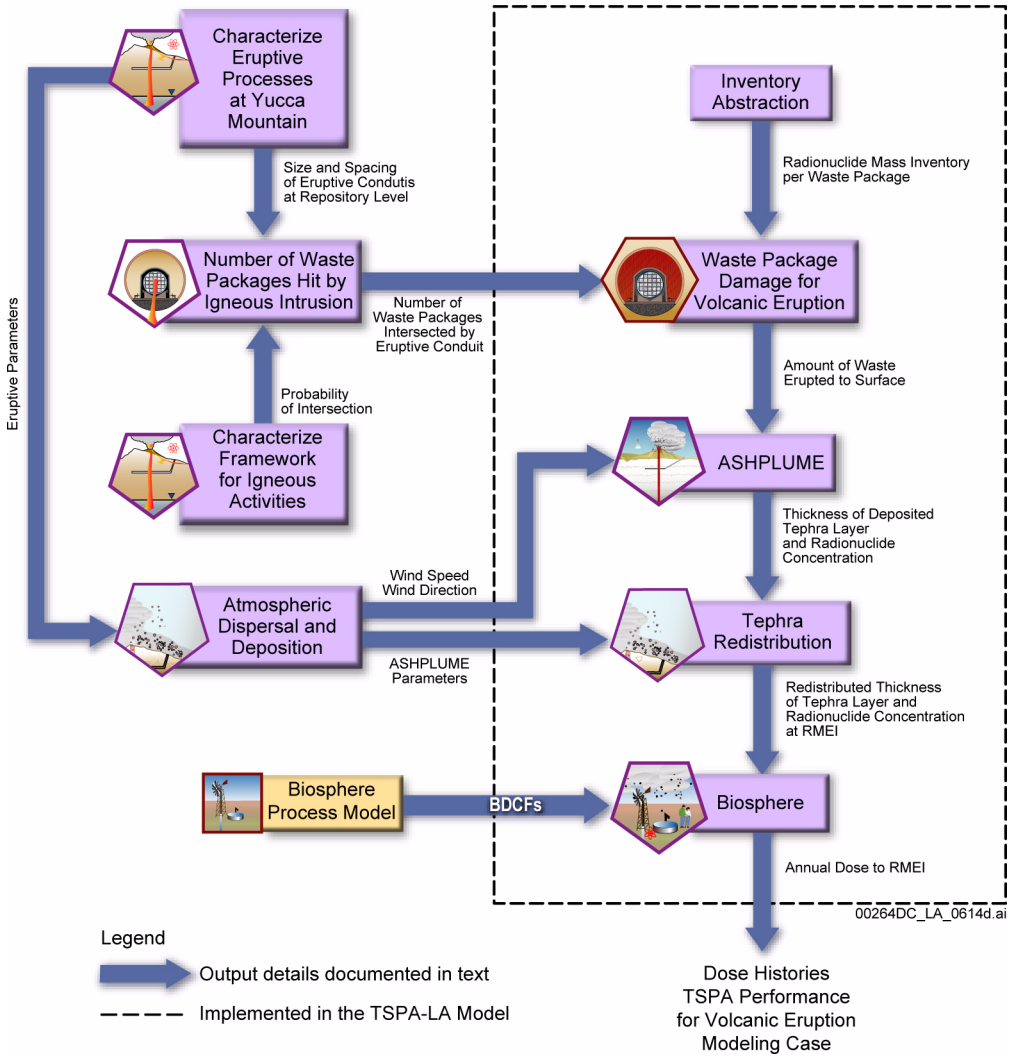

Figure 2.3.10-3. Information Transfer between the Principal Model Components of the TSPA Volcanic Eruption Modeling Case

NOTE: BDCF = biosphere dose conversion factor; RMEI = reasonably maximally exposed individual.

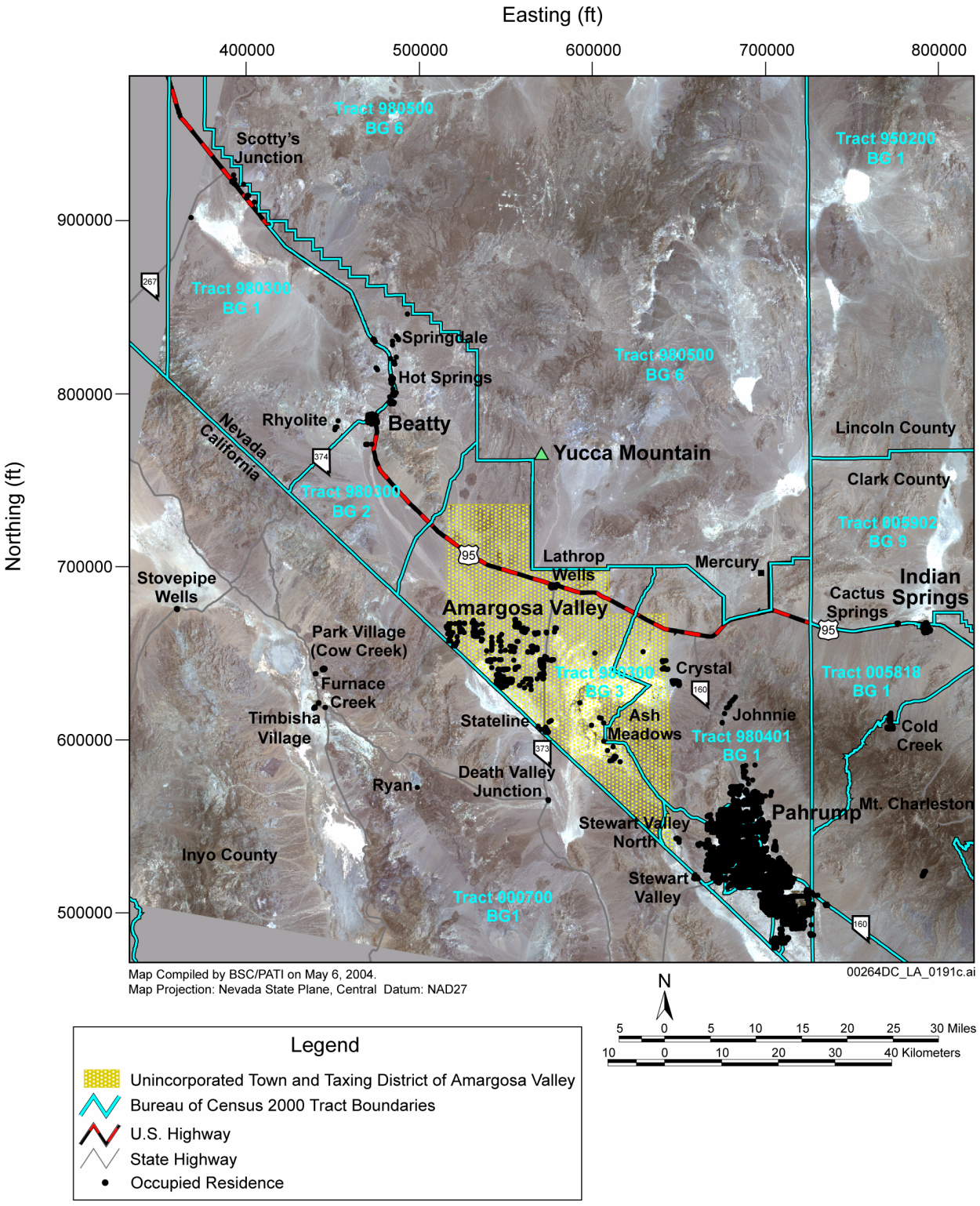

Figure 2.3.10-4. Locations of Occupied Residences in the Yucca Mountain Region (2003)

NOTE: Each dot represents one occupied residence.

Source: BSC 2005, Figure 6-1.

	1	2	3	4	5	6	7
1	**SOURCE** (groundwater)	Irrigation	Evaporation	Irrigation interception	Ingestion of water	Bio-accumulation (water use in fisheries)	Drinking water ingestion
2	Leaching	**SURFACE SOIL**	Particle resuspension, gas release, soil erosion	Root uptake	Soil ingestion	—	Soil ingestion, external exposure
3	—	Dust deposition	**AIR**	Dust deposition, photosynthesis	—	—	Inhalation of particulates, gases, and aerosols
4	—	Weathering, harvest removal	—	**PLANTS** (crops)	Ingestion of feed	—	Crop ingestion
5	—	Fertilization	—	—	**ANIMALS** (animal products)	—	Animal product ingestion
6	—	—	—	—	—	**FISH**	Fish ingestion
7	—	—	—	—	—	—	**HUMAN** (receptor)

00264DC_LA_0309a.ai

Environmental media and the RMEI are displayed in the shaded, diagonal elements. Unshaded elements represent methods of radionuclide transport among media and exposure to the RMEI. The direction of interaction between components is clockwise. Elements with a dash indicate interactions not included in the biosphere model.

Figure 2.3.10-5. Radionuclide Transfer Interaction Matrix for the Groundwater Exposure Scenario

Source: SNL 2007a, Section 6.3.1.3.

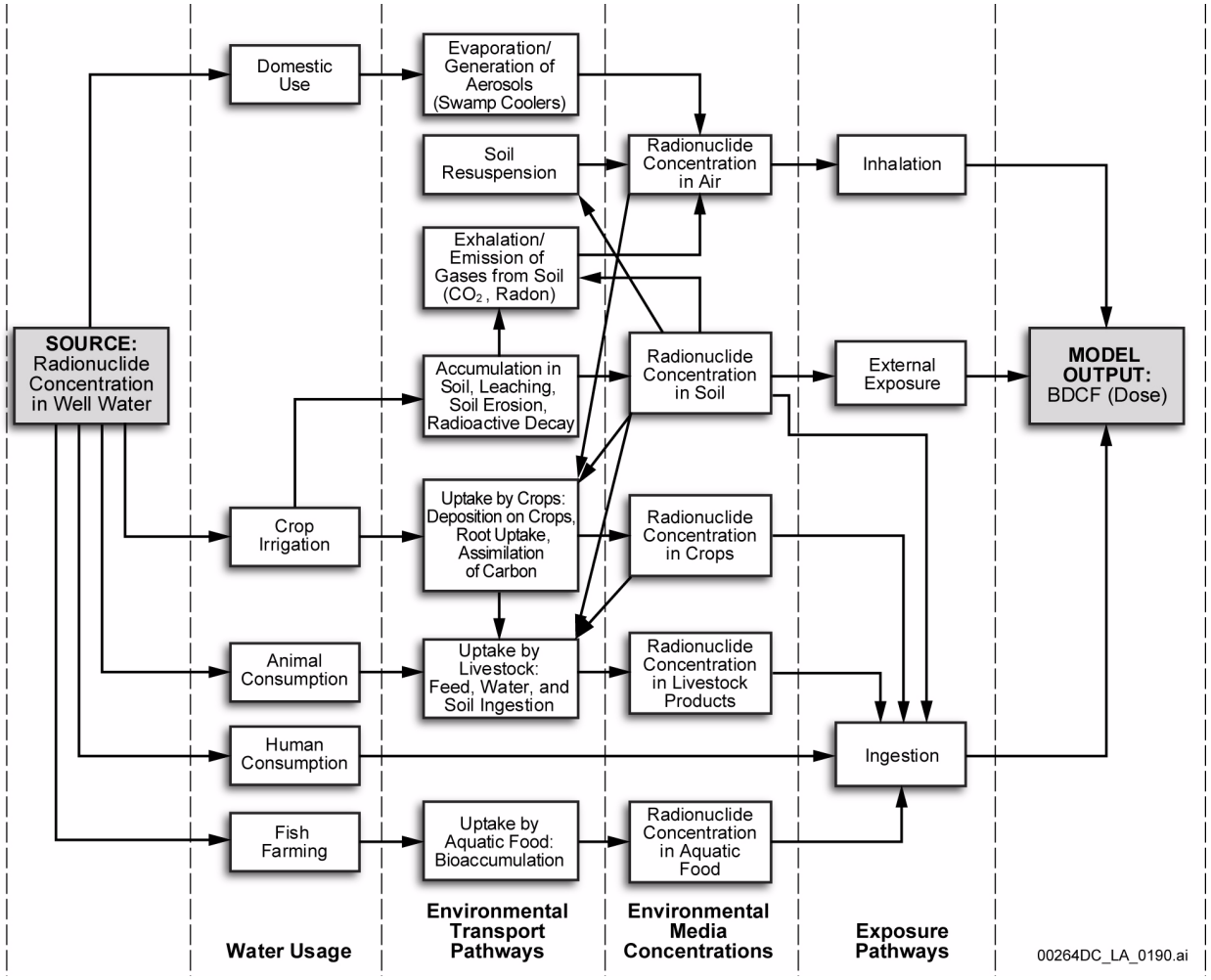

Figure 2.3.10-6. Conceptual Representation of the Transport and Exposure Pathways for the Groundwater Exposure Scenario

Source: SNL 2007a, Section 6.3.1.6.

	1	2	3	4	5	6
1	**SOURCE** (volcanic ash)	Ashfall	—	—	—	—
2	—	**SURFACE SOIL** (ash or ash-soil mixture)	Particle resuspension, gas release	Root uptake	Soil ingestion	Soil ingestion, ground exposure
3	—	Particle deposition	**AIR**	Particle deposition	—	Inhalation of particulates and gas
4	—	Weathering, harvest removal	—	**PLANTS** (crops)	Feed ingestion	Crop ingestion
5	—	Fertilization	—	—	**ANIMALS** (animal products)	Animal product ingestion
6	—	—	—	—	—	**HUMAN** (receptor)

00264DC_LA_0310a.ai

Environmental media and the RMEI are displayed in the shaded, diagonal elements.
Unshaded elements represent methods of radionuclide transport among media and exposure to the RMEI. The direction of interaction between components is clockwise. Elements with a dash indicate interactions not included in the biosphere model.

Figure 2.3.10-7. Radionuclide Transfer Interaction Matrix for the Volcanic Ash Exposure Scenario

NOTE: Atmospheric dispersion, deposition, and redistribution of volcanic tephra is modeled outside the biosphere model. The source term for the biosphere model is the radionuclide concentration in the surface soil.

Source: SNL 2007a, Section 6.3.2.3.

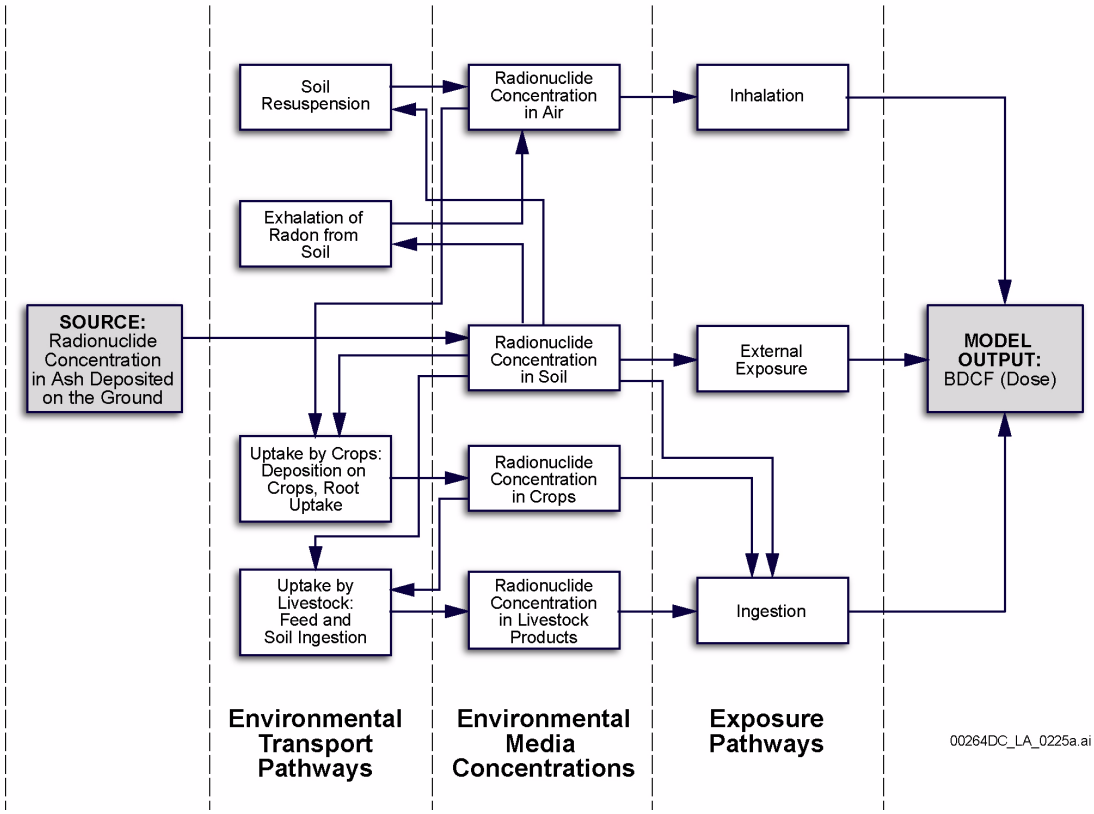

Figure 2.3.10-8. Conceptual Representation of the Transport and Exposure Pathways for the Volcanic Ash Scenario

NOTE: Atmospheric dispersion, deposition, and redistribution of volcanic tephra is modeled outside the biosphere model. The source term for the biosphere model is the radionuclide concentration in the surface soil.

Source: SNL 2007a, Section 6.3.2.6.

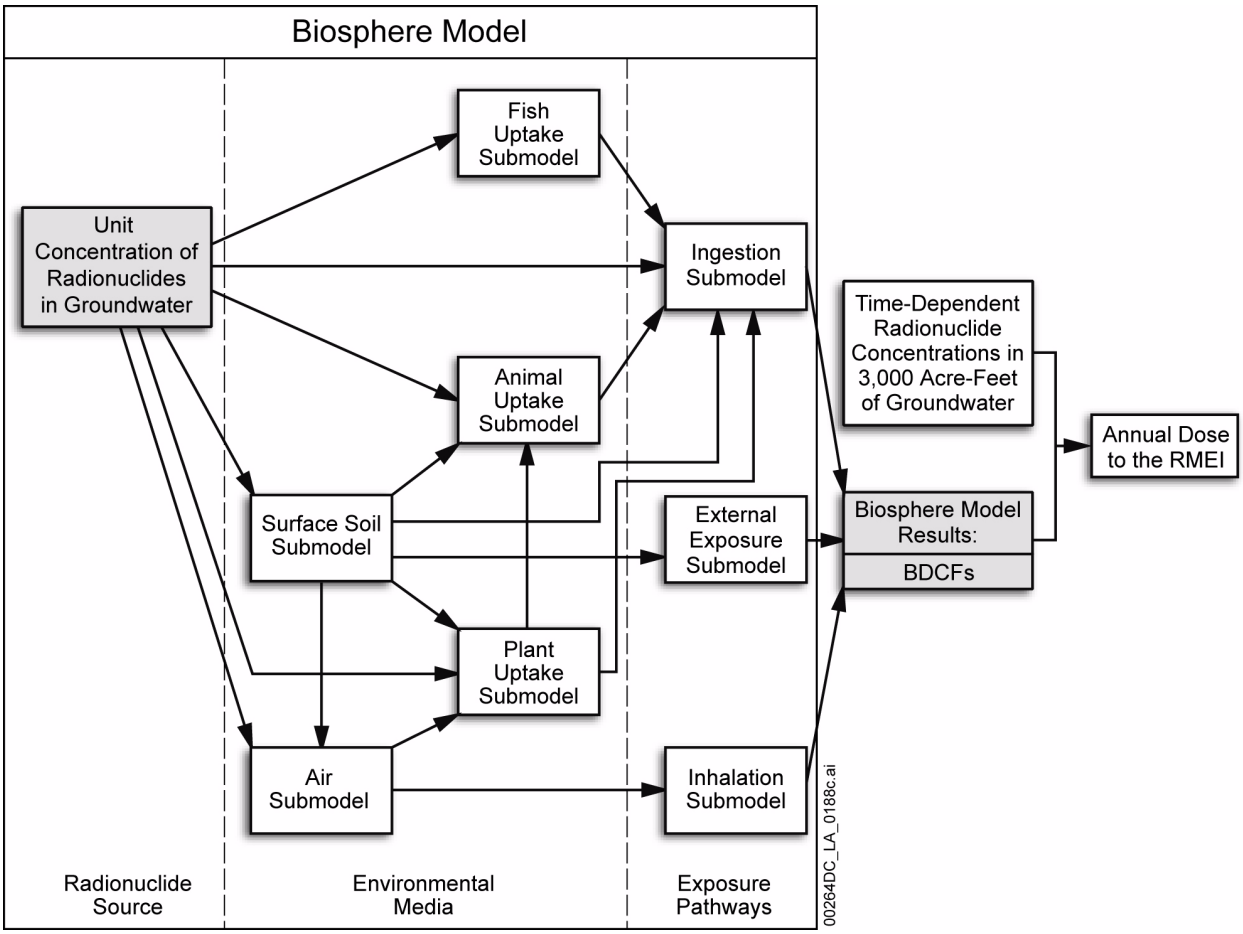

Figure 2.3.10-9. Relationships among Biosphere Submodels for the Groundwater Exposure Scenario

NOTE: The special model for ^{14}C, concerning transport of this radionuclide to soil, air, crops, and animal products, is not shown in this simplified representation of the biosphere model structure. The modeling of the ^{14}C transport pathways is included in the appropriate boxes representing surface soil, air, plant uptake, and animal uptake submodels.

Source: Modified from SNL 2007a, Figure 6.3-2.

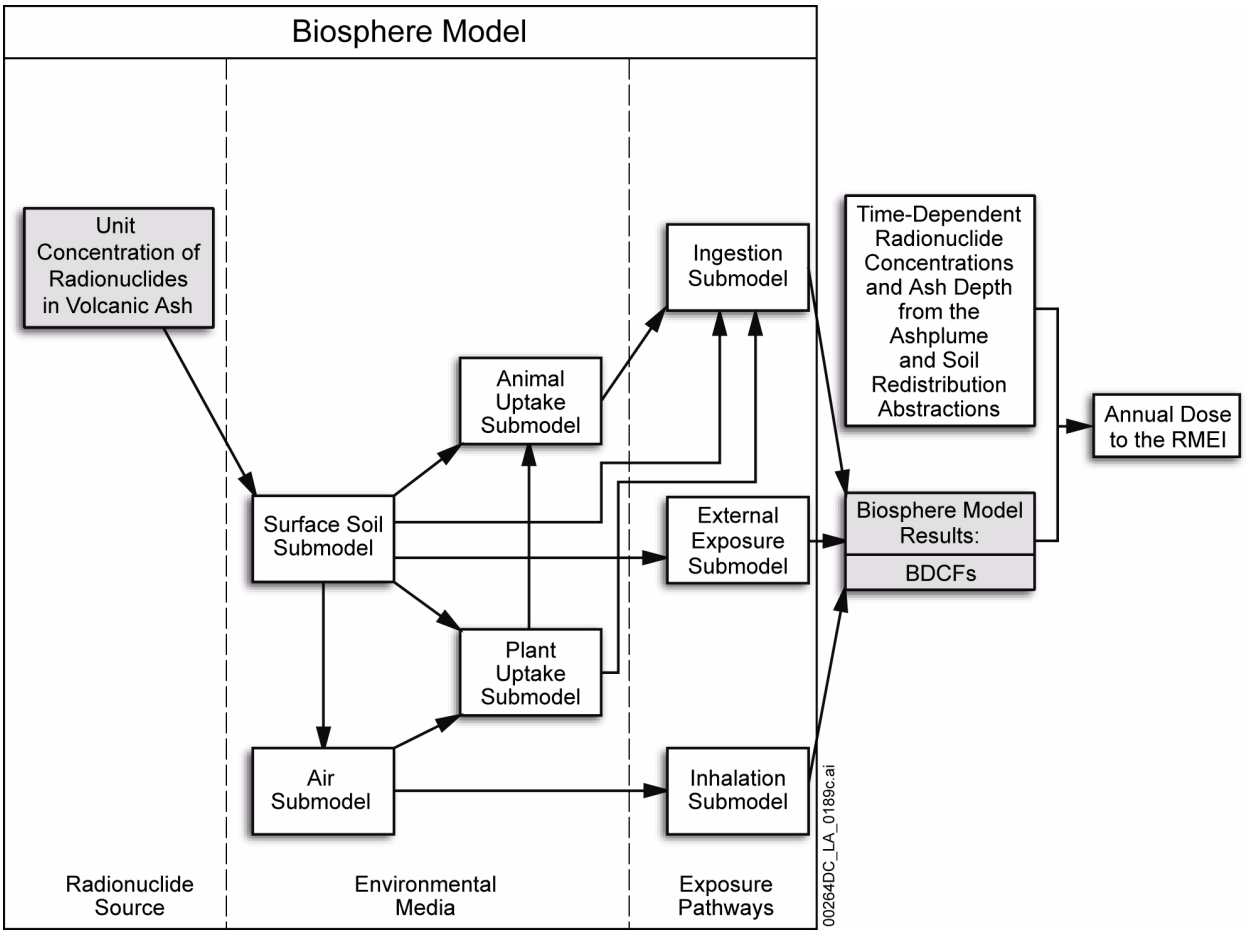

Figure 2.3.10-10. Relationship Among Biosphere Submodels for the Volcanic Ash Exposure Scenario

NOTE: Atmospheric dispersion, deposition, and redistribution of volcanic tephra is modeled outside the biosphere model. The source term for the biosphere model is the radionuclide concentration in the surface soil.

Source: Modified from SNL 2007a, Figure 6.3-5.

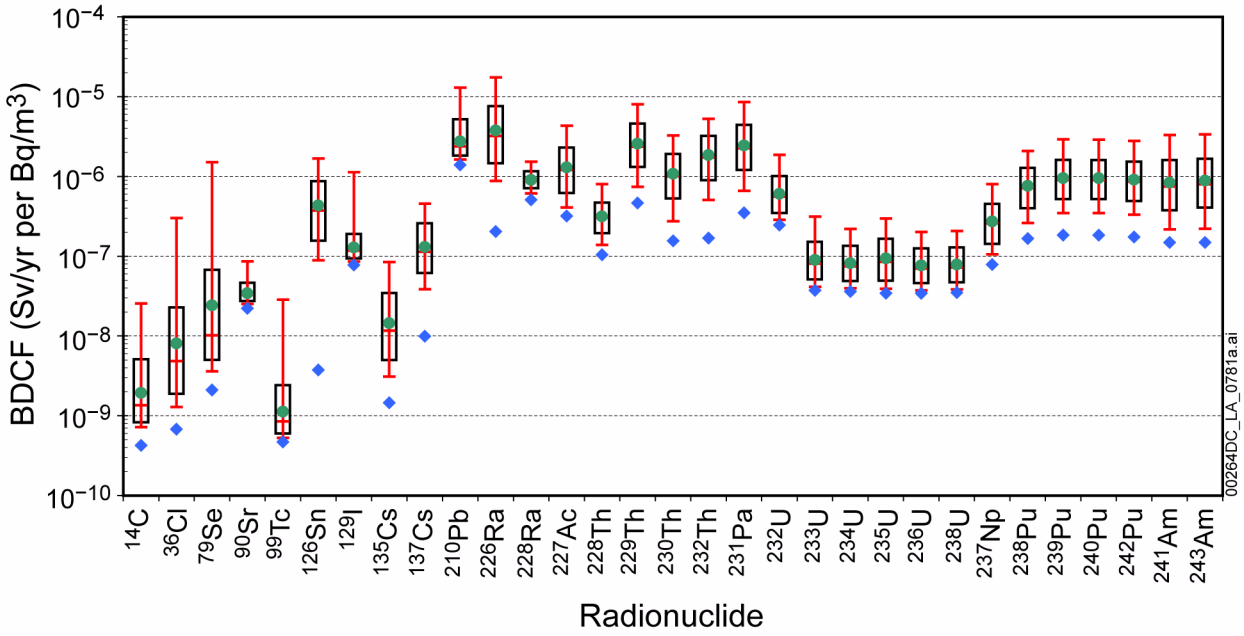

Figure 2.3.10-11. Distributions of Groundwater Exposure Scenario Biosphere Dose Conversion Factors (Present-Day Climate)

NOTE: Boxes represent the 5th to 95th percentile range. The vertical solid lines represent the range, and the tick mark on the line is the median. Diamonds represent BDCF contribution from drinking water; dots represent the mean BDCF. The BDCF statistics shown in this figure are listed in Table 2.3.10-12.

Source: SNL 2007a, Section 6.13.1.

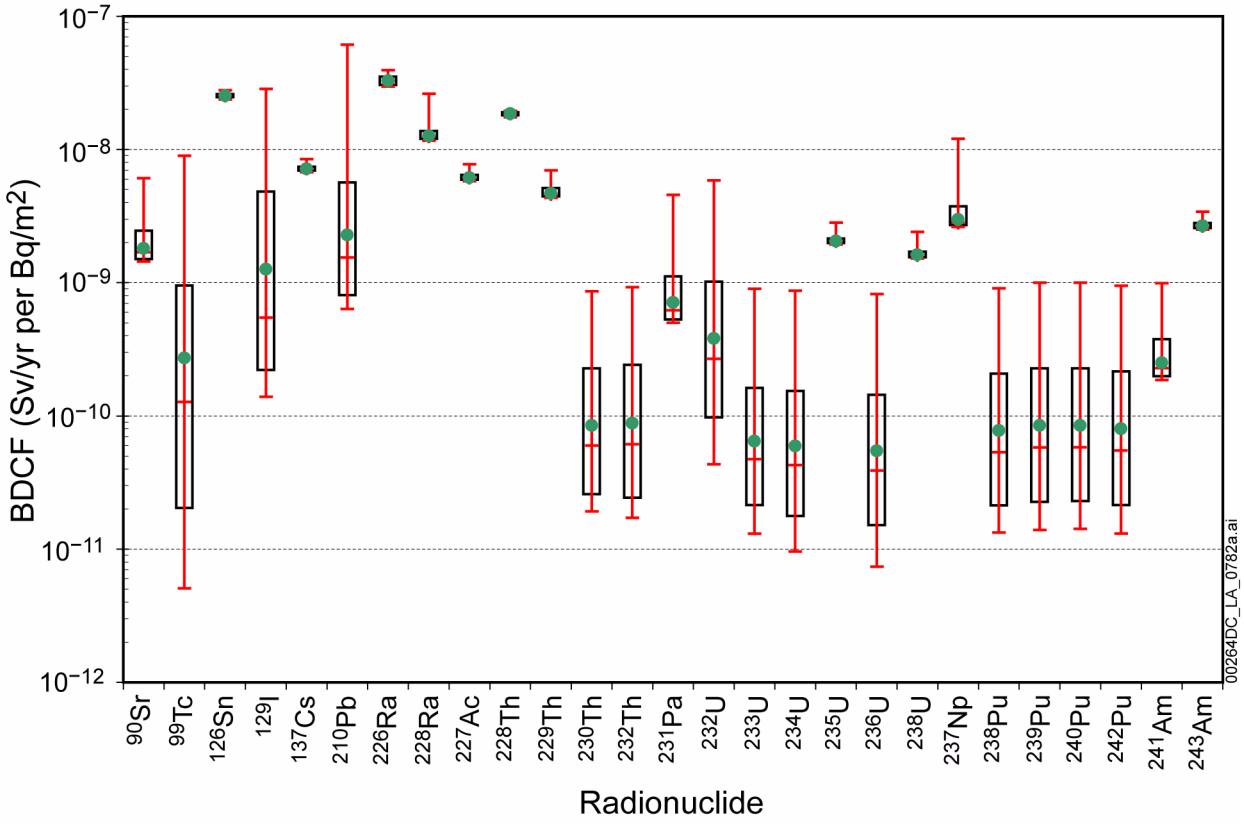

Figure 2.3.10-12. Distributions of the Biosphere Dose Conversion Factor Component for Ingestion, Inhalation of Radon Decay Products, and External Exposure for Volcanic Ash Exposure Scenario

NOTE: Boxes represent the 5th to 95th percentile range. The vertical solid lines represent the range, and the tick mark on the line is the median. Dots represent the mean BDCF (listed in Table 2.3.10-14).

Source: SNL 2007a, Section 6.14.1.

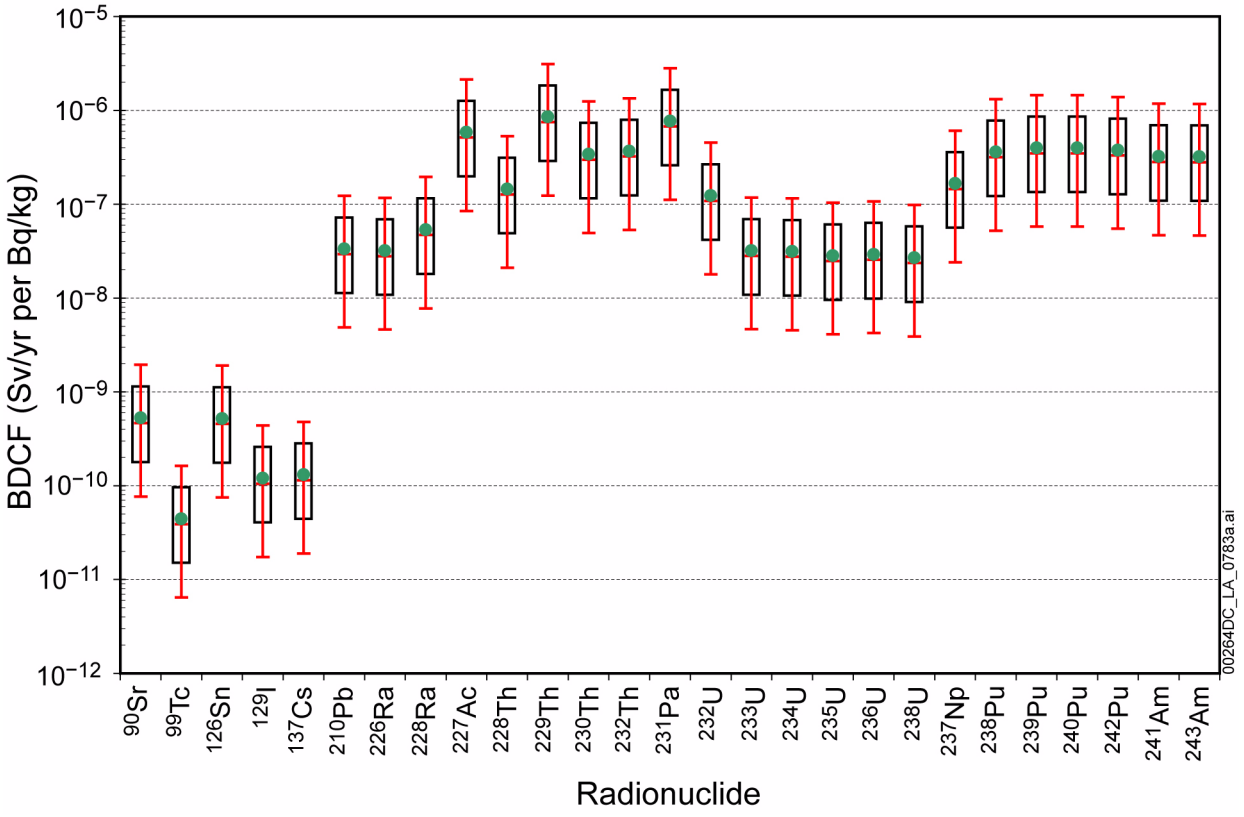

Figure 2.3.10-13. Distributions of Biosphere Dose Conversion Factor Components for Short-Term Inhalation of Particulate Matter for Volcanic Ash Exposure Scenario

NOTE: Boxes represent the 5th to 95th percentile range. The vertical solid lines represent the range, and the tick mark on the line is the median. Dots represent the mean BDCF (listed in Table 2.3.10-14).

Source: SNL 2007a, Section 6.14.1.

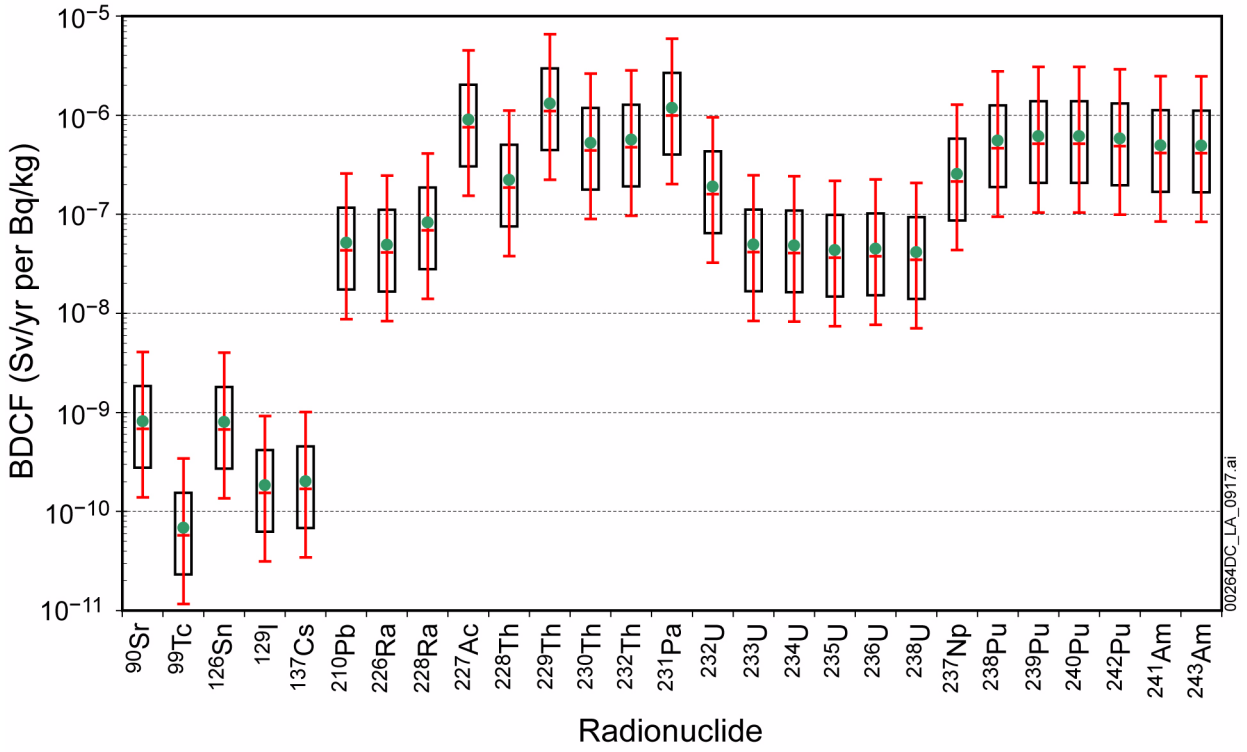

Figure 2.3.10-14. Distributions of Biosphere Dose Conversion Factor Components for Long-Term Inhalation of Particulate Matter for Volcanic Ash Exposure Scenario

NOTE: Boxes represent the 5th to 95th percentile range. The vertical solid lines represent the range, and the tick mark on the line is the median. Dots represent the mean BDCF (listed in Table 2.3.10-14).

Source: SNL 2007a, Section 6.14.1.

CONTENTS

Page

INTENTIONALLY LEFT BLANK

TABLES

Page

INTENTIONALLY LEFT BLANK

FIGURES

Page

INTENTIONALLY LEFT BLANK

2.3.11 Igneous Activity

[NUREG-1804, Section 2.2.1.2.2.3: AC 1, AC 2, AC 3, AC 4, AC 5; Section 2.2.1.3.2.3: AC 1(1) to (5), (7), AC 2, AC 3, AC 4, AC 5; Section 2.2.1.3.3.3: AC 1(1) to (8), (12), AC 2(1), (2), (4), AC 3(1) to (4), (6), AC 4(1) to (4), AC 5; Section 2.2.1.3.10.3: AC 1, AC 2, AC 3, AC 4, AC 5; Section 2.2.1.3.11.3: AC 1, AC 2, AC 3, AC 4, AC 5; Section 2.2.1.3.13.3: AC 1, AC 2, AC 3, AC 4, AC 5]

Future igneous activity at the site is included in the features, events, and processes (FEPs) that are incorporated in the total system performance assessment (TSPA) for the repository (Section 2.2.1.4), because the mean annual probability of intersection of the repository by an igneous event is slightly greater than the probability threshold value for exclusion (Section 2.2.2.2; proposed 10 CFR 63.114(a)(4)). Separate probabilities have been estimated for intersection of the repository by a basalt dike (igneous intrusion modeling case) (Section 2.3.11.2.2) and for eruption through the repository (volcanic eruption modeling case) (Section 2.3.11.4.2.1). These two cases provide the basis for analyses of the consequences of disruption of the repository by an unlikely future igneous event and for evaluation of igneous activity FEPs that are included in the TSPA (Tables 2.2-1, 2.2-7, and 2.3.11-1). Igneous activity FEPs that are excluded from the TSPA are also summarized in Table 2.2-7.

This section summarizes the conceptual model for igneous activity in the region and at the repository site and the annual frequency of intersection of the repository by an unlikely future igneous event (Section 2.3.11.2). The annual frequency of intersection was estimated for 10,000 years following closure based on patterns of igneous activity in the Yucca Mountain region (CRWMS M&O 1996, Section 4.3). The estimate has been updated to account for changes in the design of the repository between the conclusion of the probabilistic volcanic hazard analysis (PVHA) (CRWMS M&O 1996) and 2003 (BSC 2004a, Table 7-1). Because of the overall volcanic stability of the region (in terms of recurrence rate, eruptive style, volume, and location relative to the repository) over the last 2 million years (Section 2.3.11.2.1), this same estimated annual frequency of intersection is also valid for evaluations over time periods that extend beyond 10,000 years. Should intersection occur, the performance of the repository is assumed to be disrupted. The descriptions in this section include the conceptual and numerical models, data and data uncertainties, model uncertainties and alternative models, and the model abstractions used in TSPA (Section 2.4).

Consistent with the regulatory requirement to assess the effects of igneous scenarios (proposed 10 CFR 63.342(c)(1)(ii) (70 FR 53313), the igneous intrusion modeling case (Section 2.3.11.3) is based on studies of the propagation of a basaltic dike (a magma-filled fracture) from deep in the crust and its interactions with the repository. The FEPs included in the igneous intrusion modeling case are FEPs 1.2.04.03.0A, Igneous intrusion into the repository; 1.2.04.04.0A, Igneous intrusion interacts with EBS components; and 1.2.04.04.0B, Chemical effects of magma and magmatic volatiles (Tables 2.2-5 and 2.3.11-1). The studies considered the following:

- The upward propagation of the dike as a fluid-filled crack.
- The potential for diversion or focusing of the dike because of the repository openings or effects of heat from waste emplaced in the repository. This potential was evaluated as part of the analyses associated with the dike propagation modeling (SNL 2007a,

Section 6.3.7). The results showed that stress changes caused by excavation of drifts and changes associated with heat produced by emplaced waste would be of limited spatial extent. Hence, diversion of a dike by stress changes associated with drift excavation and heat effects from emplaced waste are not included the TSPA.

- The flow of magma into and within repository drifts following intersection.
- Heat flow and cooling of the magma.
- Damage to the Engineered Barrier System (EBS), principally the drip shields and waste packages, from contact by magma, and resulting damage to the waste forms.
- Changes in the pH and ionic strength of groundwater that reacts with cooled basalt.

Although considered, not all of the above studies (e.g., the potential for diversion or focusing of a dike) are implemented in the TSPA because they were found to have no significant impact on the results of the igneous intrusion modeling case.

In the sense that intersection of the repository by a dike must occur for eruption though the repository to happen, the volcanic eruption modeling case can be considered an extension of the igneous intrusion modeling case. The volcanic eruption modeling case (Section 2.3.11.4) is based on a model for eruption of a small-volume basalt volcano through the repository, ejection of contaminated material into the atmosphere, and dispersal and deposition of that material downwind of the eruption location. The model also considers mobilization by hillslope and fluvial processes of contaminated material deposited on hillslopes in the Fortymile Wash watershed, redistribution of that material along tributaries to and within the Fortymile Wash channel, and deposition of that material at the reasonably maximally exposed individual (RMEI) location, near the apex of the Fortymile Wash alluvial fan. These processes are associated with three included igneous activity FEPs: FEP 1.2.04.06.0A, Eruptive conduit to surface intersects repository; FEP 1.2.04.07.0A, Ashfall; and FEP 1.2.04.07.0C, Ash redistribution via soil and sediment transport (Tables 2.2-1 and 2.3.11-1).

Summaries of the abstractions of the two modeling cases are presented in Section 2.3.11.5, and Section 2.3.11.6 provides conclusions about the evaluations described in this section in terms of the principal effects on the repository system. In short, the information in those sections describes the model parameters that are provided to the TSPA to estimate the dose risk to the RMEI associated with the intersection of the repository by an unlikely future igneous event.

The information presented in this section addresses the requirements of proposed 10 CFR 63.114(a)(1) through (a)(7) and (b) (70 FR 53313) for conducting a performance assessment that considers igneous processes and events. This section also provides information that addresses specific regulatory acceptance criteria in Sections 2.2.1.2.2.3, 2.2.1.3.2.3, 2.2.1.3.10.3, 2.2.1.3.11.3, and 2.2.1.3.13.3 of NUREG-1804.

Section 2.3.11 presents:

- Data from the site and surrounding region related to igneous activity, including uncertainties and variabilities in parameter values, and alternative conceptual models used in the analyses
- Specific FEPs included in the analyses with the technical bases for inclusion
- Specific degradation, deterioration, and alteration processes related to the effects of igneous activity and included in the analyses taking into consideration their effects on annual dose, and the technical bases for inclusion of the processes
- Technical basis for models related to igneous activity and used in the performance assessment.

The applicable regulatory requirements and acceptance criteria for disruptive events related to igneous activity are listed in the table that follows, along with a reference to where each item is addressed within this section.

SAR Section	Information Category	Proposed 10 CFR Part 63 Reference	NUREG-1804 Reference
2.3.11	Igneous Activity	63.114(a)(1) 63.114(a)(2) 63.114(a)(3) 63.114(a)(4) 63.114(a)(5) 63.114(a)(6) 63.114(a)(7) 63.114(b) 63.342	Section 2.2.1.2.2.3: Acceptance Criterion 1 Acceptance Criterion 2 Acceptance Criterion 3 Acceptance Criterion 4 Acceptance Criterion 5 Section 2.2.1.3.2.3: Acceptance Criterion 1(1) Acceptance Criterion 1(2) Acceptance Criterion 1(3) Acceptance Criterion 1(4) Acceptance Criterion 1(5) Acceptance Criterion 1(7) Acceptance Criterion 2 Acceptance Criterion 3 Acceptance Criterion 4 Acceptance Criterion 5

SAR Section	Information Category	Proposed 10 CFR Part 63 Reference	NUREG-1804 Reference
2.3.11 (Continued)	Igneous Activity (Continued)		Section 2.2.1.3.3.3: Acceptance Criterion 1(1) Acceptance Criterion 1(2) Acceptance Criterion 1(3) Acceptance Criterion 1(4) Acceptance Criterion 1(5) Acceptance Criterion 1(6) Acceptance Criterion 1(7) Acceptance Criterion 1(8) Acceptance Criterion 1(12) Acceptance Criterion 2(1) Acceptance Criterion 2(2) Acceptance Criterion 2(4) Acceptance Criterion 3(1) Acceptance Criterion 3(2) Acceptance Criterion 3(3) Acceptance Criterion 3(4) Acceptance Criterion 3(6) Acceptance Criterion 4(1) Acceptance Criterion 4(2) Acceptance Criterion 4(3) Acceptance Criterion 4(4) Acceptance Criterion 5 Section 2.2.1.3.10.3: Acceptance Criterion 1 Acceptance Criterion 2 Acceptance Criterion 3 Acceptance Criterion 4 Acceptance Criterion 5 Section 2.2.1.3.11.3: Acceptance Criterion 1 Acceptance Criterion 2 Acceptance Criterion 3 Acceptance Criterion 4 Acceptance Criterion 5 Section 2.2.1.3.13.3: Acceptance Criterion 1 Acceptance Criterion 2 Acceptance Criterion 3 Acceptance Criterion 4 Acceptance Criterion 5
2.3.11.1	Summary and Overview	Not applicable	Not applicable
2.3.11.2	System Description and Integration	63.114(a)(1) 63.114(a)(2) 63.114(a)(3) 63.114(a)(4) 63.114(a)(5) 63.114(a)(6) 63.114(a)(7) 63.114(b) 63.342(a) 63.342(c)	Section 2.2.1.2.2.3: Acceptance Criterion 1 Acceptance Criterion 2 Acceptance Criterion 3 Acceptance Criterion 4 Acceptance Criterion 5 Section 2.2.1.3.10.3: Acceptance Criterion 2(4) Acceptance Criterion 3(3)

SAR Section	Information Category	Proposed 10 CFR Part 63 Reference	NUREG-1804 Reference
2.3.11.3	Igneous Intrusion Modeling Case	63.114(a)(1) 63.114(a)(2) 63.114(a)(3) 63.114(a)(4) 63.114(a)(5) 63.114(a)(6) 63.114(a)(7) 63.114(b) 63.342	See details in sections below
2.3.11.3.1	Conceptual Model	63.114(a)(1)	Section 2.3.1.3.2.3: Acceptance Criterion 1(2) Section 2.2.1.3.3.3: Acceptance Criterion 1(1) Acceptance Criterion 1(2) Acceptance Criterion 1(4) Acceptance Criterion 1(6) Acceptance Criterion 1(8)
2.3.11.3.2	Model and Analysis Descriptions	63.114(a)(1) 63.114(a)(5) 63.114(a)(6) 63.114(a)(7) 63.114(b) 63.342	Section 2.2.1.3.2.3: Acceptance Criterion 1(1) Acceptance Criterion 1(2) Acceptance Criterion 1(3) Acceptance Criterion 1(4) Acceptance Criterion 1(5) Acceptance Criterion 1(7) Acceptance Criterion 2 Section 2.2.1.3.3.3: Acceptance Criterion 1(1) Acceptance Criterion 1(2) Acceptance Criterion 1(3) Acceptance Criterion 1(4) Acceptance Criterion 1(5) Acceptance Criterion 1(6) Acceptance Criterion 1(7) Acceptance Criterion 1(8) Acceptance Criterion 2(1) Acceptance Criterion 2(2) Acceptance Criterion 2(4) Acceptance Criterion 3(1) Acceptance Criterion 3(2) Acceptance Criterion 3(3) Section 2.2.1.3.10.3: Acceptance Criterion 1 Acceptance Criterion 2(1) Acceptance Criterion 2(2) Acceptance Criterion 2(3)

SAR Section	Information Category	Proposed 10 CFR Part 63 Reference	NUREG-1804 Reference
2.3.11.3.3	Data Uncertainty	63.114(a)(2)	Section 2.2.1.3.2.3: Acceptance Criterion 3(1) Acceptance Criterion 3(2) Acceptance Criterion 3(3) Section 2.2.1.3.3.3: Acceptance Criterion 3(1) Acceptance Criterion 3(2) Acceptance Criterion 3(4) Section 2.2.1.3.10.3: Acceptance Criterion 3(1) Acceptance Criterion 3(2)
2.3.11.3.4	Model and Analysis Uncertainty and Alternative Models	63.114(a)(3)	Section 2.2.1.3.2.3: Acceptance Criterion 4 Section 2.2.1.3.3.3: Acceptance Criterion 4(1) Acceptance Criterion 4(2) Acceptance Criterion 4(3) Acceptance Criterion 4(4) Acceptance Criterion 5 Section 2.2.1.3.10.3: Acceptance Criterion 4
2.3.11.3.5	Igneous Intrusion Model Abstraction	63.114(a)(5) 63.114(b) 63.342	Section 2.2.1.3.2.3: Acceptance Criterion 5 Section 2.2.1.3.3.3: Acceptance Criterion 5 Section 2.2.1.3.10.3: Acceptance Criterion 5
2.3.11.4	Volcanic Eruption Modeling Case	63.114(a)(1) 63.114(a)(2) 63.114(a)(3) 63.114(a)(4) 63.114(a)(5) 63.114(a)(6) 63.114(a)(7) 63.114(b) 63.342	See details in sections below
2.3.11.4.1	Conceptual Model	63.114(a)(1)	Section 2.2.1.2.2.3: Acceptance Criterion 1(2) Acceptance Criterion 2

SAR Section	Information Category	Proposed 10 CFR Part 63 Reference	NUREG-1804 Reference
2.3.11.4.2	Model/Analysis Description	63.114(a)(1) 63.114(a)(5) 63.114(a)(6) 63.114(a)(7) 63.114(b) 63.342	Section 2.2.1.2.2.3: Acceptance Criterion 1(2) Acceptance Criterion 2 Section 2.2.1.3.10.3: Acceptance Criterion 1 Acceptance Criterion 2(1) Acceptance Criterion 2(2) Acceptance Criterion 2(3) Section 2.2.1.3.11.3: Acceptance Criterion 1 Acceptance Criterion 2(1) Acceptance Criterion 2(2) Acceptance Criterion 2(3) Section 2.2.1.3.13.3: Acceptance Criterion 1 Acceptance Criterion 2
2.3.11.4.3	Data Uncertainty	63.114(a)(2)	Section 2.2.1.3.10.3: Acceptance Criterion 3(1) Acceptance Criterion 3(2) Section 2.2.1.3.11.3: Acceptance Criterion 3(1) Acceptance Criterion 3(2) Section 2.2.1.3.13.3: Acceptance Criterion 3(1) Acceptance Criterion 3(2) Acceptance Criterion 3(3) Acceptance Criterion 3(4)
2.3.11.4.4	Model and Analysis Uncertainty and Alternative Models	63.114(a)(3)	Section 2.2.1.3.10.3: Acceptance Criterion 4 Section 2.2.1.3.11.3: Acceptance Criterion 4 Section 2.2.1.3.13.3: Acceptance Criterion 4
2.3.11.4.5	Volcanic Eruption Model Abstraction	63.114(a)(5) 63.114(b) 63.342	Section 2.2.1.2.2.3 Acceptance Criterion 1(2) Section 2.2.1.3.10.3: Acceptance Criterion 5 Section 2.2.1.3.11.3: Acceptance Criterion 5 Section 2.2.1.3.13.3: Acceptance Criterion 5

SAR Section	Information Category	Proposed 10 CFR Part 63 Reference	NUREG-1804 Reference
2.3.11.5	Summary of Igneous Scenario Class Model Abstraction	63.114(a)(1) 63.114(a)(2) 63.114(a)(3) 63.114(a)(4) 63.114(a)(5) 63.114(a)(6) 63.114(a)(7) 63.114(b) 63.342	Section 2.2.1.3.2.3: Acceptance Criterion 1(1) Acceptance Criterion 5(1) Section 2.2.1.3.3.3: Acceptance Criterion 1(1) Acceptance Criterion 5(1) Section 2.2.1.3.10.3: Acceptance Criterion 1(1) Acceptance Criterion 5(1) Section 2.2.1.3.11.3: Acceptance Criterion 1(1) Acceptance Criterion 5(1) Section 2.2.1.3.13.3: Acceptance Criterion 1(1) Acceptance Criterion 5
2.3.11.6	Conclusions	Not applicable	Not applicable

NUREG-1804, Section 2.2.1.3.2.3, Acceptance Criterion 1(6) is not referenced in the table because criticality is excluded from TSPA (Section 2.2.1.4.1). Acceptance Criteria 2(4) and 3(3) from NUREG-1804, Section 2.2.1.3.10.3 related to expert elicitations are included in the table because of the expert elicitation to estimate the annual frequency of intersection of the repository by an unlikely future igneous event (CRWMS M&O 1996, Section 4.3; Section 2.3.11.2.2). The expert elicitation was conducted in a manner consistent with NUREG-1563 (Kotra et al. 1996). However, no expert elicitations were used in direct support of the analysis of the consequences associated with the igneous intrusion modeling case (Section 2.3.11.3). Similarly for the volcanic eruption modeling case (Section 2.3.11.4), no expert elicitations were used in the development of the atmospheric dispersal model, the evaluation of the ASHPLUME code, or the evaluation of radionuclide redistribution. As a result, the following acceptance criteria from NUREG-1804 are not included in the table for the subsections of Section 2.3.11: Section 2.2.1.3.2.3, Acceptance Criterion 3(4); Section 2.2.1.3.11.3, Acceptance Criteria 2(4) and 3(3); and Section 2.2.1.3.13.3, Acceptance Criterion 3(3).

Multiple peer reviews were used to support development of the current models and analyses discussed in this section (Section 2.3.11), and the associated acceptance criteria from NUREG-1804, Sections 2.2.1.3.2.3, 2.2.1.3.10.3, 2.2.1.3.11.3, and 2.2.1.3.13.3 are shown in the table for the appropriate subsections of Section 2.3.11. However, in terms of Acceptance Criterion 1(12) from NUREG-1804, Section 2.2.1.3.3.3, no formal peer reviews were used in the development of the model for water chemistry under the igneous scenario. With regard to data qualification, this section does not discuss the approach used. However, scientific analyses, model development, and data qualification activities were conducted in accordance with project procedures that comply with Quality Assurance Program requirements. The project procedures governing data qualification are consistent with NUREG-1298 (Altman et al. 1988) in keeping with the associated acceptance criteria.

2.3.11.1 Summary and Overview

The U.S. Department of Energy (DOE) developed the igneous scenario class to evaluate the consequences of future igneous activity at the repository because the mean annual frequency of intersection of the repository by an igneous event is about 1.7×10^{-8} per year (BSC 2004a, Table 7-1), or slightly greater than the regulatory value for exclusion (proposed 10 CFR 63.342(a)) (70 FR 53313). The current estimate of the frequency of intersection was developed from the results of an expert elicitation that was completed in 1996 (CRWMS M&O 1996). Based on the understanding of the igneous framework of the region (Section 2.3.11.2.1), it is appropriate to use this same frequency of intersection for evaluations of consequences of igneous activity that extend beyond the 10,000 year postclosure period through the period of geologic stability as required by proposed 10 CFR 63.342(c) (70 FR 53313).

The postclosure performance of a repository at Yucca Mountain could be compromised by natural events, including igneous activity at the repository. As described in this section and consistent with regulatory requirements, the DOE has evaluated the consequences of an igneous event that intersects the repository. For evaluations that extend beyond the 10,000 year postclosure period, the DOE consequence analyses are limited to those causing damage to waste packages directly, and causing releases of radionuclides to the biosphere, atmosphere, or groundwater as required by proposed 10 CFR 63.342(c)(1)(ii) (70 FR 53313). The methods that the DOE has selected to evaluate the consequences of igneous activity are summarized in the following paragraphs of this section.

The igneous scenario class includes FEPs that describe the possibility that low probability igneous activity may affect repository performance (Tables 2.2-7 and 2.3.11-1). Two modeling cases in the TSPA simulate the significant FEPs: the first is the igneous intrusion modeling case, which addresses the possibility that magma could intrude into the repository and disrupt expected repository performance. The igneous intrusion modeling case is strictly limited to an event that intersects the repository because the hazard is described in terms of the annual frequency of intersection of the repository by an igneous event (BSC 2004a, Table 7-1). Once intersection has occurred, all waste packages and drip shields are assumed to be damaged by contact with magma (SNL 2007b, Table 7-1) and all the waste packages are assumed to fail, thereby making the waste available for transport once seepage of water resumes through the cooled, magma-filled emplacement drifts (SNL 2007a, Section 8.1.2). The second is the volcanic eruption modeling case, which includes FEPs that describe an eruption that rises through the repository footprint and damages a number of waste packages. The basis for this case is the number of intrusion realizations that include an eruption through the repository and intersection of waste packages by a conduit(s) (SNL 2007b, Table 7-1). The analysis recognizes that for eruption through the repository to occur, a dike must have intersected the repository. Since eruption is contingent on intersection of the repository by a dike, all waste packages are contacted by magma and damaged. However, an eruption within the repository footprint could occur, but no waste packages would be intersected by conduits (e.g., eruption through access drift or eruption through pillar separating emplacement drifts). The volcanic eruption modeling case features a low probability volcanic eruption through the repository with potential to disperse volcanic tephra and entrained waste into the atmosphere, and deposits them on land surfaces where they would be redistributed by fluvial and soil processes.

This section demonstrates the level of understanding of the igneous setting of the region, and the site, and the implications of the setting for estimating the probability and consequences of intersection of the repository by an unlikely future igneous event. The definition of an igneous event includes intersection of the repository by a dike accompanied by eruption somewhere along the dike but not necessarily within the repository footprint. The potential consequences of intersection have been evaluated, and those consequences are evaluated for the TSPA in terms of two modeling cases: (1) the igneous intrusion modeling case (intrusion case); and (2) the volcanic eruption modeling case (eruption case).

In terms of the number of failed waste packages, the igneous intrusion modeling case is much more significant than the volcanic eruption modeling case. The intrusion case describes the models for and analyses of dike propagation, magma flow, and damage to waste packages and waste forms from interaction with magma. Lacking a demonstrated natural or engineered means to limit magma flow from intersected to non-intersected drifts, the intrusion case assumes that, if intersection occurs, all waste packages in all drifts will be contacted by magma and damaged to the extent that they provide no protection for the waste. Once a waste package is contacted by magma, radionuclides in the contained waste are assumed to be immediately available for transport by groundwater, but the magnitude of the release is a function of the solubility of each radionuclide. The parameters utilized by the TSPA are the number of waste packages damaged and the drift centerline and wall temperatures, which are used to determine when percolation through cooled basalt occurs. For realizations in which intersection of any repository drift occurs, all waste packages are assumed to be damaged. In addition, the pH and ionic strength of percolating water that has reacted with cooled basalt have been investigated using published analogue information. Although the TSPA inputs for these parameters are provided by the *In-Package Chemistry Abstraction* (SNL 2007c, Section 8.2[a]), the inputs are described as part of the igneous intrusion modeling case in Section 2.3.11.3.

The volcanic eruption modeling case is conditional on intersection of a dike with the repository (i.e., the igneous intrusion modeling case), and therefore the conditional probability for development of one or more volcanic conduits within the repository is estimated. This probability is used to estimate the number of waste packages intersected by conduits. Once intersection occurs, the waste from damaged waste packages within the conduit circumference is entrained in the erupting magma. At the earth's surface, the erupting contaminated material is partitioned into three types of volcanic products based on analogue information: lava, cone forming deposits, and fallout tephra. Only the tephra is ejected high into the atmosphere, dispersed by atmospheric processes, and deposited downwind of the eruption site. The atmospheric dispersal model uses a distribution of wind speeds and wind directions to model the thickness of contaminated tephra deposited throughout the Fortymile Wash drainage basin (SNL 2007d, Section 6.5.2.8 and Figures C-8 and K-4; Section 2.3.11.4.2). One combination of wind speed and direction is used for each realization (SNL 2007d, Section 5.2.2), and the amount of material deposited at the RMEI location depends on whether the wind is blowing from the repository toward the RMEI. For most realizations, the wind is from the southwest (reflecting present-day wind patterns) (SNL 2007d, Section 5.2.1 and Appendix K, Section K1) so most tephra falls within the Fortymile Wash basin but upstream of the RMEI. Such tephra could be redistributed to the RMEI location following mobilization off slopes and movement down Fortymile Wash and its tributaries by surface water runoff.

The general location of the RMEI is described in Section 2.3.9 and is at the boundary of the controlled area as described by regulations (10 CFR 63.302) and along the predominant direction of groundwater flow. Both the igneous intrusion modeling case and the igneous eruption modeling case use the same location for the RMEI, and it is important to note that the dose results for the two cases are additive. The ASHPLUME code models atmospheric dispersal and deposition of the contaminated tephra. The Fortymile Wash ash redistribution code models redistribution of the contaminated tephra by fluvial processes. The analyses described in Section 2.3.11 describe the processes and provide the parameter values needed to implement the ASHPLUME and the Fortymile Wash ash redistribution codes in the TSPA model. The result of the eruption case modeling is a suite of simulations that estimate the amount of contaminated tephra at the RMEI location.

The intrusion of a dike or eruption of volcanic materials through the repository would not substantially affect the capability of the natural barriers at Yucca Mountain to prevent or reduce the flow of water or the movement of radionuclides in groundwater away from the repository (Table 2.2-1, FEP 1.2.04.02.0A, Igneous activity changes rock properties). However, igneous or volcanic events could adversely affect the engineered barrier system's ability to prevent the release or reduce the release rate of radionuclides from the waste, and to prevent or reduce the movement of radionuclides away from the repository (SNL 2007a, Section 8.2.3). The specific FEPs determined to be most important to the evaluation of the effects of igneous intrusion on the performance of a repository at Yucca Mountain are listed in Tables 2.2-7 and 2.3.11-1 and technical bases have been provided for their inclusion (Table 2.3.11-1).

- **Igneous Intrusion into Repository**—Following intersection of one or more repository emplacement drifts by a dike, all drifts are assumed to be inundated by magma. The annual frequency of intersection used for the igneous intrusion modeling case is summarized in *Characterize Framework for Igneous Activity at Yucca Mountain, Nevada* (BSC 2004a, Table 7-1). All waste packages contacted by magma are assumed to be damaged, and the severity of the damage is summarized as part of the description of the FEP, Igneous intrusion interacts with EBS components.

- **Igneous Intrusion Interacts with EBS Components**—An igneous intrusion into the repository in the form of a dike may occur, intersecting the repository drifts, resulting in magma, pyroclastics, and volcanic gases entering the drift and interacting with the EBS components (drip shields, waste packages, cladding, waste forms, and the waste package pallet). This could lead to accelerated drip shield and waste package breaching (e.g., damage by flowing or fragmented magma, or thermal effects) and mobilization of the waste by groundwater.

The specific FEPs determined to be most important to the evaluation of the effects of an eruption through the repository on the performance of a repository at Yucca Mountain are as follows:

- **Eruptive Conduit to Surface Intersects Repository**—As a result of an igneous intrusion, one or more volcanic vents may form at land surface. The conduit(s) supplying the vent(s) could pass through the repository, interacting with and entraining waste.

- **Ashfall**—Finely divided waste particles may be carried up a volcanic vent and deposited on the land surface from an ash cloud.

- **Ash Redistribution via Soil and Sediment Transport**—Following deposition of contaminated ash on the surface, ash deposits may be redistributed on the surface via eolian and fluvial processes.

Field geologic investigations, laboratory analyses, analogue studies, and reviews of published literature provide the technical bases for the description of past igneous activity in the Yucca Mountain region, and for the development of conceptual, process and consequence models that represent potential future events. The process models have been used to develop simplified models or abstractions that are incorporated within the TSPA model to generate a probabilistic representation of the likelihood and consequences of the igneous scenario class.

Igneous Activity—The probability of a future igneous event intersecting the repository is addressed through the PVHA (CRWMS M&O 1996, Section 4.3), which used expert elicitation to consider applicable geologic processes and uncertainty (Section 2.3.11.2.2). Probability distributions were developed to define the likelihood of a volcanic event that could intersect the repository footprint. The mean annual frequency of intersection of the repository footprint by a potential future igneous event is 1.7×10^{-8} (Section 2.3.11.2.2), equivalent to an annual probability of about 1 in 60 million (or 1 chance in 6,000 in 10,000 years). The 5th and 95th percentile uncertainties associated with the frequency of intersection span almost 2 orders of magnitude, from 7.4×10^{-10} to 5.5×10^{-8} (BSC 2004a, Table 7-1), or about 1 in 1.4 billion to 1 in 18 million per year. The results of the PVHA indicate that the mean annual probability of future igneous activity at Yucca Mountain is greater than 1×10^{-8}; therefore, the impact on repository performance of igneous scenario class for disruptive events must be considered.

Igneous Intrusion Modeling Case—In the igneous intrusion conceptual model, a basaltic dike intersects one or more emplacement drifts, and magma flows in and fills them, engulfing the waste packages and drip shields. Flow is assumed to continue until the entire repository is filled and all waste packages are contacted by magma. The magma then cools and solidifies. Waste packages in the filled drifts are heated to near-magmatic temperatures, and their strength and stability are affected. The waste packages are assumed to lose structural integrity, and their capabilities to prevent or limit the flow of water and limit the movement of radionuclides are compromised (Section 2.3.11.3). After the drifts return to temperatures less than the boiling point of water, seepage into drifts is restored. The model assumes that the cooled magma has hydrologic properties similar to the surrounding welded tuff, so that the movement of water into or radionuclides out of the waste package is not impacted. That is, the cooled magma (basalt) in the drift offers no additional resistance to flow beyond that of the surrounding host rock. The rate of transport of radionuclides depends on the temperature and chemistry of the groundwater. Thus, the percolation of water through cooled basalt provides a mechanism for radionuclide release and transport.

The igneous intrusion modeling case simulates flow and transport below the EBS and the unsaturated and saturated zones in the same manner as the nominal case (Section 2.4.2.1.2). The results of the TSPA for the igneous intrusion modeling case and for the igneous eruption modeling case are discussed in Section 2.4.2.2.1.2.

Volcanic Eruption Modeling Case—The volcanic eruption modeling case considers the intrusion of one or more dikes into the repository, and the formation of one or more eruptive conduits that intersect emplacement drifts. Waste packages within the conduits are assumed to be destroyed, and their waste entrained in the erupting magma. Contaminated volcanic tephra is erupted into the atmosphere (Section 2.3.11.4.2.2) in a column that reaches altitudes up to 13 km, and is dispersed by wind to the accessible environment. Following deposition on the ground, surface processes (erosion and deposition by fluvial action) may redistribute the tephra. Information from the PVHA (CRWMS M&O 1996, Section 4) and analogue studies (SNL 2007e, Table 7-1) was used to estimate the probability that one or more eruptive centers would form within the repository to estimate the number of waste packages that would be intersected by the eruptive conduits. The volcanic eruption modeling case provides to TSPA the eruptive center probability, which is the fraction of the intersections that include eruption, the number of waste packages intersected by volcanic conduits, the areal density of contaminated tephra, and the concentration of contaminated tephra from redistribution (Section 2.3.11.4.2.1.3).

Application in TSPA—The modeling and analytical activities associated with the two igneous activity modeling cases provide output parameters and abstractions for the TSPA model to evaluate the impacts of an igneous event. These outputs include:

- Assumptions about the severity of damage to waste packages, and the waste forms exposed to magma
- Assumption that once intersection of the repository by a basalt dike occurs, all drifts are filled with magma and all waste packages are damaged
- Temperature of the magma and drift wall as a function of time after intrusion
- Fraction of waste packages damaged by a violent Strombolian eruption (Section 2.3.11.4.1.1) through the repository
- Physical parameters for waste particle size and ratio of waste to ash for inclusion in ASHPLUME code (violent Strombolian eruption phase)
- Physical parameters for the redistribution of contaminated tephra after initial deposition.

Figure 2.3.11-1 depicts the general flow of information within the process models and TSPA abstractions for the igneous intrusion modeling case and the volcanic eruption modeling case, including the major inputs and outputs for each submodel.

For each realization of the igneous intrusion modeling case, the TSPA model selects parameter values for each of the model components and submodels. The percolation flux, the water chemistry, and the temperature of the waste package are used to simulate degradation of the radioactive waste and subsequent radionuclide mobilization. The radionuclides in the waste are considered immediately available for dissolution and transport.

The volcanic eruption modeling case is implemented in the TSPA by generating a set of realizations that produce annual dose histories associated with eruptions that occur at a rate determined by three

factors: (1) the frequency of intersection of the repository by an igneous event (mean about 1.7×10^{-8} per year (BSC 2004a, Table 7-1)); (2) the conditional probability of a conduit forming within the repository (0.28) (Section 2.3.11.4.2.1; SNL 2007b, Table 7-1); and (3) the conditional probability of a conduit that forms within the repository footprint and intersects waste (0.30), which is calculated as 1 minus the probability that zero waste packages are intersected (SNL 2008, Section 6.5.2.2). Therefore, the combined conditional probability of a conduit forming within the repository footprint and intersecting waste is 0.083 (SNL 2008, Section 6.5.2.2). The dose histories are dependent on the future time of occurrence of an eruption because of the effects of radionuclide decay. Therefore, the time of eruption is also treated as an uncertain parameter in the TSPA, and the calculated mean annual dose considers eruptions that could occur at all possible future times.

Both the igneous intrusion modeling case and the volcanic eruption modeling case consider a broad range of data and model uncertainties (Sections 2.3.11.3.3, 2.3.11.3.4, 2.3.11.4.3, and 2.3.11.4.4). The igneous intrusion modeling case incorporates uncertainties related to the probability of an igneous event intersecting the repository, as well as the number of repository drifts intersected by dikes, the number of waste packages damaged by magma (SNL 2007b, Section 7), and the durability and integrity of EBS components (SNL 2007a, Section 8). The uncertainties considered in the volcanic eruption modeling case include the number of conduits associated with the eruption, conduit geometry, amount of waste entrained in the eruption plume, wind speed and direction, and the response of deposits of contaminated tephra to surficial processes. The TSPA captures the range of uncertainty in the model cases by using parameter distributions, bounding ranges (SNL 2007d, Section 6.5), and assumptions (SNL 2007d, Section 5) to provide confidence that the dose has not been underestimated.

Summary of Features, Events, and Processes Evaluated in the Igneous Activity Models and Analyses—The complete set of FEPs, both included and excluded, is provided in Tables 2.2-1. Tables 2.2-7 and 2.3.11-1 provide summaries of the FEPs related to igneous activity that are included in the models and analyses discussed in this section. The FEPs that are evaluated in this section are principally related to igneous intrusion impacts on EBS components, transport of waste package contents to the surface, atmospheric dispersal of radionuclides from an eruption plume, and tephra deposition and redistribution processes.

2.3.11.2 System Description and Integration

[NUREG 1804, Section 2.2.1.2.2.3: AC 1, AC 2, AC 3, AC 4, AC 5; Section 2.2.1.3.10.3: AC 2(4), AC 3(3)]

This section describes the conceptual model for igneous activity, associated processes for the igneous scenario class model cases, and the probability of intersection of the repository by a volcanic event as determined by the PVHA (CRWMS M&O 1996, Section 4), and recalculated to consider subsequent changes to the repository footprint (BSC 2004a, Table 7-1). Although the repository design has changed several times since the completion of the PVHA, the probability of intersection of the repository footprint recalculated to reflect these design changes results in increases in the probability of intersection of less than 20% (BSC 2004a, Section 6.5.2.1) (Section 2.3.11.2.2.3). The mean annual probability of intersection of the repository by an igneous intrusion was last updated for the design in effect in 2003 (BSC 2004a, Section 6.5.2.1). The appropriateness of the hazard estimate based on the design in effect in 2003 for the current TSPA

is described in Section 2.3.11.2.2.3. Lastly, this section describes the integration of the model cases in the TSPA.

2.3.11.2.1 Conceptual Model of Igneous Activity

[NUREG-1804, Section 2.2.1.2.2.3: AC 1(1), 2(1), 3(1), 5(1)]

The conceptual model of igneous activity near Yucca Mountain consists of three components, each related to an aspect of unlikely future igneous processes that might impact the repository. The three components are:

1. **Igneous Framework**—The igneous framework describes the igneous and tectonic history and characteristics of the Yucca Mountain region and the assessment of the history and characteristics by PVHA experts as a basis to determine the probability of intersection of the repository by an unlikely future volcanic event (BSC 2004a).

2. **Igneous Processes**—Igneous processes describe the physical phenomena that could occur during a potential future volcanic event (SNL 2007e; SNL 2007b; SNL 2007a; SNL 2007d; SNL 2008).

3. **Postigneous Processes**—Postigneous processes describe the effects of exposure of EBS components to magmatic temperatures and gases for the igneous intrusion modeling case (SNL 2007a, Section 6.4). For the volcanic eruption modeling case, post igneous processes describe the surficial phenomena of erosion and deposition that could occur when a contaminated tephra sheet covers a portion of the landscape and is redistributed following a potential future volcanic eruption through the repository (SNL 2007d).

2.3.11.2.1.1 Igneous Framework

Basaltic volcanism is the most common form of volcanism on earth and has occurred repeatedly throughout the western United States over the past 5 million years (Figure 2.3.11-2). Basaltic volcanoes, primarily in the form of scoria cones, generally develop in clusters of several, to several hundred volcanoes that define a volcanic field. In the western United States, the largest basaltic volcanic fields erupted approximately 100 to 300 cubic kilometers of lava, generally over periods of less than a few million years (Perry, Crowe et al. 1998). The larger volcanic fields tend to occur along the margins of major physiographic provinces, such as the Colorado Plateau and Great Basin. Smaller-volume volcanic fields of less than tens of cubic kilometers tend to occur within the interior of the Basin and Range Province, including the interior of the Great Basin where Yucca Mountain is located. Basaltic volcanism in the western United States is generally correlated with regions of extensional tectonics.

The earliest volcanism in the Yucca Mountain region was dominated by a major episode of caldera-forming silicic (rhyolitic) volcanism that occurred between 15 and 11 million years ago, forming the southwestern Nevada volcanic field (Sawyer et al. 1994). Silicic volcanism was approximately synchronous with a period of major crustal extension or stretching, which occurred between 13 and 9 million years ago (Sawyer et al. 1994, Figure 4). Volcanism in the Yucca

Mountain region peaked between 13 and 11 million years ago with the eruption of the rhyolitic units of the Paintbrush and Timber Mountain Groups (Sawyer et al. 1994, Table 1).

Around 11 million years ago, the character of volcanism changed from rhyolitic (silicic) to basaltic, and the volume of material erupted decreased dramatically compared to the final rhyolitic eruptions. Silicic volcanism has not occurred in the region in the last 7 or 8 million years and, as a result, is not included as part of the igneous conceptual model. Small-volume basaltic volcanism has continued into the Quaternary as part of the general decline in eruption volume over the past 11 million years in the Yucca Mountain region (Perry, Crowe et al. 1998, Chapter 2).

Figure 2.3.11-3 shows the distribution of Miocene through Quaternary basaltic volcanism in the Yucca Mountain region. Post-Miocene volcanism (younger than 5 million years) has occurred in six episodes, at approximately 4.6 (Thirsty Mountain), 3.8 (Southeast Crater Flat), 2.9 (Buckboard Mesa), 1.1 (Crater Flat), 0.35 (Hidden Cone and Little Black Peak), and 0.08 (Lathrop Wells) million years ago (Table 2.3.11-2). The recurrence interval between episodes is thus quite long, ranging between about 300,000 to 1.8 million years.

The total eruption volume of the post-Miocene basalts exposed at the surface in the region is about 5 km^3 (Table 2.3.11-2). The volumes of individual episodes have generally decreased through time, with the three Pliocene episodes having volumes of approximately 1 to 3 km^3 each and the three Quaternary episodes (2.9 Ma, 3.8 Ma and 4.6 Ma) having a combined volume of only about 0.5 km^3 (Table 2.3.11-2). Consistent with the PVHA (CRWMS M&O 1996, Section 3.2), the conceptual model for volcanism in the Yucca Mountain region emphasizes volcanic features characteristic of the Quaternary (the past ~2 Ma): small-volume basaltic volcanoes (< 0.1 km^3) consisting of a single main scoria cone surrounded by a small field of lava flows that extend to about 1 km from the scoria cone (BSC 2004a, Section 6.1.1.1).

The decreased eruptive volume through time, together with geochemical evidence (Perry, Crowe et al. 1998, p. 4-8), indicates that the intensity of mantle-melting processes beneath the Yucca Mountain region has waned over the past 5 million years (Perry and Crowe 1992, p. 2359; Perry, Crowe et al. 1998, p. 4-1). Considered in terms of total eruption volume, recurrence intervals, and duration of volcanism during the past 5 million years, the Crater Flat volcanic field, adjacent on the west to Yucca Mountain, is one of the least active basaltic volcanic fields in the western United States (BSC 2004a, Section 6.1.1.1).

In addition to surface exposures of basaltic volcanism, several magnetic anomalies in the Amargosa Desert identified in aeromagnetic surveys conducted in the late 1970s have characteristics that indicate the presence of buried basaltic volcanic centers (Langenheim et al. 1993, p. 1,840). One of these anomalies, Anomaly B (Langenheim et al. 1993, Figure 1a), was drilled in the early 1990s (Carr et al. 1995; BSC 2004a, Section 6.1.1.1) (Drill holes FF25-1 and FF5-1, Figure 2.3.11-3). Basalt cuttings from the drill hole were dated at 3.85 million years using the $^{40}Ar/^{39}Ar$ method (Perry, Crowe et al. 1998, Table 2.B). An aeromagnetic survey conducted by the U.S. Geological Survey in 1999 (O'Leary et al. 2002) suggested the possibility of additional buried volcanic centers in the Amargosa Desert.

A high-resolution aeromagnetic survey of Crater Flat, Yucca Mountain, Jackass Flats, and the northern part of the Amargosa Desert was conducted in 2004 that was designed to optimize

detection of buried basalt or basalt intrusions. The results of the aeromagnetic survey were used to design a drilling program to identify the sources of magnetic anomalies (Perry, Cogbill et al. 2005). Seven drill holes were completed. The youngest basalt encountered by drilling (drill hole VA-2) was dated at 3.9 million years old (Table 2.3.11-3) and is located in the northern Amargosa Desert (Figure 2.3.11-3). Three other basalt units encountered by drilling ranged in age from approximately 9.5 million years to 11.2 million years (Table 2.3.11-3). Major-element, trace-element and isotopic data were obtained from the buried basalt bodies and indicate that all are broadly basaltic in composition with typical SiO_2 contents of 42-50%. These geochemical results are consistent with geochemical analyses of basalt samples from surface exposures near Yucca Mountain (Perry and Bowker 1998). Three other drill holes did not encounter basalt and demonstrated that not all magnetic anomalies are due to buried basalt (Perry, Cogbill et al. 2005). The results of the aeromagnetic survey and drilling program indicate that the essential characteristics of the age, geochemistry, and location of basaltic volcanism near Yucca Mountain were fundamentally understood when the PVHA was completed in 1996. No basalt encountered in the recent drilling had an unexpectedly young age (Table 2.3.11-3), nor was post-Miocene basalt encountered to the east of Yucca Mountain in Jackass Flats. Both results are consistent with the understanding of the spatial distribution of basalt derived from surface exposures (Figure 2.3.11-3).

Post-Miocene volcanoes of different ages in the Yucca Mountain region are spatially clustered, as shown in Figure 2.3.11-3 (Perry, Crowe et al. 1998, Figures 3.10, 3.11, and 3.12; Connor and Hill 1995, Figures 1 and 2). Clustering of volcanism is important to probability models because it indicates spatial control on location of past volcanism that may influence the location of future volcanism. The most significant clustering of post-Miocene volcanism occurs in the Crater Flat structural domain (hereinafter referred to as the Crater Flat domain) both in terms of number of episodes (3 of 6 post-Miocene episodes) and proximity to Yucca Mountain. Two of the three episodes of Quaternary volcanism, including the youngest episode at Lathrop Wells, occur within the Crater Flat domain (Figure 2.3.11-3).

The structural and geophysical features of the domain and the extent to which they influence the location of volcanism within the domain have been key factors in conceptual models of volcanism. The conceptual models provide the geologic framework for assessing hazards to the repository (CRWMS M&O 1996, Section 3.1; Smith et al. 1990, pp. 83 and 84; Connor and Hill 1995, p. 10122; Fridrich et al. 1999, pp. 197 to 212).

Structural data indicate that the southwestern part of the Crater Flat domain is more extended than the northeastern part of the domain (Fridrich 1999, p. 177; Fridrich et al. 1999, Figure 2B). Post-Miocene basaltic centers of the Crater Flat domain lie within the extended southwestern part of the domain, as shown in Figure 2.3.11-4. The youngest volcano in the Crater Flat domain, the 80,000-year-old Lathrop Wells volcano, lies within the most active area of late Quaternary faulting in the Crater Flat domain (Fridrich et al. 1999, p. 211). Thus, the Crater Flat volcanoes, including Lathrop Wells volcano, show that close spatial and temporal relationships exist between areas of extension and volcanism throughout the Crater Flat domain (Fridrich et al. 1999, p. 211). The occurrence of three episodes of post-Miocene volcanism in the more extended part of the Crater Flat domain suggests future volcanism is more likely to occur in southwestern Crater Flat and less likely to occur at Yucca Mountain, which lies outside of the more extended part of the Crater Flat domain (BSC 2004a, Section 6.1.1.1). A thin, discontinuous basalt dike is exposed intermittently along the Solitario Canyon fault and along a northwest striking fault that intersects the Solitario Canyon fault

(Day et al. 1998). The dike has been dated at about 10.4 Ma (Perry, Crowe et al. 1998 page 2-16). Significantly, no post-Miocene igneous features have been identified within the repository block (Figure 2.3-11-3; Perry, Crowe et al. 1998, Figures 2-4 and 2-5). PVHA experts generally recognized the close association between volcanism and areas of maximum extension in the Yucca Mountain region (CRWMS M&O 1996, Appendix E, pp. RC-5, BC-12, AM-5, MS-2, and GT-2). Subsequent geologic and geophysical studies provide corroborative evidence that areas of maximum extension in the Crater Flat domain correspond closely to volcanic source zones defined in the PVHA and shown in Figure 2.3.11-4 (Stamatakos et al. 1997, p. 319; Brocher et al. 1998, pp. 947 to 971; Fridrich et al. 1999, p. 210). The volcanic source zones defined in the PVHA are also consistent with the latest aeromagnetic survey and drilling program (Perry, Cogbill et al. 2005), which indicate that no post-Miocene basaltic volcanoes are present to the east of Yucca Mountain.

2.3.11.2.1.2 Igneous Processes

The onset of a volcanic event in the Yucca Mountain region begins with ascent of magma from the mantle source as a dike or dike set (swarm) that follows a crack created ahead of the ascending magma. During magma ascent and decompression, volatile gases such as H_2O and CO_2 are released, increasing the volume of the magma. This resulting volume expansion drives the basaltic magma upward through the upper few kilometers of the earth's crust. Based on analogue studies, the concentration of water in basalts of the Yucca Mountain region ranges from 1 to about 4.6 wt % (SNL 2007e, Section 6.3.2.2; Nicholis and Rutherford 2004, p. 490). This range might reflect the low degree of partial melting of a hydrous lithospheric mantle source (BSC 2004a, Section 6.1.1.2) represented by the basalts in the Yucca Mountain region.

Based on analogue studies in the Yucca Mountain region, dikes typically range in width from 1 m to about 12 m (SNL 2007e, Section 6.3.3.1), with lengths ranging from less than 500 m to about 6 km (SNL 2007e, Section 6.3.3.1). Field observations at eroded analogue volcanoes in the Yucca Mountain region suggest that the appropriate range for the number of dikes in swarms associated with a monogenetic volcano is 1 to 5 (SNL 2007e, Section 6.3.3.1). Based on observations of Miocene dikes and Pliocene-Pleistocene volcanoes in the region, dikes typically occupy preexisting normal faults and therefore may have the same orientations as the faults, although it is also possible for a potential dike to be oriented perpendicular to the current least compressive principal stress, or about N30°E (SNL 2007e, Section 6.3.3.1).

The process described here, and schematically shown in Figure 2.3.11-5, assumes that a dike propagates through the repository (SNL 2007a, Section 6.3). As the dike approaches the level of the drifts, the crack tip advances ahead of the magma front. When the magma within the dike reaches the level of the repository, magma is available to flow into drifts. The observed record of basaltic volcanism in the Yucca Mountain region during the last 10 million years indicates that volcanic centers have been constructed of both effusive and pyroclastic deposits (SNL 2007e, Section 6.3.1). Hence, two end-member possibilities exist for the behavior of the magma as it approaches the drifts. The first end-member possibility is that the magma steadily releases gas into the host rock as it approaches the drifts so that a relatively gas-poor magma flows effusively into the drifts. The second end-member possibility is that the initial magma encountering the drifts is gas-rich, resulting in pyroclastic flow into the drifts. In either case, the dike tip precedes the magma by several seconds to a few hours. For example, during the 1943 eruption of the Parícutin volcano in Mexico, the initial crack broke the surface several hours before the first manifestation of weak pyroclastic eruptions

began. This is one of the best documented historic eruptions of a new volcano and offers a basis for comparing some aspects of model results (SNL 2007a, Section 7.3.1.1.1).

The rate and degree to which an intersected emplacement drift fills with magma depends on variables such as magma rise rate, magma viscosity, and the nature (effusive or pyroclastic) of the flow into the emplacement drifts. A typical set of magma parameters includes magma far-field velocity ranging between 1 and 15 m/s (SNL 2007a, Table 6-2) and minimum (liquidus) viscosities ranging between 10 and 40 Pa·s for magma (SNL 2007a, Table 6-2).

The potential ascent of dikes and the formation of conduits at Yucca Mountain have been analyzed relative to the configuration of the repository, which consists of approximately 100 emplacement drifts of 5.5 m diameter, spaced 81 m apart (SNL 2007f; Section 1.3.1), and connected to larger diameter access and ventilation drifts. The number of emplacement drifts into which magma could be introduced depends on the orientation of a dike system intersecting the repository, the number of dikes in a dike swarm (more than one subparallel dike of the same age), and the lengths of the dikes lying within the repository footprint.

Formation of a volcano often begins with a fissure eruption as a dike or dike swarm intersects the surface. If there is more than one dike (a dike swarm), the thickest dike, also referred to as the "master" dike, is the most likely to feed the eruptions. The total eruption durations typically range from several months to a few years (some historical scoria cone eruptions have exceeded 10 years in duration). Eruption activity typically includes effusion of gas-poor lava flows and highly energetic, gas-rich pyroclastic eruptions. Both types of eruptions can occur simultaneously or in alternating cycles that include periods of inactivity (SNL 2007e, Section 6.4). Analogue studies of shallowly eroded volcanoes in the Yucca Mountain region demonstrate that subsurface intrusive processes may include the formation of multiple dikes and sills (horizontal emplacement of magma into the host rock). Figure 2.3.11-6 shows a schematic of a basaltic dike set and eruptive equivalents at Basalt Ridge East, located approximately 60 km north of Yucca Mountain. Development of a volcano can also include the establishment of small satellite eruptive vents (boccas) during the period of eruption (SNL 2007e, Appendix F).

As the fissure eruption rapidly localizes to one or more conduits along the master dike, the conduit(s) becomes the primary magma transport mechanism for the remainder of the eruption. Conduit formation also provides a potential mechanism to transport waste to the surface. The physical processes that influence the exact location of a conduit within the repository are complex, and natural analogue data suggest that a conduit can form anywhere along a dike. The location of a conduit along a dike is assumed to have a uniform distribution (SNL 2007e, Table 7-1), and the number of conduits that might form ranges between one and three, but is heavily weighted toward development of a single conduit based upon data from analogue Quaternary volcanoes in the region (SNL 2007e, Section 6.3.3.3 and Appendices C to F). Based on analogue information, if multiple conduits form along a dike, they have a spacing between about 500 m and 2 km (SNL 2007e, Section 6.3.3.3). Conduits widen within the uppermost tens of meters of the earth's surface, and become narrower with depth. Based upon data from analogue sites, conduit diameters at repository depth range from a few meters (i.e., the width of the host dike) to a mean value of 15 m and a 95th percentile value of 21 m (SNL 2007e, Section 6.3.3.3 and Appendix F).

After the eruption is localized into one or more conduits, the characteristics of the eruption may change from relatively low energy bursts of large gas bubbles with ballistic ejection of coarse magma clots and fragments (Strombolian) to more energetic eruptions that include gas jets and tephra resulting in a sustained tephra column (violent Strombolian) in the atmosphere (Figure 2.3.11-5). The change in eruptive style can result from evolving magma composition (e.g., volatile content), constriction of the conduit, and changes in the ascent rate and the volumetric flux of magmatic material being ejected. The larger-sized fraction of the total ejected material falls to the ground surface near the vent and forms scoria cone(s). The finer material (ash and fine lapilli) will be dispersed downwind (SNL 2007e, Section 6.3.5).

The material forming the violent Strombolian eruption column and plume is dispersed laterally by the prevailing winds. Atmospheric dispersal and deposition of the tephra forms a sheet-like deposit characterized by decreasing thickness and grain size with distance from the volcano. Tephra deposits might extend 10 km or more from the volcano and cover several hundred square kilometers (SNL 2007e, Appendix C). In the TSPA, only violent Strombolian activity is modeled to produce atmospheric dispersal, because other, less violent volcanic activity would result in deposition of lava and cone-forming materials but would not result in greater atmospheric dispersal.

Lathrop Wells volcano, considered the best analogue for a possible future eruption at Yucca Mountain, is one of eight small-volume (about 0.004 to 0.12 km^3) basaltic volcanoes that formed during the Quaternary within 50 km of Yucca Mountain (Figure 2.3.11-3) (SNL 2007e, Section 6.3.1). Based on observations of preserved eruptive deposits, these basaltic volcanoes share a similar eruptive history of pyroclastic activity that led to the formation of a main scoria cone and tephra sheet, and effusive activity that produced the compound lava flow fields composed of many small lava flows (SNL 2007e, Appendices C to E). The scoria cone and lava flow deposits, excluding tephra fall from violent eruptions, typically cover a few square kilometers. Based on geologic studies of these deposits, as well as analogue historic basaltic volcanoes, a future eruption that could potentially disrupt the repository is expected to have eruptive processes similar to those recorded in deposits at the Lathrop Wells volcano and analogue volcanoes in Crater Flat (SNL 2007e, Appendices C to E).

Both the igneous intrusion modeling case and the eruption modeling case examined the disruption of waste packages in the emplacement drifts. For the igneous intrusion modeling case, once intersection of the repository footprint occurs, all drifts are assumed to be inundated with magma and all waste packages damaged (SNL 2007b, Section 5.1). For the eruption modeling case, the number of packages disrupted depends on the number of conduits within the repository footprint, their diameters, and the portions of drifts that are intersected by conduits (SNL 2007b, Section 6.3.2.2). Relevant eruptive features, processes, and characteristics of igneous material are described in greater detail in *Characterize Eruptive Processes at Yucca Mountain, Nevada* (SNL 2007e, Sections 6.3 and 6.4), as well as in Section 2.3.11.4.

2.3.11.2.1.3 Postigneous Processes

For the igneous intrusion modeling case, if magma were to enter a drift, processes after intrusion related to cooling and solidification of magma become relevant (Figure 2.3.11-5). Cooling of the magma results in transfer of heat and gases to the surrounding rock. After cooling is complete,

seepage of ground water into drifts is assumed to be re-established. Sections 2.3.11.3.2.8 and 2.3.11.3.2.9 provide additional discussion of the postcooling environment.

For the eruption modeling case, after the deposition of a tephra sheet from a violent Strombolian eruption, the tephra is subject to redistribution by normal sedimentary processes (erosion and deposition) (Section 2.3.11.4.2). A hypothetical violent Strombolian eruption through the repository would disperse tephra downwind, most likely to the northeast, blanketing part of the Fortymile Wash drainage system (SNL 2007d, Figure 8-1; SNL 2007g, Figure 6.3.3-9) and less likely to the RMEI location. The tephra redistribution conceptual model (Section 2.3.11.4.2.3) applies a set of parameters that captures the effects of erosion of the initial deposit, mixing during transport, and the eventual redeposition at the RMEI location (Section 2.3.11.4.2.3). The outputs of this model are treated as an abstraction for the TSPA model (SNL 2007g, Section 8.1.1).

2.3.11.2.2 Probability of an Igneous Event Intersecting the Repository Footprint

[NUREG-1804, Section 2.2.1.2.2.3: AC 1(2), AC 3(1), AC 4(1), AC 5(1), Section 2.2.1.3.10.3: AC 2(4), 3(3)]

This section summarizes detailed information provided in Section 2.2.2.2 and addresses the requirements of proposed 10 CFR 63.114(a)(4) (70 FR 53313) that the analysis of repository performance considers volcanic events that have at least one chance in 10,000 of occurring over 10,000 years. The probability of intersection of the repository footprint by a volcanic event depends on the recurrence rate of volcanic events multiplied by the likelihood of a volcanic event intersecting the repository (CRWMS M&O 1996, Section 3.1.1). Because volcanic events have occurred very infrequently in the Yucca Mountain region during the past 5 million years (on average every few hundred thousand years), recurrence rates for volcanic events are proportionally low (10^{-5} to 10^{-6} events per year). The low recurrence rate of volcanism in the Yucca Mountain region is the primary reason that the annual probability of intersection with the repository footprint is extremely low, with a mean of 1.7×10^{-8} (BSC 2004a, Table 7-1) intersections per year, or approximately one chance in 6,000 for the 10,000 years after closure of the repository.

2.3.11.2.2.1 Definition of Event

An important consideration in the PVHA is the definition of a volcanic event. The PVHA experts defined a volcanic event to be a spatially and temporally distinct batch of magma ascending from the mantle through the crust as a dike or system of dikes (BSC 2004a, Sections 1 and 6.1). The physical manifestations of a volcanic event include the dike or dike system and any surface eruption deposits, as shown schematically in Figure 2.3.11-5. For the purposes of probability models developed in the PVHA, a volcanic event is defined as a point (x, y) in space representing the expected midpoint of the dike system involved in the magma ascent. The dike system associated with the volcanic event is represented in probability models by a line element defined in terms of a length, azimuth, and location relative to the point event (Figure 2.3.11-7). Dike length (used in the PVHA and in subsequent analyses to assess consequences from volcanic events) refers to the total length of the dike system associated with the volcanic event. Intersection of the repository footprint by a dike refers to intersection of the repository by the line element representing the dike system associated with the volcanic event.

2.3.11.2.2.2 Process Used for Probabilistic Volcanic Hazard Analysis

The probability of future igneous activity in the region used in the TSPA is based on an expert elicitation (PVHA) conducted by the DOE in 1995 and 1996 (CRWMS M&O 1996). An expert panel was convened to review pertinent data relating to volcanism at Yucca Mountain and to quantify, based on these data, both the annual probability and associated uncertainty of a volcanic event intersecting the repository footprint. Comprehensive data collected over two decades to understand the temporal and spatial characteristics of basaltic volcanism of the Yucca Mountain region provided the primary input to the expert elicitation (CRWMS M&O 1996), as described in *Characterize Framework for Igneous Activity at Yucca Mountain, Nevada* (BSC 2004a, Section 6.3.1.3). The PVHA was conducted consistent with guidance developed by the Senior Seismic Hazard Assessment Committee and later described in NUREG/CR-6372 (Budnitz et al. 1997). The manner in which the PVHA was conducted is also consistent with U.S. Nuclear Regulatory Commission (NRC) guidance for conducting expert elicitation that was later issued as NUREG-1563 (Kotra et al. 1996). The PVHA process is described in detail in Section 2.2.2.2 and Section 5.4.1.

The sparse eruptive history of Pliocene and Quaternary volcanic activity in the Yucca Mountain region permits consideration of multiple alternative assessments of future volcanic activity. To ensure that a wide range of alternative assessments and the associated uncertainties were considered in the PVHA, individual judgments were elicited from 10 members of an expert panel using a formal expert elicitation process. The judgments of the expert panel members were subsequently combined with equal weight to produce a probability distribution of the annual frequency of intersection of a basaltic dike with the repository footprint. The results of the PVHA constitute a set of alternative models for assessing the volcanic hazard at the repository, the probability of each model being an appropriate model, and probability distributions for the parameters of the models (BSC 2004a, Sections 6.3.1.5 and 6.3.1.6). Additional description of the PVHA process is provided in Section 2.2.2.2 and Section 5.4.1.

2.3.11.2.2.3 Probability of Future Igneous Intersection of the Repository

The mean annual frequency of intersection of the repository footprint by a dike calculated during the PVHA is 1.5×10^{-8} (CRWMS M&O 1996, Section 4.2). Figure 2.3.11-8a shows the computed distributions for the frequency of intersection aggregated over the 10 PVHA expert interpretations, together with the median and mean values obtained for each expert interpretation. Figure 2.3.11-8b compares the 5th to 95th percentile range for frequency of intersection obtained for each expert interpretation with that for the aggregate distributions. The value for the mean annual frequency of intersection increased slightly to 1.7×10^{-8} when recalculated for the repository footprint that was implemented in 2003 (BSC 2003; BSC 2004a, Section 6.5.1.1 and Table 7-1). The 5th and 95th percentiles of the uncertainty distribution for the recalculated annual frequency of intersection are 7.4×10^{-10} and 5.5×10^{-8} (Figure 2.3.11-8a) (BSC 2004a, Table 7-1). Changes in the mean annual frequency of intersection due to changes in repository layout between 1996 and 2003 indicate that any differences in the repository footprint between the design in effect in 2003 (BSC 2003) and the current design would have negligible effects on the estimate of the frequency of intersection. For example, the north-south lengths of the repository design in effect during the PVHA and in 2003 (BSC 2003) differ by about 1,500 m, resulting in an increase in the intersection frequency of about 13% (BSC 2004a, Section 6.5.2.1). Comparison of the north-south dimensions

of the repository design in effect in 2003 (BSC 2003) and the current design (BSC 2007e, Figure 1) show that the differences are negligible, and the differences are expected to have negligible effects on the frequency of intersection.

The major cause of the uncertainty in the estimates of the frequency of repository intersection is the statistical uncertainty in estimating volcanic event rates (CRWMS M&O 1996, Section 4.2 and Figure 4-33). The second largest cause of uncertainty is modeling the spatial distribution of future events. Although differences exist among the interpretations of the 10 experts, most of the uncertainty in the computed frequency of intersection is due to the average uncertainty that an individual expert expressed in developing his PVHA model (CRWMS M&O 1996, Section 4.3).

2.3.11.2.2.4 Probability Model Support

An objective of the PVHA (CRWMS M&O 1996) was to explicitly characterize the uncertainties associated with the assessment of the probability of disruption of the repository by a volcanic event. The PVHA was conducted in conformance with the methodology developed by the Senior Seismic Hazard Analysis Committee and later described in NUREG/CR-6372 (Budnitz et al. 1997). The process was also consistent with available NRC guidance on the use of expert elicitation that was later issued as NUREG-1563 (Kotra et al. 1996).

2.3.11.2.2.5 Geologic Basis for the Probabilistic Volcanic Hazard Analysis

The PVHA (CRWMS M&O 1996, Section 3.2) combined multiple alternative conceptual models into a single distribution that captured the uncertainty in the expert conceptual models of the physical behavior of volcanism in the Yucca Mountain region. A conceptual framework of igneous activity in the Yucca Mountain region was developed that is consistent with the igneous and tectonic history of this region and the assessment of this history by members of the expert panel for the PVHA (CRWMS M&O 1996, Section 3.2). For regional volcanism, no single base-case conceptual model is appropriate because the underlying physical processes that control the precise timing and location of volcanic events within a particular region remain uncertain (BSC 2004a, Section 6.3.1.6).

Analyses of magmatic processes in the Yucca Mountain region generally indicate that the magnitude of mantle melting has significantly decreased since the middle Miocene. The information also suggests that melts in the past few million years were generated within relatively cool ancient lithospheric mantle (compared to asthenospheric mantle), which is a factor that may contribute to the relatively small, and decreasing, volume of basaltic melt erupted in the Yucca Mountain region since the Miocene (BSC 2004a, Section 6.3.3).

On a more local and shallow crustal scale, the occurrence of volcanism in the Yucca Mountain region is correlated with zones of past or present crustal extension such that once dikes feeding volcanoes enter the shallow upper crust, their locations and orientations are influenced by the orientation of the local stress field (BSC 2004a, Section 6.2) and the presence of faults that may locally control vent location and dike orientation (SNL 2007e, Section 6.3.3.1). Evidence supporting these two conclusions includes several northeast-oriented vent alignments in the Yucca Mountain region and the association of eruptive centers with known or inferred faults with north-south orientations (BSC 2004a, Section 6.3.3; SNL 2007e, Section 6.3.3.1).

The Quaternary volcanoes in the Crater Flat basin and their proximity to Yucca Mountain result in the Crater Flat cluster playing a major role in assessing the potential for future volcanism at Yucca Mountain. Research on the Crater Flat structural domain, published largely since the PVHA (CRWMS M&O 1996) was conducted (Fridrich 1999, Figure 2B), provides evidence that the northeastern and southwestern portions of the basin have different extensional histories that may have influenced the location of basaltic volcanism within the basin (BSC 2004a, Section 6.4). These data and conclusions are consistent with the PVHA expert's assessments concerning the location of potential future volcanism, as discussed below.

The correlation between the more structurally active portion of the Crater Flat basin and sites of volcanism within Crater Flat basin indicated to the PVHA experts that Yucca Mountain is near, but not within, a local source zone that may produce small volume eruptions in the future (BSC 2004a, Section 6.4.2). Source zones were defined by the PVHA experts based largely on the location of past volcanic events. The source zones also correspond to the areas of highest cumulative extension and most active faulting in the Crater Flat basin (Fridrich et al. 1999, Figures 5 and 6), an association recognized by several of the PVHA experts. In cases in which local zones were defined, the zones were restricted to the southwestern part of the Crater Flat basin or defined as elongated, northwest-trending belts that included the southwestern part of the basin and stretched to the Sleeping Butte area, northwest of Crater Flat. The local zones excluded the northeastern part of the Crater Flat structural domain where the repository is located. Based on structural features and the past patterns of the close association of volcanism and extension, the eastern boundaries of local volcanic source zones defined in the PVHA separate more extended and less extended portions of the Crater Flat basin and therefore are reasonable assessments of the eastern extent of volcanism expected in the future (BSC 2004a, Section 6.4.2). Given that the locus of post-Miocene volcanism in the Crater Flat basin lies in the south and southwestern portion of the basin, volcanic source zones defined in the PVHA and centered in southwestern Crater Flat are consistent with the volcanic and tectonic history of the Crater Flat structural domain (BSC 2004a, Section 6.4.2).

2.3.11.2.2.6 Alternative Estimates of the Intersection Probability

Published estimates of the probability of a volcanic event intersecting the repository footprint are summarized in Table 2.3.11-4, including the mean intersection probability estimated in the PVHA. These values cluster at slightly greater than 10^{-8} per year, providing confidence that the probability estimate is robust. This confidence is warranted given the range of alternative temporal and spatial models and event geometries considered in the probability calculations (BSC 2004a, Section 6.3.1.8).

In the various estimates of the intersection probability developed between 1982 and 2000, volcanic events in hazard calculations were represented as both points and lines, as shown in Table 2.3.11-4. For point events, volcanic source zone areas or the repository area are adjusted to account for the fact that volcanic events have dimension due to the length of associated dikes. The shorter the dike length, the more comparable the intersection probability results are to calculations representing volcanic events as points. Probabilities near 10^{-7} intersections per year reflect unusually small volcanic source zone areas or unusually long vent alignments or dike lengths (BSC 2004a, Section 6.3.1.8).

Estimates of the intersection probability have also been performed to assess the sensitivity of the intersection probability to the presence of postulated buried volcanoes (Brocoum 1997; CRWMS M&O 1998; BSC 2004a, Section 6.5.4). The studies showed that the effects of postulated buried centers on the hazard estimate are not significant. *Characterize Framework for Igneous Activity at Yucca Mountain, Nevada* (BSC 2004a, Section 6.5.4) considered the effect of buried anomalies from a 1999 aeromagnetic survey (Blakely et al. 2000; O'Leary et al. 2002) that might represent buried volcanic centers. The assessment considered the likelihood that anomalies (or groups of anomalies) represent buried volcanic centers. These considerations resulted in an increase in the mean annual hazard estimate of approximately 22%, to about 1.9×10^{-8}. A related assessment examined the effect of assuming that all anomalies represented buried volcanic centers, and this assessment resulted in an increase in the mean annual hazard of about 40%, to about 2.2×10^{-8}. Aeromagnetic survey and drilling program results from 2004-2006 (Perry, Cogbill et al. 2005) indicate that these sensitivity studies overestimated the number of buried basaltic centers and therefore are not appropriate to use as alternative models to estimate the frequency of intersection of the repository footprint.

2.3.11.2.3 Model Integration

[NUREG-1804, Section 2.2.1.2.2.3: AC 1(1), (2)]

The igneous scenario class comprises two separate modeling cases: the intrusion case and the volcanic eruption case. The potential consequences of a basaltic dike (magma-filled fracture that propagates upward through the earth crust) intersecting the repository are addressed through a suite of integrated models and supporting analyses in the igneous intrusion modeling case (Section 2.3.11.3). This model case addresses both intrusion processes and processes after intrusion and their potential impacts on repository performance. The process and potential consequences of a basaltic eruption (volcano) through the repository and the effects after an eruption are addressed in the volcanic eruption modeling case (Section 2.3.11.4). Figure 2.3.11-1 shows the integration of the intrusion and eruption modeling cases that support the TSPA model.

The model cases described in the following sections (Sections 2.3.11.3 and 2.3.11.4) provide the following information:

- Model description
- Conceptual model
- Model and analysis descriptions and results
- Data uncertainty and treatment of uncertainty
- Model uncertainty, including alternative models and approaches
- Model abstractions.

2.3.11.3 Igneous Intrusion Modeling Case

[NUREG-1804, Section 2.2.1.3.2.3: AC 1(1) to (5), (7), AC 2; AC 3(1) to (3), AC 4, AC 5, Section 2.2.1.3.3.3: AC 1(1) to (8), AC 2(1), (2), (4), AC 3 (1) to (4), AC 4(1) to (4), AC 5, Section 2.2.1.3.10.3: AC 1, AC 2(1) to (3), AC 3(1), (2), AC 4, AC 5]

Representative data from the site and surrounding region form the basis to describe and model potential disruption of the repository by an unlikely future igneous event. Effects on the analyses of uncertainties and variabilities in parameter values have been considered, and alternative conceptual

models have been used in the analyses. FEPs identified in Table 2.3.11-1 have been included in the analyses. Specific processes of degradation, deterioration, and alteration that would affect waste forms exposed to basaltic magma have been included in the analyses and propagated into parameters provided to the TSPA. The technical bases have been provided for the process models used to develop abstractions for the TSPA.

The igneous intrusion modeling case represents a potential basaltic dike intersecting the repository without surface eruption within the repository boundary, the postintrusion effects from heat, potential impacts on EBS features, and changes in water chemistry following reaction with cooled basalt. As noted earlier, the event definition for PVHA (CRWMS M&O 1996) was limited to intersection of the repository by an igneous dike (CRWMS M&O 1996, Section 1.1). The principal physical processes that are modeled in this case are:

- Ascent of a basaltic dike, intersection of the dike within the repository, and the flow of magma into the drifts

- Effects after intrusion associated with heat and changes in water chemistry.

These processes provide both direct and indirect inputs to the TSPA model, as well as contribute to the understanding of the effects of the presence of a repository on dike localization and ascent. TSPA requires three parameters derived from the model and analyses developed in the igneous intrusion modeling case:

- **Number of waste packages compromised during an igneous intrusion**—All waste packages in the repository are assumed to be compromised if there is an intersection of a dike with any repository drift, including access drifts (SNL 2007b, Section 5.1).

- **Temperature of emplacement drifts as a function of time following intrusion**—This parameter provides the thermal history after a potential basaltic intrusion. This history presents the centerline and perimeter temperatures in the magma-filled drifts and adjacent drifts as functions of time. Emplacement drift temperatures are used to determine when seepage of water into the drifts is reestablished. This parameter is developed in a model that represents heat flow between drifts and magma cooling (SNL 2007a, Section 6.4.6). Development of this parameter is described in Section 2.3.11.3.2.8.

- **pH and ionic strength of basalt-equilibrated percolation as functions of time**—These parameters provide the basis for the model of influx-water chemistry for the igneous intrusion modeling case. Percolation water chemistry affects the mobilities of the radionuclide species. The pH and ionic strength parameters reflect the compositions of the fluids within or leaving breached waste packages during the postintrusion phase of the igneous intrusion modeling case (SNL 2007c, Section 6.6.2[a]).

The models and analyses that make up the igneous intrusion modeling case have addressed a range of potential conditions associated with igneous intrusion. In situations where the analyses cannot reach definitive conclusions as a result of epistemic (state of knowledge) and aleatoric (random variability in a parameter or process) uncertainties, bounding conditions are adopted.

2.3.11.3.1 Conceptual Model

[NUREG-1804, Section 2.2.1.3.2.3: AC 1(2); Section 2.2.1.3.3.3: AC 1(1), (2), (4), (6), (8)]

The igneous intrusion conceptual model considers that a dike rises from a deep (mantle) magma source through the lithosphere and intersects the repository. This dike is depicted as a vertical sheet of magma rising and driving a crack ahead of it. As the dike reaches the level of the repository, magma flows into intersected drifts, fills them, and then continues flowing into adjacent drifts until all repository drifts are filled with magma (Table 2.3.11-1, FEP 1.2.04.03.0A, Igneous intrusion into repository). Waste packages in the filled drifts are heated to near-magmatic temperatures. Strength and stability of the contacted waste packages are affected (Table 2.3.11-1, FEP 1.2.04.04.0A, Igneous intrusion interacts with EBS components). Once the drifts return to temperatures less than the boiling point of water, seepage of water into drifts is restored and percolation of water through cooled basalt provides a mechanism for radionuclide release and transport (Table 2.3.11-1, FEP 1.2.04.04.0B, Chemical effects of magma and magnetic volatiles). The cooled magma (basalt) in the drift offers no additional resistance to flow beyond that of the surrounding host rock.

A dike is similar to a hydraulic fracture, pushed upward from a high-pressure source of magma deep in the earth and by the buoyancy of the magma column compared to the surrounding rocks. The magma at depth forces the propagating fracture to open as the magma rises. This mechanism typically results in dikes with thicknesses of several meters (SNL 2007e, Section 6.3.3.1), near-surface lengths of kilometers, and depths extending to tens of kilometers. Most dikes have a short surface expressions relative to their vertical extents. As the magma ascends to the surface within the dike, the magma is preceded by the dike tip, which is a gas- and vapor-filled crack. The dike tip or crack tip, shown in Figure 2.3.11-9, represents the propagating fracture that precedes the ascending magma at some distance that depends on the properties of the magma and the surrounding rock. Field studies at eroded analogues indicate that in detail, dikes that ascend vertically from depth are typically diverted into steeply dipping normal faults within a few hundred meters of the surface (SNL 2007e, Section 6.3.1). Analyses that constrain the conditions (e.g., overburden pressure, magma pressure, fault orientation) that are required for dikes to be "captured" by preexisting faults are described in *Dike/Drift Interactions* (SNL 2007a, Section 6.3.4). For modeling purposes, the host rock is treated as a homogeneous, isotropic medium (SNL 2007a, Section 6.3.2) in spite of layering and other inhomogeneities in the rock.

Magma is a mixture of silicate melt, with or without crystals (phenocrysts and xenocrysts), and volatiles (present as dissolved constituents in the melt or as exsolved vapor bubbles in the melt). The viscosity and volatile content of the magma play a fundamental role in the intrusion and eruption style (SNL 2007e, Section 6.3.3). Magma viscosity is primarily influenced by melt composition, as represented by magma oxide chemistry (SNL 2007e, Section 6.3.2.1) and volatile constituents (SNL 2007e, Section 6.3.2.2), and by temperature, crystal, and bubble content (SNL 2007e, Section 6.3.2.4). Compared with silicic magma, basaltic magma is relatively fluid (lower viscosity) in its single phase state.

If a dike intersects a drift, analyses show that basaltic magma could fill the drift in less than 30 minutes if the magma viscosity is near its liquidus value (SNL 2007a, Section 6.3.3.5.6). This process is shown schematically in Figure 2.3.11-5. The magma enters the intersected drifts at temperatures ranging from about 1,046°C to 1,169°C (SNL 2007e, Table 7-1), and due to the low

thermal conductivity of the rocks at the repository horizon, heat loss from inflowing magma would be minimal. The waste package temperatures would increase to near-magmatic temperatures, and the waste packages would begin to lose their strength (SNL 2007a, Section 6.4.8.3.1), resulting in plastic deformation of the waste packages within days. The intruding magma also heats the surrounding host rock (SNL 2007a, Appendix D, Section D1) interrupting percolation and causing the host rock to dry. For TSPA, once a single drift is intersected by a dike, magma is modeled to fill all drifts, and the waste packages are assumed to fail upon contact with magma (SNL 2007a, Sections 6.4.8.3.1). The final configuration is not estimated, but the amount of deformation is limited by the type 304B4 stainless steel fuel basket and the type 316L fuel bundle spacers. Simulations of the postintrusion waste package degradation with the influx of water and atmospheric gases are based on the premise that the interior of the waste package is open and that all of the components are exposed to water that has seeped into the drift (SNL 2007c). In the intrusive scenario for the in-package chemistry simulations, the influent water chemistry is changed to be consistent with water that has reacted with basalt (SNL 2007c, Section 6.3.1.3.5[a]).

Modeling results show that approximately 100 years after intrusion, drift centerline temperatures return to near the temperature before intrusion (SNL 2007a, Tables 6-13, 7-9, and 7-10). As the magma continues to solidify and cools below the boiling point of water, movement of groundwater through the basalt and adjacent host rock is reestablished as joints form in the cooling basalt and seepage returns. The chemistry of water that has reacted with the host tuff(s) is presented in a series of results that show water-rock interactions as functions of time of seepage occurrence and temperature of the rock (SNL 2007h, Sections 6.13.1 and 6.13.2).

The chemistry of the seepage water entering and passing through the basalt filled drifts is changed by chemical reactions between basalt and the percolating water. Data on groundwaters in basalt from analogue sites indicate that the altered percolation water in the basalts studied had mean pH values ranging from 6.05 to 8.12 with an average of the means of 7.29. Similarly, the mean ionic strength values ranged from 0.00029 moles/kg to 0.0959 moles/kg with an average of the means of 0.0021 moles/kg (SNL 2007a, Section 6.6.7). The stability of waste forms and the dissolution of radionuclides in the water are affected by water chemistry, and results of studies of in-package chemistry show that the chemistry of in-package solutions is buffered such that the chemistry of the influent water has little effect on the pH and ionic strength of the exfluent water (SNL 2007c, Section 6.6.2[a]) (e.g., all of the waters considered in the *In-Package Chemistry Abstraction* end up with nearly the same pH and ionic strength as they exit the waste package (SNL 2007c, Figures 6-14[a] and 6-20[a])). Radionuclide release could then occur as water percolates through the basaltic mass and contacts radionuclides after the intrusion cools. The same transport mechanisms would be active as in the nominal case (i.e., advective transport of dissolved species and colloids).

2.3.11.3.2 Model and Analysis Descriptions

[NUREG-1804, Section 2.2.1.3.2.3: AC 1(1) to (5), (7), AC 2; Section 2.2.1.3.3.3: AC 1(1) to (8), AC 2(1), (2), (4), AC 3(1) to (3); Section 2.2.1.3.10.3: AC 1, AC 2(1) to (3)]

An integrated set of models and analyses support the igneous intrusion modeling case. These numerical models and supporting analyses address the phenomena associated with an igneous

intrusion and the postintrusion effects on repository performance. The models and analyses that provide the basis for the igneous intrusion modeling case are as follows:

- Natural and induced stresses at the repository, as they relate to dike propagation from depth (SNL 2007a, Section 6.2)
- Dike propagation from depth (SNL 2007a, Section 6.3)
- Magma flow into drifts at dike–drift intersections (SNL 2007a, Section 6.3.3.5.6; Dartevelle and Valentine 2007)
- Effects on waste packages and waste forms (SNL 2007a, Section 6.4.8.3)
- Secondary dike propagation (SNL 2007a, Section 6.5)
- Magma flow between drifts (SNL 2007b, Section 5.1)
- Waste packages compromised during an igneous intrusion (SNL 2007b, Figure 7-1)
- Heat flux and magma cooling (SNL 2007a, Section 6.4.6)
- Percolation flux through cooled basalt (SNL 2007c, Section 6.6.2[a] and 6.10.9[a]).

These studies support the abstraction used in TSPA for the igneous intrusion modeling case, as described in Section 2.3.11.3.5.

2.3.11.3.2.1 Natural and Induced Stresses at the Repository

The regional stresses related to the tectonic setting, stresses induced by topography, and induced stresses related to the presence of a repository (e.g., excluded FEP 1.1.02.00.0B, Mechanical effects of excavation and construction in EBS, and included FEP 2.2.01.01.0A, Mechanical effects of excavation and construction in the near-field) (Tables 2.2-1, 2.2-7, and 2.3.3-1) may potentially affect the orientation of future dikes. Thermal loading due to radioactive waste decay coupled with the presence of the repository will have an effect on the stress state within Yucca Mountain (excluded FEPs 2.1.11.07.0A, Thermal-expansion stress of in-drift EBS components; 2.2.01.02.0A, Thermally-induced stress changes in the near-field; 2.2.10.04.0A, Thermal-mechanical stresses alter characteristics of fractures near the repository; 2.2.10.04.0A, Thermal-mechanical stresses alter characteristics of faults near repository; 2.2.10.05.0A, Thermomechanical stresses alter characteristics of rocks above and below the repository). Detailed descriptions of stress analyses are found in *Drift Degradation Analysis* (BSC 2004b, Appendix C). The prerepository maximum principal compressive stress is vertical (gravitational stress affected by topography and stratigraphy), whereas the two other principal stresses of smaller magnitude are in the horizontal plane (SNL 2007a, Section 6.2.2). The rock mass is modeled as a homogeneous, isotropic medium, and in the absence of any preexisting weaknesses such as fault planes, a future dike would be expected to be oriented perpendicular to the least principal compressive stress.

Analysis results (SNL 2007a, Figure 6-2) show that topographic mass loading above the repository results in variations in the vertical stress of less than 2 MPa. This stress differential is demonstrated to have a minimal effect on dike propagation (SNL 2007a, Section 6.2.2). A similar analysis addressed the alteration of the stress field due to the presence of the emplacement drifts. These results show that stress changes from drift excavation would be of limited spatial extent. The effects related to the presence of emplacement drifts are shown to be limited to approximately three drift radii from the emplacement drift wall. Since the drift spacing is more than 14 times the drift diameter, the results indicate that the presence of repository emplacement drifts will have a minimal effect on dike propagation (SNL 2007a, Section 6.2.3).

Thermal stresses associated with the decay of radioactive waste were also analyzed. The temperature and associated stress changes caused by heat generated from the emplaced waste were simulated for a period of 10,000 years (BSC 2004b, Appendix C, Figures C-10 to C-13). The maximum increase in horizontal stress due to heating occurs between 500 and 1,000 years after waste emplacement. On average, the vertical stresses do not change as a result of heating. Analytical results indicate that dike propagation would be slowed under thermal stresses (SNL 2007a, Section 6.3.7.4), but stresses would not increase enough to result in sill formation or diversion before the dike penetrates the repository. Hence, this potential diversion effect is not modeled (SNL 2007a, Section 6.2.4).

2.3.11.3.2.2 Dike Propagation from Depth

The dike propagation model describes the mechanisms of fracture development that accompany magma ascent. The model analyzes the behavior of magma melt and gases in the ascending dike. Figure 2.3.11-9 schematically depicts the key features, processes, and properties that control the ascent of magma in dikes through the shallow crust. The ascent of magma as it approaches the surface is a complex process to model and is dependent on multiple factors, including the stress gradient and the properties of both the magma and the host rocks.

The pressure of the magma in the dike pushes aside the surrounding rock, creating typical dike widths of several meters (SNL 2007e, Section 6.3.3.1). The restricted width of the dike and the viscosity of the magma induce frictional losses in magma pressure along the length of the dike. As a result, the overall dike-propagation model is constrained by a balance between the pressure necessary to keep the crack open at a given width, the stresses from the surrounding rock acting to close the crack, and the appropriate width necessary to sustain the pressure gradient needed to maintain magma ascent. The model of dike propagation simulates the propagation of the crack tip ahead of the ascending magma, considering regional and induced stresses from topography and repository thermal effects, and the instability of crack propagation as the crack approaches the earth's surface (SNL 2007a, Section 6.3). The model also considers the physical properties and the effects of a compressible magma (SNL 2007a, Section 6.3.6).

Most dikes in the Yucca Mountain area have a small dike width (meters) compared to strike length (approximately 0.5 to 6 km) (BSC 2004a, Figure 6-2) and compared to their depths of origin (tens of kilometers) in the mantle (BSC 2004a, Section 6.1.1.2). Thus, although they are three-dimensional features, it is reasonable in near-surface environments such as the repository, to use a two-dimensional approximation of dike propagation for calculating many dike parameters. The basic components of the dike propagation model include: (1) the elastic deformation of a crack

due to the internal pressure of the fluid resisted by the stresses acting on the surrounding rock; (2) the viscosity of the moving magma within the fracture; (3) fluid and gas losses into the surrounding medium; and (4) a crack propagation criterion that accounts for the resistance, if any, of the rock to fracture. These components must be calculated interactively to ensure proper coupling of the various mechanisms. A detailed description of the mathematical formulation of the dike-propagation model is presented in *Dike/Drift Interactions* (SNL 2007a, Section 6.3.3.1).

The effects of magma expansion on propagation of the leading crack have been analyzed. Results show that expansion of rising magma would be accompanied by acceleration of the magma. In turn, the crack tip would accelerate as it approaches the surface. Generally, the results show that the crack tip arrives at the surface sooner than it would if no expansion of the magma occurred (SNL 2007a, Section 6.3.6).

Analyses were conducted to quantify conditions within a magma-drift-volcano system if the volcanic vent were blocked, as might occur during the months to years duration of a volcanic event in order to determine what effect these conditions would have on the potential development of secondary dikes. The additional analyses considered three configurations: (1) blockage of a conduit feeding a scoria cone by slumping; (2) blockage by solidification of magma within a conduit; and (3) blockage by a co-volcanic fault (SNL 2007a, Section 6.4.8.1.3.3). These three cases are illustrated in Figure 2.3.11-10. The analyses for Configurations 1 and 2 applied increasing increments of pressure to the magma/basalt boundary until the blocking structure failed. The analysis for Configuration 3 supplied magma at a steady rate to the bottom of the dike until a new steady flow state was achieved. Results indicate that magma overpressures as high as 10 MPa could be attained in Configuration 2 before either the blockage or the surrounding rocks would fail and relieve the pressure. The other two configurations failed at lower pressures. Thus, total pressure within a magma-filled drift might attain values up to 10 MPa plus the lithostatic overburden pressure, due to temporary blockages during the full duration of a volcanic event (SNL 2007a, Section 6.4.8.1.3.3). The potential for sustaining magma flow in secondary dikes under these conditions is remote (Section 2.3.11.3.4.4) (SNL 2007a, Section 6.5.1.2). However, assuming dose from the eruptive case scales linearly with waste packages intersected by a conduit, and assuming that all waste packages in the drift are involved in the development of a secondary conduit, the increase in dose for the volcanic eruption modeling case can be no more than one to two orders of magnitude compared to the case where waste packages are entrained only in the primary conduit. As discussed in Section 2.4, the estimated dose from the volcanic eruption modeling case is a small fraction (less than 0.1) (Sections 2.4.2.2.1.2.3.1 and 2.4.2.2.1.2.3.2) of the estimated dose from the igneous intrusion modeling case.

2.3.11.3.2.3 Magma Flow in Drifts

Data from Quaternary analogue volcanoes in the Yucca Mountain region (SNL 2007e, Sections 6.3.1, Appendices C to E) preserve evidence for a range of eruptive processes that occur when magma rising through a dike or conduit flows (erupts) into the atmosphere. These are considered to be analogous to the range of processes that might occur if rising magma were to intersect a repository drift. The processes can be considered in terms of two end members:

1. Magma with or without gas bubbles, but where the silicate melt is a continuous (interconnected) phase, flows into a drift. On the earth's surface such a flow would

produce a lava flow. The term "effusive" is commonly used in reference to the flow of lava from a vent at the surface, and that term is also used to refer to the end member behavior of lava flowing into a drift.

2. A mixture of gas (continuous phase) containing dispersed fragments or drops of magma flows into a drift. On the earth's surface such a flow would produce a violent Strombolian eruption with a tephra plume that rises hundreds to thousands of meters into the atmosphere. Such eruptions are commonly referred to as "pyroclastic" and that term is also used in reference to the flow of such a mixture into a drift.

The factors that determine which type of process occurs include the initial volatile content of the rising magma, the solubilities of those volatiles as a function of pressure, the ascent rate of magma, magma viscosity, and the rate of volatile loss to the surrounding country rocks. Field data indicate that both end member types of processes, as well as transitional processes, can occur at various stages during an igneous event and can even occur simultaneously (SNL 2007e, Sections 6.3.1, Appendices C to E). Therefore, the approach taken is to model the dynamic conditions as rising magma first intersects and then flows into a drift for both the effusive and pyroclastic end member cases. For the purposes of TSPA, the details of these processes are simplified such that all waste packages that are contacted by magma are assumed to fail in terms of their ability to contain spent fuel (SNL 2007b, Section 5.1).

Magma ascent in a rising dike would be influenced by magma flowing into the drifts, with the rate of ascent reduced directly above the drift until the drift is filled. This effect may be diminished at the pillar centerline between the drifts (SNL 2007a, Section 6.3.3.5.6). The net effect would be that initial magma ascent above the pillars could be faster than above the drifts. As the magma fills the drifts, it engulfs the waste packages (SNL 2007a, Section 1.4.3) and all other EBS components in the drifts.

The analyses of pyroclastic flow into drifts consider two-phase expansion of magma as it rises in the dike (BSC 2005a, Section 6.4.2; Dartevelle and Valentine 2007, Section 3.2). The analysis considers the potential diversion of pyroclastic flow into repository drifts after initial interaction between rising magma under relatively high flow pressures and a repository drift at atmospheric pressure. The distance within a drift from the point of dike-drift intersection, at which the pyroclastic flow drops to the floor, depends upon the volatile content and particle size in the mixture. At the highest expected water contents (4.6 wt %) and with small (100 micron) particles, the pyroclastic flow initially may travel several hundred meters down a drift until it is turned back at the drift end. Conversely, for the same water content but with coarser particles (e.g., 1 cm), the gas particle mixture falls back to the floor within a few tens of meters, and the drift fills as weak pyroclastic flows move away from the fall-back point (Dartevelle and Valentine 2007, Sections 7.2.1 and 7.2.2).

2.3.11.3.2.4 Effects on Waste Packages and Waste Forms

For TSPA, it is assumed that (1) following intersection of the repository, all drifts are rapidly filled with magma; (2) all waste packages in drifts are engulfed in magma; and (3) the waste packages contacted by magma are damaged and fail, providing no protection for the waste from groundwater (SNL 2007b, Section 5.1). Damage to drip shields, waste packages, and cladding is presented in

terms of igneous EBS failure fractions (SNL 2007a, Section 8.2.3), which describe the extent of damage to these components when they are contacted by magma. For all components, the EBS failure fraction is 1, that is, the components are totally damaged and fail.

Waste Packages—Based on analysis of magma flow in drifts and analogue information about the environmental conditions associated with intrusion of a basaltic magma, the temperature in an intruded drift is expected to increase rapidly to near the magma temperature of about 1,046°C to 1,169°C (SNL 2007e, Table 7-1). Results from a design calculation (BSC 2005b, Section 6.3.3.1) indicate that at near magmatic temperatures, the waste packages would begin to lose their strength (SNL 2007a, Section 6.4.8.3.1), resulting in plastic deformation of the waste packages within days. Hence, failure of waste packages in drifts intruded by magma is expected to occur as soon as the waste packages approach magmatic temperatures. Additional analyses describe damage to the waste package from external magmatic pressures as low as 4 MPa; as a result of this response to magmatic pressures, magma could fill the waste packages (SNL 2007a, Section 6.4.8.3.1).

Waste Forms—If the waste packages fail, waste forms would also be subject to disruption. Possible effects include exposure to high temperature and chemical interactions with magma and associated fluids and gases that could degrade the waste forms. The nature of the effects would depend upon factors such as the degree and duration of magma contact with waste forms, the contact pressure, the magma viscosity, the temperature, the redox conditions at the time of intrusion, and the physical and chemical characteristics of the waste forms. For example, commercial spent nuclear fuel (SNF) has a high melting temperature ranging from approximately 2,600°C (for light water reactor fuels) to 2,800°C (for UO_2) (SNL 2007a, Section 6.4.8.3.3). Therefore, the commercial SNF is not expected to melt at temperatures up to the upper-bound magma temperature on the order of 1,200°C. However, under some oxygen fugacity conditions, zirconium in the cladding can reduce UO_2 to produce uranium-zirconium alloy at temperatures between 800°C and 1,150°C. In turn, several other solid solution layers of interactive uranium-zirconium and zirconium oxides could form at lower temperatures. As temperatures decrease after intrusion, and under oxidizing conditions, cladding damage is expected, and uranium oxide is expected to fragment, which would increase the surface area of the waste (SNL 2007a, Section 6.4.8.3.3).

Another example is high-level radioactive waste (HLW) contained in borosilicate glass. When this waste is subjected to magmatic temperatures, the glass could remelt and possibly devitrify as the glass slowly cools. The slow cooling would be expected to result in less cracking than in the original glass, and therefore, a lower release rate, although no credit is taken for this phenomenon. The extent of devitrification depends on the composition of the glass, temperature, and cooling rate. Borosilicate glasses are currently formulated to minimize devitrification (SNL 2007a, Section 6.4.8.3.3).

In summary, commercial SNF is expected to be unaffected by exposure to magmatic temperatures alone because commercial SNF is a refractory ceramic material with a very high melting point (SNL 2007a, Section 6.4.8.3.3). However, under magmatic temperatures and oxidizing conditions, uranium oxide and HLW could undergo fragmentation, substantially increasing their surface areas (SNL 2007a, Section 6.4.8.3.3) and facilitating solution and transport after percolation has been reestablished. However, to avoid underestimating radionuclide mobility, for TSPA, all waste in the drifts is conservatively assumed to be unprotected, instantaneously degraded, and the radionuclides

are assumed to be immediately available for mobilization by groundwater (SNL 2007a, Section 8.1).

2.3.11.3.2.5 Secondary Dike Propagation

Analyses have also been performed to evaluate the possibility of propagating a secondary pathway by opening a preexisting crack that would allow magma to ascend to the surface. Key factors considered in these analyses were crack orientation, initial crack aperture, magma pressure in drifts, confining stresses, host rock physical properties, and magma properties. Results of these analyses show that during the early stages of a volcanic event, magma would be expected to follow the path of the main dike to the surface, rather than develop a secondary dike that extends to the surface (SNL 2007a, Section 6.5.2; Dartevelle and Valentine 2007, Section 7.2.1.1). As mentioned in Section 2.3.11.3.2.2, pressures that might occur during the full duration of the volcanic event (e.g., due to conduit blockage) might also effect the development of secondary dikes. If such a secondary dike formed and entrained waste packages into a secondary eruptive conduit, dose would increase by no more than one to two orders of magnitude (Section 2.3.11.3.2.2). Analysis results indicate that formation of secondary dikes and associated conduits is unlikely (SNL 2007a, Section 8.1.3). Furthermore, if secondary dikes (and conduits) were to form, they could affect only the volcanic eruption modeling case. As discussed in Section 2.4, the estimated dose from the volcanic eruption modeling case is a small fraction of the estimated dose from the igneous intrusion modeling case.

2.3.11.3.2.6 Magma Flow between Drifts

As described in Section 2.3.11.3.1, once the repository footprint is intersected by a dike, magma is assumed to flow into all drifts (SNL 2007a, Section 5.1).

2.3.11.3.2.7 Waste Packages Compromised During Igneous Intrusion

The analysis presented in *Number of Waste Packages Hit by Igneous Events* (SNL 2007b, Section 6.3.2) calculates the location and number of drifts intersected by a dike or dike swarm when an igneous event intrudes (intersects) the repository (Figure 2.3.11-11). Although the results of the calculation indicate that the number of drifts intersected during an igneous intrusion is typically less than the total number of drifts in the repository, it is assumed that all drifts in the repository are filled with magma if any drift (including access and exhaust drifts) in the repository is intersected (SNL 2007b), Section 5.1). Because all drifts are assumed to be filled with magma following an igneous intrusion, all waste packages in the repository are contacted by magma. Once contacted by magma, the waste packages are assumed to fail and provide no protection for waste from contact by groundwater (SNL 2007b, Section 5.1).

2.3.11.3.2.8 Heat Flow and Magma Cooling

Heat from the magma would increase host rock temperatures near the magma-filled drifts for a period of time (host rock temperatures would characteristically cool to within 10°C of pre-intrusion temperatures after 20 years). Modeling of heat flow between drifts and magma cooling was performed to estimate drift centerline and wall temperatures and to constrain the post-intrusion environment to which waste packages and waste forms in magma-filled drifts would be subjected.

The dispersal of heat following intrusion has been assessed by numerical simulations of non-steady-state heat conduction, with radial flow of heat from the drifts filled with basalt magma (SNL 2007a, Appendix C).

The initial temperature of the magma is taken as 1,150°C (SNL 2007a, Section 6.4.1.1), which is near the upper bound of analogue basaltic magma temperatures (SNL 2007e, Table 6-5). In the model, the magma is assumed to immediately fill the drifts, and the temperature decreases with time and distance from the centerline of the drift. The rate of heat flow depends on the thermal diffusivity of the welded tuff and the basalt, which are assumed to be the same (SNL 2007a, Section 5.4). The model uses thermal properties of both dry and saturated tuff. The repository drift wall temperature at the time of intrusion is assumed to be between 25°C (ambient) and 200°C (SNL 2007a, Section 6.4.3). The high end of the range represents rock heated during the thermal period.

For TSPA, the model provides a lookup table of temperatures in intruded drifts (drift centerline and wall temperatures) at 0 to 100 years after intrusion, and as functions of five specified repository temperatures between 25°C and 200°C (SNL 2007a, Table 8-2). The time-temperature data are used to estimate when seepage is restored to drifts and percolation through the cooled basalt begins. For the 25°C case, temperatures at the rib would permit seepage by the end of year 3 following intrusion. For the 200°C case, temperatures at the rib are 202°C at the end of 100 years following intrusion (so water seepage would not return until sometime after 100 years following intrusion) (SNL 2007a, Table 8-2).

2.3.11.3.2.9 Percolation Flux through Cooled Basalt

Following an igneous intrusion and after drift temperatures have decreased to less than the boiling point of water, percolation of groundwater through the repository would begin to be restored. The analysis assumes that the cooled magma (basalt) in the drift offers no additional resistance to flow beyond that of the surrounding host rock. The chemistry of water seeping into drifts would be affected by basalt–water interactions within the drift. Of particular importance to the TSPA are changes in pH and ionic strength (SNL 2008, Section 6.5.1.4.1).

The igneous intrusion modeling case conceptual model for groundwater chemistry is a mixing cell in which waste package components are reacted with liquid water from a basalt reservoir and atmospheric gases over time following waste package breach (SNL 2007c, Section 6.3[a]). The waste package configuration (surface areas and moles of constituents) are the same as those used in the nominal case in which the waste package is simply breached. The TSPA uses the pH and ionic strength from the in-package chemistry lookup tables (SNL 2007c, Table 6-21[a]) as input for their realizations. The in-package simulations are conducted using the EQ3/6 code and the Data0.R5 thermodynamic database (SNL 2007c, Section 6.3.1.1[a]).

Because the igneous intrusion modeling case considers transport of radionuclides by groundwater and radionuclide mobility is influenced by groundwater chemistry, the intrusion modeling case requires consideration of the chemistry of groundwater that has been in contact with the basalt surrounding the waste packages. Three groundwater samples from large fractured basalt reservoirs were selected for simulations that examined pH and ionic strength of water that has interacted with cooled basalt. Two of the samples are from the Columbia River Plateau basalts at the Hanford Reservation in Washington, and one is from basalt in Iceland (SNL 2007c, Section 4.1.2[a];

Tables 4-4[a] and 4-5[a]). The samples from the Columbia River Plateau represent the two predominant water types observed there: a sodium-rich groundwater (BW, pH 8.57, *I*: 0.0040) from a deep well screened in the Wanapum and Grande Ronde formations and a calcium-rich groundwater (BS, pH 8.00, *I*: 0.0066) from a shallower well screened in the Saddle Mountain and Wanapum formations (SNL 2007c, Section 4.1.2[a]). The Icelandic sample is from a shallower aquifer, has not been in contact with the reservoir rock for as long as have the Hanford samples, and apparently is in equilibrium with the basaltic glass as indicated by its elevated pH (9.0 S.U., *I*: 0.0014). Sensitivity studies from the *In-Package Chemistry Abstraction* (SNL 2007c, Section 6.6.2[a]) were used to estimate solution development during reactions between basalt-equilibrated water and the in-package materials.

In addition to the water samples used in the analysis, a literature review was conducted of groundwater chemistry in basaltic rocks. More than 400 articles were reviewed, and a total of 15 sites were chosen to assess basalt-groundwater interactions. A total of 1,229 sample pH values were used in the analyses. The 15 sites had groundwater pH values that were summarized by mean values and standard deviations. The mean pH from these sites ranged from 6.05 to 8.12, with an average of the means of 7.29. The mean ionic strengths ranged between 0.00029 mol/kg and 0.0959 mol/kg, with an average of the means of 0.0021 mol/kg (SNL 2007a, Section 6.6.5).

2.3.11.3.3 Data Uncertainty

[NUREG-1804, Section 2.2.1.3.2.3: AC 3(1) to (3); Section 2.2.1.3.3.3: AC 3(1), (2), (4); Section 2.2.1.3.10.3: AC 3(1), (2)]

Parameter distributions related to the implementation of the igneous intrusion modeling case are the probability of intersection of the repository by a basalt dike (Section 2.2.2.2.5), the parameters needed to model the propagation of the dike and the effects of magma on various components of the EBS, and the number of waste packages in drifts intersected by dikes. The following sections discuss how uncertainties in data supporting specific analyses are addressed.

2.3.11.3.3.1 Natural and Induced Stresses at the Repository

Natural and induced stresses at the repository location primarily affect dike propagation characteristics for the igneous intrusion modeling case. Data uncertainties associated with analysis of these stresses depend on the orientation and magnitude of the stress. The orientations of regional stresses acting upon the repository host rock are determined by in situ measurements and are well established (BSC 2004b, Table 4-1, Section 6.3.1.1, and Appendix C, Section C2). Locally, in situ stresses vary in response to the static load of overlying stratigraphy, plus any tectonic activity (fault movement and associated stress drops), and induced stresses from repository excavation and thermal loading after waste emplacement. Local variation in the stress field around the repository could influence the orientation of an ascending dike but, because spacing between drifts is more than 14 times the drift diameter, the presence of emplacement drifts would have a minimal effect (SNL 2007a, Section 6.2.3).

Overburden density affects the magnitude of the horizontal stress components at repository depths. Variation in the density of the overlying rocks is an important source of uncertainty in the magnitude of the vertical component of natural stress. At Yucca Mountain, density variations with depth are well known from laboratory tests performed on rock cores from the North Ramp geotechnical

boreholes and the systematic boreholes (BSC 2004b, Section 4.1.3, Appendix E). Horizontal stresses vary spatially but are of less magnitude than vertical stresses. Uncertainties are also associated with measurements of in situ stresses (BSC 2004b, Section 6.3.1.1) and elastic properties of the rock (BSC 2004b, Section 6.3.1.1, pp. 6-58 and 6-59). These uncertainties are represented through use of ranges of parameter values in the analyses (BSC 2004b, Appendix C) even though the effects of these uncertainties on the analysis of dike propagation are not significant compared to the natural variabilities associated with geologic processes related to dike propagation (SNL 2007a, Section 6.3.3.2; SNL 2007e, Section 6.3.1 and Appendix F.3).

2.3.11.3.3.2 Dike Propagation from Depth

Data uncertainties concerning the analysis of dike propagation include the water content of the magma, magma physical properties, and host rock properties, including regional in situ stresses and induced stresses due to the presence of repository drifts. Water content is a crucial factor in determining properties, including magma density, viscosity, temperature, and intrusion style (related to volatile content). To address the uncertainties in individual properties, the dike propagation model considers a wide range of parameter inputs for the fluid magma. The host rock properties are modeled as those at the repository level (SNL 2007a, Section 6.3.3.3). The results of simulations are reformulated and evaluated as dimensionless quantities. Use of dimensionless quantities keeps the number of numerical simulations to a minimum while allowing the model to address large variations in magma density and viscosity, confining stress or dike tip cavity pressure (SNL 2007a, Sections 6.3.3.1.2), and host rock fracture toughness (SNL 2007a, Section 6.3.3.3). The effect of magmatic volatile expansion on dike propagation is approximated by combining results for different magma densities. Results show that the magma front and the crack tip accelerate upward in response to magmatic expansion (SNL 2007a, Section 6.3.6) as the magma ascends.

2.3.11.3.3.3 Magma Flow in Drifts

Data uncertainties associated with the analysis of magma flow into drifts include magma properties (e.g., water content, density, viscosity, temperature, supply rate, and pressure), intrusion properties, especially dike width, drift properties (open diameter, rockfall frequency, and block size), and waste package diameter. Results of the modeling using wide ranges of these properties account for uncertainties for effusive flow (SNL 2007a, Sections 6.3.3.5.6 and 6.3.3.5.7). Uncertainties associated with magma flow in drifts are accommodated in the TSPA through the assumption that once the repository footprint is intersected by a dike, all drifts are inundated by magma and all waste packages fail (SNL 2007b, Section 5.1; and SNL 2007a, Section 8.2.3).

2.3.11.3.3.4 Effects on Waste Packages and Waste Forms

Data uncertainties associated with the analysis of impacts on waste packages and waste forms include the mechanical properties of alloys at high (magmatic) temperatures, mechanical loads on waste packages, nature of chemical reactions between waste packages, waste materials and magma, and the chemical species present in magmatic gas (SNL 2007a, Sections 6.4.8.3.1 and 6.4.8.3.3). These data uncertainties are accommodated by the assumption that once any drift is intersected by a dike, magma flows from the intersected drift(s) into all emplacement drifts, and all waste packages in the repository are damaged to the extent that they provide no protection for waste (SNL 2007b, Section 5.1; SNL 2007a, Section 8.2.3).

2.3.11.3.3.5 Secondary Dike Propagation

Data uncertainties associated with analysis of secondary dike propagation include rock properties (e.g., joint frequency, initial joint opening, and thermal diffusivity), magma properties (e.g., density, viscosity, temperature, and pressure), magma chemistry, and intrusive style (effusive or pyroclastic). Uncertainties related to rock and magma properties and to magma chemistry (i.e., differing water contents) are addressed by considering a range of input values for the respective parameters in the analysis (SNL 2007a, Sections 6.5.1.1.1 and 6.5.1.1.2). Uncertainty related to intrusion style is addressed by including analyses of propagation of both an effusive secondary dike and a pyroclastic secondary dike (two-phase flow) (SNL 2007a, Sections 6.5.1 and 6.5.2; Dartevelle and Valentine 2007, Section 7.2.1.1).

Additional uncertainty associated with whether partial solidification would halt secondary dike propagation arises from the value for effective solidification temperature, which determines the temperature–viscosity relationship for partially crystallized magma. The presence of 10% to 20% crystals causes the magma viscosity to increase 1.5 to 2 orders of magnitude (SNL 2007a, Section 6.4.8.2.1). Thus, the effective solidification temperature for each water content was selected as the temperature at which the calculated magma viscosity reached 1,000 Pa·s (SNL 2007a, Section 6.4.8.2.1).

2.3.11.3.3.6 Magma flow Between Drifts

Once intersection of the repository occurs, all drifts are assumed to be inundated by magma (SNL 2007b, Section 5.1).

2.3.11.3.3.7 Waste Packages Compromised During an Igneous Intrusion

Uncertainties associated with a future igneous event are addressed using distributions for the various parameters included in the analysis to calculate intersection of the repository footprint by igneous features. The distributions account for uncertainties associated with number of dikes, dike orientation, length, width, and spacing. Uncertainties in interaction effects between dikes and host rock are considered by including a “buffer zone” to address uncertainties in proximal effects of dikes on drifts related to rock failure processes (SNL 2007b, Section 6.4).

2.3.11.3.3.8 Heat Flow and Magma Cooling

Principal data uncertainties associated with the magma cooling and solidification model include the initial magma temperature, which for the analysis is considered to be 1,150°C. The 1,150°C temperature is within the range of liquidus temperatures for dry magma (SNL 2007e, Table 6-5). Magma temperatures could be as low as 1,046°C, principally because of variations in water content of the magma (SNL 2007e, Table 6-5). The effects of thermal property contrasts between the magma and the tuff host rock have been shown to be small. The analysis shows that variations of as much as 10% in a thermal property produces approximately a 3% change in calculated temperatures (SNL 2007a, Appendix D, Section D6). Latent heat of crystallization was shown to affect magma cooling and solidification, increasing by one-third the time required for temperatures at the drift axis to decrease below 325°C and causing early-time temperatures within the magma and tuff near the contact to be approximately 100°C hotter (SNL 2007a, Appendix D, Section D6). This

effect is approximated by using a higher starting temperature in the analysis. Thermal properties of tuff are better constrained than are those of basalt magma, but the main uncertainties are the spatial variations in porosity and saturation. While such variations can cause thermal conductivity variations of 10% or more, their main influence is on convective heat transport. The analytical model is conductive and magma convection is not expected to occur within emplacement drifts because of the limited height of the drifts (SNL 2007a, Appendix D, Section D3).

Uncertainties in various input parameters have been addressed, including thermal conductivity, grain density of tuff, specific heat capacity, matrix porosity, saturation, lithophysal porosity, and initial temperature (SNL 2007a, Section 7.3.2.2.1.2 and Appendices C and D). Analysis indicates that the results are fairly insensitive to natural parameter variations. Only the initial temperature has any appreciable effect on the outcome of the analysis (SNL 2007a, Section 8.3.1). In addition, a two-dimensional numerical model was developed to model heat flow with a configuration that included an idealized waste package and the invert fill material. This model included the latent heat of crystallization of the magma and the radiogenic heat from the waste packages in one case, simulating heat flow in the first century following closure of the repository. The uncertainty in temperature is reflected in the comparison between the model output (SNL 2007a, Table 8-2) and the results of the two-dimensional alternative model (SNL 2007a, Tables 7-7 and 7-8).

2.3.11.3.3.9 Percolation Flux through Cooled Basalt

Because the basalt water compositions used in the analyses supporting the igneous intrusion modeling case are based on measured data, the uncertainties are limited to those of sampling and analysis of groundwaters. The Hanford Reservation groundwater analyses were published in a U.S. Geological Survey Water Resources investigation report (Turney 1986).

The Columbia Plateau and Iceland basalts studied were selected to give a wide range of chemical compositions consistent with basalt reservoir environments such that the composition of a basalt that might intrude the repository would be within the compositional range represented by the Columbia Plateau and Iceland basalts. Analyses using waters equilibrated with the Columbia Plateau and Iceland basalts have shown that the pH and ionic strength of the incoming water has little effect on the resulting water pH and ionic strength because the intra-package reactions dominate the effluent (SNL 2007c, Sections 6.6.2[a] and 6.10.8.2[a]). The result shows that the uncertainty associated with not knowing the actual composition of a future repository basalt would not affect the effluent chemistry, which represents solutions in equilibrium with and buffered by the in-package corrosion products.

The uncertainty of groundwater analyses is a function of the concentrations of the constituents being measured. The U.S. Environmental Protection Agency's Contract Laboratory Program states that analyses can be ±100% near the detection limits for the constituent and can be no more than ±10% at the estimated quantitation limit. The detection limit for any specific instrument is the lowest concentration at which a pure solution of a component can be detected. The estimated quantitation limit is the lowest concentration that can be measured using routine methods on a groundwater (complex) solution (EPA 1992, Section 5.0).

2.3.11.3.4 Model and Analysis Uncertainty and Alternative Models

[NUREG-1804, Section 2.2.1.3.2.3: AC 4; Section 2.2.1.3.3.3: AC 4(1) to (4), AC 5; Section 2.2.1.3.10.3: AC 4]

This section discusses uncertainty associated with both models and analyses and provides a discussion of alternative models. The uncertainty includes the consideration of uncertainties associated with the conceptual models used in the igneous intrusion modeling case, and considers alternatives for specific FEPs. Limitations of the models and analyses developed for the igneous intrusion modeling case have also been considered.

2.3.11.3.4.1 Natural and Induced Stresses at the Repository

The igneous intrusion modeling case includes an analysis of natural and induced (thermal) stresses at the repository. The analysis of natural and thermal stresses considers that all material is linear elastic, except that two cohesionless coulomb slip interfaces are used to represent the Ghost Dance and Solitario Canyon faults. Anelastic effects, which are likely to exist at Yucca Mountain, are not considered. Not including anelastic effects is expected to have a very limited impact on the analysis results because (1) gravitational stresses are statically determined and, therefore, are correctly computed; and (2) the analyses of horizontal stresses have been calibrated using field measurements (SNL 2007a, Section 1.4.1).

2.3.11.3.4.2 Dike Propagation from Depth

The igneous intrusion model includes a submodel for dike propagation from depth. Dike ascent is a complex process involving nonlinear behavior of both magma and the surrounding rock mass. To develop a practical model of the dike ascent process, several simplifications are employed. The overall approach taken in the modeling is using a two-dimensional model of a three-dimensional process. This approach is reasonable because of the horizontal (strike) and vertical (dip) extents are favorable for creating essentially two-dimensional processes in the center of the dike (SNL 2007a, Section 6.3.3.2). The rock mass is modeled as linearly elastic, and the process of dike-tip propagation is analyzed according to linear elastic fracture mechanics. In reality, rock is not linearly elastic, but the assumptions of linear elasticity and linear elastic fracture mechanics provide a tractable mathematical formulation for the analysis. The effect of deviations from linear elastic fracture mechanics are considered by variations in the fracture toughness input parameter (SNL 2007a, Section 6.3.1.2). Magma is assumed to be an incompressible, single-phase fluid. In reality, as magma rises in a dike, water and other volatile components exsolve in response to decreasing pressure, and the exsolution, in turn, changes the bulk density and viscosity of the magma. Uncertainty in the viscosity of the magma is addressed by using a range of values for Newtonian viscosity that has been selected as appropriate for the magma and flow regime expected (SNL 2007a, Sections 1.4.2 and 6.3.3.2; Dartevelle and Valentine 2007, Section 3.2).

Several analytic and commercial oil and gas hydraulic-fracture models, including those used in geothermal hot-dry-rock and waste-injection applications, were considered to determine if they would be appropriate to model igneous dike propagation. Analytic solutions for hydraulic fractures are useful for parameter estimation, but they do not address dike propagation in the vicinity of the free surface or losses of driving fluid (magma) at a single location such as a drift. Thus, these models

cannot be used to provide the detail needed for understanding magma flow into a shallow repository due to an intersecting dike (SNL 2007a, Section 6.3.3.5.1).

Industrial hydraulic-fracture models (oil and gas applications) were reviewed as well (Warpinski, Abou-Sayed et al. 1993; Warpinski, Moschovidis et al. 1994). The reviews show that these models can result in widely different fracture geometries (and pressures) for the same input parameters, largely because of many unknown factors in the algorithms. In addition, these models are primarily appropriate for fracturing far away from the free surface in layered media (where fractures are relatively confined between horizontal strata). These limitations make the industrial models unsuitable for modeling propagation of a dike near the earth's surface (SNL 2007a, Section 6.3.3.5.2). Hydraulic-fracture dike propagation models were evaluated as well. Buoyancy was found to be important for its effect on upward growth of the dike and for the effect of magma density on the width profile of the dike, but buoyancy is normally ignored in most hydraulic-fracture models because they are generally applied to high viscosity fluids. In addition, none of these models has a free surface that can model the changing behavior of the dike as the surface is approached. Hence, these models are used only for validation comparisons (SNL 2007a, Section 6.3.3.5.3).

2.3.11.3.4.3 Magma Flow in Drifts

The igneous intrusion modeling case includes a submodel that considers magma flow in drifts. One source of uncertainty in the model of magma flow in drifts is the extent to which the flow is effusive or pyroclastic and the associated properties of the magma (SNL 2007a, Section 1.4.3; Dartevelle and Valentine 2007, Section 7.1). The conceptual model employed for TSPA, however, is insensitive to the details of effusive or pyroclastic flow in drifts because the model assumes that intersected drifts will completely fill with magma and that waste packages and drip shields contacted by magma would provide no protection for the waste form from aqueous transport of radionuclides (SNL 2007a, Section 8.2.3; SNL 2007b, Section 5.1).

Results of analyses (SNL 2007a, Section 6.5.2) have shown that effusive magma would be expected to continue to flow along the trajectory of the original dike following intrusion of the repository. But an alternative model for magma flow into drifts (Woods et al. 2002) has also been evaluated (SNL 2007a, Section 6.5). The Woods et al. (2002) model assumes that the magma flow is pyroclastic and produces a shock wave in a drift. The Woods et al. model also assumes that the vapor is always at equilibrium with the liquid (that is, that vapor exsolves (or dissolves) from the liquid instantaneously in response to pressure changes, and the vapor and pyroclastic particles have the same velocity and temperatures). Recent analyses have shown that shock waves in intruded drifts could occur during an igneous event as results of a variety of processes, including multiphase flow effect (Darteville and Valentine 2007, Section 5.3). Based on that result, the Woods et al. (2002) analysis is considered as a possible alternative model for magma flow in drifts (BSC 2005a, Section 6.1) and also for secondary dike propagation (Section 2.3.11.3.4.4; SNL 2007a, Section 6.5; BSC 2005a, Section 1.2).

2.3.11.3.4.4 Secondary Dike Propagation

Woods et al. (2002) also describe a conceptual model in which, after a dike intersected a drift at Yucca Mountain, the drift was filled with magma and the magmatic system, including the drift, was pressurized. This pressurization generated a new opening at some distance down the drift or caused

magma flow to the surface through access drifts. In this model, the new opening propagated to the surface and became the main vent of the system. Based on the results of modeling of magma flow in drifts (SNL 2007a, Sections 6.3.3.5.6 and 8.1.3), the Woods et al. (2002) model of magma expansion into a drift is not expected to initiate secondary breakout conditions in the intersected drift (SNL 2007a, Section 6.5.2; Detournay et al. 2003, Section 3.4) because of heat loss and stoppage due to solidification of the magma in the secondary fracture (SNL 2007a, Section 8.1.3). A separate analysis of pressures needed to initiate pyroclastic flow in a secondary dike indicates that the pressure conditions are not expected to be met and, even if they occur, they are not expected to sustain pyroclastic flow in a secondary dike (BSC 2005a, Section 7; SNL 2007a, Section 5.1). These results are corroborated by the findings in the *Final Report of Igneous Consequences Peer Review Panel* (Detournay et al. 2003, Section 3.4.8).

Additional analyses evaluated alternative models related to processes that occur during the full duration of an igneous event. The results indicate that a preexisting crack would not open wider and propagate greater distances (tens of meters) even if an igneous event is sustained and the temperatures of the host rock at the drift wall are substantially elevated (SNL 2007a, Section 6.5.1.2). Even under these conditions the magma would also freeze as it moves beyond the area thermally affected by magma in the host rock (i.e., tens of meters) (SNL 2007a, Section 6.5.1.2).

A set of analyses considered the magmatic pressures that would lead to failure of a blockage of the conduit that had developed due to slumping of the volcanic cone, magma solidification near the surface, or fault-induced displacement of the conduit (Figure 2.3.11-10) (SNL 2007a, Section 6.4.8.1.3). Magmatic overpressures that would lead to failure of the blockage are generally greater than the tensile strength of the conduit wall rock (SNL 2007a, Table 6-26). Therefore, prior to failure of the blockage itself, fractures in the wall rock around the conduit are expected to occur. Based on observations and modeling of the 2001 eruption of Mount Etna (Taddeucci et al. 2004), an analogue for certain aspects of possible future volcanism in the Yucca Mountain region (SNL 2007e, Section 6.3.3.6), the cinder cone at Mount Etna failed at estimated overpressures of 3 to 5 MPa.

Pressures necessary to fail the wall rock around the conduit (SNL 2007a, Section 6.4.8.1.4) are below the range of pressures used in the secondary dike propagation analysis for preexisting fractures at the repository (SNL 2007a, Section 6.5.1.2). With the addition of hydrostatic pressure from a column of magma above the repository level, the wall rock pressures could increase by factors of two or three (BSC 2005a, Section 7.0). However, a subsequent analysis has shown that even under the most favorable assumptions for growth, a subsidiary dike will never be able to propagate effusively more than a few meters from the drift because the magma will be halted by solidification (SNL 2007a, Section 8.1.3). The same cooling effects should apply to pyroclastic flow.

The computational fluid dynamics code, GMFIX (BSC 2005a, Section 3.1; Dartevelle and Valentine 2007, Section 5.1), was used to simulate two-phase (pyroclastic) flow conditions, during initial interaction between the dike and drift (Section 2.3.11.3.2.3), and a condition later in time following sudden decompression in the drifts (Section 2.3.11.3.2.5). A limitation of the analysis is that the two-dimensional calculations approximate flow from dike to drift as flow from a dike to a sill. This limitation is expected to overpredict the fraction of magma diverted into a drift. The

analysis also does not include any effects of waste packages in the drift, which would lead to overprediction of the amount of magma flowing into a drift.

Finally, Dartevelle and Valentine (2007, Section 3.2) describe work by Menand and Phillips, who conducted experiments to study the effect of a horizontal body on mass transfer processes in a vertical conduit with bubbles. Results of their study showed that flow patterns similar to those described for the time-dependent, two-phase model can develop (Dartevelle and Valentine 2007, Section 3.2).

2.3.11.3.4.5 Magma Flow Between Drifts

Once intersection of the repository by a dike occurs, all drifts are assumed to be inundated by magma (SNL 2007b, Section 5.1).

2.3.11.3.4.6 Effects on Waste Packages and Waste Forms

Since the range of possible interactions encompasses an unusually broad range of uncertainty, it is appropriate to consider that waste packages, cladding, and drip shields contacted by magma provide no added protection for waste forms (SNL 2007a, Section 8.3.2). The uncertainty in the assumption is addressed by analyses to corroborate the assumption. Specifically, the analysis results show that emplacement drifts intersected by a dike would be filled with magma within minutes (SNL 2007a, Section 6.3.3.5.7). Another analysis addresses the response of waste packages to external total pressures as little as 4 MPa (SNL 2007a, Section 6.4.8.3.1 and Appendix E), and to a mixture of volatile species dominated by water but including CO_2, SO_2, HCl, H_2S and HF (SNL 2007a, Section 6.4.8.3.1). This environment would develop over a period of a few months within magma-filled drifts as the magma began to solidify from the edge of the drift inward. The pressures would deform the waste packages (already weakened by thermal effects) to such an extent that they would provide no protection for the waste from contact by percolation once seepage into drifts is restored (SNL 2007a, Sections 6.4.8.3.1 and 6.4.8.3.5).

An independent analysis of impacts on waste packages and waste forms was developed by the Electric Power Research Institute (EPRI 2004). That analysis concludes that no waste packages will be compromised by an igneous event. There are differences between the Electric Power Research Institute analysis and the analysis described in this report that are attributable to differences in input parameters and assumptions (SNL 2007a, Section 6.4.8.3.4).

The Electric Power Research Institute modeling examines a 4-m-diameter by 5-m-long cylinder of magma moving vertically at 100 m/s and impacting a horizontal 21-PWR waste package at midlength (EPRI 2004, Section 5.2), and the analysis considers the structure of the waste package and its internal components. Contact between the magma and the waste package produces damage to the waste package but does not result in tearing of the inner structural shell, and integrity of the end closures is maintained (SNL 2007a, Section 6.4.8.3.4). The analysis also examined the thermal effects of pressurization of the waste package and "pinhole" rupture and creep failure and concluded for the "pinhole" rupture analysis that internal pressure after a package has been engulfed in magma would be compressive and would not produce failure. Similarly, for ductile failure the analysis concluded that (already weakened by thermal effects) the waste package shell is not expected to

plastically deform, let alone undergo ductile failure, during the thermal transient (SNL 2007a, Section 6.4.8.3.4).

The Electric Power Research Institute report also addressed corrosion of waste packages by magma. Their results estimated a maximum corrosion depth of 5.26 mm that occurred when corrosion continued as temperatures decreased to as low as 800°C (EPRI 2004, Section 5.5.2). The differences between the Electric Power Research Institute results and results described in *Dike/Drift Interactions* (SNL 2007a, Section 6.4.8.3.1) are attributed to the absence of reactive gases, sulfur species, and halides (SNL 2007a, Section 6.4.8.3.4) in the Electric Power Research Institute corrosion analysis, and to the fact that the DOE analysis used different methods to represent the effects of magmatic temperatures on the deformation properties of waste package materials. Since the analysis of the effects of magma on waste packages and drip shields include the effects of reactive gases, sulfur species and halides, and a more realistic treatment of temperature effects (SNL 2007a, Section 6.4.8.3.1), the analysis reflects more representative conditions than does the analysis by the Electric Power Research Institute (SNL 2007a, Section 6.4.8.3.4).

2.3.11.3.4.7 Waste Packages Compromised During an Igneous Intrusion

Once the repository is intersected by a dike, all waste packages and drip shields are assumed to be damaged and fail (SNL 2007b, Section 7.2; SNL 2007a, Section 8.2.3). This assumption represents an extreme condition and hence incorporates all the analysis uncertainties associated with the analysis of how many waste packages might actually fail during an igneous intrusion.

2.3.11.3.4.8 Heat Flow and Magma Cooling

The igneous intrusion model of magma cooling and solidification evaluates the thermal effects of the intrusion on drift centerline and wall temperatures. One-dimensional cylindrical solutions for magma cooling and solidification do not directly include the effects of latent heat of crystallization and the contrasts in thermal properties of the magma and host rocks (SNL 2007a, Section 6.4.1.1 and 6.4.7.2). These uncertainties mainly affect the magma cooling times and tuff temperatures within a few drift radii (SNL 2007a, Appendix D4). At greater distances from the emplacement drifts, uncertainties in tuff temperatures related to uncertainties in input values are insignificant (SNL 2007a, Section C2).

Two alternative models were considered. The first is an analytical solution that approximates the effects of latent heat (SNL 2007a, Section 6.4.7.1 and Appendix D). The analysis (SNL 2007a, Appendix D, Section D6) showed that latent heat prolongs the cooling times within the magma and causes early-time temperatures within the magma and tuff near the contact to be hotter. The second alternative consists of numerical solutions in two dimensions that include the effects of latent heat and of radioactive heat from emplaced waste (SNL 2007a, Section 6.4.7.2).

The results of the two-dimensional numerical analysis that included both a waste package and invert fill indicates that the one-dimensional model overestimates temperatures of the waste package, crown, and invert at early times. However, within about 10 years following intrusion, temperatures in the one-dimensional model would be within 20% of the values from the two-dimensional model, and the one-dimensional model overpredicts thermal effects for long times (SNL 2007a, Section 7.3.2.1.1). Using either the one-dimensional model or the two-dimensional model, peak

temperatures in the waste packages would be high enough to result in failure of EBS components. Because latent heat effects are not included (SNL 2007a, Section 6.4.1.1), using the one-dimensional model results for TSPA provides an underestimate of the peak temperatures and, as a result, of the time needed for crown and invert temperatures to decrease to less than 100°C (SNL 2007a, Tables 7-7 and 8-2) for the TSPA model.

2.3.11.3.4.9 Percolation Flux Through Cooled Basalt

The sensitivity of the in-package chemistry process model outputs to input parameter values were evaluated (SNL 2007c, Section 6.6[a]).

Temperature Sensitivity—Temperature has a substantial influence on pH of incoming fluids when increased to 90°C (SNL 2007c, Section 6.6.6). Actinide solubilities decrease with increasing temperature (SNL 2007i, Section 6.3.3.3), and the uncertainty in radionuclide solubilities increases with increasing temperature. Therefore, to ensure that radionuclide solubilities were not underestimated, the solubilities used in TSPA are those calculated at 25°C from *Dissolved Concentration Limits of Elements with Radioactive Isotopes* (SNL 2007i, Section 6.3.3.3).

pH Sensitivity—Sensitivity analyses on the volumetric ratio of water to reactants and liquid influx rates indicate negligible effects on the range of pH but a distinct effect on the calculated pH and ionic strength. As the ratio of water to reactant decreases, the calculated pH values shift in time (SNL 2007c, Section 6.6.1[a]). The inherent buffering capacity of the degradation phases limits the pH range. Therefore, since the pH abstraction is the range of pH and not the calculated pH, liquid influx rate is not included in the abstraction (SNL 2007c, Section 6.6.4[a]).

Sensitivity analyses using waters from the basalt aquifers (two samples from the Columbia River Plateau basalts and one of basalt from Iceland) showed that, in general, the composition of the liquid influx has little effect on the In-Package Chemistry model estimates (Section 2.3.11.3.2.9; SNL 2007c, Section 6.6.2[a]).

Ionic Strength Sensitivity—The parameters that most affect ionic strength are liquid influx rate and time (SNL 2007c, Section 6.10.2.1[a]). The sensitivity of ionic strength in three mixing cells to variations in degradation rates and liquid influx water compositions was evaluated (SNL 2007c, Figures 6-33[a], 6-35[a], and 6-37[a]). Nominal case simulations (waste package breach with influx of local groundwaters) with EQ6 are listed in the *In-Package Chemistry Abstraction* (SNL 2007c, Table 6-10[a]). The nominal case estimates are not the most probable; rather, they represent the mid range process model estimates (SNL 2007c, Section 6.5.1[a]). Based on these simulations and results of the nominal case liquid influx simulations, extreme values of degradation rates cause ionic strength to depart from nominal case predictions in both positive and negative directions, justifying an uncertainty distribution with a central tendency (SNL 2007c, Section 6.10.8.2[a]). The sensitivity to liquid influx rate is demonstrated by the fact that as it increases, the residence time decreases and there is less time for degradation reactions to contribute to the solution composition. Indeed, at very high influx rates (1,000 L/yr) into the waste packages, there is little change between influent and effluent solutions (SNL 2007c, Section 6.6.4[a]).

2.3.11.3.5 Igneous Intrusion Model Abstraction

[NUREG-1804, Section 2.2.1.3.2.3: AC 5; Section 2.2.1.3.3.3: AC 5; Section 2.2.1.3.10.3: AC 5]

The igneous intrusion modeling case is implemented as an abstraction directly within the TSPA (SNL 2008, Section 6.5.1). The TSPA model uses the igneous event probability to calculate the probability-weighted mean annual dose for the igneous intrusion modeling case (SNL 2008, Section 6.5.1.1). Three input parameters developed from igneous consequences analyses are used by TSPA to implement the modeling case:

1. The parameter Num_WPs_Hit_Intrusive_a is nominally a tabular representation of the cumulative frequency distribution for the number of waste packages hit by igneous intrusion. For TSPA, it is assumed that once a dike intersects the repository footprint, all emplacement drifts are inundated by magma, and all waste packages are damaged. This assumption allows TSPA to treat the Num_WPs_Hit_Intrusive_a parameter as the single value of 11,629 (Figure 2.3.11-12a; SNL 2007b, Section 7.1; Section 2.3.7.4.1.2). Implicit in this parameter is an estimate of the severity of damage to EBS components contacted by magma. This estimate is provided in the form of EBS failure fraction of 1 for all EBS components (e.g., drip shields, waste packages and cladding) contacted by magma, which for all EBS components = 1 (all components fail) (SNL 2007a, Section 8.2.3).

2. A lookup table of drift centerline and wall temperatures for times up to 100 years after intrusion into the repository and for ambient temperatures between 25°C and 200°C to reflect effects of heat produced by emplaced waste (SNL 2007a, Section 8.2.2).

3. Descriptions of the TSPA abstraction for pH and ionic strength are provided in the *In-Package Chemistry Abstraction* Report (SNL 2007c, Sections 8.2.1[a] and 8.2.2[a]). The TSPA parameters have been defined for the *In-Package Chemistry Abstraction* (SNL 2007c, Sections 8.2.1[a] and 8.2.2[a]), and the details of TSPA implementation of these abstractions are also provided (SNL 2007c, Section 6.10.9[a]) and are described in Section 2.3.7.5.1.

pH—The secondary minerals that accumulate in each In-Package Chemistry model cell are the dominant pH buffers (SNL 2007c, Section 6.10.8.1[a]). The pH distribution for TSPA is defined to be uniform between the minimum and maximum pH values (4.97 to 8.32). A uniform distribution is chosen because sensitivity analyses indicate no clear central tendency for pH (SNL 2007c, Section 6.10.8.1[a]).

Time-dependent base case simulations and sensitivity analyses confirm that the established minimum and maximum pH limits are reasonable. Sensitivity simulations include varying the composition of the liquid influx, varying the fugacity of carbon dioxide, varying liquid flux rates, and varying degradation rates of the In-Package Chemistry cell materials and waste forms. The minimum and maximum pH limits (4.97 to 8.32) were not exceeded in those simulations (SNL 2007c, Section 6.10.8.1[a]). In addition, all of the potential influent solutions (e.g., pore waters, basalt waters, etc.) are within this pH range.

Ionic Strength—In the liquid influx case, ionic strength is a function of liquid influx rate and time since waste package breach. Because of the uncertainties in the distributions of representative degradation rates, the distribution of ionic strength values used in TSPA is log triangular with a range of –2.5 to 1 log units (SNL 2007c, Figures 6-47[a], 6-48[a], and 6-49[a]). The results show that maximum log *I* deviation from base case values is approximately one (SNL 2007c, Section 6.10.8.2[a]).

2.3.11.4 Volcanic Eruption Modeling Case

[NUREG-1804, Section 2.2.1.2.2.3: AC 1(2), AC 2; Section 2.2.1.3.10.3: AC 1, AC 2(1) to (3), AC 3(1) to (2), AC 4, AC 5; Section 2.2.1.3.11.3: AC 1, AC 2(1) to (3), AC 3(1) to (2), AC 4, AC 5, (2); Section 2.2.1.3.13.3: AC 1, AC 2, AC 3(1) to (4), AC 4, AC 5]

The volcanic eruption modeling case considers the processes associated with localization of upward magma flow into one or more conduits along a dike(s) that intersected the repository, eruption of contaminated magma products to the earth's surface, dispersal of the contaminated tephra by wind and deposition downwind, and redistribution of contaminated tephra by surface sedimentary (geomorphic) processes. The volcanic eruption modeling case develops an estimate of the number of waste packages that are intersected by eruptive conduits and provides this estimate to the TSPA model as a direct input. Another component of the case considers the airborne transport and deposition of contaminated tephra during the eruption, that is, atmospheric dispersal predicting the distribution of contaminated tephra fallout on the ground downwind of the site of an eruption. A final component of the model considers redistribution of contaminated tephra by surface sedimentary processes after deposition. This component is the Fortymile Wash ash redistribution model, which is executed within the GoldSim code and also provides an estimate of the amount of contaminated tephra that would be eroded from hillslopes, transported down Fortymile Wash, and deposited at the RMEI location as a result of fluvial processes.

Representative data from the site and surrounding region and observations from natural analogues form the basis for parameters used to calculate the number of waste packages intersected by eruptive conduits, to model airborne transport of radionuclides, and to evaluate subsequent redistribution of radionuclides in soil following an unlikely future volcanic eruption through the repository. Effects on the analyses of uncertainties and variability in parameter values have been considered, and alternative conceptual models have been used in the analyses. Analysis considerations discussed in this section are described below:

- Degradation, deterioration, and alteration that would affect waste forms exposed to erupting basaltic magma have been included in the analyses by assuming that waste packages intersected by volcanic conduits fail (SNL 2007b, Section 5.2). The effects of the assumption are propagated into the model for airborne dispersal of waste and the model for redistribution of contaminated tephra. Outputs of these models are propagated into parameters provided to the TSPA.

- Specific parameters needed to estimate the number of waste packages intersected by eruptive conduits have been estimated from analogue information and include dike length and orientation, the number of dikes in a swarm, the number of conduits that could occur along a dike, and conduit size and shape. These parameters are inputs to the analysis

(SNL 2007b, Table 4-1) that provides the TSPA abstraction of the number of waste packages intersected, which is provided as a distribution.

- For each model realization, the airborne dispersal and deposition model includes the parameter eruptive power, which is used to estimate the altitude to which contaminated tephra would be erupted and the height from which dispersal by prevailing winds would occur. Other inputs to the model include parameters controlling the proportion of waste mass incorporated into ash particles in the eruption column and wind speed and wind direction for the altitude at which dispersal occurs (SNL 2007d, Section 8.2). The output of each realization of the model is the concentration of waste in ash at the RMEI location.

- Specific tephra redistribution processes and parameters have been included in the analyses and propagated into parameters provided to the TSPA model. Parameter values used are consistent with characteristics of the RMEI, future climate data, and fluvial processes in Fortymile Wash and alluvial fan. Field data and analogue information are used to develop parameters for the redistribution model, including slope angles and areas on which tephra could be remobilized, channel scour depths (SNL 2007g, Section 4), and erosion rates that affect channels (SNL 2007g, Section 5.1.4) and the stability of interchannel divides (SNL 2007g, Section 5.1.3). Effects on the analyses of uncertainties and variabilities in parameter values have been considered. Similar to the airborne dispersal model, the output of the soil redistribution model is the concentration of waste in ash at the RMEI location.

Specific FEPs have been included in the analyses (Table 2.3.11-1), and technical bases for process models used to develop abstractions for the TSPA are described in the following sections.

2.3.11.4.1 Conceptual Model

[NUREG-1804, Section 2.2.1.2.2.3: AC 1(2), 2]

The conceptual model for the volcanic eruption modeling case includes eruption of a volcano through the repository, and entrainment of waste in the eruption products, followed by airborne dispersal, deposition, and redistribution of the contaminated tephra. Most observed basaltic eruptions begin as fissure eruptions, discharging magma where a master dike intersects the earth's surface, but the eruptions rapidly become focused into roughly cylindrical conduit eruptions along the master dike. Quaternary basaltic volcanoes in the Yucca Mountain region are likely to have evolved in this manner, although the dominant products of eruptions from the central conduits buried the earlier fissure-fed products. Studies at older, eroded Miocene basaltic volcanoes in the region also support this sequence of events (SNL 2007e, Section 6.3.1).

The transition from magma flow in a subplanar dike to flow in a conduit has been inferred at many field locations. From a continuum mechanics view, a planar dike is the preferred form for propagation of magma through brittle and elastic host rock, whereas a cylindrical conduit is the preferred form for magma flow and delivery to the surface (SNL 2007e, Section F.1).

The volcanic eruption modeling case includes a model that assumes a dike intersects the repository. The dike continues to the earth's surface to begin an eruption, and magma flow quickly focuses into 1-3 conduits that form along the dike, although the model is heavily weighted toward

the formation of a single conduit based upon characteristics of the Quaternary volcanoes in the Yucca Mountain region (SNL 2007e, Table 7-1). It is assumed that most of the eruptions, particularly the violent Strombolian phases, are fed through these conduits and, therefore, radioactive waste that is intersected by a conduit is assumed to mix with volcanic products and erupt. Some of this mixture is ejected in violent Strombolian eruption plumes into the atmosphere, and eventually deposited as contaminated tephra on the ground surface downwind from the eruptive center (Figure 2.3.11-5). Following deposition, the contaminated tephra is subject to redistribution by geomorphic processes. The volcanic eruption modeling case thus addresses three processes:

1. Eruption of magma and radioactive waste at the surface at 1-3 eruptive centers, each fed by a conduit (Table 2.3.11-1, FEP 1.2.04.06.0A, Eruptive conduit to surface intersects repository). Based on analogue studies, a fraction of the contaminated erupted material (10% to 50% (SNL 2007d, Section 6.5.2.22)) is dispersed by violent Strombolian activity, and the remaining fraction is erupted in Strombolian or effusive activity whose erupted products (cone forming material and lava) are typically found proximal to the vent location.

2. Transport of contaminated tephra into the atmosphere by violent Strombolian activity, dispersal by prevailing winds, and deposition on the ground surface as a tephra sheet (Table 2.3.11-1, FEP 1.2.04.07.0A, Ashfall).

3. Redistribution of contaminated tephra to the RMEI location via hillslope and fluvial processes and time-dependent vertical migration of radionuclides into the soil at the RMEI location. (Table 2.3.11-1, FEP 1.2.04.07.0C, Ash redistribution via soil and sediment transport).

The consequences of a volcanic eruption include consideration of the potential for increased waste concentration at the location of the RMEI from the transport of contaminated ash by geomorphic processes. This potential consequence is associated with a specific included disruptive events FEP (Table 2.3.11-1, FEP 1.2.04.07.0C, Ash redistribution via soil and sediment transport). The Fortymile Wash ash redistribution model, enumerated as the FAR V 1.2 code, represents the processes related to redistribution of contaminated ash (tephra) to and at the RMEI location. The objective of the Fortymile Wash ash redistribution model is to numerically represent the range of conditions that allow for the transport of contaminated volcanic tephra to the location of the RMEI by geomorphic processes. The tephra redistribution model also addresses the temporal near-surface and at-depth concentrations of fuel (waste) in soil at the location of the RMEI (SNL 2007g, Section 1). The terms fuel and waste are used interchangeably in the *Atmospheric Dispersal and Deposition of Tephra from a Potential Volcanic Eruption at Yucca Mountain, Nevada* (SNL 2007d) model report and supporting documentation.

2.3.11.4.1.1 Eruption Model

Volcanic centers within Crater Flat show evidence of effusive flow, mildly explosive Strombolian volcanic activity, and violent Strombolian activity. Strombolian eruptions are generally characterized by scoria cone building (ejection of coarse fragments with ballistic trajectories) (SNL 2007e, Section 6.1.3.2). Fifty to ninety percent of the fragments are deposited immediately

around the vent as cone forming facies or lava flows (SNL 2007d, Section 6.5.2.22), and the balance of the material consists of finer particles that rise higher and are dispersed by wind to form fallout sheets (SNL 2007e, Section 6.3.5.1).

More explosive, violent Strombolian activity is also inferred to have occurred on the basis of field observations. Violent Strombolian eruptions are higher-energy eruptions featuring tephra columns capable of rising kilometers into the atmosphere (SNL 2007e, Section 6.3.5.1). Such eruptions produce a fallout sheet of varying thickness extending from the volcanic vent. The thickness of the deposit depends on factors such as particle density, eruption parameters, wind speed and direction, and distance from the vent (Suzuki 1983, Figures 6, 7, 9, and 10).

Strombolian and violent Strombolian natural analogue eruptions from other igneous systems have been characterized as sporadic, consisting of periods of intermittent lava fountaining and fuming and, occasionally a few days of continuous violent Strombolian activity. Measurements of tephra-fall volume associated with such eruptions are documented in the literature (SNL 2007e, Appendices C and E) and have been used as case studies in atmospheric dispersal model validation activities.

The Quaternary Lathrop Wells volcano is the representative analogue for a future hypothetical eruption through the repository and provides the primary technical basis for description of the kind of igneous eruptive activity that could disrupt the repository (SNL 2007e, Section 1). The Lathrop Wells volcano retains many volcanic products and features of a young vent and, therefore, provides the best analogue of a potential eruptive center. It is the youngest example of the waning basaltic volcanism that characterizes the Yucca Mountain region (SNL 2007e, Section 1 and Appendix C). The Lathrop Wells volcano is interpreted as a complex monogenetic volcanic center, which produced a cone, lava flows, and tephra-fall deposit within a span of a few months or years (SNL 2007e, Sections C.5 and C.8.3).

The lower part of the Lathrop Wells Cone is composed of welded scoria typical of mild Strombolian activity, but the cone and tephra deposits have characteristics that indicate much of the eruptive style was violent Strombolian (SNL 2007e, Section 6.3.5.1 and Appendix C). The tephra-fall deposit from the Lathrop Wells volcano has been estimated to be 0.07 km^3. The total erupted volume is estimated to be 0.12 km^3, with 0.02 km^3 comprising the cone and 0.03 km^3 comprising lava (SNL 2007e, Appendix C).

The Fortymile Wash ash redistribution model uses a spatially-distributed Geographic Information System framework (SNL 2007g, Sections 1 and 6.2.2) to calculate the ash and associated waste transported to the RMEI location from the upper Fortymile Wash watershed by hillslope and fluvial processes. This redistributed and contaminated ash is combined with the primary contaminated ash (if any) that was deposited directly on the RMEI location during an eruption through some portion of the repository. Because of the prevailing wind direction, in the majority of the TSPA realizations the initial tephra deposit from ASHPLUME is directed away from the RMEI location. Therefore, in most realizations, the redistributed portion of the contaminated ash exceeds that which is deposited directly at the RMEI location. By explicitly modeling the primary ash fall and redistribution processes, the model directly computes the amount of contaminated ash (tephra) deposited directly at the RMEI location or transported to the RMEI location by fluvial processes (SNL 2007d, Section I1.1; SNL 2007g, Section 1).

2.3.11.4.1.1.1 Number of Waste Packages Intersected by Eruptive Conduits

As analyzed, an eruption through the repository includes localization of flow into 1-3 eruptive conduits that may intersect waste packages. The intersected waste packages are assumed to be damaged to the extent that they provide no protection for the contained waste (SNL 2007a, Section 8.2.3). Analogue information from volcanoes in the Yucca Mountain region is used to develop specific parameters such as number of dikes in a swarm, dike length and orientation, number and spacing of eruptive conduits or centers along a dike, and diameter of eruptive conduits (SNL 2007e, Table 7-1). These parameters are sampled from probability distributions, and realizations are generated that place dikes and conduits within the repository footprint. The number of waste packages intersected by an eruptive conduit is determined by the size of the conduit at repository depth, and whether or not it intersects a drift (Section 2.3.11.4.3.1).

2.3.11.4.1.1.2 Atmospheric Dispersal and Deposition of Tephra

In the conceptual model for the atmospheric dispersal and deposition of contaminated tephra, the volcanic eruption is preceded by (1) ascent of a basaltic dike through the earth's crust; intersection of the repository at Yucca Mountain; and (2) subsequent propagation of the dike to the ground surface. An eruptive conduit, or conduits, forms when a portion of the erupting dike begins to widen and provides a preferential pathway to focus magma flow to the surface. Physical damage to the waste package in this energetic conduit environment is assumed to provide a means for waste package failure and entrainment of fragmented waste (particle size 1 micrometer to 0.2 cm (SNL 2007d, Section 6.5.2.16)) within the rising magma.

These waste particles are suspended and well mixed with the magma, carried to the surface through the conduit, and erupted at the vent. The eruption typically involves several styles, including Strombolian and violent Strombolian activity (cone building and effusion of lava flows), and tephra sheet deposition; each of these eruptive styles might occur in multiple phases during the formation of a scoria cone volcano. For example, violent Strombolian activity in a volcano might occur as many phases during the months-to-years time scale during which a volcano is active. The atmospheric dispersal model abstraction assumes that the violent Strombolian eruption activity is adequately represented by modeling a single violent Strombolian phase (SNL 2007d, Section 5.1.1 and Table 5-1), with concurrent effusion of lava, construction of a scoria cone, and sustained eruption column. Over the course of the eruption, the waste incorporated into the magma (a well-mixed suspension) is deposited in various eruptive products: scoria cone, lava flows, and tephra blanket. The sustained eruption column produced by the violent Strombolian eruptive style deposits a tephra blanket that may result in dose to the RMEI and is the only eruptive process that is modeled for TSPA. Waste incorporated into the scoria cone and lava flows (50% to 90% of the waste released from waste packages (Section 2.3.11.4.1)) is part of geologically resistant landforms and is not considered to contribute dose to the RMEI because transport to the RMEI is not expected (Section 2.3.11.4.1.1.3).

Existing data are limited regarding the expected state of the waste particles resulting from a basaltic disruptive event and associated thermal, chemical, and physical effects, but an expected grain size distribution has been developed (0.001 mm to 2 mm) using a combination of the results of diverse analyses of degraded spent nuclear fuel (SNL 2007d, Section 6.5.2.16 and Appendix F). The model assumes that fine-grained waste particles are mixed directly into the magma prior to magma

fragmentation, and accounting is made for the proportion of waste-containing magma that is eventually deposited in geologically resistant eruptive products (scoria cone, lava flows) (SNL 2007d, Section 6.5.2.22) that do not contribute to dose. The waste particles within the magma are treated as refractory particles that form a component of tephra particles upon magma fragmentation (SNL 2007d, Section 5.1.3 and Table 5-1). For transport calculations, the combined ash/waste particles are modeled as density-corrected ash particles (SNL 2007d, Section 6.3).

A violent Strombolian eruption is characterized by the eruption of a high-speed column of pyroclast-waste particle mixture. The column consists of two regions. The lower region directly above the vent is called the gas-thrust region and flows upward due to its initial eruption momentum. The upper region of the column is called the convective-thrust region, in which the mixture rises by buoyant convection (Self and Walker 1994). The atmospheric dispersal model begins with the thermal and mass characteristics of the erupted material entering the convective-thrust part of the eruption column.

As the eruptive mixture rises in the plume of a violent Strombolian eruption, it entrains and heats air. This, in turn, reduces the bulk density of the mixture, and the plume becomes buoyant and continues to rise (SNL 2007e, Section 6.4). The plume rises to an altitude of neutral buoyancy compared to the surrounding atmosphere, where it spreads laterally as an anvil shaped cloud and is transported downwind. Tephra particles fall out from the vertical eruption column and from the anvil cloud according to their settling velocities. Such eruptions produce a tephra blanket of varying thickness extending tens of kilometers from the volcanic vent (SNL 2007d, Figure 7-1; Section 2.3.11.4.2.2.3). The thickness of the deposit (meters near the vent to millimeters 10's of kilometers downwind) depends on such factors as particle density, eruptive parameters, wind speed and direction, and distance from the vent (Suzuki 1983, p. 95).

2.3.11.4.1.1.3 Tephra Redistribution

The conceptual model for tephra redistribution has three main elements. First, proximal products of a potential volcano at Yucca Mountain, namely the scoria cone and lavas, are considered to be relatively immobile and therefore are not available for transport by fluvial processes to the RMEI location. This is supported by observations of Quaternary volcanoes in the Yucca Mountain region. The approximately 80,000 year old Lathrop Wells volcano has lava fields that are relatively uneroded; in fact, surficial processes at Lathrop Wells are dominated by accumulation of eolian sediment (SNL 2007e, Appendix C) rather than erosion of volcanic material and remobilization by sedimentary processes. The scoria cone at Lathrop Wells volcano has also experienced little erosion. This erosion is mainly focused in the upper part of the cone such that little if any cone scoria has yet been remobilized to the base of the cone where it would be available for fluvial transport. Only the fallout tephra from violent Strombolian eruptive phases has been variably remobilized and entrained into fluvial sediment (SNL 2007e, Appendix C). Two volcanoes that are ~350,000 years old (Little Black Peak and Hidden Cone) also show very little erosional modification of lava fields; their cone deposits have only been partially mobilized to form small aprons around the bases of the cones (SNL 2007e, Appendix D). However, no remnants of fallout deposits have been observed around these two volcanoes, which are inferred to have had similar eruptive styles as the Lathrop Wells volcano. This implies that the inferred tephra fallout deposits have been completely removed by erosion or buried beneath younger sediments. The five volcanoes in Crater Flat (Little Cones, Red Cone, Black Cone, and Makani volcano; 1.1 million years old) exhibit varying degrees of

erosion of their lava fields (SNL 2007e, Appendix E). The lava fields of two volcanoes in the southern part of Crater Flat (SW and NE Little Cones) have been buried by younger sediments. Makani volcano, in the northern part of Crater Flat, exhibits little erosional remobilization of its small lava field. At Red Cone and Black Cone volcanoes, in the central part of Crater Flat, lava fields south of the cones have abundant pyroclastic debris on their tops due to eruptive processes. This debris is rilled and channeled and has been partly remobilized into fluvial systems. Other lava fields associated with these two volcanoes have only minor erosion along their margins with little remobilization into fluvial systems. Scoria cones in Crater Flat are all highly eroded, but it appears that much of the cone scoria has been transported relatively small distances onto the surrounding lava fields and valley floor. Any remnants of inferred fallout tephra deposits have been removed by erosion and remobilization, or buried by later sediments. The observations summarized above support a conceptual model wherein the material that is most susceptible to fluvial remobilization and transport to the RMEI during the time period of interest is the fallout tephra produced by violent Strombolian activity. Therefore only the fraction of tephra from a potential eruption that might occur as violent Strombolian activity is dispersed downwind of the eruption site (SNL 2007d, Section 6.5.2.22) and considered to be available for remobilization.

The second element of the conceptual model for tephra redistribution is that remobilization of tephra depends upon hill slope gradient and that tephra mixes with channel sediments according to stream power of channels as it is transported down the Fortymile Wash upper drainage basin (Figure 2.3.11-13). For a given eruptive scenario realization, the atmospheric dispersal model predicts a spatial distribution of tephra thickness for deposits from violent Strombolian activity. The Fortymile Wash ash redistribution model simplifies the consideration of remobilization processes with an unambiguous criterion that if tephra is deposited on slopes steeper than a threshold slope, subsequent flood events will move that tephra into channels (SNL 2007g, Section 6.2.2). The threshold, or critical, slope is a model input parameter that is derived from combined erosion observations and slope measurements made at analogue sites near Flagstaff, Arizona (SNL 2007g, Section 6.5.2). Any slope or channel that is outside the Fortymile Wash upper drainage basin is excluded from the model, since it cannot contribute material to the RMEI. Once tephra has been remobilized into channels, it mixes with other channel sediments as it is transported downstream toward the alluvial fan environment of the RMEI location (SNL 2007g, Section 6.2.2). Mixing is determined by the depth of entrainment of channel bed sediments during flood events (the scour depth), which describes the depth to which the entrained channel sediments mix within the flood flow prior to redeposition downstream. The conceptual model implemented in the Fortymile Wash ash redistribution model accounts for the ensemble effects of tephra remobilization and transport by many flood events, rather than a single hypothetical flood event.

The third element of the conceptual model for tephra redistribution focuses on the disposition of contaminated tephra (mixed with sediment) once it reaches the Fortymile Wash alluvial fan (labeled as RMEI location Figure 2.3.11-13). This depositional setting is characterized by shallow distributary channels separated by inter-channel divides (SNL 2007g, Section 6.5.4 and Appendix A). The alluvial fan, while hosting sediment deposition, is modeled as an open system and therefore remobilized tephra can move through and beyond the RMEI area during large flood events. The tephra redistribution model partitions the RMEI location into two subdomains (channels and interchannel divides). Channels represent the area that is subject to active fluvial deposition and redistribution over the regulatory period. The fraction of the RMEI location that is treated as channels is controlled by a model input parameter. The divides are the remaining fraction

of the RMEI location that is not subject to fluvial deposition. A geomorphic map of the Fortymile Wash alluvial fan was generated and the relative areas of units deposited in the Holocene (channels) and Pleistocene (divides) are used as the basis for this fraction. Uncertainty in the geologic ages assigned to various units is translated into uncertainty in the range of the fraction parameter (SNL 2007g, Appendix A). The initial depth of tephra in the channels of the alluvial fan is equal to the scour depth at the fan apex and the concentration is calculated as the sum of direct volcanic fallout and the average concentration of the mobilized sediments leaving the upper drainage basin. On interchannel divides, tephra is only deposited by direct volcanic fallout (i.e., eruption plume directed toward the south), with no contribution from the remobilization and fluvial transport processes (SNL 2007g, Section 6.2.2). Each of these environments (channels and divides) is represented by a one-dimensional domain in which waste concentration with time is simulated. Once contaminated tephra are deposited on the Fortymile Wash alluvial fan (by fallout and/or fluvial processes), the radionuclides are able to migrate downward into the underyling soil. Thus the model provides a spatial distribution of radionuclide concentrations in the RMEI area.

The tephra redistribution model assumes that eolian transport of contaminated tephra to the RMEI location is negligible compared with the direct deposition and fluvial redistribution (SNL 2007g, Sections 1.2 and 5.2.2). The rationale for making this assumption is based on a number of observations. First, eolian transport processes would tend to reduce radionuclide concentrations near the surface at the RMEI location due to removal of contaminants from the ground surface and by further dilution and mixing with uncontaminated material. The reason for this is that the highest wind speeds (which dominate eolian transport) are generally directed to the north and northeast (SNL 2007g, Section 5.2.2), which means that the source of eolian deposition at the RMEI location is further from the repository and therefore less contaminated by the primary ashfall deposit. It is likely that some amount of contaminated tephra redistributed from the upper Fortymile Wash basin and deposited in the channels at the RMEI location would be transported by wind short distances on to the adjacent divides. While this process is not explicitly included in the tephra redistribution model, the consequence of this occurrence is included in the uncertainty range assigned to the parameter that defines the fraction of the RMEI location that is represented as active fluvial channels, which includes a relatively large upper bound. Based on a description of dilution of contaminated tephra on divides by burial beneath diluted (and redistributed) channel sediments (SNL 2007g, Section 7.3.2.1 Item 5, Response), eolian transport of contaminated tephra from channels to the divides at the RMEI location would result in the concentration profiles in the divides to be similar to that predicted in the channels. Based on consideration of the need to explicitly include eolian transport in the tephra redistribution model (SNL 2007g, Section 7.3.2.1, Item 3, Response), by increasing the fraction of the RMEI location that is represented as channels in some of the TSPA model realizations, the possible consequences of this eolian transport are effectively included.

2.3.11.4.2 Model/Analysis Description

[NUREG-1804, Section 2.2.1.2.2.3: AC 1(2), AC 2; Section 2.2.1.3.10.3: AC 1, AC 2(1) to (3); Section 2.2.1.3.11.3: AC 1), AC 2(1) to (3); Section 2.2.1.3.13.3: AC 1, AC 2]

The eruption modeling case includes intersection of the repository by a basaltic dike, localization of magma flow into one or more eruptive conduits within the repository, eruption, and entrainment of waste in the erupting material and atmospheric dispersal of contaminated tephra during a violent

Strombolian eruptive phase. The model case also includes redistribution of contaminated tephra by geomorphic processes that erode, dilute, and redistribute the contaminated tephra. The waste source term for the modeling is provided by an analysis of the number of waste packages intersected by eruptive conduits, which is provided as a distribution. This source term is multiplied by a sampled value for the magma partitioning factor (0.1 to 0.5) to limit the transported waste to that which is carried by the tephra cloud from violent Strombolian eruptive activity.

2.3.11.4.2.1 Number of Waste Packages Intersected by Conduits During an Eruption

The analysis of the number of waste packages intersected (hit) by conduits during an eruption (SNL 2007b, Section 7.1) produces a distribution of the number of volcanic conduits that are associated with a single volcanic event that affects the repository. Each conduit is assumed to create a cylindrical path through the repository, damaging any intersected waste packages (SNL 2007b, Section 5.2) and transporting waste to the surface. The distribution for number of waste packages intersected during an eruption ranges from zero to seven, with a most likely value of zero, because in most cases, a volcanic conduit intersects the rock pillars between drifts and no waste is transported out of the repository during the eruption (SNL 2007b, Section 7.2).

The TSPA parameters used in the calculation of the probability that conduits would intersect waste packages consist of: (1) the frequency of intersection of the repository footprint by an igneous event (mean value about 1.7×10^{-8} per year (BSC 2004a, Table 7-1)); (2) the conditional probability that a conduit would form within the repository footprint (0.28; SNL 2007b, Table 7-1); and (3) the conditional probability that a conduit intersects waste packages, which is calculated as 1 minus the probability that zero waste packages are intersected (SNL 2008, Section 6.5.2.2). The combined conditional probability that a conduit forms within the repository and intersects waste packages is $0.28 \times (1 - 0.703)$ or about 0.083 (SNL 2008, Section 6.5.2.2).

2.3.11.4.2.1.1 Formulation

A volcanic eruption could occur through the repository and result in the development of eruptive conduits. As described in Section 6.4 of *Characterize Eruptive Processes at Yucca Mountain, Nevada* (SNL 2007e), a potential eruption at the Yucca Mountain repository could proceed as follows:

1. A tabular dike penetrates vertically upward through the repository and reaches the surface.

2. Irregularities in the dike and/or the materials through which the dike travels promote the evolution of one or more cylindrical conduits.

3. The conduit transmits all material in its path upward to the surface. This material includes waste from failed packages if they are intersected by the conduit.

2.3.11.4.2.1.2 Analysis Parameters

The number of waste packages damaged by eruptive conduits is treated as a cumulative distribution function, dependent on the number of conduits, their diameters, and their locations on the dikes that

represent a single volcanic event. Accordingly, underlying distributions were developed for both the potential number of conduits and the variability in conduit diameter at the horizon of the repository. Distributions for the number of waste packages intersected by conduits are then developed considering numbers, locations, and sizes of conduits that could form (SNL 2007b, Section 6.3.2). Waste package dimensions and spacings, drift orientation and width, and distributions for dike length, orientation, thickness, and number of dikes in a swarm are considered. The distribution of conduit diameters is characterized by a minimum of 1 m, a mean of 15 m, and a 95th percentile value of 21 m (SNL 2007e, Table 7-1). The expected range of conduit diameters defined by the distribution is smaller than the distance between drifts (81 m) (SNL 2007f, Table 4-1, Parameter 01-13). Conduits are therefore expected to form more frequently between drifts, within the pillars, assuming that conduits are located randomly along a dike. If the conduit is located entirely within a pillar (the most likely location), no waste will leave the repository during the course of a volcanic eruption through the repository. The distribution for the number of conduits is provided as a probability distribution with the probability for one conduit of 0.85; two conduits of 0.10, and three conduits of 0.05 (SNL 2007e, Table 7-1). The spacing between conduits along the master dike is provided as a random uniform distribution with a minimum of 0.4 km and a maximum of 2 km (SNL 2007e, Table 7-1).

Field observations indicate that subsurface intrusions beneath monogenetic volcanoes in the Yucca Mountain region may consist of one to five vertical or subvertical basaltic dikes that form a parallel swarm. In the two observed cases where there are multiple dikes, East Basalt Ridge and Paiute Ridge (SNL 2007e, Appendix F), only one of the dikes hosts eruptive conduits. This "master dike" is also wider than most other dikes in the swarm and in detail might branch into several very closely spaced dikes (separation distances measured in meters) in the uppermost tens of meters beneath the surface and might also consist of several en echelon segments.

For the volcanic eruption modeling case it is necessary to have a model for location of a conduit(s) along a master dike, in the event that the subsurface feeding system (dikes) intersects the repository footprint. The following alternative models could be used:

1. Conduit location is random along the master dike. Model 1 implies that there is no geologic reason for a conduit to be more likely to form anywhere along a dike, nor is there any reason that the repository itself would affect conduit location in any way.

2. Conduit location is preferentially focused toward certain parts of the master dike (e.g., at the ends of a dike, or in the middle). Model 2 implies that there are geological reasons to expect a conduit to form in certain locations along a master dike, but that the repository has no additional impact on conduit formation.

3. Conduit location preferentially occurs within or outside the repository footprint. Model 3 implies that the presence of the repository as a whole (including drifts, pillars) would influence the formation of conduits.

4. Conduit location preferentially occurs where a dike intersects a drift. Model 4 implies that it is the individual drifts that would affect conduit formation, rather than the repository as a whole.

5. Some combination of the above (for example, there might be a "background" probability that a conduit will be randomly located along a master dike, but with additional weighting to increase the probability that it would form within the repository footprint). Model 5 implies that both geological reasons and the presence of the repository have an affect on conduit formation.

Field observations (SNL 2007e, Table F-1) of basaltic volcanic centers in the Yucca Mountain region that are sufficiently eroded to allow mapping of feeder dikes and conduits suggest that some conduits form along the central part of the master dike's length, while others form near the ends. Based upon this small data set, the approach in model 2 is not justified. Modeling by Gaffney and Damjanac (2006) does indicate that if an ascending dike intersects variable surface topography, then conduit formation is most likely to be focused at the lowest point on that topography rather than at the higher points. However, the likely trends of dikes in the Yucca Mountain block (SNL 2007e, Table 7-1) are parallel or subparallel to the linear ridge-type topography, therefore it is unlikely that an ascending dike would intersect significantly lower topography along its length (mean length of ~2 km (SNL 2007e, Table 7-1)) that would favor conduit formation at a point in a predictable way. This reasoning, based upon field analogue and modeling, therefore suggests that the approach of model 2 is not justified (nor, by implication, model 5).

Most of the repository footprint (at least 90%) will be within intact host rock. This is because the drifts, with their diameters of 5.5 m, will be separated by 81 m wide pillars (SNL 2007f; Section 1.3.1) of unmined rock. Studies reported in *Dike/Drift Interactions* (SNL 2007a, Section 6.2.3) show that the state of stress within the pillars will be unaffected by the excavation of drifts except within a distance of ~3 drift radii of the drifts. During the initial period of ~2,000 years the repository block would experience heating due to radioactive decay of waste. Heating of the host rock would affect the state of stress within the repository block. However, analyses in *Dike/Drift Interactions* indicate that while dike propagation might be slowed due to the heat-related stress field, the dominantly vertical propagation direction of dikes would be unaffected. Analogue studies indicate that conduits grow downward from the intersection of their feeder dikes with the earth's surface (SNL 2007e, Appendix F). Because ascending dikes would not have their propagation paths affected by the presence of the repository as a whole, and conduits form from the surface downward, the repository footprint in the broad sense would be unlikely to impact conduit formation. This suggests that there would be no basis for using the approach in model 3.

In detail, the stress field and magma flow field in proximity to an intersected drift might have roles in conduit formation. This is because an open drift is a stress void and a sink for ascending magma, and because the rocks within ~3 drift radii have an altered state of stress compared to more distant rocks. Modeling in *Dike/Drift Interactions* indicates that the magma front in an ascending dike would be slowed compared to the rise speed of the magma front in the centerline of a pillar. This slowing is caused by the diversion of magma into the open drift. Once the drift is filled, the magma front would continue on its upward trajectory. Therefore the magma front would be expected to reach the earth's surface above a pillar centerline before the magma front directly above a drift reaches the surface. Because the overall upward path of dike propagation does not consider the presence of a drift (SNL 2007a, Section 6.3.6), and because conduits grow from the surface downward, it is expected that an individual drift would not affect conduit location. Thus an approach such as that in Model 4 seems unwarranted.

The above arguments support a model wherein the location of a conduit along a master dike is simply treated as random (note that if more than one conduit forms, conduit spacing rules are also used).

In the analysis, the number of waste packages intersected by an eruptive conduit is estimated by considering the conduits as "cookie cutters" (Figure 2.3.11-14) (SNL 2007b, Sections 5.2 and 6.3.2.2). In this method, for drifts intersected by conduits, the number of waste packages within, or partially within, the conduit outline are considered to fail and become entrained within the eruptive conduit (SNL 2007b, Section 5.2).

2.3.11.4.2.1.3 Results

The result of the conduit intersection analysis for the number of waste packages intersected is provided directly to TSPA through a tabulated cumulative frequency distribution (SNL 2007b, Section 7.1 and Table 7-1) shown in Figure 2.3.11-12b. Because a conduit forming within the repository is not expected to intersect a drift (approximately 90% of the repository area is comprised of pillars), the median number of waste packages intersected by eruptive conduits is zero and no waste is transported into the atmosphere by the eruption (SNL 2007b, Section 7.2).

The results of the analyses indicate that the proportion of intersections in which eruption within the repository footprint would occur is 0.28 (Section 2.3.11.4.2.1; SNL 2007b, Section 7.2). This value, the eruptive center probability (SNL 2007b, Table 7-1), is less than 1 because a conduit can form at any location on a dike and therefore would not necessarily form within the repository (Section 2.3.11.1). The value for the eruptive center probability primarily depends on the distribution for the number of dikes in a swarm (probability of 0.6 of more than one dike (SNL 2007b, Table 4-1, Row 13)), the distribution for number of conduits in an event (probability of 0.85 of only one conduit (SNL 2007b, Table 4-1, Row 15)) and their spacing (SNL 2007b, Section 5.3), and the observation that conduits only form on the thickest dike of a dike swarm (SNL 2007b, Section 5.4). Given the above event characteristics, a conduit is more likely to form outside, rather than inside, the repository if the repository is intersected by a dike swarm.

2.3.11.4.2.2 Atmospheric Dispersal and Deposition of Tephra

The conceptual model for the eruption, atmospheric dispersal, and deposition of waste-containing tephra simulates a violent Strombolian eruption (SNL 2007d, Section 5.1.1 and Table 5-1). This conceptual model is implemented in the mathematical model that underlies the ASHPLUME code.

The ASHPLUME code is based on a two-dimensional diffusion model in which only horizontal turbulent diffusion is considered. The movement of air in the atmosphere is relatively random due to the many eddy currents that exist (Suzuki 1983, p. 96), and as a result, the movement of particles within the air mass is treated as random. Particles diffuse in the atmosphere in both vertical and horizontal directions, but because the scale of horizontal turbulence is much greater than the scale of the vertical turbulence (Suzuki 1983, pp. 96 to 98), horizontal diffusion is the dominant factor in determining the width of a plume as it moves downwind. Therefore, ASHPLUME is based on a two-dimensional diffusion equation in which only horizontal turbulent diffusivity is considered (SNL 2007d, Section 6.31).

Under these violent Strombolian conditions, most particles rise to near the top of the plume before dispersal downwind (SNL 2007d, Section 5.2.3). This aspect of the conceptual model is implemented by using parameter values whereby the majority of erupted material is dispersed from the upper half of the column (SNL 2007d, Section 5.2.3). ASHPLUME models a steady-state column (plume) instantaneously loaded with particles moving at some upward velocity. ASHPLUME stipulates that the convective rise velocity of tephra particles decreases linearly from the initial rise velocity at the base of the plume to zero at the top of the plume. The initial rise velocity of tephra particles in the plume is consistent with the minimum velocity required to provide the modeled thermal power (i.e., minimizing momentum from the gas thrust region of the column) (SNL 2007d, Section 5.2.5).

2.3.11.4.2.2.1 Formulation

The ASHPLUME software code is integrated within the TSPA through a dynamically linked library (DLL) called within the GoldSim performance assessment code (SNL 2007d, Section 1.2.1). Suzuki (1983) originally developed a mathematical formulation for atmospheric dispersal of tephra from a volcanic eruption. Jarzemba et al. (1997, pp. 132 to 141) adapted ASHPLUME to include the incorporation of waste particles with tephra particles (SNL 2007d, Section 6.5). The source term for radionuclides in the contaminated tephra comes from the separate analysis of the number of waste packages intersected by eruptive conduits during a hypothetical eruption through the repository (Section 2.3.11.4.2.1.3). In subsequent sections the terms "fuel" and "waste" are used interchangeably.

As stated in Section 2.3.11.4.2.2, the atmospheric dispersal mathematical model accounts for horizontal turbulent diffusion of particles in a laterally-advecting plume (SNL 2007d, Section 6.5.1). Particle movement in the vertical direction is accounted for by settling velocity in the Suzuki (1983) model (SNL 2007d, Section 6.5.1). Particle deposition from the column and downwind plume is defined by a probabilistic model that balances upward momentum and settling velocity. The duration of transport is the fallout time for the particles and is a function of the terminal fall velocity (SNL 2007d, Section 1.3.1).

The mathematical formulation of the atmospheric dispersal model (SNL 2007d, Section 6.5.1) includes:

- The areal concentration of accumulated tephra and waste as a function of the total mass erupted
- Probability density distribution function for particle diffusion (based on particle terminal velocity)
- Particle density (combined value for tephra and waste)
- Particle fall time
- Height of eruption column (based on eruptive power)
- Atmospheric characteristics (e.g., air viscosity and density)

- Wind speed and direction
- Particle size distribution
- Waste incorporation ratio
- Fuel fraction.

The transported fraction of available waste ("fuel" fraction) is derived from the particle size distributions of tephra and waste and the waste incorporation ratio. The fuel fraction is calculated by summing the incremental contributions of the fuel mass to the volcanic tephra mass using the waste incorporation ratio as a control on the waste-to-tephra particle size comparison. The density of the combined tephra-waste particles is adjusted to account for the presence of the high-density waste. To determine the mass of waste deposited at a particular location, the main model equation that calculates tephra distribution (SNL 2007d, Eq. 6-2) is multiplied by this fuel fraction term and re-integrated by particle size and eruption column height (SNL 2007d, Section 6.5.1).

2.3.11.4.2.2.2 Model Parameters

Key parameters in the atmospheric dispersal model are described in *Atmospheric Dispersal and Deposition of Tephra from a Potential Volcanic Eruption at Yucca Mountain, Nevada* (SNL 2007d, Section 6.5.2) and are summarized as follows:

Eruption Parameters—Parameters describing the eruption process include power, duration, initial rise velocity, and column diffusion constant. The eruptive column height is calculated from the input value for eruptive power within the ASHPLUME code. Eruptive column height, in turn, defines the altitude at which wind speed and direction conditions are sampled for a given realization. The eruptive power and duration parameter ranges are derived from observations at analogue volcanoes (SNL 2007d, Table 6-4; SNL 2007e, Table 7-1). The range for eruptive power is defined as log-uniform, ranging from 10^9 to 10^{12} W (SNL 2007d, Section 6.5.2.1). The duration of a single explosive phase constituting a violent Strombolian eruption ranges from 18 hours to 75 days (SNL 2007e, Table 7-1). The actual limits on the range of eruption duration used in each TSPA model realization are established at run-time (SNL 2007d, Section 8.2), such that the total volume of the eruption remains within the bounds established from analogue volcanoes in the Yucca Mountain region (SNL 2007e, Table 7-1). The initial rise velocity parameter defines the velocity at the base of the convective thrust portion of the eruption column. The minimum practical value for initial rise velocity (0.01 m/s) is defined for magma ascent velocity below the fragmentation depth (SNL 2007d, Section 6.5.2.10). The maximum value (100 m/s) reflects the upper end of possible velocities of the plume as it transitions from the gas-thrust to convective rise portions of the plume (SNL 2007d, Section 6.5.2.10). This parameter range is defined as a uniform distribution (SNL 2007d, Section 6.5.2.10).

The column diffusion constant (β) parameter affects the distribution of particles vertically in the eruption column and determines where particles exit the plume. The values for β, which are unitless, are defined as a range with a minimum value of 0.01 and a maximum value of 0.5 (SNL 2007d, Section 6.5.2.3). To properly simulate the anvil-shaped cloud associated with a violent Strombolian eruption, a uniform distribution of values for β is used (SNL 2007d, Section 6.5.2.3).

Tephra and Waste Particle Parameters—The size, shape, and density of tephra and waste particles are defined by several parameters. The size distribution for tephra particles is defined by the mean ash particle diameter and ash particle diameter standard deviation statistics. The mean ash particle diameter is defined as a log-triangular distribution with a minimum value of 0.001 cm, a mode value of 0.01 cm, and a maximum value of 0.1 cm (SNL 2007d, Section 6.5.2.4), which is representative of tephra deposits from the Lathrop Wells volcano and other violent Strombolian analogue volcanoes. The ash particle diameter standard deviation is treated as a uniform distribution of 1 to 3 phi (φ) units, based on analogue eruptions at Cerro Negro, Tolbachik, and Etna (SNL 2007e, Section 6.3.5.1). Phi (φ) units are defined to be the negative logarithm in base 2 of the particle diameter in millimeters (SNL 2007d, Section 6.5.2.5).

A waste particle size distribution (minimum 0.0001 cm, mode 0.0013 cm, maximum 0.2 cm) has been developed using a combination of the results of diverse analyses of degraded SNF (SNL 2007d, Section 6.5.2.16 and Appendix F). Waste mass is treated as a log-triangular distribution with particle size in the atmospheric dispersal model. For the purpose of estimating waste particle diameters in the eruptive environment, the waste is assumed to be unaltered commercial SNF (SNL 2007d, Section 5.2.4).

A limitation of ASHPLUME is its inability to accurately represent the transport of tephra particles of mean diameter less than approximately 0.0015 cm because atmospheric turbulence tends to retard settling of these small particles. However, the typical mean diameter of tephra particles after an eruption is generally much larger than 0.0015 cm, and the model tends to overpredict settling of particles less than 0.0015 cm in diameter in the vicinity of Yucca Mountain (SNL 2007d, Section 1.3.1).

In violent Strombolian eruptions, transport and deposition of pyroclasts depends on their settling velocities in air, which, in turn, depends on their shapes and bulk densities (the melt density corrected for the porosity, or vesicularity, of the clasts). The ash particle shape factor is given a constant value of $F = 0.5$, for $F = (b + c)/2a$, where *a, b,* and *c* are the lengths of the longest, medium, and shortest axes of the clasts (SNL 2007d, Section 6.5.2.12). The density of tephra particles is a function of magma density and particle size. Assuming a Lathrop Wells-type magma, the magma density would be 2.6 g/cm^3 (SNL 2007e, Section 6.3.5.2). For tephra particles less than or equal to 0.001 cm, tephra particle density is 80% of the magma density, or 2.08 g/cm^3. For particles greater than or equal to 1.0 cm, particle density is 40% of the magma density (SNL 2007e, Section 6.3.5.2), or 1.04 g/cm^3 (SNL 2007d, Section 6.5.2.11). Particle density varies linearly for particles with diameters between 0.001 cm and 1.0 cm. It is important to note that the densities apply to a range of particles sizes, defined by $f(\rho)$, the distribution function for particle log diameters in the atmospheric dispersal model (SNL 2007d, Section 6.5.1). The density of the combined tephra-waste particles is corrected for the presence of waste.

Areal ash densities can be converted to deposit thickness by dividing the areal density by the value of settled (deposit) density, referred to as the ash settled density (SNL 2007d, Section 6.5.2). The value used for ash settled density ranges from 300 to 1500 kg/m^3 with a mean of 1000 kg/m^3 (SNL 2007e, Table 7-1); a standard deviation of 100 kg/m^3 is chosen based on expectations that the value will be near 1000 kg/m^3 (SNL 2007e, Section 6.3.5.3 and Table 7-1).

The waste incorporation ratio parameter enables the mathematical combination of tephra and waste particles within the ASHPLUME code for transport purposes. This parameter determines the fuel fraction (ratio of waste mass to tephra mass) in the erupted tephra, which is used to calculate the concentration of waste deposited on the ground in a given model realization (SNL 2007d, Section 6.5.2.6). Flow dynamics within the magma in the drift and conduit prior to eruption are assumed to produce a well-mixed (homogeneous) suspension of waste particles throughout the magma. At the vent, the waste-containing magma erupts to produce various deposits (scoria cone, lava flows, and tephra blanket), and the portion destined for the tephra blanket is fragmented and becomes entrained in the buoyant plume. In this conceptual model the waste is already incorporated into the melt prior to magma fragmentation, and the mathematical formulation of waste incorporation ratio is used by prescribing a neutral value (zero) for the waste incorporation ratio, which allows waste particles to combine with tephra particles of the same size or larger. Thus, the waste particles can be treated as refractory "xenoliths" in the melt, which, upon magma fragmentation, will reappear in the tephra as mixed particles of waste and silicate melt (glass). The constant value for waste incorporation ratio is 0 (that is, the ratio of the particle sizes is 1) (SNL 2007d, Section 6.5.2.6).

Atmospheric and Wind Parameters—The transport of tephra by diffusion and advection in the ASHPLUME code is controlled by several parameters, including eddy diffusivity constant, air density and viscosity, and wind speed and direction. The constant (C) controlling eddy diffusivity relative to particle fall time was modeled by Suzuki (1983, pp. 98 and 99) and is used in the mathematical model to determine the areal density on the ground. A constant value for C equal to 400 $cm^2/s^{5/2}$ is defined for the ASHPLUME code (SNL 2007d, Section 6.5.2.15).

Air density and viscosity are used to calculate particle settling velocity. Values of 0.001734 g/cm^3 and 0.000185 g/cms, respectively, are specified, based on tables of physical data (Lide 1994, pp. 6-1 and 6-239; SNL 2007d, Sections 6.5.2.13 and 6.5.2.14).

Values for wind speed and direction for each model realization are sampled from the probability distribution functions that characterize conditions at the elevations at the top of the eruption column. In any given calculation, wind speed is sampled from a distribution of wind speeds from near zero to maximum wind speeds observed at altitudes up to 13 km. For modeling purposes, wind speed and wind direction are assumed to be constant during an eruption (SNL 2007d, Section 5.2.2). Over the course of multiple model runs, the entire distributions for wind speed and direction are sampled.

The stochastic treatment of wind speed and wind direction produces results that capture the uncertainty that exists in future wind speeds at the altitudes of the vertical eruptive column and reflects the wind directions actually observed. The consideration of wind speed and direction is reasonable, given the relatively short duration of violent igneous eruptions that have been recorded (SNL 2007d, Section 5.2.2). This representation is considered to be a reasonable characterization of wind conditions in future climates. The magnitude of short-term variability in meteorological phenomena is great compared to changes in long-term averages. Modeling demonstrates that wind speeds and directions in the southwestern United States did not vary significantly during the transition from glacial to interglacial climates. The largest changes, which occurred during full glacial conditions 18,000 years ago according to a general circulation model (Kutzbach et al. 1993, Figures 4-14 and 4-15), support a decrease in the relative frequency of winds blowing toward the RMEI location south of Yucca Mountain. Consequently, the stochastic approach used in the TSPA

captures variability in present short-term wind conditions and is considered to be a reasonable characterization of variability in future conditions (SNL 2007d, Section 5.2.1).

The National Oceanic and Atmospheric Administration provided wind speed data for the Desert Rock Station (NOAA 2004), located approximately 40 miles east of Yucca Mountain. After converting data for the altitude above mean sea level to the altitude above Yucca Mountain, the converted data were grouped into 1 km increments from 0- to 13-km altitude. The wind speed data for each height interval were then used to calculate cumulative distribution functions at 100 cm/s intervals. (SNL 2007d, Section 6.5.2.7 and Appendix D)

The National Oceanic and Atmospheric Administration (NOAA 2004) data described above also provide the source for the distribution of wind directions for the tephra transport model. The wind direction data for each height interval are used to calculate probability distribution functions and associated wind rose diagrams at 30° intervals (Figure 2.3.11-15).

Mass of Waste Available for Incorporation—The mass of waste available for incorporation into tephra is an input for each atmospheric dispersal model run. The waste mass depends upon factors such as waste inventory and the number of waste packages damaged during an eruption. These factors are calculated within GoldSim from the number of waste packages intersected by conduits, the radionuclide inventory of a waste package, and the magma-partitioning factor (see below). The resulting waste mass available is passed to ASHPLUME at run time (SNL 2007d, Section 6.5.2.9).

Magma Partitioning Factor—The model of the eruption column, downwind transport, and tephra deposition assumes that violent Strombolian eruptive activity dominates, and it considers only the portion of the eruption products that is transported aerially away from the vent (SNL 2007d, Section 5.1), thereby excluding the volume of magma and waste incorporated into the scoria cone and lava flows. The input parameter values for the atmospheric dispersal model are based on estimates of eruptive style and tephra volumes in the Yucca Mountain region, especially the Lathrop Wells volcano, which is the youngest and best preserved of the scoria cones in the region (SNL 2007e, Section 6.3.3.1). The Ashplume model of the eruption column, ash dispersal and ash deposition assumes that violent Strombolian activity dominates, and the model considers only the portion of the eruption products that are transported aerially away from the vent (SNL 2007d, Section 6.5.2.22). Therefore, the mass of waste available for magmatic transport due to waste package failure must be reduced by a factor that reflects the proportion of waste-containing magma that is erupted to form the scoria cone and lava flows (SNL 2007d, Section 6.5.2.22). This reduced mass of waste (mixed with magma) is then provided to ASHPLUME for transport and deposition in the tephra sheet.

Model Configuration Parameters—ASHPLUME requires several other input parameters to control code operations that are not directly related to the mathematical model described in this section. These parameters are computational grid locations, maximum particle diameter for transport, minimum height of eruption column considered in transport, and threshold limit on tephra accumulation (SNL 2007d, Section 6.5.2).

2.3.11.4.2.2.3 Results

The atmospheric dispersal model calculates the distribution of tephra and waste in terms of areal concentration (g/cm^2). For a typical set of ASHPLUME input values, the tephra is distributed in a east- to north-east-directed blanket extending downwind from the eruptive vent (Figure 2.3.11-16). In the example ASHPLUME result shown in Figure 2.3.11-16, midpoint values were chosen for distributed (stochastic) parameters: eruptive power = 2×10^{11} W, eruption duration = 1.5 days, eruption column height = 6 km, wind speed = 713 cm/s. In this example, the region blanketed with at least 10 cm of ash extends 13 km downwind, and the region covered by at least 1 cm of ash extends 35 km downwind. The distribution of waste on the landscape follows that of tephra; in this example, the concentration of waste at a given point is 6 orders of magnitude lower than the concentration of tephra.

The Ashplume model for airborne transport is integrated with the TSPA through a DLL called within the GoldSim performance assessment code. The ASHPLUME code is called twice in each TSPA realization; the first call calculates the primary tephra and waste deposition for a single point at the RMEI location, and the second call calculates the distribution of tephra and waste in the Fortymile Wash watershed, using many grid points (SNL 2007d, Section 6.0). The results of these two atmospheric dispersal model runs provide input to the tephra redistribution model within TSPA.

2.3.11.4.2.3 Tephra Redistribution

Because the prevailing winds in the Yucca Mountain area are directed toward the northeast (SNL 2007d, Appendix K, Section K-1), most ASHPLUME realizations will result in little if any contaminated tephra deposited directly on the RMEI. However, any such tephra that is deposited in the Fortymile Wash drainage basin could be remobilized and transported to the RMEI location by hillslope and fluvial processes. The Fortymile Wash ash redistribution model is designed to predict the concentration of remobilized, contaminated tephra at the RMEI.

2.3.11.4.2.3.1 Formulation

The main elements of the Fortymile Wash ash redistribution model are described below: (1) tephra mobilization after initial deposition by fallout of aerially dispersed tephra; (2) tephra transport and mixing; (3) characteristics of the Fortymile Wash alluvial fan in the vicinity of the RMEI location; and (4) deposition of mixed tephra and radionuclide migration from the mixed deposits into underlying soils at the RMEI location. Item 4 is the end result of the eruptive scenario and provides input for biosphere calculations of potential dose to the RMEI.

Tephra Mobilization—The tephra redistribution model calculates the mass and concentration of tephra and waste transported from the upper drainage basin to the RMEI location by hillslope and fluvial processes. This is accomplished within the model using a spatial analysis of a digital elevation model that represents the upper basin. The model assumes that primary fallout is mobilized and transported downstream toward the RMEI location if it falls on steep slopes or on active channels (SNL 2007g, Section 6.2.2), that connect to the main channel in the Fortymile Wash. The model performs a series of geographic calculations using as inputs a 30 m digital elevation model of the upper drainage basin and grids of primary tephra and waste deposited (mass per unit area) provided by the ASHPLUME model. The tephra redistribution model first

interpolates the primary tephra and waste grids from ASHPLUME to the scale of the digital elevation model and then performs a series of calculations aimed at classifying whether tephra in each digital elevation model grid cells will be mobilized. These include: (1) calculating local slope angles for comparison with the critical slope angle; (2) calculating contributing area using a divergent flow algorithm (Freeman 1991); and (3) identifying channel networks by comparing stream power (product of the slope angle and square root of contributing area) to a threshold defined as $1/X$, where X is the drainage density, which is provided as a model input parameter. Tephra is mobilized if it is initially deposited in grid cells with a slope greater than the critical slope or in cells classified as part of the channel network (stream power is greater than $1/X$). Next, the model performs calculations aimed at estimating the concentration and thickness of tephra (and waste) in the channels of the RMEI location. These calculations include estimating scour depth in every channel cell in the upper basin and then routing tephra (and clean sediment) between the surface and the scour depth in grid cells where tephra is mobilized. As tephra and clean sediment is routed through the channel network mixing occurs along the way and the resulting tephra concentration at a single grid cell near the alluvial fan outlet is used to calculate the concentration in the channels at the RMEI location. These calculations are described in more detail in the sections that follow.

Tephra Transport and Mixing—Before the mobilized tephra and waste are deposited at the RMEI location, they are transported through the alluvial channel system of the upper drainage basin where mixing with uncontaminated channel sediments leads to dilution. Mixing occurs during flood events as sediment and tephra are entrained from the bed, mixed by turbulent flow, and redeposited on the bed. The depth to which tephra and channel sediment are mixed is the scour depth as estimated from major flood events. This mixing depth is proportional to the square root of unit discharge (SNL 2007g, Section 6.3.3). The dilution factor at each point (i.e., the fraction of channel sediment composed of tephra in each channel grid cell) is calculated using the local thickness of mobilized tephra and the local scour depth. Tephra is routed downstream from locations of primary fallout using a divergent flow (bifurcation routing) algorithm (Freeman 1991). The same technique is also used to route grid-cell area in order to calculate contributing area. The ratio of the routed tephra thickness to the routed scour depth at the fan apex, which is defined as a particular channel grid cell just upstream from the RMEI location, is used to determine the fraction of channel-bed material composed of tephra when the redistributed tephra and waste reach the RMEI location (SNL 2007gSection 6.3.3).

Characteristics of the Fortymile Wash Alluvial Fan at the RMEI Location—At the RMEI location, the model partitions the fan into two subdomains, channels and inter-channel divides. In the natural system, the fan is composed of a complex suite of "terraces" that result from episodes of aggradation, incision, and lateral channel migration. Soil geomorphic mapping has been performed to group these terraces into two types: inter-channel divides that have not been subject to fluvial erosion and deposition for the last 10,000 years or longer, and channels that have been subject to erosion and deposition over the last 10,000 years (including both active channels and Holocene age terraces that may be reoccupied over the next 10,000 years) (SNL 2007g, Section 6.2.3 and Appendix A).

On inter-channel divides, waste is considered to be deposited only from primary fallout. Tephra and waste redistributed from the Fortymile Wash drainage basin cannot be deposited on divides because divides, by definition, have not been subject to fluvial erosion or deposition for at least 10,000 years.

In channels, the initial waste concentration includes the primary fallout as well as the waste redistributed from the Fortymile Wash drainage basin. Both of these components are mixed with channel sediments by fluvial scour and redeposition (SNL 2007g, Section 6.2.3 and Appendix A).

The active channels on the alluvial fan are not expected to provide a perfect depozone during large floods. Instead, a portion of the tephra transported from the upper drainage basin (particularly the silt-sized "wash load" fraction of the tephra and waste) is expected to be transported past the RMEI area into the Amargosa River (SNL 2007g, Section 5.2.3). The tephra redistribution model treats the RMEI location as an open system with respect to sediment deposition, allowing throughflow of tephra and waste (SNL 2007g, Section 5.2.4). In most realizations, the fluvial component of the model mixes and deposits the material at the RMEI location instantaneously, capturing maximum concentrations (SNL 2007g, Section 5.2.1).

Deposition of Mixed Tephra and Radionuclide Diffusion—The spatially distributed model of tephra redistribution in the upper basin is assumed to transport diluted tephra and waste to the RMEI location instantaneously following the eruption (SNL 2007g, Section 5.2.1). In reality, such transport would be delayed until sufficient flood events are able to transport the material, but the assumption is considered necessary because otherwise the model would have to simulate time-dependant future flood events, which is impractical. The essential purpose of the spatial analysis performed in the upper basin is to estimate the initial thickness and concentration of the contaminated tephra deposited in the two subdomains representing the RMEI location. In the channel subdomain, the model assigns the thickness and tephra (and waste) concentration to be equal to the scour depth and tephra (and waste) concentration at the fan apex (SNL 2007g, Sections 6.2.2, 7.1.3, and 7.2.5), which are calculated by the model. The fan apex is a reasonable location for estimating these quantities for the RMEI location channels because there are no major tributaries on the alluvial fan, which might cause scour to increase, resulting in greater dilution. In the divides subdomain, the model assumes that the only source of tephra and waste is from primary deposition from the ash fall and the initial thickness and concentration is taken directly from ASHPLUME model results. Following the instantaneous transport to the RMEI location, the tephra redistribution model estimates the time-dependent vertical migration of radionuclides via suspension and redeposition of fine particles by infiltrating water, and physical mixing of soil particles by freeze-thaw cycles and bioturbation. The model estimates this complex transport with a one dimensional diffusion submodel. This representation is supported by analogue studies that have shown that over time, radionuclides deposited on the ground surface establish a concentration profile that is very similar to that predicted by a diffusion model (e.g., Pelletier, Harrington et al. 2005).

Diffusion is modeled to occur within an active layer whose thickness corresponds to the depth of carbonate and clay-rich soil horizons with reduced permeability compared to the active zone. Soils in arid environments develop a petrocalcic horizon by solution and reprecipitation of calcium carbonate over time scales of tens to hundreds of thousands of years (Machette 1985). Deposition of calcium carbonate at depth in the soil decreases permeability locally forming a boundary beneath the active layer (SNL 2007g, Section 6.2.2). Field observations from the alluvial fan were used to estimate appropriate values and uncertainties for this depth (SNL 2007g, Section 6.5.5).

The diffusivity values vary between the divide and channel. Diffusion within the channel is likely to occur faster because of the higher permeability of channel bed sediments (which increases the

rate of fine particle transport by suspension and redeposition) and the additional physical mixing of sediments that can occur by freeze-thaw cycles and bioturbation (SNL 2007g, Section 6.2.2). The diffusivity values and uncertainties used by the model are estimated by fitting ^{137}Cs concentration profiles measured in the soils at the site to the diffusion model (SNL 2007g, Section 6.5.8).

2.3.11.4.2.3.2 Model Parameters

Key parameters in the Fortymile Wash ash redistribution model are as follows:

- **Digital Elevation Model of the Fortymile Wash Drainage Basin**—The tephra redistribution model requires a grid of elevation values (in meters) for the Fortymile Wash drainage basin. To meet this need, a 30-m resolution digital elevation model (SNL 2007g, Section 6.5.1) was created by merging U.S. Geological Survey 7.5 minute quadrangle digital elevation models that cover the entire drainage basin. This digital elevation model also includes a "mask" that defines the watershed.

- **Critical Slope**—The critical slope is reported as the elevation change over the horizontal distance. It represents the steepest stable slope for tephra-blanketed hillslopes. The critical slope field measurements at analogue sites were made to determine the slope angle below which tephra is not remobilized, based on observed indicators for tephra mobilization such as incipient rilling and debris lobes. Values for critical slope are taken to be a uniform distribution between 0.21 and 0.47 (SNL 2007g, Section 6.5.2).

- **Drainage Density**—The drainage density is defined as the total length of channels in a basin divided by the basin area (SNL 2007g Section 6.5.3). To account for uncertainty in the drainage density value through time, a uniform range of values from 20 per km to 33 per km is used in TSPA. This distribution was determined by model calibration to field observations (SNL 2007g, Section 6.5.3).

- **Area of Fortymile Wash Alluvial Fan**—This parameter refers to the depositional area (km^2) of the upper Fortymile Wash alluvial fan. It represents the area bounded by the large mid- to late-Pleistocene terraces on either side of the active fan. The value for area, A, is a single value of 33 km^2 (SNL 2007g, Section 6.5.4.1).

- **Channel Area Fraction**—This parameter defines the fraction of the Fortymile Wash alluvial fan (representing the RMEI location) that is subject to active fluvial deposition. This fraction is estimated as the fraction of the fan area composed of surfaces (channels and terraces) younger than 10,000 years. Significant uncertainty in the exact age of the surfaces on the fan translates into uncertainty in this fraction, which is represented as a uniform distribution from 0.09 to 0.54 (SNL 2007g, Section 6.5.4).

- **Permeable Depth on Divides**—The permeable depth (cm) on the divides, L_d, defines the vertical extent of the subdomain for the one dimensional diffusion calculation. Determination of the parameter, L_d, was made from field measurements on soil pits dug into inter-channel divides of the Fortymile Wash alluvial fan. The depth to the petrocalcic horizon was measured at each soil pit, and a range of depths was recorded to provide data for L_d. The permeable depth was assumed to coincide with the top of the stage-IV

carbonate development in the soil pit. Stage-IV carbonate development refers to the presence of a platy, continuous laminar cap and carbonate matrix that cements the gravel and results in very low soil permeability (SNL 2007g, Section 6.5.5.1). The oldest (Qa3) surface was encountered at a reasonably consistent depth, and the value for the parameter L_d is a uniform distribution between 102 cm and 140 cm (SNL 2007g, Section 6.5.5.1).

- **Permeable Depth in Channels**—The permeable depth (cm) in channels, L_c, defines the vertical extent of the subdomain for the one dimensional diffusion calculation. Determination of the parameter, L_c, was made from field measurements on soil pits dug into channels of the Fortymile Wash alluvial fan. Soil pits were dug on the late Pleistocene alluvial unit (Qa4) surface to 140 cm with minimal carbonate development (i.e., Stage II (carbonate coatings on clasts) was the maximum observed soil-carbonate development). Furthermore, U.S. Geological Survey scour chain data have been measured to a depth of >120 cm. Therefore, the permeable depth is at least 140 cm, but could be much larger. Based on field observations, the parameter L_c is considered to be a single value of 200 cm (SNL 2007g, Section 6.5.5.2).

- **Scour Depth at the Fortymile Wash Fan Apex**—The scour depth, *H*, used by the tephra redistribution model represents the total scour depth over many large floods at a specific location in the upper basin (U.S. Geological Survey Narrows station). However, because no direct measurement for *H* is available over geologic time scales, *H* is constrained using U.S. Geological Survey measurements during a single flood in 1995 at this location. The value for the scour depth, *H*, is taken to be a uniform distribution between 73 cm and 152 cm (SNL 2007g, Section 6.5.6).

- **Vent Location**—This parameter represents the location of the hypothetical volcanic vent through the repository (UTM, NAD27, Zone 11 in meters). The hypothetical volcanic vent could feasibly penetrate anywhere within the waste emplacement area of the repository. However, the center of this area is selected for simplicity. The location and extent of the repository footprint were determined from *Total System Performance Assessment Data Input Package for Requirements Analysis for Subsurface Facilities* (SNL 2007f), which presents the subsurface layout of the repository. For TSPA, the vent location shown in Figure 2.3.11-13 has the coordinates 548500 m E, 4078840 m N (*xvent, yvent*) UTM, NAD27, Zone 11 in meters (SNL 2007g, Section 6.5.7.1).

- **Vent Radius**—This parameter is used to eliminate the tephra and waste deposited within a distance less than *rvent* (meters). For TSPA, *rvent* is set to equal zero. Setting this to equal to zero maximizes the amount of contaminated tephra that can be mobilized by the model (SNL 2007g, Section 6.5.7.2).

- **Diffusivity of Radionuclides on Divides**—This parameter describes the effective diffusivity (cm^2/yr) of radionuclides on the inter-channel divides at the RMEI location. The parameter distribution was developed using measured ^{137}Cs profiles on inter-channel divides of the upper Fortymile Wash alluvial fan (Pelletier, Harrington et al. 2005). The measured data are represented cumulatively as the fraction of total concentration to a given depth. The downward migration of radionuclides into a soil beneath a contaminated tephra deposit is modeled with a diffusion equation. The data against which diffusivities

are calculated incorporates all transport processes that occur (e.g., advection, bioturbation), and the parameter range calculated incorporates measurement errors. The parameter has a uniform distribution from 0.001 to 0.095 cm^2/yr, which incorporates measurement errors (SNL 2007g, Section 6.5.8.1).

- **Diffusivity of Radionuclides in Channels**—This parameter describes the effective diffusivity (cm^2/yr) of radionuclides in the channels of the RMEI location. This parameter value was developed using measured ^{137}Cs profiles on channels and young terraces of the upper Fortymile Wash alluvial fan (Pelletier, Harrington et al. 2005). Similar to the parameter for diffusivity of radionuclides on divides, the downward migration of radionuclides in channels modeled with a diffusion equation. The data against which diffusivities are calculated incorporates all transport processes that occur (e.g., advection, bioturbation). The parameter has a uniform distribution from 0.035 to 0.266 cm^2/yr, which incorporates the full range of measurement errors (SNL 2007g, Section 6.5.8.2).

2.3.11.4.2.3.3 Model Results

The model is run directly within TSPA and produces as outputs the surface and depth integrated concentrations of waste in channels and inter-channel divides at the RMEI location as a function of time following the eruption. TSPA actually runs the Fortymile Wash ash redistribution model twice for each realization with the only difference being the depth over which the concentrations are integrated. One run uses the tillage depth, which defines the layer thickness for calculating the dose from agricultural sources and the other uses the critical depth, which defines the layer thickness for material that is resuspended by wind and available for inhalation dose by the RMEI. Figure 2.3.11-17 presents several example results of integrated waste concentration over time within the tillage layer of the RMEI channels. The difference between these curves reflects the model sensitivity to diffusivity values that vary between runs.

2.3.11.4.3 Data Uncertainty

[NUREG-1804, Section 2.2.1.3.10.3: AC 3(1), (2); Section 2.2.1.3.11.3: AC 3(1), (2); Section 2.2.1.3.13.3: AC 3(1) to (4)]

This section summarizes the parameter values developed to propagate data uncertainty in the TSPA abstraction, as well as data and numerical analyses used to justify the volcanic eruption modeling case abstraction and eruption model parameter distributions. Parameter distributions and values used to implement the igneous eruption model, and the abstractions for number of waste packages intersected by conduits and airborne transport, were summarized in Section 2.3.11.4.2.2.2. Parameter distributions and values used to implement the tephra redistribution model are listed in Section 2.3.11.4.2.3.2.

The physical parameters of the Fortymile Wash fluvial system contain some uncertainty because of the difficulty in quantifying some of the variables (e.g., scour depth at the Narrows station (SNL 2007g, Figure 7.1.3-2)) and because of spatial heterogeneity in certain parameters (e.g., diffusivity in channels and divides). Parameters that may vary spatially, such as critical slope, drainage density, diffusivities, and permeable depths are represented in the model as homogeneous properties of the domain which they describe. Uncertainty from possible spatial variability is accounted for by sampling from probability distributions assigned to the homogeneous properties.

Upper and lower bounds for distributions are constrained by the minimum and maximum parameter values measured or inferred from field data and therefore do not underestimate the uncertainty in the homogeneous property. Section 6.5 of *Redistribution of Tephra and Waste by Geomorphic Processes Following a Potential Volcanic Eruption at Yucca Mountain, Nevada* (SNL 2007g) describes the development of each parameter in the model and contains information on the range of each parameter of the physical system.

2.3.11.4.3.1 Number of Waste Packages Intersected by Eruptive Conduits

The number of waste packages intersected by eruptive conduits depends upon the diameter of conduits at repository depths, and the number of conduits that might form if a monogenetic volcano erupted through the repository. Conduit size at repository depth is estimated from field data at eroded volcanoes (Miocene and Pliocene in age), which indicate that conduit diameter is largest at the earth's surface and rapidly decreases with depth (SNL 2007e, Appendix F), as well as from xenolith data from the Quaternary Lathrop Wells volcano (SNL 2007e, Appendix C). Uncertainty in conduit size at repository depth is constrained by the range of values determined from the analogue data and is incorporated in the range of values that are used to calculate waste packages intersected by conduits (minimum size is the dike width for a given realization, mean diameter is 15 m, and the 95th percentile value is 21 m) (SNL 2007e, Table 7-1). The 95th percentile value for conduit diameter (21 m) is based on analogue studies at the Lathrop Wells volcano. This value is considered to be the maximum conduit diameter for the Lathrop Wells volcano based on reconstruction of conduit geometry from xenolith studies (SNL 2007e, Section 6.3.3.3). The uncertainty in conduit size distribution further assumes that the Lathrop Wells volcano is the expected type of volcano (in terms of volume and eruptive style) for a future eruption in the region (SNL 2007e, Section 6.3.3.1). The distribution for conduit size is consistent with measurements made at a limited number of eroded analogue sites in the region (SNL 2007e, Section 6.3.3.3).

Field analogue studies indicate that most of the Quaternary volcanoes in the Yucca Mountain region probably each had a single main conduit with shallow breakouts that laterally fed lavas that vented around the bases of the cones (SNL 2007e, Appendices C, D, and E). Therefore the number of conduits modeled in TSPA is heavily weighted (85% probability) toward one conduit per eruption (SNL 2007e, Section 6.3.3.3; Tables 6-8 and 7-1), but allows for potential formation of up to three conduits along the master dike (as observed at eroded analogue sites (SNL 2007e, Appendix F)), albeit with low probabilities (SNL 2007e, Table 6-8). This allowance is based on observations of older (Pliocene and Miocene) basaltic volcanoes in the region. However, the volcanoes with multiple conduits also are likely to have had larger eruptive volumes than Quaternary volcanoes, which is why the probability of two or three conduits forming is considered to be relatively low compared to the formation of a single conduit. This treatment incorporates uncertainty in the number of conduits that would form if a monogenetic volcano, similar to Quaternary volcanoes, erupted through the repository.

2.3.11.4.3.2 Atmospheric Dispersal and Deposition of Tephra

Quantification of the treatment of uncertainty for the data underlying each uncertain parameter is discussed as part of the description of each parameter in *Atmospheric Dispersal and Deposition of Tephra from a Potential Volcanic Eruption at Yucca Mountain, Nevada* (SNL 2007d, Section 6.5.2) and in Section 2.3.11.4.2.2.2. ASHPLUME input parameters defined by stochastic distributions

include eruptive power, eruption duration, column diffusion coefficient, ash particle diameter mean and standard deviation, initial eruption velocity, wind speed and direction, and the magma partitioning coefficient. The distributions for parameter values have been derived from observations of basaltic volcanoes worldwide, and the distributions are defined to reflect the generally low level of statistical knowledge. For example, the distribution of values for eruptive power is based on values calculated for six observed (historical) eruptions and spans three orders of magnitude. The distribution is defined as log-uniform to reflect an equal likelihood of small or large events. Data are not sufficiently abundant to define a more specific distribution, such as log-normal. In contrast, abundant (1.4 million data lines) wind speed and direction data at the Desert Rock Station for the years 1978 through 2003 (NOAA 2004) have been tabulated as probability density functions and cumulative distribution functions for each 1-km altitude bin above Yucca Mountain (for 1 km to 13 km) (SNL 2007d, Sections 6.5.2.7 and 6.5.2.8). As a result of the abundance of these wind data, uncertainties associated with wind speed and direction are well represented in the associated distribution functions (SNL 2007d, Tables 8-3 and 8-4).

2.3.11.4.4 Model and Analysis Uncertainty and Alternative Models

[NUREG-1804, Section 2.2.1.3.10.3: AC 4; Section 2.2.1.3.11.3: AC 4; Section 2.2.1.3.13.3: AC 4]

Uncertainties for the volcanic eruption modeling case include uncertainty in the number of conduits that could form within the repository footprint, the potential for development of secondary conduits and uncertainties associated with the ability for the ASHPLUME code to appropriately model the atmospheric dispersal and subsequent surface redistribution of contaminated tephra.

2.3.11.4.4.1 Number of Waste Packages Intersected by Eruptive Conduits

Uncertainty in the results of the number of waste packages hit analysis is represented by a cumulative distribution function that represents the discretized cumulative probability of zero to seven waste packages being intersected if one or more conduits form within the repository footprint (Figure 2.3.11-12b). The output uncertainty reflects the use of stochastic input parameters that define the uncertainty in the characteristics of a volcanic event (SNL 2007e, Table 7-1).

Uncertainty in the number of waste packages intersected is described in terms of three components: (1) repository design uncertainty, such as drift end point coordinates (SNL 2007b, Section 6.4.1); (2) epistematic uncertainties associated with the development of one of more conduits within the repository (SNL 2007b, Section 6.4.2); and (3) numerical uncertainty due to sampling of input parameter distributions using the Latin Hypercube Sampling method (SNL 2007b, Section 6.4.3). Additional uncertainties associated with the way the analysis is formulated are assessed through evaluation of alternative analyses and formulations (SNL 2007b, Section 6.4.2).

Numerical uncertainty is associated with the values of the random number seeding that is part of the Latin Hypercube Sampling method to sample input parameter distributions. To evaluate variability in the sampling due to the random number seeding, the analysis is divided into four independent replicate analyses (based on different random seeds), each providing 1,000 samplings of the input distributions (SNL 2007b, Section 6.4). The replicates are combined to produce the final composite result as shown in Figure 2.3.11-12b. The maximum number of waste packages intersected by eruptive conduits in the replicate analyses ranges from 5-7, while the median number of waste

packages intersected in all four replicates is 0 (SNL 2007b, Table 6-4). The conditional probability of at least one eruptive center within the repository footprint ranges from 0.20-0.34 in the replicate analyses (SNL 2007b, Table 6-5). These results indicate that the value of the random number seed does not significantly impact the final results of number of waste packages intersected.

The results of the analysis indicate that the mean conditional probability of an eruption (given a dike intersection) within the repository footprint is 0.28 (Section 2.3.11.4.2.1.3) (SNL 2007b, Section 6.3.4 and Table 7.1). Alternative analyses, using different interpretations of volcanic event characteristics and behavior, result in conditional probabilities of at least one eruptive center within the repository footprint that range from 0.43 to 0.78 (SNL 2007b, Section 6.4.2 and Table 7-1; BSC 2004a, Section 6.5.2.2 and Table 7-1). These alternative analyses are not used for the volcanic eruption modeling case (SNL 2007b, Section 6.4.3) because they are less consistent with recent analogue data for volcanic events in the Yucca Mountain region (SNL 2007e, Table 7-1).

Four alternative probabilities of formation of an eruptive center, that could increase the number of waste packages intersected by a conduit, are formulated based on different concepts of an event:

1. The mean value of 0.28 is derived from observations at eroded analogues that events include multiple dikes (likelihood of 60%) and that the widest (highest volume flux) dike will host all conduits (SNL 2007b, Section 5.4). Thus, a dike intersection can occur while the conduit-bearing dike lies wholly outside the repository footprint, precluding conduit formation within the footprint. The conduit-bearing dike can host up to 3 conduits, but is heavily weighted towards a single conduit (likelihood of 85%) consistent with analogue observations (SNL 2007e, Table 7-1). The presence of the repository is assumed to have no effect on conduit location.

2. The value of 0.43 is the result of a sensitivity analysis for Alternative 1 to determine the eruptive center probability if the conduit-bearing dike always intersects the repository (SNL 2007b, Section 6.4). The presence of the repository is assumed to have no effect on conduit location.

3. The PVHA-based value of 0.56 is based on a formulation that the event has only a single dike that hosts conduits with the likelihood of multiple conduits (up to 13) being more likely than in the first two scenarios of the current analysis. The conduits are spaced along the dike in several variations of a uniform distribution (BSC 2004a, Section 6.5.1.3). In this case, as in the previous two alternatives, the presence of the repository is assumed to have no effect on conduit location.

4. The value of 0.78 is based on the formulation in Alternative 3 but also includes an equally weighted formulation that the repository always induces conduit formation within the repository footprint, thereby increasing the probability of an eruptive center within the footprint.

Given observations that volcanic events are expected to include multiple dikes, and that a conduit(s) is expected to form on the widest dike, the first alternative, with an eruption probability value of 0.28 is the most consistent with analogue data and the most appropriate to use in the volcanic eruption modeling case. Alternatives 3 and 4 assume a single dike, which is considered less

probable based on analogue observations (SNL 2007e, Table 7-1). The most directly comparable are Alternatives 2 and 3, each involving the possibility of only a single dike that hosts conduits, and where the presence of the repository is assumed to have no effect on conduit location. The resulting values (0.43 and 0.56) are similar and differ, at least in part, because the PVHA-based scenario allows a greater number of conduits on the dike (BSC 2004a, Section 6.5.1.3).

Another uncertainty in the number of conduits and the potential number of waste packages that could be incorporated into a volcanic eruption is presented by the alternative model of Woods et al. (2002). They suggested that transient high pressures due to reflection of shock waves at the closed ends of drifts might cause upward propagation of a secondary dike at some distance from the location of the initial intersection of a drift by the main dike. Results of analyses (SNL 2007a, Section 6.5; BSC 2005a, Section 6.3.2) show that even in the unlikely case that magma invades a preexisting fracture, flow of magma would be interrupted by magma cooling and solidification (freezing) long before the magma could reach the surface (Section 2.3.11.3.4.4; SNL 2007a, Section 8.1.3).

2.3.11.4.4.2 Atmospheric Dispersal and Deposition of Tephra

Uncertainty is addressed through model validation activities that include parameter sensitivity studies and comparisons to observed natural analogues. Such simulations are used to show that the parameter ranges encompass the range of expected eruptive behavior and that the model is valid for the entire range of parameters represented by distributions (SNL 2007d, Section 7.2). The analysis indicates that the atmospheric dispersal model results are most sensitive to variations in wind speed and wind direction, which produce orders-of-magnitude changes in tephra and waste thickness (<mm to 10s of cm) at the RMEI location. Moderate sensitivity (factor of 2 to 10 variability in output) was displayed for variations in values for the parameters defining eruptive power, duration, and tephra particle size (mean and standard deviation). The model showed only minor sensitivity (less than factor of two variability in output) to variations in column diffusion constant, initial rise velocity, eruption duration, waste incorporation ratio, and waste particle size.

Additional analyses have been undertaken to evaluate the sensitivity of the coupled atmospheric dispersal and Fortymile Wash ash redistribution models to variations in column height (i.e., unsteady eruption) and variability of wind speed and direction during eruption (conditions not represented by the base-case atmospheric dispersal model). Variations in tephra dispersal resulting from model realizations featuring unsteady column height and variable wind conditions produced up to a factor of two increase in tephra concentration in sediment transported to the RMEI area compared to a base case featuring a simple plume directed due east of the repository (SNL 2007d, Section 7.6). However, the nature of the watershed geometry and terrain produces up to a factor of three variability in tephra concentration in redistributed sediment at the RMEI location. These watershed geometry and terrain effects encompass effects of variation in eruption parameters (SNL 2007d, Sections 7.6 and K4).

Three natural analogue studies addressed the adequacy and accuracy of the atmospheric dispersal model by comparing model results to observed tephra fall thickness distributions at Cerro Negro volcano, Nicaragua; Lathrop Wells volcano, Nevada; and Cinder Cone, California. The studies emphasized fits of distal (SNL 2007d, Sections 7.3.2, 7.3.3, and 7.3.4) data because the distal deposits are those that would be the dominant contributors to the dose to the RMEI. At Cerro Negro,

for distances greater than 10 km, the model results gave ash thicknesses that compared well with the observed data (SNL 2007d, Section 7.3.2). At Lathrop Wells, the overall pattern of the centerline profile of the deposit was reproduced. The model generally provided a good fit for thinner deposits and over-predictions for thicker proximal deposits (SNL 2007d, Section 7.3.3). At Cinder Cone, model fits to observed medial and distal data are generally good, and the overall pattern of the centerline profile of the deposit was reproduced. Generally, the fit was good for thinner deposits and over-predictions for thicker proximal deposits (SNL 2007d, Section 7.3.4). The results of the validation studies indicate that the model can successfully reproduce the pattern and thickness of tephra deposits when the model input parameters are derived from available site specific eruption information supplemented by generalized "base case" parameter values derived from the volcanological literature and field studies (SNL 2007d, Section 7.7).

The results from the ASHPLUME code have been compared to those from another ash dispersal code, ASHFALL (Hurst and Turner 1999), using equivalent input parameters (SNL 2007d, Section 7.5 and Appendix J). The code comparison was carried out by configuring the inputs to the ASHPLUME code to simulate conditions of the 1995 and 1996 eruptions of Ruapehu volcano in New Zealand. The ASHPLUME code was used in two sets of model runs to attempt to match published output from the ASHFALL code for constant wind conditions and a variable wind field (Hurst and Turner 1999, Figures. 1b and 1d; SNL 2007d, Section 7.5 and Appendix J). The results of the ASHPLUME code were similar to ASHFALL in terms of the shape and distribution of the tephra deposit. ASHPLUME input parameter values were adjusted within reasonable ranges to fine-tune the match between the two models. In both cases the best fits were obtained using base-case parameter values (those derived from direct equivalencies between the two mathematical models) with adjustment to wind speeds appropriate for the center of mass of the eruptive column and to values of the Suzuki constant (including the column diffusion constant) to match the usage of Hurst and Turner (1999). This code comparison activity demonstrated that the ASHPLUME code can use reasonable input parameter values to produce results comparable to the ASHFALL code, which uses more complex treatments of tephra particle settling velocities and variable wind conditions with height and with time.

Several alternative models were considered to evaluate the violent Strombolian eruption and transport of the tephra-waste mixture. The alternative models include Gaussian Plume, PUFF, Gas-Thrust, an Alternative Igneous Source Term model, ASHFALL, and TEPHRA (SNL 2007d, Section 6.4). Based on the screening of the alternative models considered, the ASHPLUME code was determined to be the most appropriate code for use in TSPA calculations of atmospheric dispersal and deposition of tephra due to a volcanic eruption through the repository (SNL 2007d, Section 6.4.7). The ASHPLUME code was specifically chosen because it incorporates both the ash dispersal and waste incorporation mechanisms required for the TSPA analysis of ash waste deposition, redistribution, and dose to humans. In addition, the mathematical model embodied in the ASHPLUME code has been confirmed as robust and valid compared to more complex simulation codes (e.g., waste incorporation into tephra) (e.g., ASHFALL and TEPHRA) (SNL 2007d, Section 6.4.7). The alternative conceptual models considered do not provide the full functionality required for the TSPA analysis nor do they provide additional value in the context of the long time frame for the risk assessment. For example, it is not reasonable to explicitly define complex, time-varying wind conditions for a tephra dispersal model realization that estimates tephra dispersal thousands of years in the future.

2.3.11.4.4.3 Tephra Redistribution

The uncertainty and limitations associated with the Fortymile Wash ash redistribution model include the following:

- The model does not explicitly include the effects of future climate on model processes and parameters. Future climate is estimated to be wetter than present-day climate and several model parameters may be affected by changes in climate. For example, the vertical migration rate of radionuclides into the soil at the RMEI location, which is controlled by diffusivity values, may increase with increasing precipitation due to higher net infiltration flux. Such climate feedbacks are not considered by the model (SNL 2007g, Section 5.1.1). Neglecting climate feedbacks in the model tends to overestimate radionuclide concentrations in the surface layer of the soil at the RMEI location because wetter climate conditions tend to increase vertical transport rates and thus near-surface soil concentrations would decrease more quickly.

- The long term geologic dynamics of fan inter-channel divides and channel interactions are not represented. Alluvial fans are dynamic landforms that can evolve topographically over both long and short time scales. Uncertainty in the fraction of the alluvial fan that is subject to active fluvial deposition is assumed to adequately account for future changes in the Fortymile Wash alluvial fan (SNL 2007g, Sections 1.2 and 6.5.4.2).

- The model is only applicable to channels without active floodplains. This limitation is inconsequential for the drainage networks in the Yucca Mountain region because these drainage networks have no significant active floodplains (SNL 2007g, Section 5.1.3).

- Processes which may cause accumulation of contaminants within the soils at the RMEI location, such as chemical precipitation, placering, or bioaccumulation, are not included in the model. Such processes are unlikely to occur in this environment (SNL 2007g, Section 5.1.5).

- The model does not explicitly incorporate time in the fluvial remobilization calculations. Mobilization of the tephra in the upper drainage basin domain is assumed to be instantaneous, as is the transfer of tephra to the RMEI location; additionally, eventual removal of nonmobilized tephra is not considered.

- Based on analogue studies, including at Franklin Lake Playa, the model does not include the effects of eolian erosion or deposition. Eolian sediment transport is a significant geomorphic process in this environment. However, because of prevailing wind directions, eolian deposition and erosion will tend to further dilute contaminated tephra redistributed to the RMEI location by fluvial processes beyond that estimated by the model. Therefore, neglecting to simulate these effects explicitly in the model is considered conservative (SNL 2007g, Section 5.2.2).

- The model assumes that channel geomorphology does not change over time. Following a volcanic eruption, it is expected that channel geomorphology would change in certain parts of the upper drainage basin, especially close to the vent. Such changes could result

in changes in surface elevation and slope and associated changes in stream power and even drainage density and possibly affect the initial concentration at the RMEI location. None of these complex feedbacks are simulated by the model. It is assumed that the existing uncertainty considered in the input parameters accounts for the uncertainties in such possible changes (SNL 2007g, Sections 1.2 and 5.1.4).

- The model assumes that the contaminant and channel-bed material is transported primarily as bed-material load. The silt sized fraction of the contaminated tephra is transported as suspended load and would be transported past the RMEI location and into the Amargosa River valley. By treating this material as bedload, which can be deposited at the RMEI location, the model tends to overestimate tephra and waste concentration at the RMEI location (SNL 2007g, Sections 1.2 and 5.2.3).

- The model assumes that the thickness and concentration of the contaminated tephra deposited in the RMEI area is the same as that calculated at the upper drainage basin fan apex (SNL 2007g, Section 1.2). This assumption presumes that the drainage system is open, allowing some portion of the tephra and radionuclides initially mobilized in the upper drainage domain to flow through and out of the lower drainage domain (the RMEI domain is not considered to be a perfect depozone) (SNL 2007g, Sections 1.2 and 5.2.4).

- The model assumes that the concentration of waste associated with the ash in a particular location can be calculated after the ash has been re-distributed using the ratio of the total mass of waste and the total mass of ash mobilized in the upper drainage basin (SNL 2007g, Sections 1.2 and 5.2.5).

- The model assumes that once the tephra and radionuclides are deposited at the RMEI location, redistribution of the radionuclides into the soil is governed by a diffusive process. Advection of the radionuclides is not explicity modeled (although it should be noted that the data against which diffusivities are calculated incorporates all transport mechanisms that occur, such as advection and bioturbation), nor is additional mixing of the contaminants in the channels included (SNL 2007g, Sections 1.2 and 5.3). The assumption of no further mixing may overestimate waste concentrations in the channels at the RMEI location because, if additional mixing were to occur, further dilution of the waste concentration would be expected.

Alternative models of tephra redistribution were considered in the development of the Fortymile Wash ash redistribution model. The main process represented by the Fortymile Wash ash redistribution model is referred to as the scour-dilution-mixing model in Sections 6.2.2 and 6.3.3 of *Redistribution of Tephra and Waste by Geomorphic Processes Following a Potential Volcanic Eruption at Yucca Mountain, Nevada* (SNL 2007g). This model is used to represent the process of tephra and clean sediment being mixed as they are transported down the drainage system. The result of this mixing process is that waste concentrations become diluted once sediment is deposited at the RMEI location. The main difference is that the classic approaches consider only the contributing area in the calculation of dilution. The scour-dilution-mixing model estimates scour depth as a function of contributing area, which results in a estimate of sediment volume available for mixing.

Other alternative modeling approaches are described in *Redistribution of Tephra and Waste by Geomorphic Processes Following a Potential Volcanic Eruption at Yucca Mountain, Nevada* (SNL 2007g, Sections 7.1 and 7.2) (e.g., bicubic versus bilinear interpolation schemes, steepest descent versus central differences for calculating slopes, steepest descent versus divergent flow (bifurcation) algorithm for calculating contributing area, etc.). These alternative approaches were considered in the development and validation of the tephra redistribution model. The model validation presented in *Redistribution of Tephra and Waste by Geomorphic Processes Following a Potential Volcanic Eruption at Yucca Mountain, Nevada* (SNL 2007g, Section 7) provides confidence that the modeling approach taken is consistent with available data and current scientific understanding.

For example, the FAR V. 1.2 code permits tracking of tephra mass in calculations and thereby demonstrates that accounting has been made for all tephra in the system (SNL 2007g, Section 7.2.8). Similarly, sensitivity studies related to three parameters (critical slope, drainage density, and scour depth) have shown that the model works as designed and gives reasonable results (SNL 2007g, Section 7.2.9). Finally, a published description of the application of the scour-dilution-mixing model to the Lathrop Wells volcanic area (Pelletier, DeLong et al. 2008) demonstrated that the model adequately represents the redistribution of tephra by hillslope and fluvial processes in an environment very similar to that which would occur in the eruption scenario (modeling case) at Yucca Mountain. The model adequately predicted the changes in concentration associated with the tributary influxes along channels on each side of Lathrop Wells volcano. The results provided confidence that the model implemented in the FAR V. 1.2 software is adequate and valid for its intended use (SNL 2007g, Section 7.3.1.5).

2.3.11.4.5 Volcanic Eruption Model Abstraction

[NUREG-1804, Section 2.2.1.2.2.3: AC 1(2); Section 2.2.1.3.10.3: AC 5; Section 2.2.1.3.11.3: AC 5); Section 2.2.1.3.13.3: AC 5]

The volcanic eruption modeling case is implemented in TSPA using four submodels to describe the processes considered. The volcanic interaction with the repository submodel determines the number of waste packages that may be affected by a volcanic eruption and the amount of waste available for atmospheric transport. The atmospheric transport submodel describes the atmospheric transport of this erupted tephra/waste mixture and its eventual deposition on the land surface. The tephra redistribution submodel describes the surface redistribution of contaminated tephra to the location of the RMEI, and the volcanic ash exposure submodel uses volcanic ash biosphere dose conversion factors to estimate the annual dose to the RMEI due to the calculated waste concentration at the RMEI location. Details of the TSPA integration and implementation of the volcanic eruption modeling case are described in Section 2.4 and *Total System Performance Assessment Model/Analysis for the License Application* (SNL 2008, Sections 6.5.2.1 and 6.5.2.2).

Implementation of the volcanic eruption modeling case for the TSPA model includes determination of both the probability of the event and its consequences. The approach employs a Monte Carlo technique to account for parameter uncertainties including the future time at which an eruption could occur and the possibility that more than one event could occur in the future evolution of the repository. The probability of an event is represented as a conditional probability that one or more eruptive conduits would form within the repository footprint given the intersection of the repository by a basaltic dike. The annual frequency of an eruption through the repository is estimated by

multiplying the sampled frequency of intrusion (mean approximately 1.7×10^{-8}/yr) (BSC 2004a, Table 7-1) by the fraction of dike intersections within the repository that include eruption (0.28; SNL 2007b, Section 7.2). Details of the treatment of uncertainty in the volcanic eruption modeling case are described in *Total System Performance Assessment Model/Analysis for the License Application* (SNL 2008, Section 6.1.2.4.3)

2.3.11.4.5.1 Number of Waste Packages Intersected by Eruptive Conduits

The analysis of the number of waste packages intersected by eruptive conduits provides a direct input to TSPA. This input provides the source term for calculations of the amount of waste that is available for eruption as contaminated ash followed by atmospheric dispersal and deposition downwind of the eruption. Results of the analysis (SNL 2007b, Section 7.2) showed that the number of waste packages intersected by conduits ranged from zero to seven. The median number of waste packages intersected by eruptive conduits is zero (SNL 2007b, Figure 7-1, Sections 6.4 and 7.2).

2.3.11.4.5.2 Atmospheric Dispersal and Deposition of Tephra

The atmospheric dispersal model represents a violent Strombolian eruption and simulates the entrainment of radioactive waste in the eruption plume as waste particles attached to the pyroclastic fragments in the plume. Multiple inputs are used to define the characteristics of the eruption, the environmental conditions, and the mass of waste included in the eruption (SNL 2007d, Section 8.2). Input distributions for the volcanic eruption modeling case account for parameter uncertainties as well as uncertainties associated with the time of occurrence of a portion of the eruption (SNL 2008, Section 6.5.2). The model components consider the damage to the EBS components and describe the amount of waste erupted to the surface, the atmospheric transport of the erupted waste, and the deposition of contaminated tephra on the ground surface. The mean and median annual doses for the volcanic eruption modeling case are determined using Monte Carlo methods and averaging the expected annual dose for a set of realizations that sample probability distributions for the epistemically uncertain parameters.

The consideration of damage to EBS components is included in the modeling by the amount of waste entrained in the eruption plume. The mass of waste incorporated in the plume depends on the amount of waste available and the number of waste packages damaged by the eruption. For the abstraction, all waste packages damaged during an eruption are assumed to provide no protection for the contained waste, and all waste in damaged waste packages is assumed to be erupted (SNL 2007d, Section 5.1.4). The amount of waste transported in the tephra plume is a fraction (0.1 to 0.5) of the total mass of waste mixed into the magma, excluding the proportion of the waste-containing magma that forms geologically resistant lava flows and scoria cone (SNL 2007d, Section 6.5.2.22).

The abstraction provided by the atmospheric dispersal model is the concentration of waste and tephra on the ground surface. Development of the abstraction requires a waste concentration in the erupted material as well as wind speed and direction information to calculate the concentrations of waste in tephra at grid points downwind of the eruption site. The waste concentration in the eruption plume is calculated using the waste incorporation ratio parameter, which is a mathematical representation of the ratio of tephra to waste particle sizes that can be combined (SNL 2007d,

Section 6.5.2.6). Wind speed and direction data are represented by distribution functions (SNL 2007d, Sections 6.5.2.7 and 6.5.2.8).

The concentrations of radionuclides in the waste provide the basis to determine the concentrations of the radionuclides in the tephra deposited on the ground surface. The waste inventory is apportioned according to the relative amounts of the different wastes in the repository, as expressed by the different kinds of waste packages that compose the waste package inventory for the repository (SNL 2008, Section 6.5.2.1.4). The annual dose associated with each radionuclide in the waste is calculated by multiplying the concentration of the radionuclide at a specified location by the respective biosphere dose conversion factor for that radionuclide.

2.3.11.4.5.3 Tephra Redistribution

The Fortymile Wash ash redistribution tephra redistribution model is implemented directly in TSPA without further abstraction (Section 2.4). In TSPA, the results of that model are combined with the biosphere dose conversion factors (Section 2.3.10.5.2) to evaluate the annual dose to the RMEI. The biosphere dose conversion factors are calculated by the biosphere model (Section 2.3.10) using the volcanic ash exposure scenario for modeling of radionuclide transport and exposure pathways in the reference biosphere.

The reference biosphere for the volcanic ash scenario is divided into two areas: cultivated land and noncultivated land. Because mixing of soil and tephra would differ between cultivated and noncultivated lands, and because radiation exposure would differ between those areas, radionuclide concentrations in soil on cultivated and noncultivated areas were treated separately in the model (SNL 2007j, Section 6.3.2.6). Radionuclide concentrations in cultivated soil were calculated by using the areal radionuclide concentration. For noncultivated soil, radionuclide concentration in the resuspendable soil layer was used (Section 2.3.10.2.6). The corresponding two source terms for the dose calculations are calculated in the TSPA model using the results of the tephra redistribution model. The two source terms are the radionuclide concentration in the resuspendable layer of soil in units of mass activity concentration (e.g., Bq/kg) and the tillage (biosphere) depth-integrated (areal) radionuclide concentration in surface soil in units of surface activity concentration (e.g., Bq/m^2) (SNL 2007j, Section 6.5.1). Both source terms are calculated in TSPA by weighting the appropriate radionuclide concentrations by the respective expected areas of the distributary channels and the interchannel divides at the location of the RMEI (SNL 2007j, Section 6.12.3). There is no relationship between the aerial distribution of the cultivated/noncultivated land in the reference biosphere and the channel/interchannel divide regions of the tephra redistribution model. The agricultural land farmed by the hypothetical community that includes the RMEI is assumed to be located on the Fortymile Wash alluvial fan irrespective of the location of the distributary channels and interchannel divides.

2.3.11.5 Summary of Igneous Scenario Class Model Abstraction

[NUREG-1804, Section 2.2.1.3.2.3: AC 1(1), AC 5(1); Section 2.2.1.3.3.3: AC 1(1), AC 5(1); Section 2.2.1.3.10.3: AC 1(1), AC 5(1); Section 2.2.1.3.11.3: AC 1(1), AC 5(1); Section 2.2.1.3.13.3: AC 1(1), AC 5]

As noted in Section 2.3.11.1, the consequences of disruption of the repository by igneous activity are examined in the TSPA through analysis of the igneous scenario class. The igneous scenario class consists of two modeling cases: igneous intrusion and volcanic eruption.

The base-case igneous scenario class involves coupling igneous disruption abstractions, as defined above, that are used to calculate the cumulative igneous dose consequence to the RMEI. The probability-weighted doses from both eruptive and igneous intrusion abstractions are added together to give the total probability-weighted dose that could result from an unlikely igneous event.

Representative data from the site and surrounding region form the basis to describe and model potential disruption of the repository by an unlikely future igneous event. Effects of uncertainties and variabilities in parameters on the analyses have been considered, and alternative conceptual models have been considered in the analyses. Specific FEPs have been included in the analyses (Table 2.3.11-1), and technical bases have been provided for their inclusion. Detailed technical bases have been provided for models and their associated parameters and parameter uncertainty used in the performance assessment.

The igneous intrusion modeling case describes the effects of an igneous intrusion on the repository. The intrusion is modeled to intersect one or more emplacement drifts. The intruding magma is assumed to flow into all emplacement drifts in the repository, engulfing all waste packages, and then cool and solidify. All waste packages in the repository are assumed to be compromised and to provide no further protection for the waste from groundwater. When seepage is restored and percolation through the cooled basalt is established, the radionuclides are assumed to be immediately available for transport because the EBS components are assumed to provide no protection for the waste. Dose to the RMEI is modeled to occur through the same pathways that are represented in the nominal scenario and seismic and early failure class. TSPA uses the pH and ionic strength values from the *In-Package Chemistry Abstraction* (SNL 2007c, Sections 8.2.1[a] and 8.2.2[a]). The solution values are inherently buffered by the degradation products between pH 5.3 and 8.5 and the ionic strength is a maximum of 0.43 moles/kg. The ionic strength has a triangular distribution with minimum and maximum factors of ±50% (SNL 2007c, Table 6-21[a]).

The volcanic eruption modeling case describes the potential impacts of an eruption through the repository. The model case considers an eruption that develops along a basalt dike and the height and dispersal direction of the ash plume. Waste packages intersected by volcanic conduits are assumed to provide no protection for the radioactive waste. The waste is partitioned into three eruptive materials: lava, cone forming deposits, and tephra. The fraction of waste that is disaggregated into fine grains is attached to the erupted tephra, facilitating airborne transport. Contaminated tephra erupts in a column or plume that reaches altitudes up to 13 km. The eruptive column is dispersed in the atmosphere as a buoyant plume that moves in the direction of the prevailing wind at the time of the eruption. The model estimates the thickness and waste concentration of the tephra sheet at the location of the RMEI. The tephra redistribution model then addresses the sedimentary processes and associated concentrations of contaminated tephra from

these processes for abstraction into the TSPA model. After the contaminated tephra is deposited on the ground surface, it is immediately subjected to redistribution by mass-wasting and fluvial processes. The model evaluates the concentrations of radionuclides in the tephra and underlying soils through time. The TSPA then uses the abstractions of this model to estimate the dose to the RMEI through contact, ingestion, and inhalation pathways.

2.3.11.6 Conclusions

The igneous scenario class includes low probability future igneous activity that could affect repository performance. Two igneous modeling cases in TSPA simulate the applicable FEPs: the first is the igneous intrusion modeling case, which addresses the possibility that magma could intrude into the repository and damage waste packages by contact with magma, and the second is the volcanic eruption modeling case, which includes eruptive conduits that develop through the repository footprint, damage waste packages intersected by the conduits, and erupt contaminated tephra into the atmosphere and deposit the tephra on the land surface. This volcanic tephra and entrained waste would then be redistributed by fluvial and diffusion processes.

2.3.11.6.1 Igneous Features, Events, and Processes

Igneous or volcanic events could significantly impact the ability of the EBS to prevent or substantially reduce the release rate of radionuclides from the waste, and to prevent or reduce the rate of movement of radionuclides away from the repository. The specific FEPs related to igneous activity that were determined to be most important to the evaluation of the consequences of igneous activity at the repository at Yucca Mountain include (Table 2.3.11-1):

- **Igneous Intrusion into Repository**—Magma from an igneous intrusion may flow into the drifts forming a sill, dike, or dike swarm, depending on the stress conditions. This intrusion could involve multiple drifts. The sill could be limited to the drifts or a continuous sill could form along the plane of the repository, impacting a potentially significant number of waste packages.

- **Igneous Intrusion Interacts with EBS Components**—An igneous intrusion in the form of a dike may intersect the repository drifts, resulting in magma, pyroclastic, and volcanic gases entering the drift and interacting with the EBS components (drip shields, waste packages, cladding, waste forms, and the waste package pallets). This could lead to accelerated drip shield and waste package breaching and dissolution or volatilization of waste.

- **Eruptive Conduit to Surface Intersects Repository**—As a result of an igneous intrusion, one or more volcanic vents may form at land surface. The conduit(s) supplying the vent(s) could pass through the repository, interacting with and entraining waste.

- **Ashfall**—Finely divided waste particles may be carried up a volcanic vent and deposited on the land surface from an ash cloud.

- **Ash Redistribution via Soil and Sediment Transport**—Following deposition of contaminated ash on the surface, ash deposits may be redistributed on the surface via eolian and fluvial processes.

2.3.11.6.2 Probability of Future Intersection and Consequences

The probability of a future igneous event intersecting the repository is addressed through a PVHA that used expert elicitation to develop an annual mean probability and associated uncertainty (Section 2.3.11.2.2). Probability distributions were developed to define the likelihood of a volcanic event (BSC 2004a, Table 7-1). The distributions for the length and orientation of dikes that could intersect the repository footprint are based on analogue information (SNL 2007e, Table 7-1). The current mean annual frequency of intersection of the repository footprint by a potential future igneous event is 1.7×10^{-8} (BSC 2004a, Table 7-1), equivalent to an annual probability of about 1 in 60 million (or 1 chance in 6,000 in 10,000 years) (Section 2.3.11.2.2).

To represent radionuclide releases to groundwater, following intrusion, cooling of the magma, and establishment of percolation through the cooled basalt consequence models were developed to simulate the igneous event processes leading to radionuclide transport, including dike–drift interactions, magma flow into drifts, and the effect of magma on waste packages and changes in water chemistry. The igneous intrusion modeling case provides intermediate products to TSPA that are used to estimate radionuclide releases based on simulation of flow and transport through the EBS and the unsaturated and saturated zones in the same manner as the nominal case (Section 2.4.2.3.2.1). Changes in the pH and ionic strength of water that has reacted with cooled basalt were addressed by a review of analogue studies reported in the published literature (SNL 2007a, Section 6.6). The TSPA inputs for pH and ionic strength needed for the intrusion modeling case are provided by the *In-Package Chemistry Abstraction* (SNL 2007c, Sections 8.2.1[a] and 8.2.2[a]).

The volcanic eruption modeling case considers the development of one or more eruptive volcanic conduits through the repository. Waste packages intersected by the conduits are assumed to be destroyed, and their waste entrained in the erupting magma. Contaminated tephra is erupted into the atmosphere, dispersed by wind, and deposited on the ground surface of the accessible environment. Erosion and deposition by hillslope and fluvial processes result in redistribution of the contaminated tephra.

The volcanic eruption modeling case provides to TSPA the number of waste packages intersected by volcanic conduits, the concentration of contaminated tephra, and the concentration of contaminated tephra from redistribution through time (Sections 2.3.11.4.2.1.3, 2.3.11.4.2.3, and 2.3.11.4.3.2). The TSPA integrates this output using biosphere dose conversion factors (Section 2.3.10) and the annual probability of eruption to provide a probability-weighted mean annual dose to the RMEI through contact, ingestion, and inhalation pathways (Section 2.4).

2.3.11.6.3 Uncertainties Associated with Igneous Activity

The analysis of the effect of igneous activity on the performance of the natural and engineered barriers at Yucca Mountain is subject to uncertainties derived from the applicability of the

conceptual and numerical models of processes, the level of understanding of the characteristics of Yucca Mountain, and the understanding of igneous processes.

In evaluating the probability of future volcanic events, uncertainties in both data and models has been incorporated directly into performance assessment models through the use of a structured process of hazard analysis relying on expert elicitation as implemented in the PVHA (Section 2.3.11.2.2). Variability and uncertainty associated with the data used to characterize the igneous intrusion modeling case and the volcanic eruption modeling case are described in Sections 2.3.11.3.3 and 2.3.11.4.3, respectively. The model uncertainties associated are described in Sections 2.3.11.3.4 and 2.3.11.4.4.

To accommodate both variability and uncertainty in the description of the site, many of the input parameters to the igneous activity models have been defined as probabilistic distributions. These distributions incorporate uncertainties associated with field or laboratory data, the use of parameters in the model, and theoretical considerations. Geologic uncertainty with respect to the selection of appropriate models is considered by evaluating alternative conceptual models to test the sensitivity of model results.

Data uncertainties considered in the igneous intrusion modeling case include uncertainties associated with dike–drift interaction, such as magma and rock properties, dike emplacement characteristics, drift properties and waste package properties. In some cases, assumptions (i.e., that drifts fill with magma instantaneously after intersection) have been used in the place of probabilistic distributions. For each analysis realization, the number of packages contacted by magma is estimated based on consideration of uncertainties in dike length, orientation, number of dikes, dike spacing, and drift orientation and diameter. Uncertainties associated with impacts on waste packages and waste forms include the mechanical properties of alloys at high temperatures, mechanical loads on waste packages, nature of reactions between waste packages, waste materials and magma, and chemical species present in magmatic gas, and changes in water chemistry after interaction with cooled basalt. After the number of waste packages damaged has been estimated for each realization, a postprocessing step is applied to implement the assumption that all waste packages fail to produce the TSPA abstraction value of 11,629 waste packages failed (SNL 2007b, Section 7.2).

The uncertainties considered in the volcanic eruption modeling case are related to the characteristics of the system and eruptive processes, and to the processes that determine the amount and distribution of waste entrained and transported in the plume. The TSPA captures the range of uncertainty in the model cases by using parameter distributions, bounding ranges, and conservative assumptions to provide confidence that the dose risk has not been underestimated. Parameters include the eruptive probability, the number and geometry of conduits associated with the eruption, the number of waste packages intersected by conduits, the amount of waste entrained in the ash plume, parameters needed to model the airborne transport of contaminated tephra (e.g., tephra and waste particle size, density and shape, waste incorporation ratio, wind speed and direction, air density and viscosity), and the response of deposits of contaminated tephra to surface geologic processes.

2.3.11.6.4 Assumptions in Models Used to Assess Igneous Activity

Several assumptions are incorporated in models of igneous activity for the igneous intrusion and volcanic eruption modeling cases. The consequence of these assumptions is that the models generally predict greater transport of radionuclides and higher doses than would result if less conservative assumptions were used.

The assumptions incorporated in the igneous intrusion modeling case ensure that the model does not underestimate radionuclide releases in groundwater. For example, although the details of magma flow within emplacement drifts intersected by a dike are not well constrained, the TSPA model assumes that once the repository footprint is intersected by a dike, all drifts would rapidly fill with magma so that every waste package in the repository is contacted by magma and damaged (Section 2.3.11.3.2.4). The model further assumes that the cooled, solidified magma offers no additional resistance to flow beyond that of the surrounding host rock, so that the entire seepage flux is available to contact waste packages. These assumptions result in the instantaneous exposure (in the model) of the waste inventory to percolating water once seepage into the drifts has been restored.

The volcanic eruption modeling case also contains assumptions that relate to radionuclide releases and concentrations. For example, it is assumed that all waste packages that are intersected by conduits offer no protection for the waste and the waste is available for entrainment in the erupting magma. The tephra redistribution model assumes mixing and diluting of radionuclide concentrations in modeling the redistribution of contaminated tephra.

2.3.11.6.5 Conservatism in Models Used to Assess Igneous Activity

Several conservative assumptions are incorporated in models of igneous activity for the igneous intrusion and volcanic eruption modeling cases.

The conservative assumptions incorporated in the igneous intrusion modeling case ensure that the model does not underestimate radionuclide releases in groundwater. For example, although the details of magma flow within emplacement drifts intersected by a dike are not well constrained, the TSPA model assumes that dike-intersected drifts would immediately fill with magma so that every waste package in the intersected drift (and the whole repository) is contacted by magma (Section 2.3.11.3.2.4). The model further assumes that the cooled, solidified magma does not impede the flow of water from the drift wall, so that the entire percolation flux is available to contact waste packages. These assumptions result in the instantaneous exposure (in the model) of the waste inventory in the intruded drift to percolating water once seepage into the drifts restored.

The volcanic eruption modeling case likewise contains several conservative assumptions that probably lead to an overestimate of radionuclide releases. Studies of analogue volcanoes such as the Lathrop Wells volcano demonstrate a variety of eruptive styles including effusive flow, Strombolian, and violent Strombolian activity (Section 2.3.11.2.1.2). The effects of lava flows and Strombolian eruptions are restricted to the vicinity of the volcanic center and would have little or no effect on the accessible environment near Yucca Mountain. Only highly energetic violent Strombolian eruptions have the potential to eject tephra to sufficient altitude that atmospheric dispersal could carry radionuclides to the location of the RMEI, about 18 km south of the repository (but also to Forty Mile Wash for redistribution). The modeling of atmospheric dispersal and

deposition assumes all available waste is captured only in the violent Strombolian phase of the eruption. The ASHPLUME model used to simulate eruptive processes and radionuclide releases only models violent Strombolian activity.

2.3.11.6.6 Summary of Consistency Between TSPA Model Abstractions and Process Models

The models of igneous activity incorporated in the igneous intrusion modeling case and the volcanic eruption modeling case in the TSPA are consistent with their underlying process models. The uncertainty in predicted TSPA results following an unlikely igneous event is also consistent with the uncertainty in the models and parameters used to develop these results. However, as summarized above, several simplifying assumptions have been incorporated to ensure that the models do not underestimate radionuclide releases and estimated doses.

The igneous intrusion modeling case uses the same assumptions and models regarding climate change, infiltration, unsaturated and saturated zone flow and transport, and the biosphere as the nominal case. The volcanic eruption modeling case does not simulate groundwater flow and transport, but does couple with the same biosphere models and assumptions to generate dose estimates.

2.3.11.6.7 Summary of Key Output Parameters Provided to TSPA

The igneous intrusive modeling case provides the following outputs to the TSPA model:

- The number of failed waste packages due to igneous intrusion
- Lookup tables for temperature at the drift centerline and drift perimeter in intersected drifts

The pH and ionic strength of water that has reacted with cooled basalt, needed for TSPA radionuclide transport calculations, are provided by the *In-Package Chemistry Abstraction* (SNL 2007c).

The volcanic eruption modeling case provides the following outputs to the TSPA model:

- Eruptive center probability or the fraction of the intersections that include eruption within the repository footprint
- Number of waste packages intersected by conduits
- Amount of waste erupted into the atmosphere and deposited on the ground surface
- Transport parameters for the atmospheric dispersal and tephra redistribution models
- Layer thickness and radionuclide concentration in deposited tephra

- Layer thickness and radionuclide concentration in redistributed tephra
- Postdeposition residual concentrations.

2.3.11.7 General References

70 FR 53313. Implementation of a Dose Standard After 10,000 Years.

Altman, W.D.; Donnelly, J.P.; and Kennedy, J.E. 1988. *Qualification of Existing Data for High-Level Nuclear Waste Repositories: Generic Technical Position*. NUREG-1298. Washington, D.C.: U.S. Nuclear Regulatory Commission. TIC: 200652.

Blakely, R.J.; Langenheim, V.E.; Ponce, D.A.; and Dixon, G.L. 2000. *Aeromagnetic Survey of the Amargosa Desert, Nevada and California: A Tool for Understanding Near-Surface Geology and Hydrology.* Open-File Report 00-188. Denver, Colorado: U.S. Geological Survey. TIC: 248767.

Brocher, T.M.; Hunter, W.C.; and Langenheim, V.E. 1998. "Implications of Seismic Reflection and Potential Field Geophysical Data on the Structural Framework of the Yucca Mountain-Crater Flat Region, Nevada." *Geological Society of America Bulletin*, *110* (8), 947–971. Boulder, Colorado: Geological Society of America. TIC: 238643.

Brocoum, S.J. 1997. "Evaluation of Data Provided at U.S. Department of Energy (DOE) and U.S. Nuclear Regulatory Commission (NRC) Igneous Activity Technical Exchange, February 25-26, 1997." Letter from S.J. Brocoum (DOE/YMSCO) to J.T. Greeves (NRC), June 4, 1997, with enclosure. ACC: MOL.19970722.0276;MOL.19970722.0277.

BSC (Bechtel SAIC Company) 2003. *Underground Layout Configuration.* 800-P0C-MGR0-00100-000-00E. Las Vegas, Nevada: Bechtel SAIC Company. ACC: ENG.20031002.0007; ENG.20050817.0005.

BSC 2004a. *Characterize Framework for Igneous Activity at Yucca Mountain, Nevada.* ANL-MGR-GS-000001 REV 02. Las Vegas, Nevada: Bechtel SAIC Company. ACC: DOC.20041015.0002.

BSC 2004b. *Drift Degradation Analysis*. ANL-EBS-MD-000027 REV 03. Las Vegas, Nevada: Bechtel SAIC Company. ACC: DOC.20040915.0010.

BSC 2005a. *Magma Dynamics at Yucca Mountain, Nevada*. ANL-MGR-GS-000005 REV 00. Las Vegas, Nevada: Bechtel SAIC Company. ACC: DOC.20050829.0006.

BSC 2005b. *Waste Package Damage Due to Interaction with Magma*. CAL-WIS-MD-000013 REV 00A. Las Vegas, Nevada: Bechtel SAIC Company. ACC: DOC.20050706.0006.

BSC 2007. *Underground Layout Configuration for LA*. 800-KMC-SS00-00200-000-00B. Las Vegas, Nevada: Bechtel SAIC Company. ACC: ENG.20070727.0004.

Budnitz, R.J.; Apostolakis, G.; Boore, D.M.; Cluff, L.S.; Coppersmith, K.J.; Cornell, C.A.; and Morris, P.A. 1997. *Recommendations for Probabilistic Seismic Hazard Analysis: Guidance on the Uncertainty and Use of Experts.* NUREG/CR-6372. Two volumes. Washington, D.C.: U.S. Nuclear Regulatory Commission. TIC: 235076; 235074.

Carr, W.J.; Grow, J.A.; and Keller, S.M. 1995. *Lithologic and Geophysical Logs of Drill Holes Felderhoff Federal 5-1 and 25-1, Amargosa Desert, Nye County, Nevada.* Open-File Report 95-155. Denver, Colorado: U.S. Geological Survey. TIC: 218310.

Connor, C.B. and Hill, B.E. 1995. "Three Nonhomogeneous Poisson Models for the Probability of Basaltic Volcanism: Application to the Yucca Mountain Region, Nevada." *Journal of Geophysical Research*, *100* (B6), 10107–10125. Washington, D.C.: American Geophysical Union. TIC: 237682.

Connor, C.B.; Stamatakos, J.A.; Ferrill, D.A.; Hill, B.E.; Ofoegbu, G.I.; Conway, F.M.; Sagar, B.; and Trapp, J. 2000. "Geologic Factors Controlling Patterns of Small-Volume Basaltic Volcanism: Application to a Volcanic Hazards Assessment at Yucca Mountain, Nevada." *Journal of Geophysical Research*, *105* (B1), 417–432. Washington, D.C.: American Geophysical Union. TIC: 247906.

Crowe, B.M.; Johnson, M.E.; and Beckman, R.J. 1982. "Calculation of the Probability of Volcanic Disruption of a High-Level Radioactive Waste Repository within Southern Nevada, USA." *Radioactive Waste Management and the Nuclear Fuel Cycle*, *3* (2), 167–190. New York, New York: Harwood Academic Publishers. TIC: 222179.

Crowe, B.; Perry, F.; Geissman, J.; McFadden, L.; Wells, S.; Murrell, M.; Poths, J.; Valentine, G.A.; Bowker, L.; and Finnegan, K. 1995. *Status of Volcanism Studies for the Yucca Mountain Site Characterization Project.* LA-12908-MS. Los Alamos, New Mexico: Los Alamos National Laboratory. ACC: HQO.19951115.0017.

Crowe, B.M.; Perry, F.V.; Valentine, G.A.; Wallmann, P.C.; and Kossik, R. 1993. "Simulation Modeling of the Probability of Magmatic Disruption of the Potential Yucca Mountain Site." *Proceedings of the Topical Meeting on Site Characterization and Model Validation, FOCUS '93, September 26–29, 1993, Las Vegas, Nevada*, 182–191. La Grange Park, Illinois: American Nuclear Society. TIC: 102245.

CRWMS M&O (Civilian Radioactive Waste Management System Management and Operating Contractor) 1996. *Probabilistic Volcanic Hazard Analysis for Yucca Mountain, Nevada.* BA0000000-01717-2200-00082 REV 0. Las Vegas, Nevada: CRWMS M&O. ACC: MOL.19971201.0221.

CRWMS M&O 1998. *Synthesis of Volcanism Studies for the Yucca Mountain Site Characterization Project.* Deliverable 3781MR1. Las Vegas, Nevada: CRWMS M&O. ACC: MOL.19990511.0400.

Dartevelle, S. and Valentine, G. A. 2007. *Interaction of Multiphase Magmatic Flows with Underground Openings at the Proposed Yucca Mountain Radioactive Waste Repository (Southern Nevada, USA).* LA-UR-07-3579. Los Alamos, New Mexico: Los Alamos National Laboratory. ACC: LLR.20070807.0153.

Day, W.C.; Dickerson, R.P.; Potter, C.J.; Sweetkind, D.S.; San Juan, C.A.; Drake, R.M., II; and Fridrich, C.J. 1998. *Bedrock Geologic Map of the Yucca Mountain Area, Nye County, Nevada.* Geologic Investigations Series I-2627. Denver, Colorado: U.S. Geological Survey. ACC: MOL.19981014.0301.

Detournay, E.; Mastin, L.G.; Pearson, J.R.A.; Rubin, A.M.; and Spera, F.J. 2003. *Final Report of the Igneous Consequences Peer Review Panel.* Las Vegas, Nevada: Bechtel SAIC Company. ACC: MOL.20031014.0097; MOL.20030730.0163.

EPA (U.S. Environmental Protection Agency) 1992. "Quality Control." Chapter 1 of *Test Methods for Evaluating Solid Waste, Physical/Chemical Methods*. SW-846. Washington, D.C.: U.S. Environmental Protection Agency. ACC: LLR.20071114.0081.

EPRI (Electric Power Research Institute) 2004. *Potential Igneous Processes Relevant to the Yucca Mountain Repository: Extrusive-Release Scenario*. EPRI TR-1008169. Palo Alto, California: Electric Power Research Institute. TIC: 256654.

Fleck, R.J.; Turrin, B.D.; Sawyer, D.A.; Warren, R.G.; Champion, D.E.; Hudson, M.R.; and Minor, S.A. 1996. "Age and Character of Basaltic Rocks of the Yucca Mountain Region, Southern Nevada." *Journal of Geophysical Research, 101* (B4), *8205-8227.* Washington, D.C.: American Geophysical Union. TIC: 234626.

Freeman, T.G. 1991. "Calculating Catchment Area with Divergent Flow Based on a Regular Grid." *Computers & Geosciences, 17* (3), 413–422. New York, New York: Pergamon Press. TIC: 257286.

Fridrich, C.J. 1999. "Tectonic Evolution of the Crater Flat Basin, Yucca Mountain Region, Nevada." *Cenozoic Basins of the Death Valley Region*, Chapter 7. Wright, L.A. and Troxel, B.W., eds. Special Paper 333. Boulder, Colorado: Geological Society of America. TIC: 248054.

Fridrich, C.J.; Whitney, J.W.; Hudson, M.R.; and Crowe, B.M. 1999. "Space-Time Patterns of Late Cenozoic Extension, Vertical Axis Rotation, and Volcanism in the Crater Flat Basin, Southwest Nevada." *Cenozoic Basins of the Death Valley Region*, Chapter 8. Wright, L.A. and Troxel, B.W., eds. Special Paper 333. Boulder, Colorado: Geological Society of America. TIC: 248054.

Gaffney, E.S. and Damjanac, B. 2006. "Localization of Volcanic Activity: Topographic Effects on Dike Propagation, Eruption and Conduit Formation." *Geophysical Research Letters*, *33*, 1–4. Washington, D.C.: American Geophysical Union. TIC: 258505.

Heizler, M.T.; Perry, F.V.; Crowe, B.M.; Peters, L.; and Appelt, R. 1999. "The Age of Lathrop Wells Volcanic Center: An $^{40}Ar/^{39}Ar$ Dating Investigation." *Journal of Geophysical Research*, *104* (B1), 767–804. Washington, D.C.: American Geophysical Union. TIC: 243399.

Ho, C.H. and Smith, E.I. 1998. "A Spatial-Temporal/3-D Model for Volcanic Hazard Assessment: Application to the Yucca Mountain Region, Nevada." *Mathematical Geology*, *30* (5), 497–510. New York, New York: Plenum Publishing Corporation. TIC: 245110.

Hurst, A.W. and Turner, R. 1999. "Performance of the Program ASHFALL for Forecasting Ashfall During the 1995 and 1996 Eruptions of Ruapehu Volcano." *New Zealand Journal of Geology and Geophysics*, *42* (4), 615–622. Thorndon, Wellington, New Zealand: RSNZ Publishing. TIC: 257647.

Jarzemba, M.S.; LaPlante, P.A.; and Poor, K.J. 1997. *ASHPLUME Version 1.0—A Code for Contaminated Ash Dispersal and Deposition, Technical Description and User's Guide.* CNWRA 97-004, Rev. 1. San Antonio, Texas: Center for Nuclear Waste Regulatory Analyses. ACC: MOL.20010727.0162.

Kotra, J.P.; Lee, M.P.; Eisenberg, N.A.; and DeWispelare, A.R. 1996. *Branch Technical Position on the Use of Expert Elicitation in the High-Level Radioactive Waste Program.* NUREG-1563. Washington, D.C.: U.S. Nuclear Regulatory Commission. TIC: 226832.

Kutzbach, J.E.; Guetter, P.J.; Behling, P.J.; and Selin, R. 1993. "Simulated Climatic Changes: Results of the COHMAP Climate-Model Experiments." Chapter 4 of *Global Climates Since the Last Glacial Maximum*. Wright, H., Jr.; Kutzbach, J.; Webb, T., III; Ruddiman, W.; Street-Perrott, F., Bartlein, P., eds. Minneapolis, Minnesota: University of Minnesota Press. TIC: 234248.

Langenheim, V.E.; Kirchoff-Stein, K.S.; and Oliver, H.W. 1993. "Geophysical Investigations of Buried Volcanic Centers Near Yucca Mountain, Southwest Nevada." *High Level Radioactive Waste Management, Proceedings of the Fourth Annual International Conference, Las Vegas, Nevada, April 26–30, 1993*, *2*, 1840–1846. La Grange Park, Illinois: American Nuclear Society. TIC: 208542.

Lide, D.R., ed. 1994. *CRC Handbook of Chemistry and Physics, A Ready-Reference Book of Chemical and Physical Data.* 75th Edition. Boca Raton, Florida: CRC Press. TIC: 102972.

Machette, M.N. 1985. "Calcic Soils of the Southwestern United States." *Soils and Quaternary Geology of the Southwestern United States*. Weide, D.L. and Faber, M.L., eds. Special Paper 203. Pages 1–21. Boulder, Colorado: Geological Society of America. TIC: 239387.

Nicholis, M.G. and Rutherford, M.J. 2004. "Experimental Constraints on Magma Ascent Rate for the Crater Flat Volcanic Zone Hawaiite." Geology, *32* (6), 489–492. Boulder, Colorado: Geological Society of America. TIC: 256878.

NOAA (National Oceanic and Atmospheric Administration) 2004. *Upper Air Data for Desert Rock, Nevada Years 1978–2003.* NCDC (National Climatic Data Center) Digital Upper Air Files TD 6201 and 6301. Asheville, North Carolina: National Oceanic and Atmospheric Administration. ACC: MOL.20040817.0103.

O'Leary, D.W.; Mankinen, E.A.; Blakely, R.J.; Langenheim, V.E.; and Ponce, D.A. 2002. *Aeromagnetic Expression of Buried Basaltic Volcanoes Near Yucca Mountain, Nevada.* Open-File Report 02-020. Denver, Colorado: U.S. Geological Survey. ACC: MOL.20020627.0225.

Pelletier, J.D.; DeLong, S.B.; Cline, M.L.; Harrington, C.D.; and Keating G.N. 2008. "Dispersion of Channel-Sediment Contaminants in Distributary Fluvial Systems: Application to Fluvial Tephra and Radionuclide Redistribution Following a Potential Volcanic Eruption at Yucca Mountain." *Geomorphology*, *94*, 226–246. New York, New York: Elsevier B.V. TIC: 260064.

Pelletier, J.D.; Harrington, C.D.; Whitney, J.W.; Cline, M.; DeLong, S.B.; Keating, G.; and Ebert, K.T. 2005. "Geomorphic Control of Radionuclide Diffusion in Desert Soils." *Geophysical Research Letters*, *32* (L23401), 1–4. Washington, D.C.: American Geophysical Union. TIC: 257905.

Perry, F.V. and Bowker, L.M. 1998. "Petrologic and Geochemical Constraints on Basaltic Volcanism in the Great Basin." Chapter 4 of *Volcanism Studies: Final Report for the Yucca Mountain Project*. Perry, F.V.; Crowe, B.M.; Valentine, G.A.; and Bowker, L.M.; eds. LA-13478. Los Alamos, New Mexico: Los Alamos National Laboratory. TIC: 247225.

Perry, F.V.; Cogbill, A.H.; and Kelley, R. E. 2005. "Uncovering Buried Volcanoes at Yucca Mountain." *Eos, Transactions*, *86* (47), 485, 488. Washington, D.C.: American Geophysical Union. TIC: 258001.

Perry, F.V. and Crowe, B.M. 1992. "Geochemical Evidence for Waning Magmatism and Polycyclic Volcanism at Crater Flat, Nevada." *High Level Radioactive Waste Management, Proceedings of the Third International Conference, Las Vegas, Nevada, April 12–16, 1992*, *2*, 2356–2365. La Grange Park, Illinois: American Nuclear Society. TIC: 204231.

Perry, F.V.; Crowe, B.M.; Valentine, G.A.; and Bowker, L.M., eds. 1998. *Volcanism Studies: Final Report for the Yucca Mountain Project.* LA-13478. Los Alamos, New Mexico: Los Alamos National Laboratory. TIC: 247225.

Sawyer, D.A.; Fleck, R.J.; Lanphere, M.A.; Warren, R.G.; Broxton, D.E.; and Hudson, M.R. 1994. "Episodic Caldera Volcanism in the Miocene Southwestern Nevada Volcanic Field: Revised Stratigraphic Framework, $^{40}Ar/^{39}Ar$ Geochronology, and Implications for Magmatism and Extension." *Geological Society of America Bulletin*, *106* (10), 1304–1318. Boulder, Colorado: Geological Society of America. TIC: 222523.

Self, S. and Walker, G.P.L. 1994. "Ash Clouds: Characteristics of Eruption Columns." *Volcanic Ash and Aviation Safety: Proceedings of the First International Symposium on Volcanic Ash and Aviation Safety held in Seattle, Washington in July 1991.* Casadevall, T.J., ed. U.S. Geological Survey Bulletin 2047. Pages 65–74. Washington, D.C.: U.S. Government Printing Office. TIC: 254494.

Slate, J.L.; Berry, M.E.; Rowley, P.D.; Fridrich, C.J.; Morgan, K.S.; Workman, J.B.; Young, O.D.; Dixon, G.L.; Williams, V.S.; McKee, E.H.; Ponce, D.A.; Hildenbrand, T.G.; Swadley, W C; Lundstrom, S.C.; Ekren, E.B.; Warren, R.G.; Cole, J.C.; Fleck, R.J.; Lanphere, M.A.; Sawyer, D.A.; Minor, S.A.; Grunwald, D.J.; Laczniak, R.J.; Menges, C.M.; Yount, J.C.; Jayko, A.S.; Mankinen, E.A.; Davidson, J.G.; Morin, R.L.; and Blakely, R.J. 2000. *Digital Geologic Map of the Nevada Test Site and Vicinity, Nye, Lincoln and Clark Counties, Nevada, and Inyo County, California, Revision 4; Digital Aeromagnetic Map of the Nevada Test Site and Vicinity, Nye, Lincoln, and Clark*

Counties, Nevada, and Inyo County, California; and Digital Isostatic Gravity Map of the Nevada Test Site and Vicinity, Nye, Lincoln, and Clark Counties, Nevada, and Inyo County, California. Open-File Report 99-554–A, –B, and –C. Denver, Colorado: U.S. Geological Survey. TIC: 248049; 251985; 251981.

Smith, E.I.; Feuerbach, D.L.; Naumann, T.R.; and Faulds, J.E. 1990. "The Area of Most Recent Volcanism Near Yucca Mountain, Nevada: Implications for Volcanic Risk Assessment." *High Level Radioactive Waste Management, Proceedings of the International Topical Meeting, Las Vegas, Nevada, April 8–12, 1990*, *1*, 81–90. La Grange Park, Illinois: American Nuclear Society. TIC: 202058.

SNL (Sandia National Laboratories) 2007a. *Dike/Drift Interactions.* MDL-MGR-GS-000005 REV 02. Las Vegas, Nevada: Sandia National Laboratories. ACC: DOC.20071009.0015.

SNL 2007b. *Number of Waste Packages Hit by Igneous Intrusion*. ANL-MGR-GS-000003 REV 03. Las Vegas, Nevada: Sandia National Laboratories. ACC: DOC.20071002.0001.

SNL 2007c. *In-Package Chemistry Abstraction.* ANL-EBS-MD-000037 REV 04 ADD 01. Las Vegas, Nevada: Sandia National Laboratories. ACC: DOC.20070816.0004.

SNL 2007d. *Atmospheric Dispersal and Deposition of Tephra from a Potential Volcanic Eruption at Yucca Mountain, Nevada*. MDL-MGR-GS-000002 REV 03. Las Vegas, Nevada: Sandia National Laboratories. ACC: DOC.20071010.0003.

SNL 2007e. *Characterize Eruptive Processes at Yucca Mountain, Nevada.* ANL-MGR-GS-000002 REV 03. Las Vegas, Nevada: Sandia National Laboratories. ACC: DOC.20070301.0001.

SNL 2007f. *Total System Performance Assessment Data Input Package for Requirements Analysis for Subsurface Facilities.* TDR-TDIP-PA-000001 REV 00. Las Vegas, Nevada: Sandia National Laboratories. ACC: DOC.20070921.0007.

SNL 2007g. *Redistribution of Tephra and Waste by Geomorphic Processes Following a Potential Volcanic Eruption at Yucca Mountain, Nevada*. MDL-MGR-GS-000006 REV 00. Las Vegas, Nevada: Sandia National Laboratories. ACC: DOC.20071220.0004.

SNL 2007h. *Engineered Barrier System: Physical and Chemical Environment.* ANL-EBS-MD-000033 REV 06. Las Vegas, Nevada: Sandia National Laboratories. ACC: DOC.20070907.0003.

SNL 2007i. *Dissolved Concentration Limits of Elements with Radioactive Isotopes.* ANL-WIS-MD-000010 REV 06. Las Vegas, Nevada: Sandia National Laboratories. ACC: DOC.20070918.0010.

SNL 2007j. *Biosphere Model Report*. MDL-MGR-MD-000001 REV 02. Las Vegas, Nevada: Sandia National Laboratories. ACC: DOC.20070830.0007.

SNL 2008. *Total System Performance Assessment Model/Analysis for the License Application*. MDL-WIS-PA-000005 REV 00 ADD 01. Las Vegas, Nevada: Sandia National Laboratories. ACC: DOC.20080312.0001.

Stamatakos, J.A.; Connor, C.B.; and Martin, R.H. 1997. "Quaternary Basin Evolution and Basaltic Volcanism of Crater Flat, Nevada, from Detailed Ground Magnetic Surveys of the Little Cones." *Journal of Geology*, *105*, 319–330. Chicago, Illinois: University of Chicago. TIC: 245108.

Suzuki, T. 1983. "A Theoretical Model for Dispersion of Tephra." *Arc Volcanism: Physics and Tectonics, Proceedings of a 1981 IAVCEI Symposium, August–September, 1981, Tokyo and Hakone*, 95–113. Tokyo, Japan: Terra Scientific Publishing Company. TIC: 238307.

Taddeucci, J.; Spieler, O.; Kennedy, B.; Pompilio, M.; Dingwell, D.B.; and Scarlato, P. 2004. "Experimental and Analytical Modeling of Basaltic Ash Explosions at Mount Etna, Italy, 2001." *Journal of Geophysical Research*, *109* (B8), 1–9. Washington, D.C.: American Geophysical Union. TIC: 257706.

Turney, G.L. 1986. *Quality of Ground Water in the Columbia Basin, Washington, 1983*. Water-Resources Investigations Report 85-4320. Tacoma, Washington: U.S. Geological Survey. ACC: LLR.20070321.0001.

Warpinski, N.R.; Abou-Sayed, I.S.; Moschovidis, Z.; and Parker, C. 1993. *Hydraulic Fracture Model Comparison Study: Complete Results*. GRI-93/0109. Chicago, Illinois: Gas Research Institute. TIC: 254276.

Warpinski, N.R.; Moschovidis, Z.A.; Parker, C.D.; and Abou-Sayed, I.S. 1994. "Comparison Study of Hydraulic Fracturing Models—Test Case: GRI Staged Field Experiment No. 3." *SPE Production & Facilities*, *9* (1), 7–16. Richardson, Texas: SPE Production & Facilities. TIC: 254277.

Woods, A.W.; Sparks, S.; Bokhove, O.; LeJeune, A-M.; Conner, C.B.; and Hill, B.E. 2002. "Modeling Magma—Drift Interaction at the Proposed High-Level Radioactive Waste Repository at Yucca Mountain, Nevada, USA." *Geophysical Research Letters*, *29* (13), 19-1 through 19-4. Washington, D.C.: American Geophysical Union. TIC: 254467.

Table 2.3.11-1. Igneous Activity Features Events, and Processes Included in Total System Performance Assessment

FEP Number and FEP Name	FEP Description	Summary of Technical Basis/Approach for FEP Inclusion
1.2.04.03.0A Igneous intrusion into repository	Magma from an igneous intrusion may flow into the drifts and extend over a large portion of the repository site, forming a sill, dike, or dike swarm, depending on the stress conditions. This intrusion could involve multiple drifts. The sill could be limited to the drifts or a continuous sill could form along the plane of the repository, bridging between adjacent drifts.	The modeling includes the in-drift conditions that would accompany the intersection of one or more emplacement drifts by an ascending basaltic dike and subsequent cooling and solidification of the basaltic intrusion (Section 2.3.11.3). This section also addresses estimating the number of waste packages damaged in the intersected drifts. For TSPA, once intersection of the repository footprint by a dike is modeled, all drifts are assumed to be inundated by magma. The mean annual frequency of intersection of the repository by a basalt dike is 1.7×10^{-8} (BSC 2004, Table 7-1). An igneous event includes intersection of the repository footprint accompanied by eruption at some location along the dike. The conditional probability of eruption given intersection of the repository is, therefore, 1. However, as explained in Section 2.3.11.4.2.1.3 the fraction of intersections that result in eruption through the repository is much less than 1, and the fraction of eruptions in which conduits intersect waste packages is even less. However the basis for inclusion is the event probability, or the mean annual frequency of intersection, which is 1.7×10^{-8} (BSC 2004, Table 7-1).
1.2.04.04.0A Igneous intrusion interacts with EBS components	An igneous intrusion in the form of a dike may occur through the repository, intersecting the repository drifts, resulting in magma, pyroclastics, and volcanic gases entering the drift and interacting with the EBS components (drip shields, waste packages, pallet, and invert). This could lead to accelerated drip shield and waste package failure (e.g., attack by magmatic volatiles, damage by flowing or fragmented magma, thermal effects) and dissolution or volatilization of waste.	In-drift conditions that would accompany intersection of one or more emplacement drifts by an ascending basaltic dike are described (Section 2.3.11.3). The expected behavior of waste packages exposed to magma is described. This supports the TSPA assumption that waste packages, drip shields, and cladding contacted by magma provide no protection for the waste. Rather, the waste is assumed to be instantaneously degraded (Section 2.3.11.3.2.4), and waste volatilization is not considered as a separate process. Because of strong buffering provided by degraded waste package contents, the igneous intrusion modeling case uses the liquid influx abstraction for the nominal case (Section 2.3.11.5).

Table 2.3.11-1. Igneous Activity Features Events, and Processes Included in Total System Performance Assessment (Continued)

FEP Number and FEP Name	FEP Description	Summary of Technical Basis/Approach for FEP Inclusion
1.2.04.04.0B Chemical effects of magma and magmatic volatiles	An igneous intrusion into the repository may be accompanied by the release of magmatic volatiles. The volatiles may affect in-drift chemistry (potentially leading to increased waste package corrosion), or may be absorbed by the host rock, where they could change the chemistry of the water seeping back into the drift following the intrusive event. Seepage water chemistry following magma cooling could also be affected by flowing through and interacting with the intruded basalt.	Chemistry of water percolating into drifts that have cooled after an igneous intrusion could be affected by basalt–water interactions (Section 2.3.11.3.2.9). Analogue data on basalt-water chemistry is included in Section 2.3.11.3.2.10 to support the abstraction of basalt-water chemistry used in the TSPA.
1.2.04.06.0A Eruptive conduit to surface intersects repository	As a result of an igneous intrusion, one or more volcanic vents may form at land surface. The conduit(s) supplying the vent(s) could pass through the repository, interacting with and entraining waste.	The modeling of eruption, dispersal, and transport of radionuclides is described (Section 2.3.11.4.2.2), as well as the estimation of the number of waste packages intersected by eruptive conduits, and the fraction of igneous events that include development of eruptive conduits (Section 2.3.11.4.2.1). The descriptions provide the primary inputs for ASHPLUME to model the volcanic eruption modeling case in TSPA.
1.2.04.07.0A Ash fall	Finely divided waste particles may be carried up a volcanic vent and deposited on the land surface from an ash cloud.	The volcanic eruption modeling case includes entrainment of waste in an ascending tephra plume and deposition of contaminated tephra on the land surface (Section 2.3.11.4.2.1). The result is the areal concentration of contaminated tephra on the ground surface at the RMEI location.
1.2.04.07.0C Ash redistribution via soil and sediment transport	Following deposition of contaminated ash on the surface, ash deposits may be redistributed on the surface via eolian and fluvial processes.	The ash redistribution model is described, as are the results of surficial processes acting on primary tephra deposited on the two primary landforms near the RMEI location: distributary channels and interchannel divides (Section 2.3.11.4.2.3.1). The model evaluates the effects of surficial processes on concentrations of waste as contaminated tephra is transported to the RMEI location. Eolian processes are not included in the model; see description in Section 2.3.11.4.4.3.

Table 2.3.11-2. Approximate Estimated Volumes and $^{40}Ar/^{39}Ar$ Ages of Pliocene and Quaternary Volcanoes in the Yucca Mountain Region

Volcano	Estimated Volume (km^3)	Estimated Age (Ma)
Lathrop Wells Cone	0.12	0.08
Hidden Cone	0.03	0.35
Little Black Peak	0.014	0.35
Makani Cone	0.004	1.1
Black Cone	0.06	1.1
Red Cone	0.06	1.1
Little Cones	0.03	1.1
Buckboard Mesa	0.92	2.9
Southeast Crater Flat	0.68	3.8
Thirsty Mountain	3.0	4.6

Source: SNL 2007e, Table 6-2; Perry, Crowe et al. 1998 for Volumes; Fleck et al. 1996; Heizler et al. 1999.

Table 2.3.11-3. Summary of 2005-2006 Drilling Results and Age of Buried Basaltic Rocks

Drill hole	Location	Aeromagnetic Anomaly	Depth to basalt (m)	Age (Ma) from $^{40}Ar/^{39}Ar$ method	Uncertainty (1σ)
USW VA-2	Amargosa Desert	G	118.3	3.91	0.11
UE-25 VA-10	Jackass Flats	JF-5	77.7	9.48	0.02
USW VA-1	Crater Flat	A	148.4	9.99	0.10
USW VA-4a	Crater Flat	Q	139.9	11.19	0.29

NOTE: The best estimate age represents the weighted-mean age (weighted by the inverse of the analytical error) for individual sample analyses.

Table 2.3.11-4. Published Estimates of the Probability of Intersection of the Repository at Yucca Mountain by a Volcanic Event

Reference	Intersection Probability (per year)	Comment	Event Representation
Crowe, Johnson et al. 1982, pp. 184 to 185	3.3×10^{-10} to 4.7×10^{-8}	Range of alternative probability calculations	point
Crowe, Perry, Valentine et al. 1993, p. 188	2.6×10^{-8}	Median value of probability distribution	point
Connor and Hill 1995, pp. 10, 121	1 to 5×10^{-8}	Range of three alternative models	point
Crowe, Perry, Geissman et al. 1995, Table 7.22	1.8×10^{-8}	Median value of 22 alternative probability models	point
Ho and Smith 1998, pp. 507 and 508	(1) 1.5×10^{-8} (2) 1.09×10^{-8} 2.83×10^{-8} (3) 3.14×10^{-7}	Three alternative models are presented; the third model assumes a spatial intersection ratio (using a Bayesian prior) of 8/75 or 0.11, approximately one order of magnitude higher than other published estimates because volcanic events are forced to occur within a small zone enclosing Yucca Mountain.	point
Perry, Crowe et al. 1998, Chapter 6, p. 6-84	2.5×10^{-8}	Sensitivity analysis that conservatively assumes all aeromagnetic anomalies in Amargosa Valley are Quaternary age	point
Connor et al. 2000, pp. 428 and 429	10^{-8} to 10^{-7}	Value of 10^{-7} assumes maximum event length of 20 km, regional recurrence rates of five events per million years, and that crustal density variations contribute to event location.	line
CRWMS M&O 1996, Section 4.3	1.5×10^{-8}	Results of 10-member expert elicitation panel	line

NOTE: Events were originally represented as point occurrences or the intersection of the repository by a point event. The original definition has been refined to describe intersection of the repository by a dike, which is a linear feature having an orientation and a length.

Source: Modified after BSC 2004, Table 6-5.

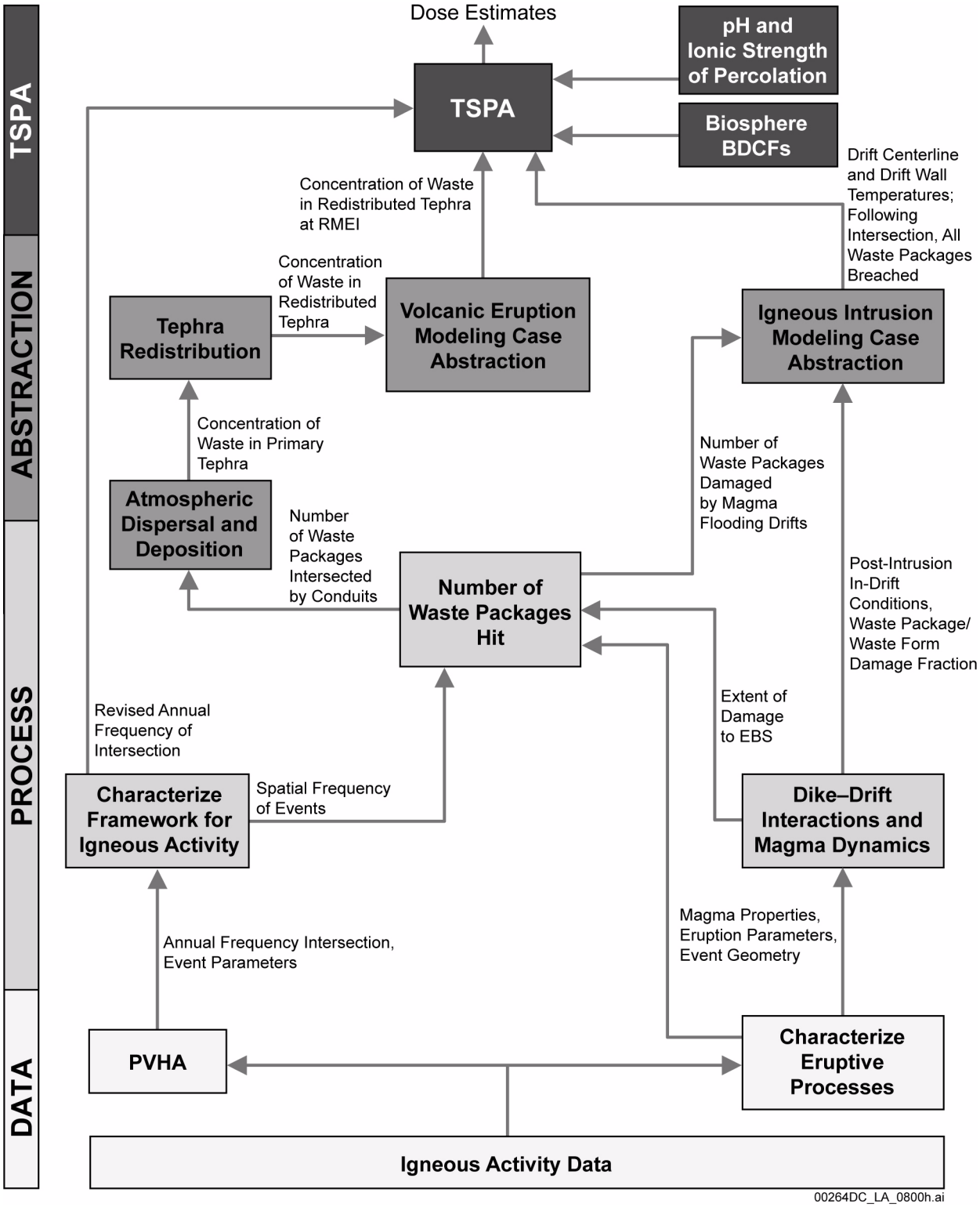

Figure 2.3.11-1. Information Flow Supporting TSPA Igneous Intrusion and Volcanic Eruption Model Cases at the Data, Process, Abstraction, and TSPA Levels

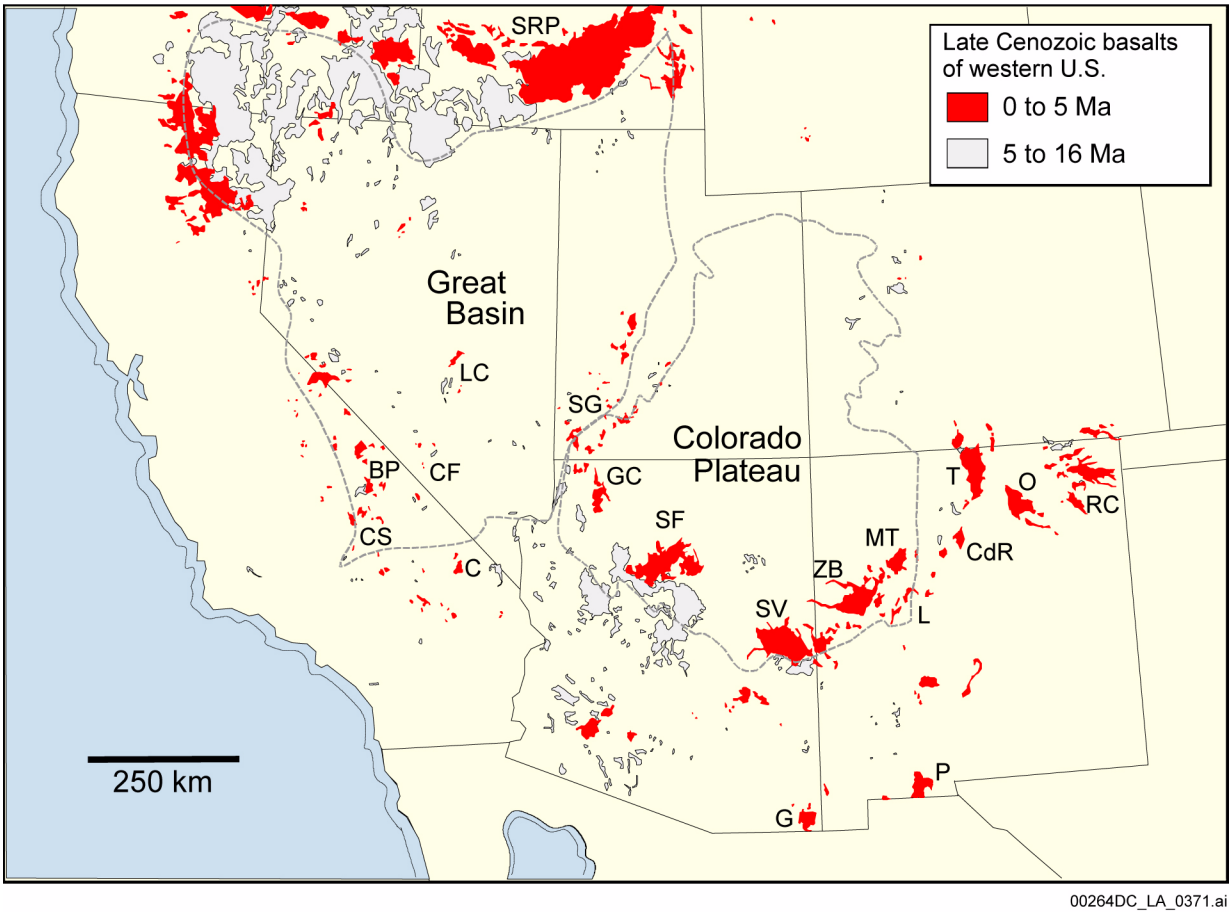

Figure 2.3.11-2. Distribution of Basalts in Southwest United States

NOTE: CF (Crater Flat) is adjacent to Yucca Mountain.
BP = Big Pine; C = Cima; CdR = Cerros del Rio; CF = Crater Flat; CS = Coso; G = Geronimo; GC = Grand Canyon; L = Lucero; LC = Lunar Crater; MT = Mount Taylor; O = Ocate; P = Potrillo; RC = Raton-Canyon; SF = San Francisco; SG = Saint George; SRP = Snake River Plain; SV = Springerville; T = Taos; ZB = Zuni-Banderra.

Source: Modified after Perry, Crowe et al. 1998, Figure 4.1.

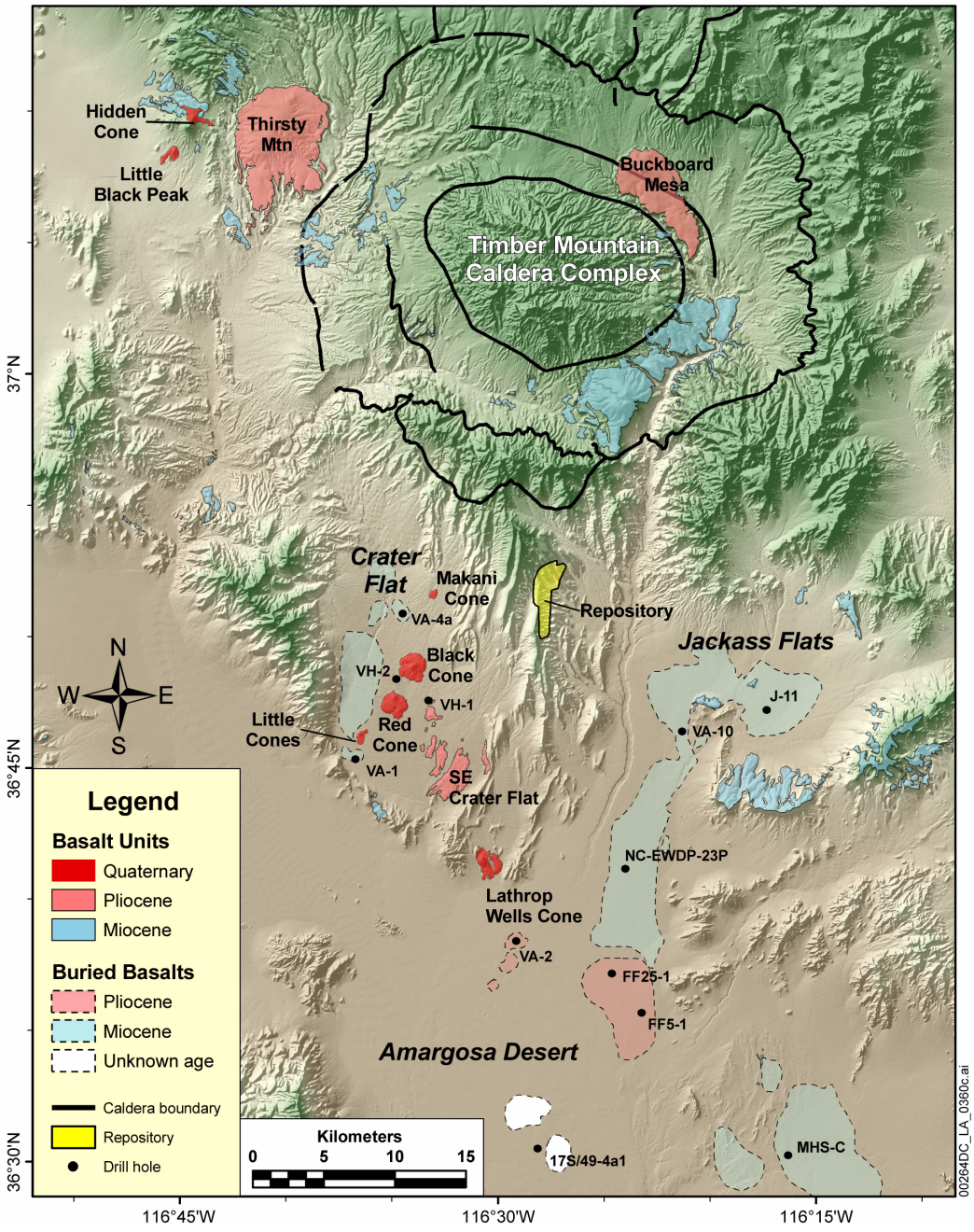

Figure 2.3.11-3. Distribution of Quaternary, Pliocene and Miocene Basaltic Rocks in the Yucca Mountain Region

NOTE: All drill holes shown encountered buried basalt. Distribution of buried basalt (areas enclosed by dashed lines) based on interpretation of aeromagnetic data and drill hole results. Buried basalts are Miocene in age except for approximately 3.8-Ma basalts in drill holes VH-1, VA-2, FF5-1 and FF-25-1 in Crater Flat and northern Amargosa Desert.

Source: Based on information presented in Slate et al. 2000; SNL 2007e, Table 6-2; Fleck et al. 1996; Perry, Crowe et al 1998; Heizler et al. 1999.

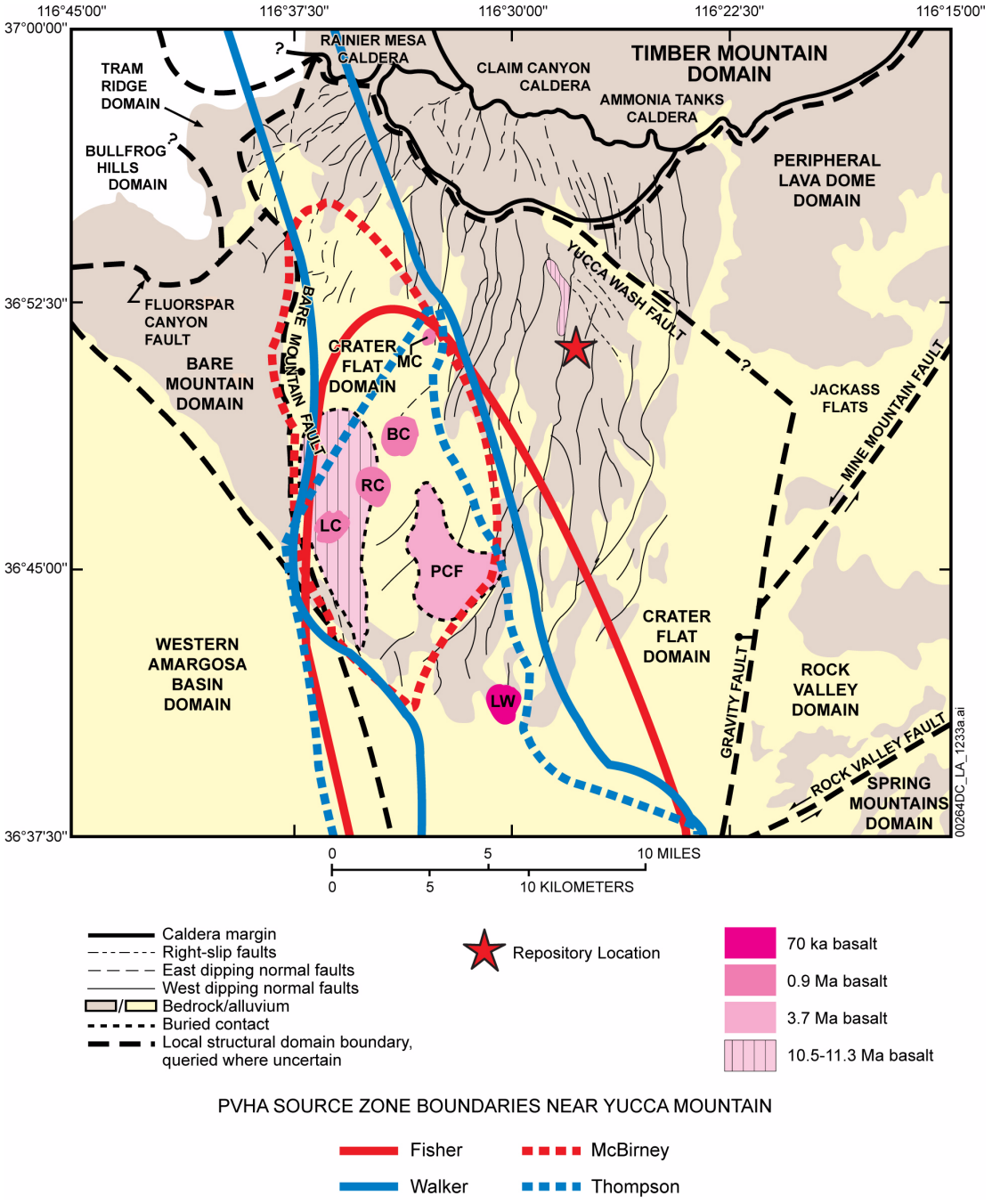

Figure 2.3.11-4. Local Structural Domains and Volcanic-Source Zones of the Yucca Mountain Region

NOTE: Superimposed on the Fridrich et al. (1999, Figure 1) map are boundaries of selected volcanic source zones (locally homogeneous spatial and temporal model (CRWMS M&O 1996, Section 3.1.3)) that lie within the Crater Flat basin, as defined by the PVHA experts (CRWMS M&O 1996, Appendix E). Other experts (not shown for clarity) used similar source-zone boundaries. The 70 ka age indicated in the figure legend for Lathrop Wells has been superseded by an age of 77 ka (Heizler et al. 1999), which has been rounded to 80 ka in this section.
BC = Black Cone; LC = Little Cones; LW = Lathrop Wells; MC = Makani Cone; PCF = Pliocene Crater Flat; RC = Red Cone.

Source: BSC 2004, Figure 6-7b.

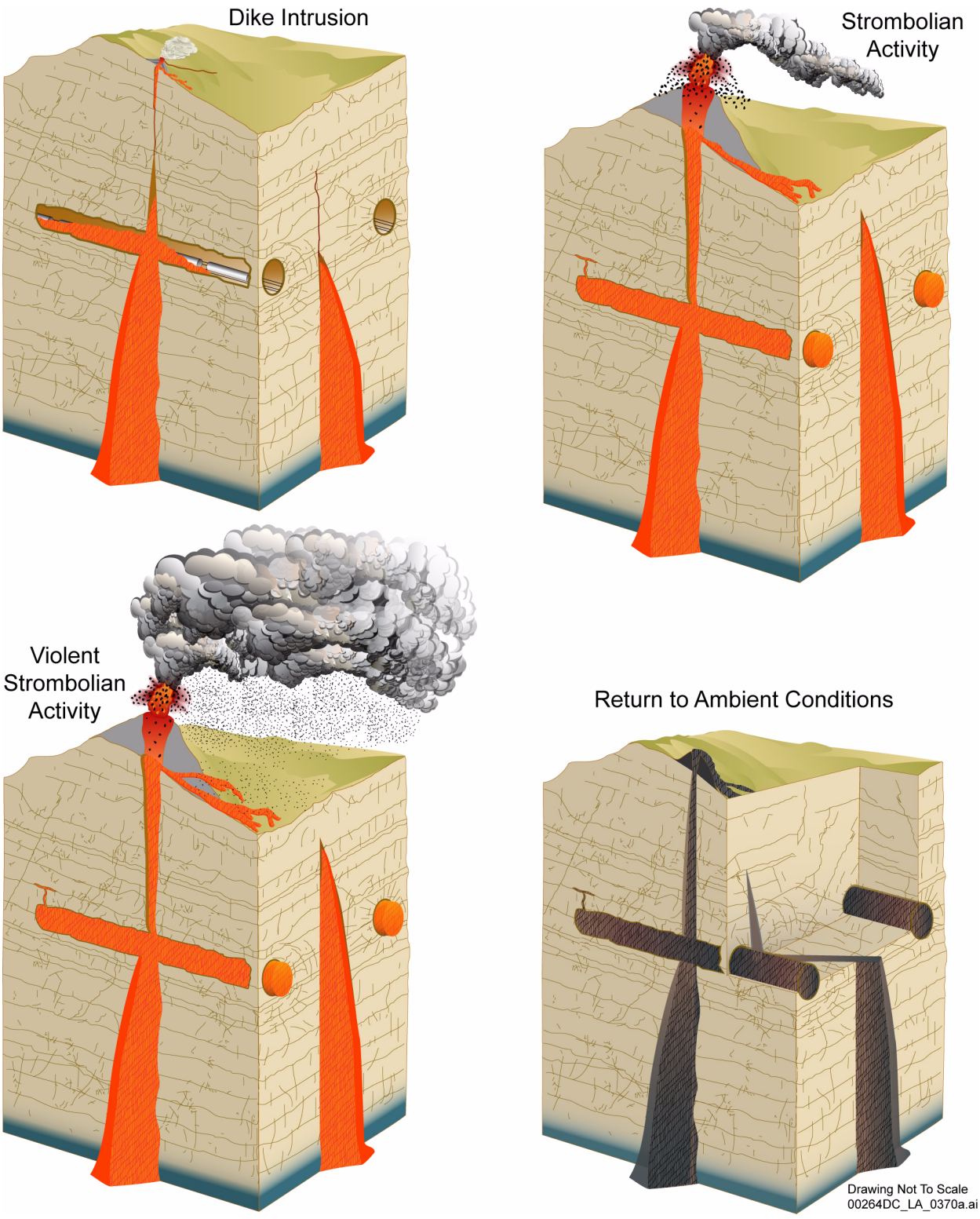

Figure 2.3.11-5. Schematic Drawing of the Processes Associated with a Hypothetical Dike Intrusion into and Eruption through a Repository

Source: SNL 2007a, Figure 1-1.

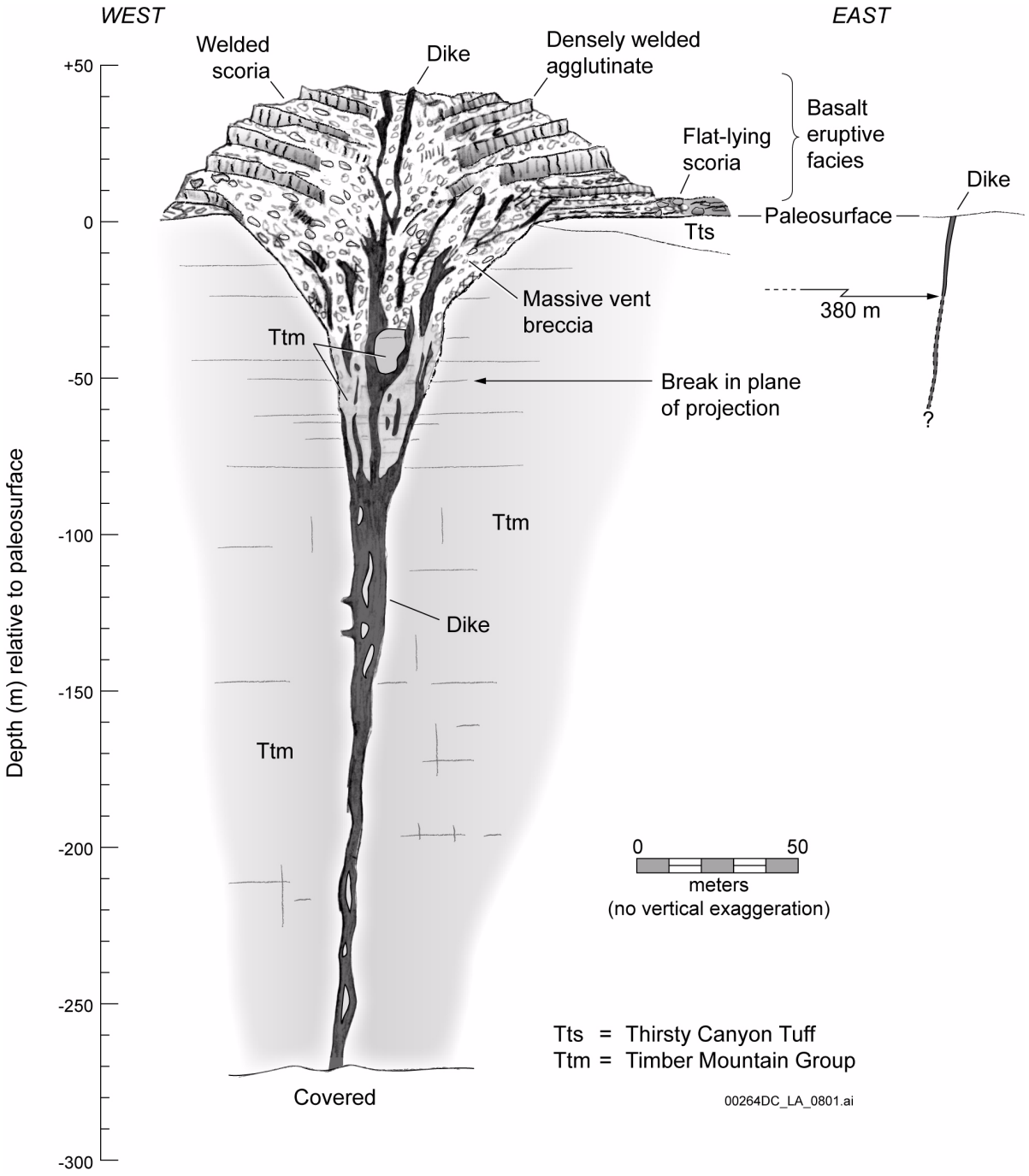

Figure 2.3.11-6. Cross Section of Basaltic Dike Set and Conduit, with Vent-Filling Facies on South Edge of Basalt Ridge East

NOTE: The view is along the plane of the dike set. The eruptive pile shows welded scoria and densely welded agglutinates dipping inward toward the fissure eruption marked by the location of the dikes. All loose scoria material has been removed by erosion. The upper one-third of the figure is displaced from the lower two-thirds by about 100 m because of canyon geometry, so that the subsurface part of the system is juxtaposed with the surface features. The arrow labeled 380 m on the right of the figure shows the approximate distance to the nearest dike. The vertical extent of the dike is unknown, as indicated by the question mark.

Source: Modified after BSC 2005a, Figure 6-7.

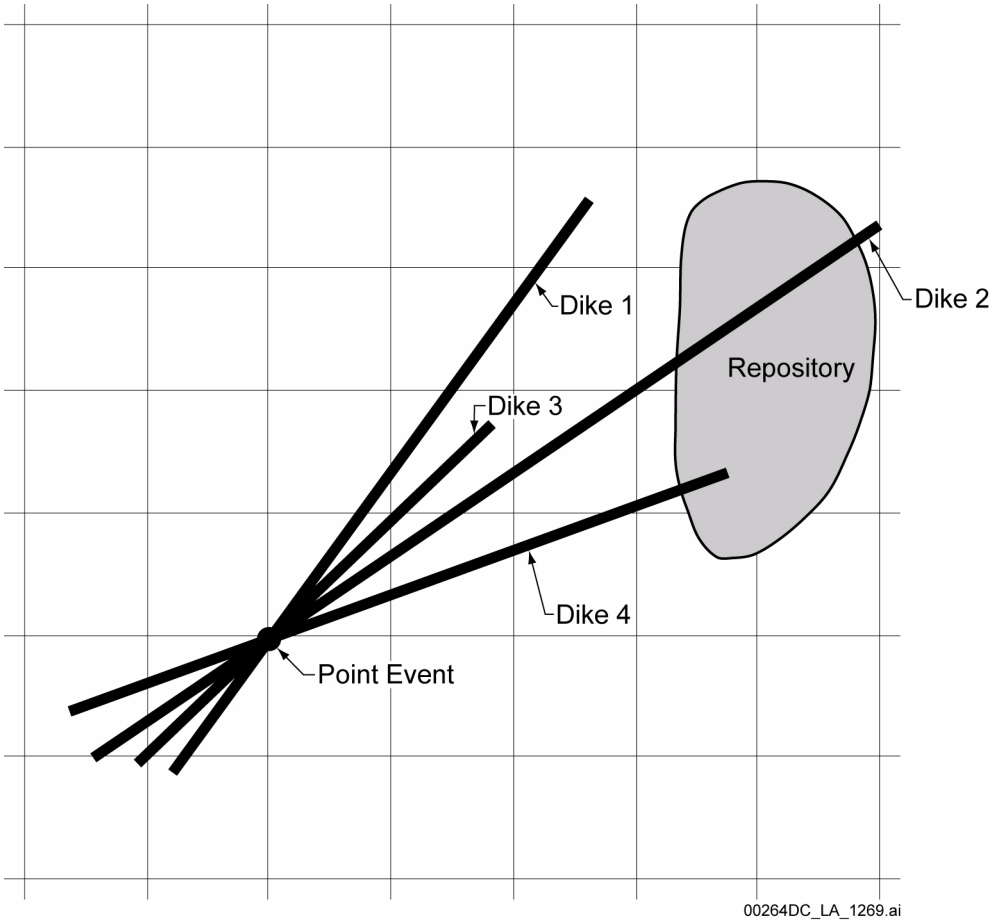

Figure 2.3.11-7. Schematic Illustrating Procedure for Computing the Frequency of Intersection of the Repository by a Dike or Dikes

NOTE: For Illustration Only.

Source: Modified after BSC 2004, Figure 6-8.

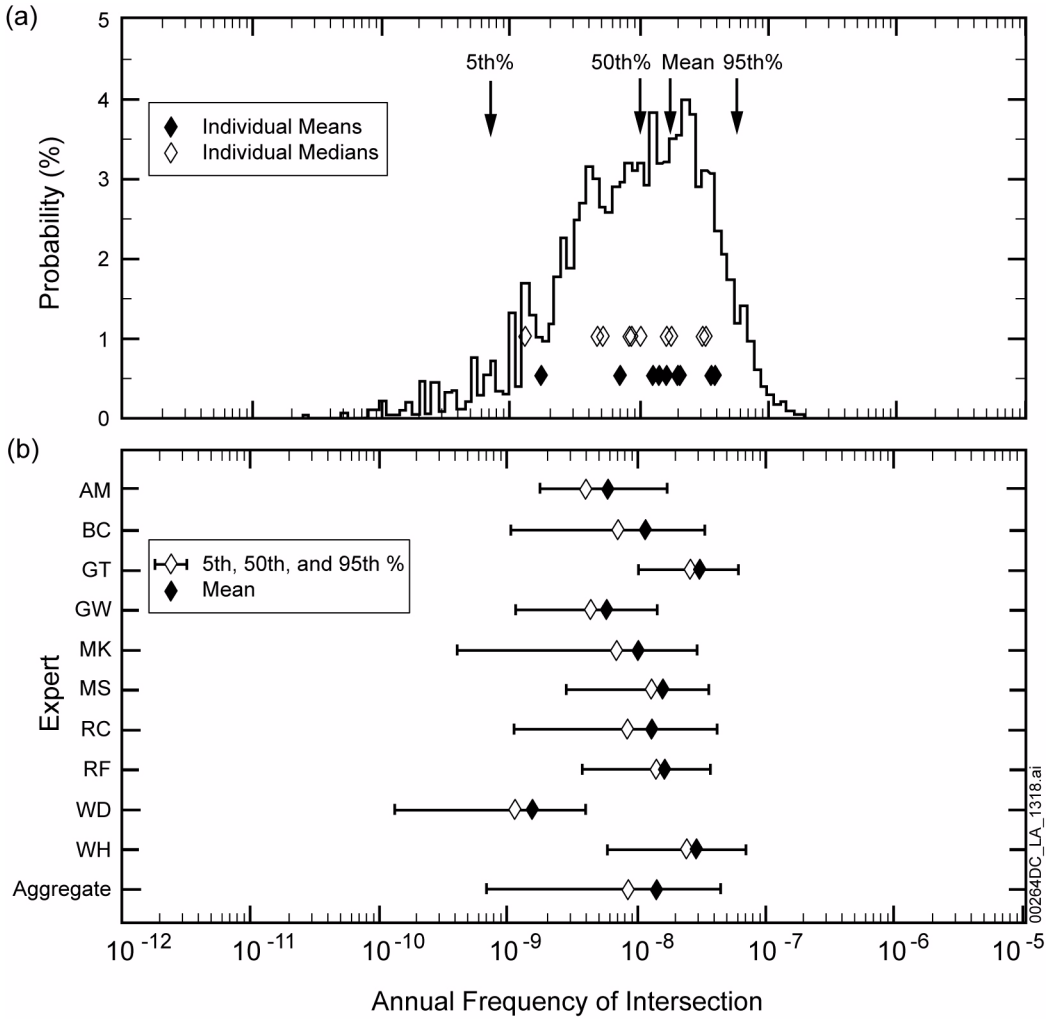

Figure 2.3.11-8. Annual Frequency of Intersecting the 2003 Repository Footprint

NOTE: (a) Aggregate distribution and median and means for individual PVHA expert interpretations.
(b) Range for 5th to 95th percentiles for results from individual PVHA expert interpretations compared to range for aggregate distribution. Two-letter code indicates initials of experts. Expert names and affiliations are listed in *Characterize Framework for Igneous Activity at Yucca Mountain, Nevada* (BSC 2004, Table 6-3).

Source: Modified after BSC 2004, Figure 6-18.

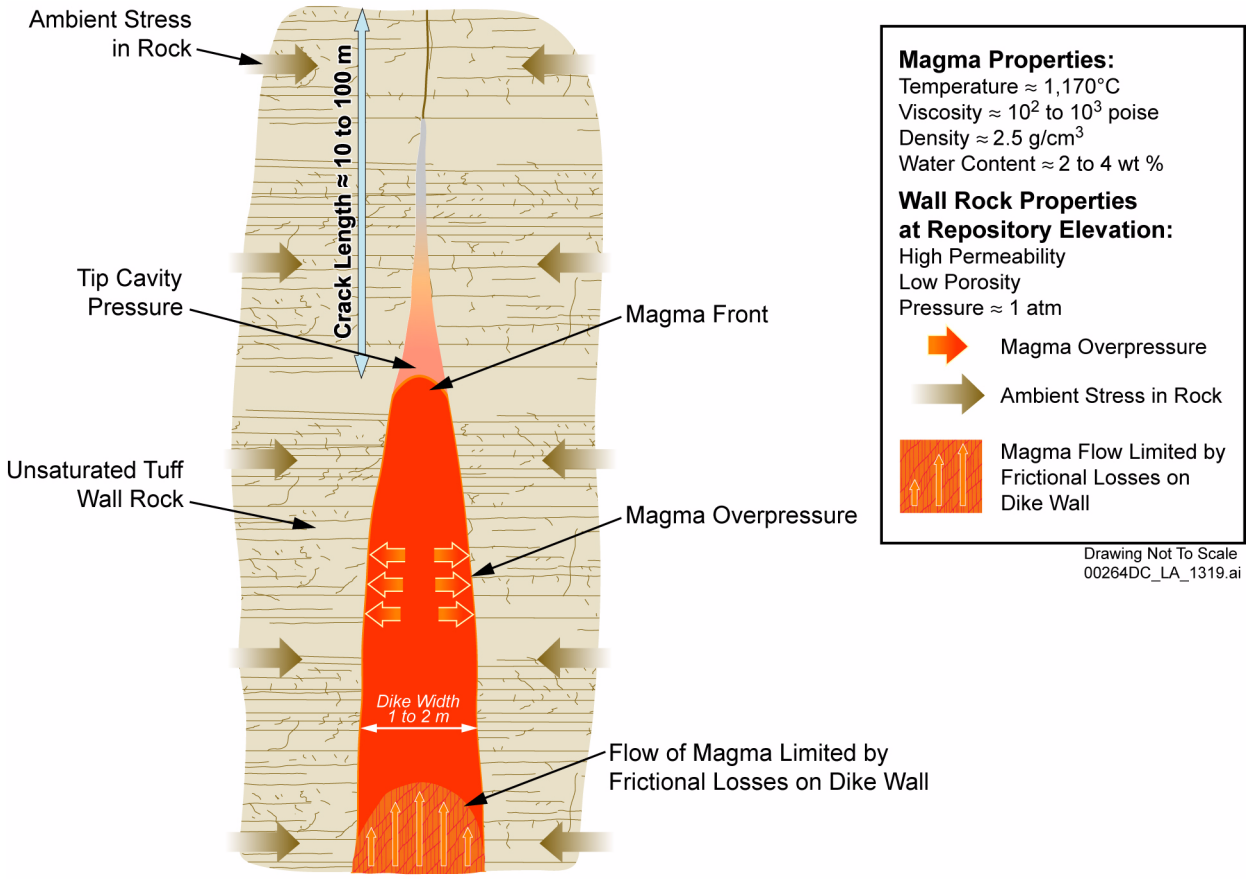

Figure 2.3.11-9. Schematic Depicting a Magma-Filled Dike Ascending through the Crust

NOTE: For illustration only. Host tuff is modeled as homogeneous, isotropic material (SNL 2007a, Section 6.3.2, Assumption 5.2, Homogeneous, Isotropic Surrounding Rock).

Source: Modified after Detournay et al. 2003, Figure 3-1.

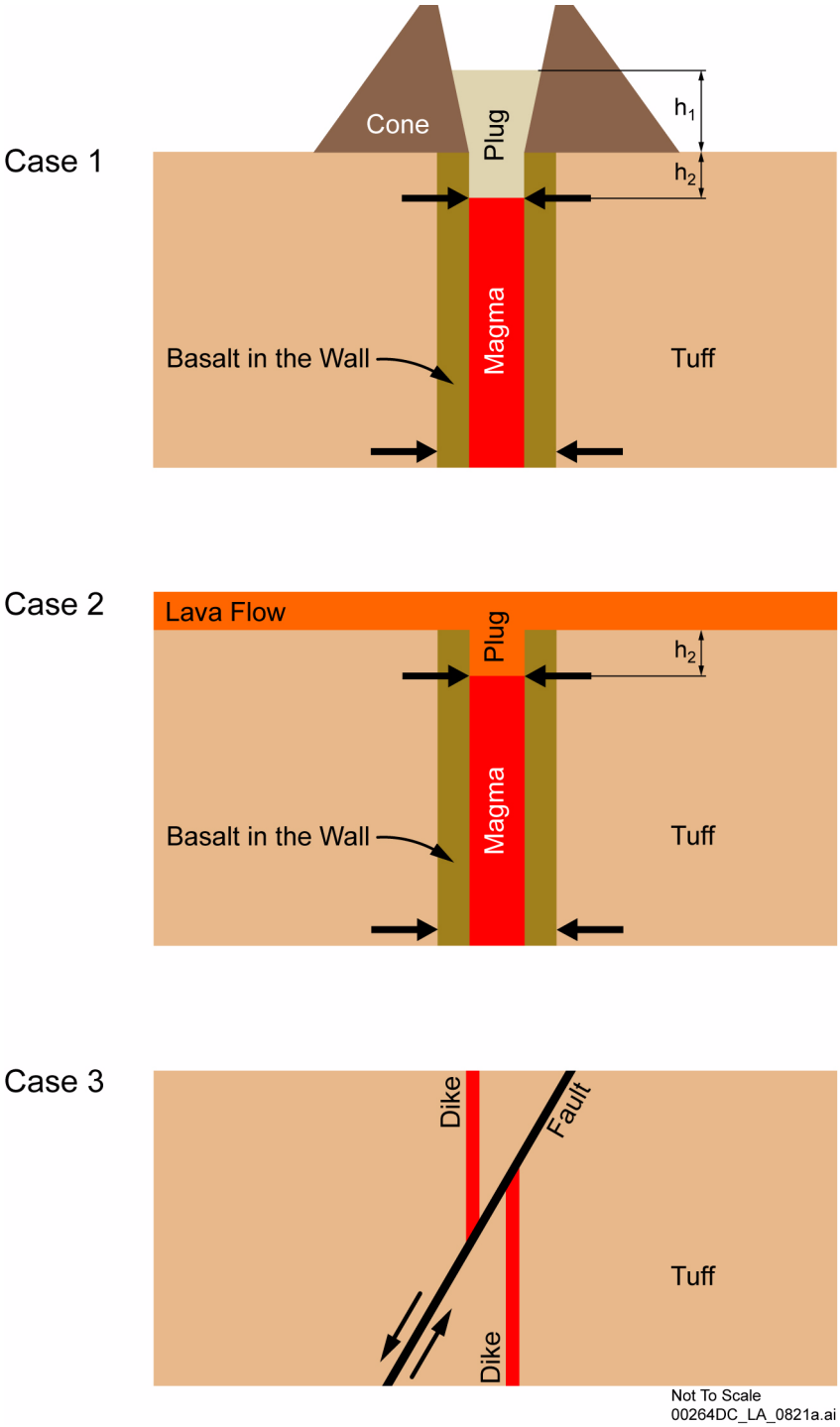

Figure 2.3.11-10. Schematic Diagram Showing Configuration of Initial Conditions for Analysis of Magma Blockage and Overpressure

NOTE: For illustration only.
h_1= height of the plug in the scoria cone; h_2 = depth of solidified magma in the conduit.

Source: Modified after SNL 2007a, Figures 6-140, 6-141, and 6-142.

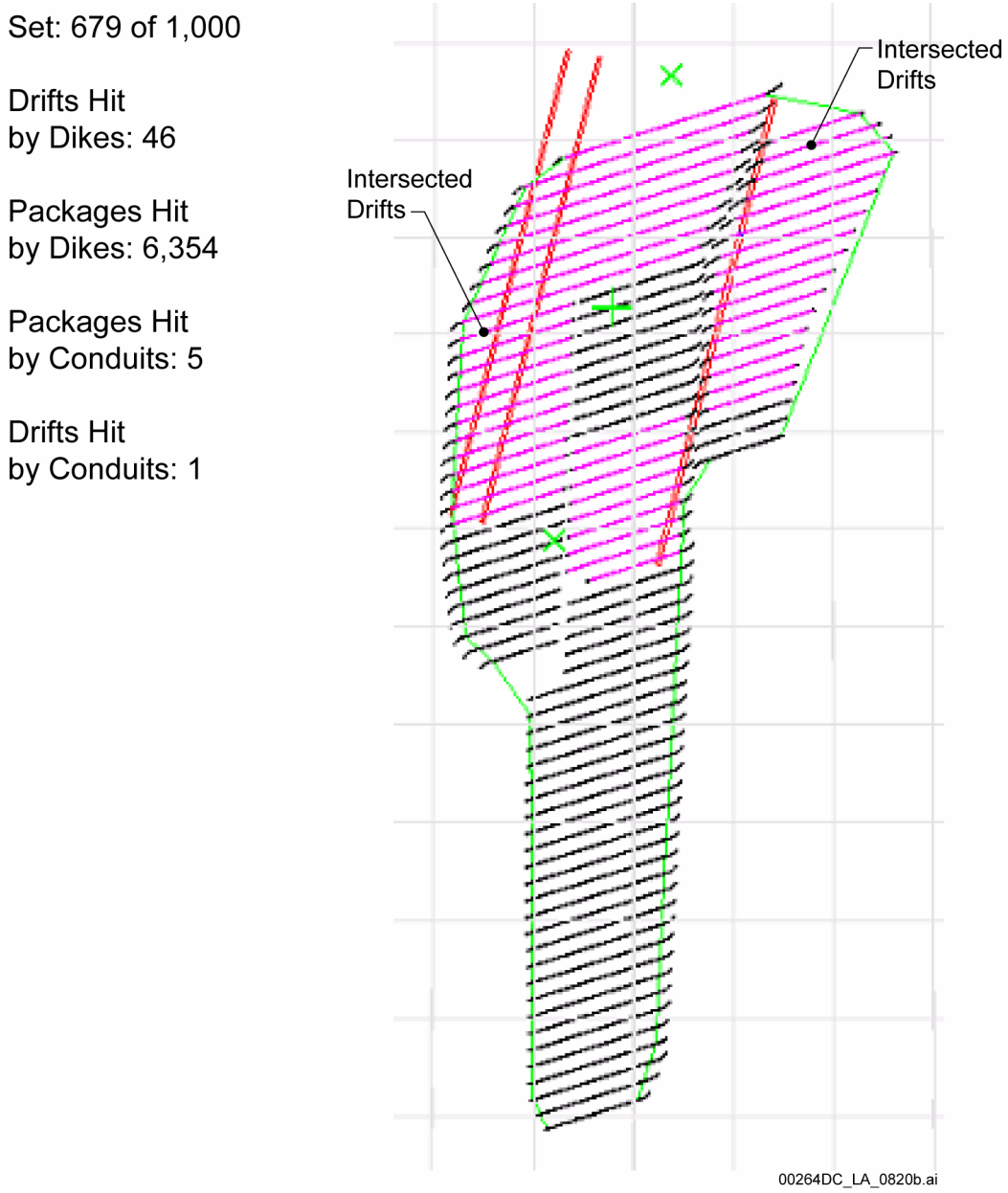

Figure 2.3.11-11. Example of Dike Swarm Configuration Intersecting Repository Drifts from the Screen Capture of the DIRECT Code

NOTE: Configuration shown indicates drifts initially contacted by dikes. It is assumed that all drifts are flooded with magma following initial dike intersection. The green cross represents the sampled center (centroid) of the dike swarm. The two green Xs (not to be confused with the green cross) represent the dike length extent for a hypothetical dike centered at the centroid.

Source: Modified after SNL 2007b Figure 6-7.

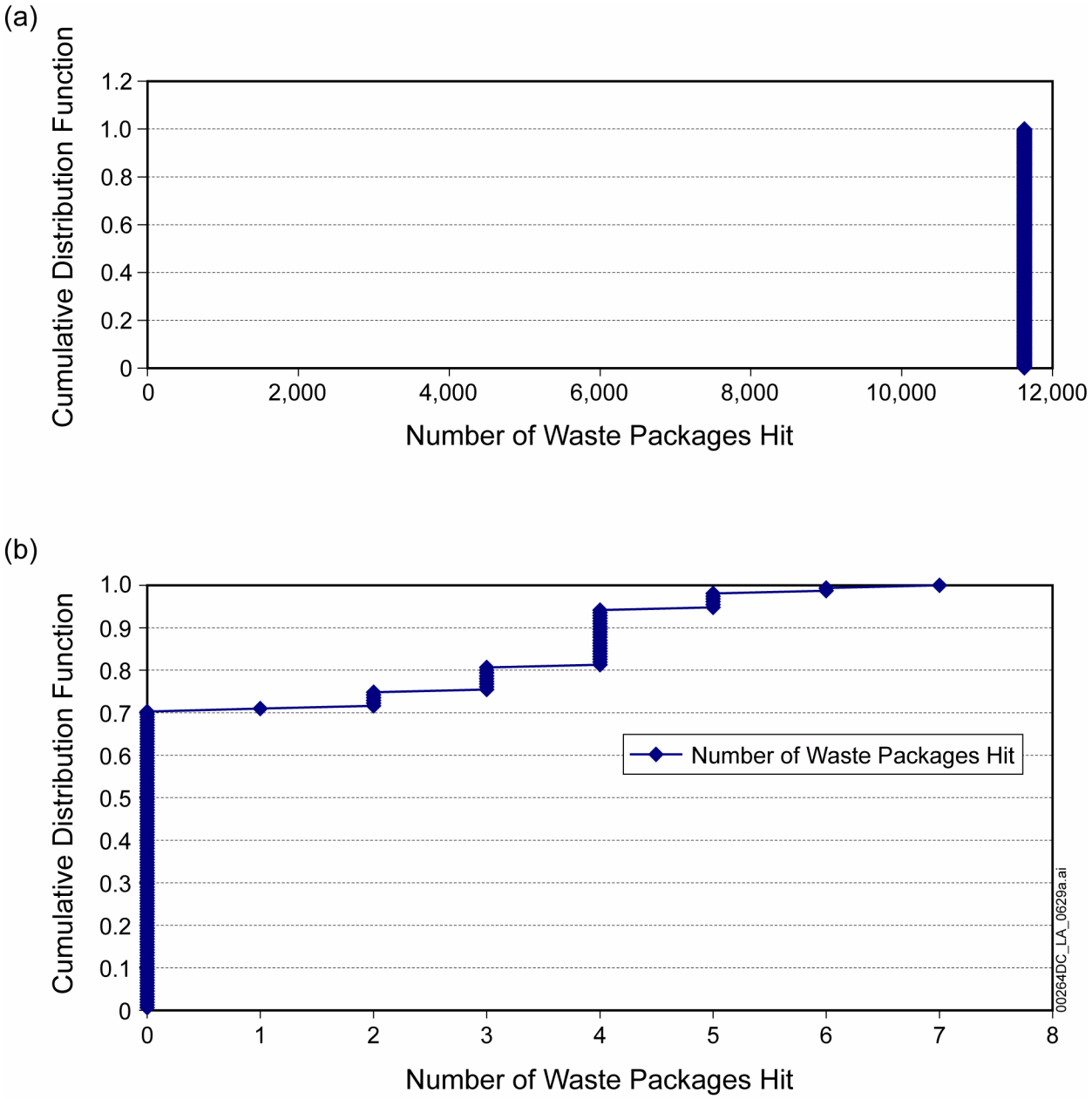

Figure 2.3.11-12. Number of Waste Packages (a) Hit by a Dike or Dike Swarm in the Igneous Intrusion Modeling Case and (b) Intersected by Conduits in the Volcanic Eruption Modeling Case

Source: SNL 2007b Figures 7-1 and 7-2.

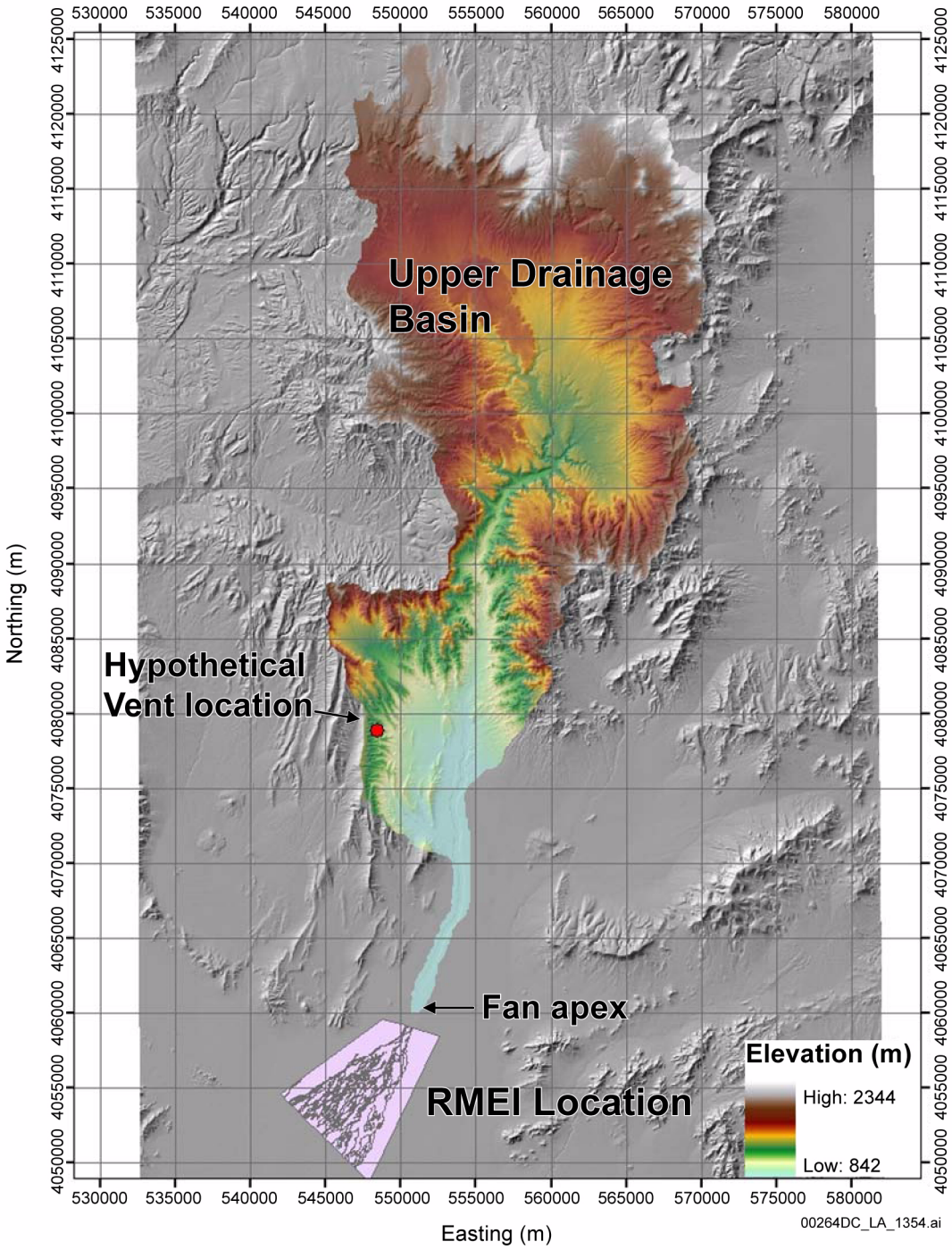

Figure 2.3.11-13. Map Showing the Upper Drainage Basin Domain (Colored by Elevation), the RMEI Location (Pink), and the Hypothetical Vent Location

NOTE: The hypothetical vent location is at the center of the repository (SNL 2007g, Section 6.5.7.1). Coordinates are Universal Transmercator Zone 11.

Source: Modified after SNL 2007g, Figure 1-2.

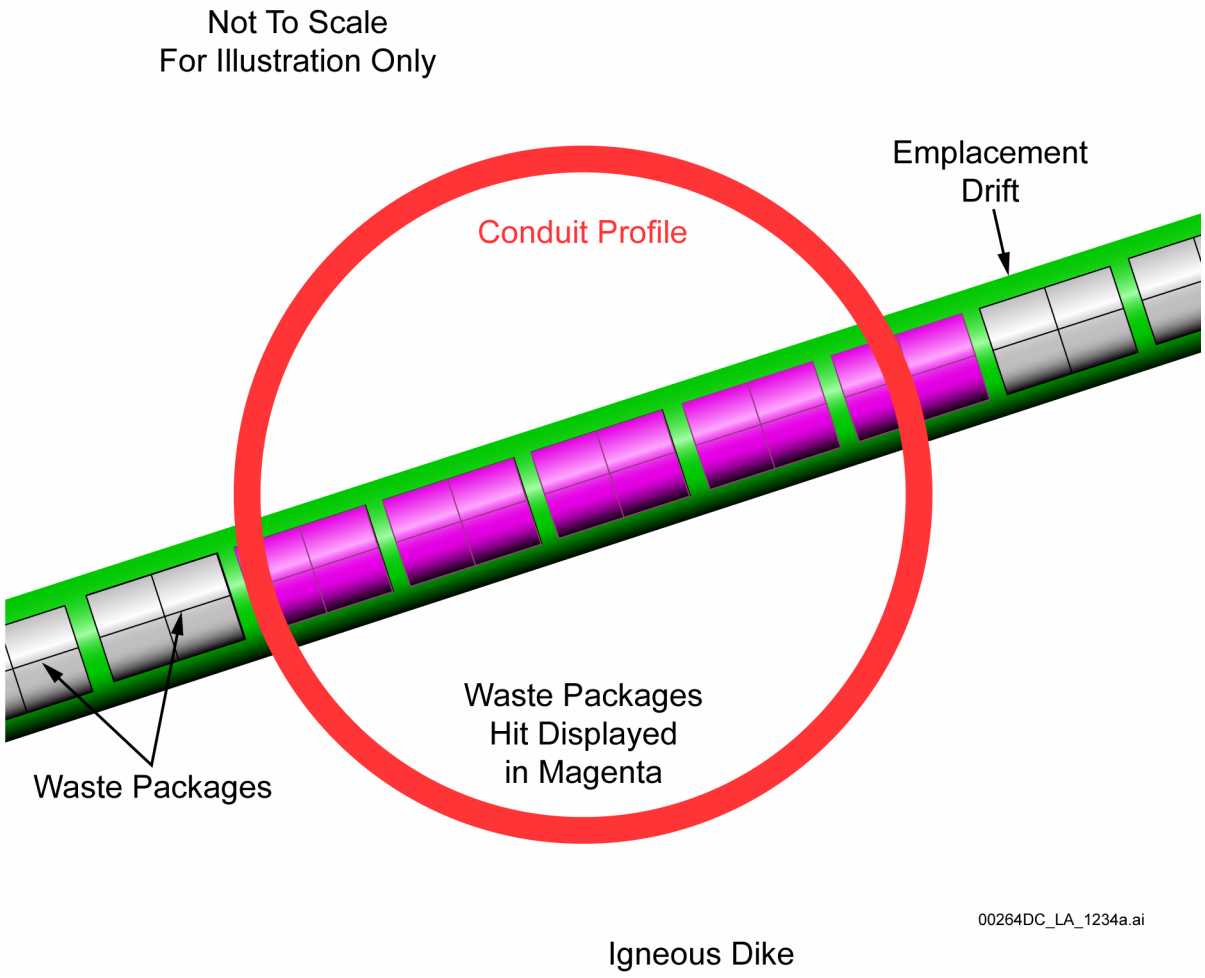

Figure 2.3.11-14. Illustration of Eruptive Conduit “Cookie Cutter” Treatment

NOTE: Waste packages displayed in magenta are directly intersected by the eruptive conduit and the waste package contents are assumed to be available for incorporation in the rising magma. Other waste packages in drifts are assumed to be engulfed by magma following dike intersection and their contents available for groundwater transport.

Source: SNL 2007b, Figure 5-1.

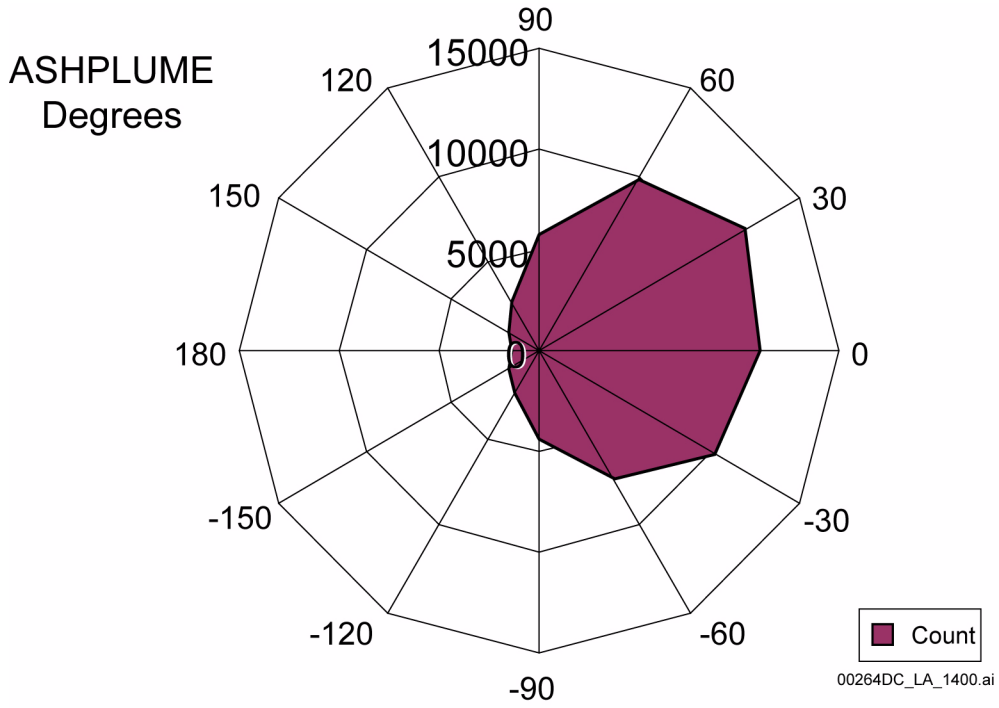

Figure 2.3.11-15. Wind-Rose Frequency of Occurrences at 3 to 4 km Above Yucca Mountain

Source: SNL 2007d, Figure 8-1.

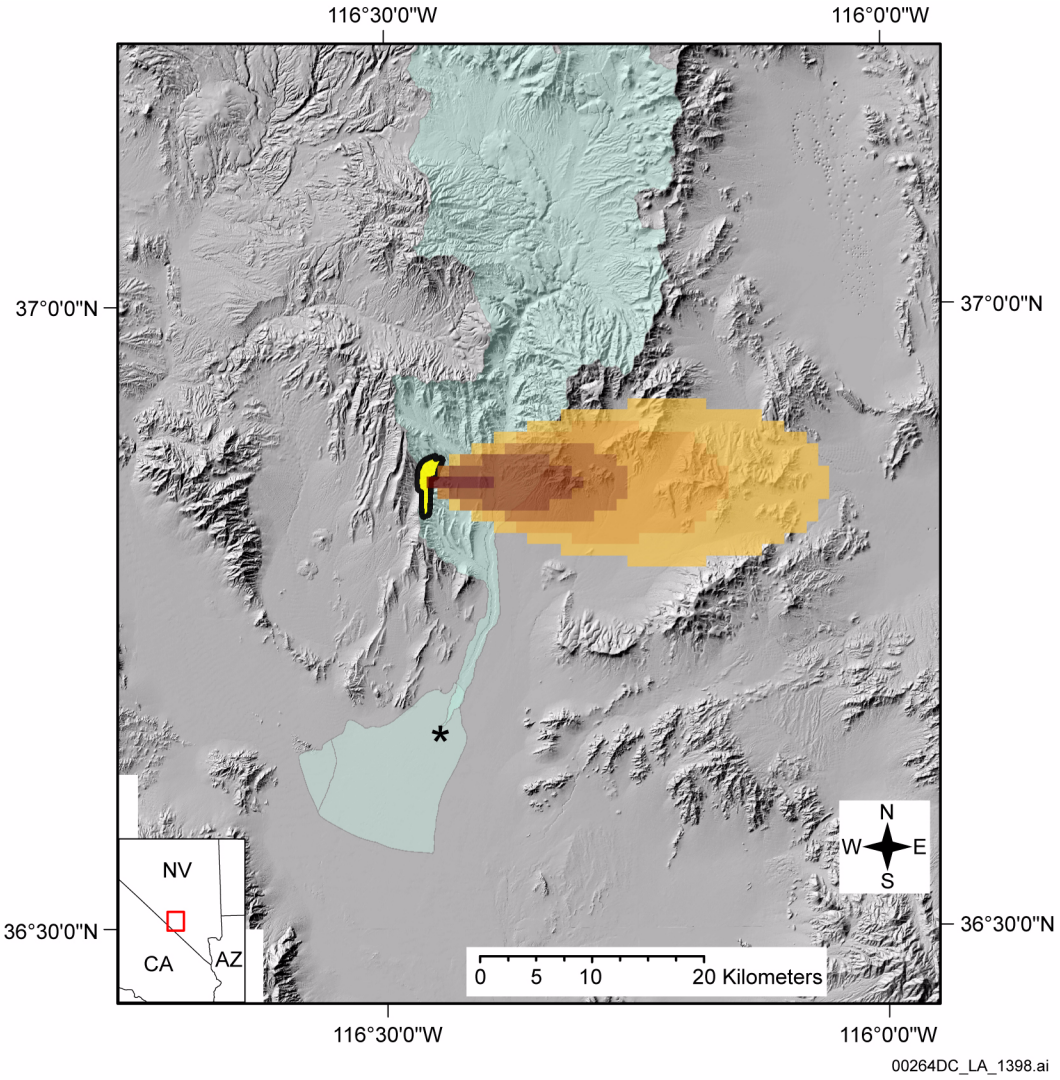

Figure 2.3.11-16. Schematic Illustration of Tephra Deposit from Example Atmospheric Dispersal Model Realization in Relation to the Fortymile Wash Watershed

NOTE: The map includes the outline of the repository (yellow), Fortymile Wash watershed (light blue), the approximate location of the RMEI (*), and a typical ASHPLUME tephra distribution (yellow-brown; > 1 cm thickness; contours at 2, 5, 10, 50 cm).

Modified after SNL 2007g, Figure 6.3.3-9 to provide additional thickness estimates and extent of tephra more than 1 cm thick.

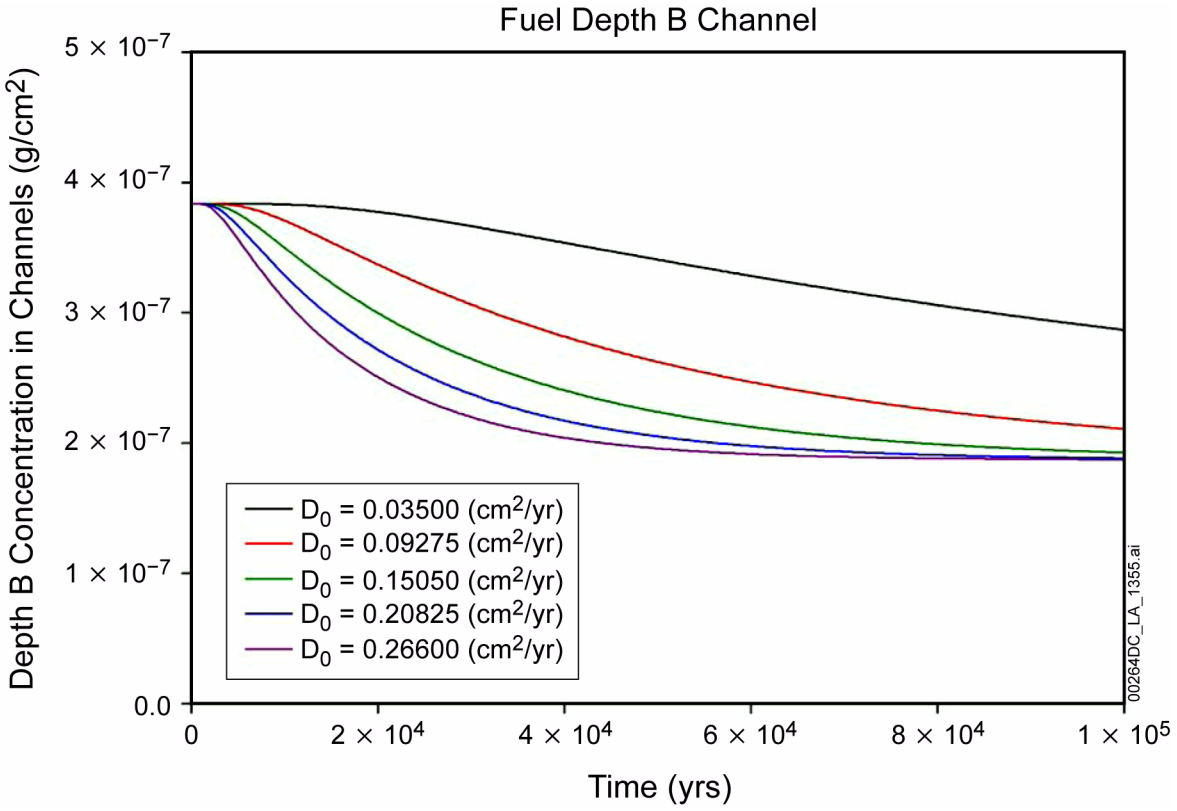

Figure 2.3.11-17. Integrated Waste to the Biosphere Depth in Channels Versus Time for Various Channel Diffusivity Values

NOTE: Consistent with the description in Section 2.3.11.4.1, the term fuel is used in this figure, but the term should be considered synonymous with the term waste.

Source: SNL 2007g, Figure 6.6.2-4.

INTENTIONALLY LEFT BLANK